4. SITE 671[1]

Shipboard Scientific Party[2]

HOLE 671A

Date occupied: 0845, 27 June 1986

Date departed: 1430, 28 June 1986

Time on hole: 29 hr, 45 min

Position: 15°31.55′N, 58°43.95′W

Water depth (sea level; corrected m, echo-sounding): 4914.5

Water depth (rig floor; corrected m, echo-sounding): 4925.0

Bottom felt (rig floor; m, drill-pipe measurement): 4941.6

Distance between rig floor and sea level (m): 10.5

Total depth (rig floor; m): 4988

Penetration (m): 46.4

Number of cores (including cores with no recovery): 1

Total length of cored section (m): 5

Total core recovered (m): 5

Core recovery (%): 100

Oldest sediment cored:
Depth (mbsf): 5
Nature: nannofossil ooze
Age: late Pleistocene
Measured velocity (km/s): 1.5

HOLE 671B

Date occupied: 1430, 28 June 1986

Date departed: 2315, 10 July 1986

Time on hole: 12 days, 8 hr, 45 min

Position: 15°31.55′N, 58°43.95′W

Water depth (sea level; corrected m, echo-sounding): 4914.5

Water depth (rig floor; corrected m, echo-sounding): 4925.0

Bottom felt (rig floor; m, drill-pipe measurement): 4942.2

Distance between rig floor and sea level (m): 10.5

Total depth (rig floor; m): 5633.4

Penetration (m): 691.2

Number of cores (including cores with no recovery): 74

Total length of cored section (m): 691.2

Total core recovered (m): 562.62

Core recovery (%): 79

Oldest sediment cored:
Depth (m): 691.2
Nature: sand
Age: early Oligocene
Measured velocity (km/s): n/a

HOLE 671C

Date occupied: 2315, 10 July 1986

Date departed: 0730, 15 July 1986

Time on hole: 4 days, 8 hr, 15 min

Position: 15°31.68′N, 58°43.97′W

Water depth (sea level; corrected m, echo-sounding): 4930.5

Water depth (rig floor; corrected m, echo-sounding): 4941.0

Bottom felt (rig floor; m, drill-pipe measurement): 4947.0

Distance between rig floor and sea level (m): 10.5

Total depth (rig floor; m): 5461.7

Penetration (m): 514.7

Number of cores (including cores with no recovery): 2

Total length of cored section (m): 19

Total core recovered (m): 16.66

Core recovery (%): 87.6

Oldest sediment cored:
Depth (mbsf): 514.7
Nature: radiolarian mudstone
Age: early Miocene
Measured velocity (km/s): 1.7

HOLE 671D

Date occupied: 2330, 6 August 1986

Date departed: 0715, 10 August 1986

---

[1] Mascle, A., Moore, J. C., et al., 1988. *Proc., Init. Repts. (Pt. A), ODP*, 110: College Station, TX (Ocean Drilling Program).

[2] J. Casey Moore (Co-Chief Scientist), Dept. of Earth Sciences, University of California at Santa Cruz, Santa Cruz, CA 95064; Alain Mascle (Co-Chief Scientist), Institut Français du Pétrole, 1–4 Ave Bois-Preau, B.P. 311, 92506 Rueil Malmaison Cedex, France; Elliott Taylor (Staff Scientist), Ocean Drilling Program, Texas A&M University, College Station, TX 77840; Francis Alvarez, Borehole Research Group, Lamont-Doherty Geological Observatory, Columbia University, Palisades, NY 10964; Patrick Andreieff, BRGM, BP 6009, 45060 Orleans Cedex-2, France; Ross Barnes, Rosario Geoscience Associates, 104 Harbor Lane, Anacortes, WA 98221; Christian Beck, Département des Sciences de la Terre, Université de Lille, 59655 Villeneuve d'Ascq Cedex, France; Jan Behrmann. Institut für Geowissenschaften und Lithosphärenforschung, Universität Giessen, Senckenbergstr. 3, D6300 Giessen, FRG; Gerard Blanc, Laboratoire de Géochimie et Métallogénie U. A. CNRS 196 U.P.M.C., 4 Place Jussieu, 75252 Paris Cedex 05, France; Kevin Brown, Dept. of Geological Sciences, Durham University, South Road, Durham, DH1 3LE, U.K. (current address: Dept. of Earth Sciences, University of California at Santa Cruz, Santa Cruz, CA 95064); Murlene Clark, Dept. of Geology, LSCB 341, University of South Alabama, Mobile, AL 36688; James Dolan, Earth Sciences Board, University of California at Santa Cruz, Santa Cruz, CA 95064; Andrew Fisher, Division of Marine Geology and Geophysics, University of Miami, 4600 Rickenbacker Causeway, Miami, FL 33149; Joris Gieskes, Ocean Research Division A-015, Scripps Institution of Oceanography, La Jolla, CA 92093; Mark Hounslow, Dept. of Geology, Sheffield University, Brook Hill, Sheffield, England S3 7HF; Patrick McLellan, Petro-Canada Resources, PO Box 2844, Calgary, Alberta Canada (current address: Applied Geotechnology Associates, 1-817 3rd Ave. NW, Calgary, Alberta T2N OJ5 Canada); Kate Moran, Atlantic Geoscience Centre, Bedford Institute of Oceanography, Box 1006, Dartmouth, Nova Scotia B2Y 4A2 Canada; Yujiro Ogawa, Dept. of Geology, Faculty of Science, Kyushu University 33, Hakozaki, Fukuoka 812, Japan; Toyosaburo Sakai, Dept. of Geology, Faculty of General Education, Utsunomiya University, 350 Minemachi, Utsunomiya 321, Japan; Jane Schoonmaker, Hawaii Institute of Geophysics, 2525 Correa Road, Honolulu, HI 96822; Peter J. Vrolijk, Earth Science Board, University of California at Santa Cruz, Santa Cruz, CA 95064; Roy Wilkens, Earth Resources Laboratory, E34-404 Massachusetts Institute of Technology, Cambridge, MA 02139; Colin Williams, Borehole Research Group, Lamont-Doherty Geological Observatory, Columbia University, Palisades, NY 10964.

Time on hole: 3 days, 7 hr, 45 min

Position: 15°31.48'N, 58°43.88'W

Water depth (sea level;, corrected m, echo-sounding): 4921

Water depth (rig floor; corrected m, echo-sounding): 4931.5

Bottom felt (rig floor; m, drill-pipe measurement): 4953

Distance between rig floor and sea level (m): 10.5

Total depth (rig floor; m): 5463

Penetration (m): 510

Number of cores (including cores with no recovery): 1

Total length of cored section (m): 9

Total core recovered (m): 0

Core recovery (%): 0

Principal results. Site 671 penetrated through the décollement zone separating accreted sequences (above) from underthrust ones (below) at the front of the Barbados Ridge, the wide accretionary complex resulting from the subduction of the Atlantic Plate below the Caribbean Plate. Drilling penetrated about 500 m of lower Pleistocene through lower Miocene imbricately thrusted, offscraped sediment, a 40-m décollement zone, and 150 m of Oligocene, little deformed, underthrust sediment. The offscraped sediment is composed of locally ashy hemipelagic mud-mudstone, calcareous mud-mudstone, and marl-marlstone that accumulated on the Tiburon Rise above the influence of terrigenous sediment flows. In contrast, the Oligocene underthrust section contains claystones and mudstones with cyclic variation in carbonate content, and a conspicuous terrigenous component, including discrete quartzose, fine-grained sand to silt that must have been derived from South America. Penetration at Site 671 was limited by unconsolidated quartz sand at about 690 mbsf.

Thrust faults at 128 and 447 mbsf bound major imbricate slices, which have been internally thickened by folding and faulting. Locally steep or even vertical dips occur in the offscraped material, in contrast to the consistently shallow dip beds observed below the décollement zone. The décollement zone is characterized by a 40-m-thick zone of scaly fabric that has also developed to a lesser extent along most faults in the offscraped sequence. A noticeable increase in density at the base of the Miocene, as already observed at an oceanic reference hole, DSDP Site 543, could mark the origin of the initial location of the décollement zone. Biostratigraphic control suggests that the age of faulting at 128 mbsf is not older than 0.5 Ma.

Pore-water chemistry results in the décollement zone show anomalies in chloride, calcium, magnesium, and silica, which can be most simply explained by fluid flow and membrane filtration along this surface. Other pore-water chemistry trends in the offscraped sequence are explicable by the alteration of volcanic ash. A decrease in chloride content approaching the sand layer at the base of the hole suggests that this unit may also make up a dewatering conduit for the underthrust sediment.

BACKGROUND AND OBJECTIVES

The Lesser Antilles intraoceanic subduction zone lies at the eastern boundary of the Caribbean plate where it is underthrust by Atlantic Ocean crust at a rate estimated between 2 to 4 cm/yr (Minster and Jordan, 1978; Sykes et al. 1983). Magmatic activity in the Lesser Antilles volcanic arc suggests that underthrusting has been occurring since at least mid-Eocene. This volcanic arc is flanked on the west by the Grenada Basin, a possible back-arc basin, and to the east by a broad forearc. The forearc is principally underlain by the Barbados Ridge complex, an extensive accretionary prism (e.g., Chase and Bunce, 1969; Biju-Duval et al., 1982; Westbrook, 1982) which narrows in extent to the north (Fig. 1). In the southern portion of the forearc the accretionary prism and the arc are separated by the Tobago Trough, which contains more than 4 km of sediment; the accretionary prism overthrusts the basin on its eastern flank (Speed et al., 1984).

Owing to its longevity and high sediment supply, the Lesser Antilles subduction zone has developed a very large accretionary prism, the Barbados Ridge complex. The seaward boundary of the accretionary prism is marked not by a typical oceanic trench but a deformation front characterized by folding and thrust faulting. In the south, where the underthrusting sediment is greater than 5 km thick, frontal accretion is characterized by folds and thrusts developed on a large scale (Valery, et al., 1985); in the north, where the incoming sediment blanket is only about 1 km thick, the initial deformation is dominated by small-scale thrusting (Biju-Duval et al., 1982).

During Leg 78A of the Deep Sea Drilling Project, drilling at Sites 541 and 542 (3.5 and 2 km arcward of the deformation front, respectively), successfully penetrated the Barbados Ridge complex to near the décollement (Fig. 2; Biju-Duval, Moore et al., 1984). There the accretionary prism is composed of lower Miocene to Holocene pelagic clays, nannofossil muds and radiolarian clays (near the base only). Ash layers were a conspicuous but volumetrically minor part of the cored section. The sediments have been deformed along minor and major low-angle thrust faults; the most prominent thrust fault was the décollement zone separating the accreted from subjacent underthrust sediments. The sediments recovered at Sites 541 and 542 are quite similar in both thickness and sedimentary facies to those of equivalent age drilled at the reference Hole 543; Site 543 is located 3 km seaward of the front of deformation and about 20 km north of Sites 541 and 542. At Site 543 basal pillow basalts of the Atlantic oceanic crust are overlain by 410 m of lower Campanian to Holocene pelagic to hemipelagic sediments.

Leg 78A clearly demonstrated tectonic accretion at the deformation front of an active margin and for the first time biostratigraphically documented thrust faulting; however, the drilling failed to completely penetrate through the décollement and the underthrust sedimentary sequence to oceanic basement. Collapse of the holes in overpressured unstable zones near and within the décollement prevented complete penetrations at Sites 541 and 542. At Site 542 the hole collapsed and "packed-off" or filled the space outside of the drill-in casing providing a closed conduit to the ship. Subsequent recording of near lithostatic fluid pressures (300 to 350 psi) at Site 541 and temperature anomalies at both Sites 541 and 542 suggest that faults act as fluid conduits (Davis and Hussong, 1984; Moore and Biju-Duval, 1984). Owing to time and equipment limitations during Leg 78A, extensive measurements on fluid pressures, temperatures, and compositions were not carried out. However, the available results suggest that concentrated flow occurs along faults, thus having potentially vital effects on the tectonics, thermal history, and diagenesis of accreted sediments.

Site 671, and indeed all of ODP Leg 110, was designed to solve problems raised by the previous drilling in this area. Results from DSDP Site 541 and 542 suggested that core recovery would be good and that faults could be identified biostratigraphically. Moreover, refined processing of the high-resolution multichannel seismic profile (IFP-ELF line CRV 128, Fig. 2) allowed better definition of seismic sequences as well as clearer resolution of the internal structure of the accretionary complex. Accordingly, the specific objectives of Site 671 were:

1. To completely penetrate through the accretionary prism, the subjacent underthrust sediments, and into oceanic crust.
2. To better define the structural geology, physical properties, and water content of the accreted sequences as well as to determine fluid migration pathways in the deformed sediments.
3. To drill through the main décollement, to measure *in situ* pore-water pressure and temperatures, to take pore-water samples in and out of fault zones, and to examine the diagenetic effects of these fluids along fault zones.
4. To compare the compaction, diagenesis, and physical properties of the subducted sequences with the ones of equivalent age in the abyssal plain.

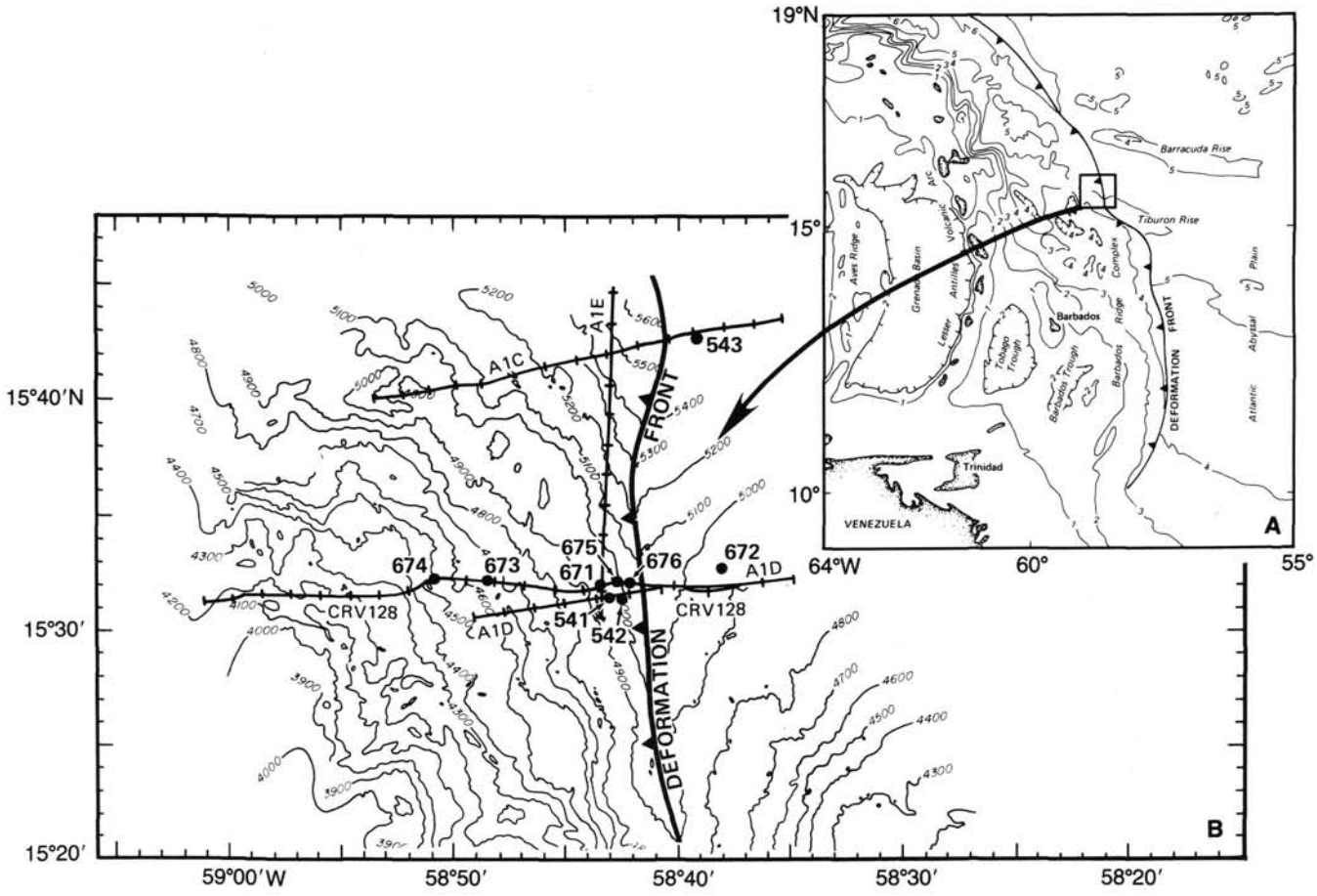

Figure 1. A: Regional location map. The deformation front defines the eastern boundary of the Barbados accretionary complex. Contour intervals are in kilometers. The Leg 110 drilling area is enclosed in box. B: Detailed site location map (box, A.). Contours are water depths (m) derived from a Seabeam map (Valery et al, 1985). Locations and shotpoint references shown for seismic profiles were obtained by IFP-IFREMER and IFP-ELF AQUITAINE-TOTAL from 1973 to 1982.

5. To set a reentry cone at the surface with subjacent casing through the décollement that would allow subsequent reentry of this fluid-rich zone for experimental purposes.

OPERATIONS

Barbados Port Call

Leg 110 had its official beginning when the first mooring line was put ashore in Bridgetown Harbor of Barbados, West Indies, at 2200 hr, 19 June 1986. Several work days were spent there transferring and inspecting drill pipe, replacing drilling equipment, and carrying out logistical tasks. About 405,000 U.S. gallons of fuel were taken aboard before sailing on Leg 110.

Barbados to Site 671

The last line was cast off from Barbados at 1230 hr on 26 June 1986. After clearing the harbor the vessel proceeded to proposed drill site LAF-1. Seismic gear was deployed to aid in site selection and the beacon was dropped at 0445 hr on 27 June 1986 for a total transit time of 16 hr 45 min. Global Positioning Satellite (GPS) navigation did not coincide with site arrival time and the last 2 hr of the presite survey were conducted using dead reckoning. Sea conditions prevented the use of the cranes until arrival on site.

Site 671

Site 671 was chosen primarily from seismic record CRV-128 as a good location to penetrate the décollement and reach the underlying basement. The final site location was moved landward about 1 km from proposed Site LAF-1 to avoid an active fault zone observed in seismic records. The multichannel seismic record CRV-128 indicated two inactive fault zones overlying the décollement. The décollement was estimated to be 400 mbsf and basement 400 m below the décollement. Table 1 gives the coring summary.

Hole 671A

Hole 671A was used to both position the mudline and to perform a jet-in test for setting 20-in. casing. For this latter purpose, an 11-7/16 APC-XCB bit and bottom hole assemble was assembled and lowered to within 100 m of the seafloor. GPS positioning data received after dropping the beacon indicated the need to offset 800 m to the east of our original position. The bit was positioned 2 m above the precision depth recorder (PDR) seafloor depth of 4925 m, and three water cores were taken before a drill-pipe seafloor depth was indicated at 4942 m. Mudline was penetrated at 1000 hr, 28 June 1986.

An XCB barrel was dropped and a jet-in test was performed to estimate sediment resistance to setting the 20-in. casing string. At 45 m below the seafloor, penetration slowed and it was apparent that 20-in. casing could not be washed below this point. The pipe was pulled clear of the mudline and the test terminated.

A total of 5.0 m of cored material was recovered from Hole 671A, for a 100% recovery. The total depth of this hole was 46.4 mbsf, and the time on hole was 29 hr, 45 min.

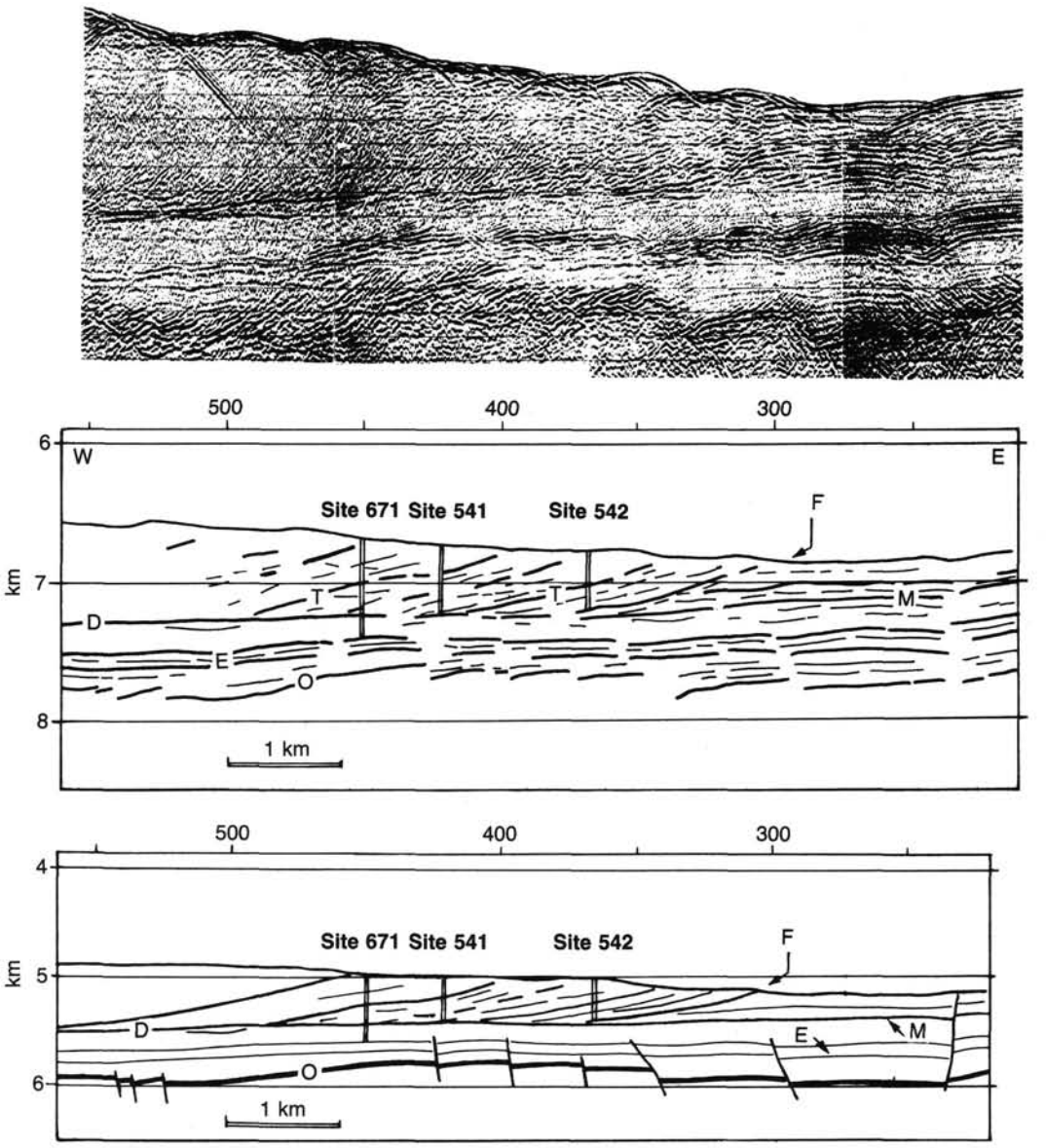

Figure 2. Migrated high-resolution multichannel seismic profile CRV 128. Seismic section (top); interpreted (prior to drilling at Site 671) line drawing (middle) and depth section (bottom). Location on Figure 1. F: deformation front of the accretionary prism facing the Atlantic abyssal plain; D: Décollement separating the accreted sequences (above) from the subducted ones (below); O: Top of the oceanic crust that was covered at Site 543 by Campanian calcareous and ferrigenous claystones; T: Possible thrusts in the accretionary complex; M: Reflector of assumed mid-Miocene age; E: Reflector of assumed mid-Eocene age.

Hole 671B

Hole 671B was spudded at 1430 hr, 29 June 1986. The hole was offset 20 m to the south of Hole 671A. The bit was positioned at 4940 m and Core 110-671B-1H established the mudline at 4942 m. APC cores were taken to 91.6 mbsf, where overpull of 40,000 lb on the last three cores indicated that the sediment was becoming too sticky for safe operation of the APC.

APC shoes, modified to carry the Von Herzen temperature recorder, were deployed on Cores 110-671B-2H, -4H, -6H, and -8H until core-barrel pull-out force raised concerns of having the core barrel stick. The core orientation (multishot) equipment was deployed on each APC coring run (Cores 110-671B-1H to -10H).

The Barnes-Uyeda heat-flow and pore-water sampler (WSTP) tool was attached to the end of a modified XCB coring assembly and deployed after Cores 110-671B-5H and -18X. In both tests 10,000 lb of weight was applied to the bit. Dwell time on bottom was 20 and 15 min, respectively. A drill string overpull of 40,000 lbs was required to free the bit at the conclusion of each test. A short probe spaced to stop 10 in. outside the bit was used on the second test to minimize the danger of bending the probe in the firmer sediment.

The coring system was switched to XCB at 5033 m (91.6 mbsf). The drilling strategy used to maintain good hole conditions consisted of:

1. Short wiper trips at three points in the hole to remove bridges forming above the bottom hole assembly (BHA).

Table 1. Coring summary for Site 671.

Core no.	Date June/ July 1986	Time	Sub-bottom Top (m)	Sub-bottom Bottom (m)	Meters cored	Meters recovered	Percent recovery
Hole 671A							
110-671A-1H	28	1037	0.0	5.0	5.0	5.02	100.0
Hole 671B							
110-671B-1H	28	1530	0.0	7.4	7.4	7.43	100.0
110-671B-2H	28	1705	7.4	16.9	9.5	10.06	105.9
110-671B-3H	28	1835	16.9	26.4	9.5	8.81	92.7
110-671B-4H	28	2015	26.4	35.9	9.5	9.91	104.0
110-671B-5H	28	2130	35.9	45.4	9.5	9.73	102.0
110-671B-6H	28	0200	45.4	54.9	9.5	10.06	105.9
110-671B-7H	29	0325	54.9	64.4	9.5	8.72	91.8
110-671B-8H	29	0505	64.4	73.9	9.5	9.80	103.0
110-671B-9H	29	0610	73.9	83.4	9.5	9.48	99.8
110-671B-10H	29	0800	83.4	91.6	8.2	8.20	100.0
110-671B-11X	29	1030	91.6	101.1	9.5	9.77	103.0
110-671B-12X	29	1225	101.1	110.6	9.5	7.60	80.0
110-671B-13X	29	1350	110.6	120.1	9.5	9.17	96.5
110-671B-14X	29	1605	120.1	129.6	9.5	9.81	103.0
110-671B-15X	29	1750	129.6	139.1	9.5	9.72	102.0
110-671B-16X	29	2005	139.1	148.6	9.5	9.75	102.0
110-671B-17X	29	2210	148.6	158.1	9.5	8.94	94.1
110-671B-18X	29	2345	158.1	167.6	9.5	5.94	62.5
110-671B-19X	30	0500	167.6	177.1	9.5	2.66	28.0
110-671B-20X	30	0656	177.1	186.6	9.5	9.57	101.0
110-671B-21X	30	1000	186.6	196.1	9.5	2.85	30.0
110-671B-22X	30	1250	196.1	205.6	9.5	9.70	102.0
110-671B-23X	30	1500	205.6	215.1	9.5	4.82	50.7
110-671B-24X	30	1711	215.1	224.6	9.5	3.82	40.2
110-671B-25X	30	2005	224.6	234.1	9.5	9.32	98.1
110-671B-26X	30	2245	234.1	243.6	9.5	4.81	50.6
110-671B-27X	1	0240	243.6	253.1	9.5	6.71	70.6
110-671B-28X	1	0545	253.1	262.6	9.5	9.35	98.4
110-671B-29X	1	0838	262.6	272.1	9.5	4.43	46.6
110-671B-30X	1	1055	272.1	281.6	9.5	9.74	102.0
110-671B-31X	1	1305	281.6	291.1	9.5	2.30	24.2
110-671B-32X	1	1900	291.1	300.6	9.5	9.72	102.0
110-671B-33X	1	2155	300.6	306.1	5.5	2.48	45.1
110-671B-34X	2	0020	306.1	315.6	9.5	8.58	90.3
110-671B-35X	2	0320	315.6	325.1	9.5	9.68	102.0
110-671B-36X	2	0530	325.1	334.6	9.5	9.76	103.0
110-671B-37X	2	0810	334.6	344.1	9.5	4.73	49.8
110-671B-38X	2	1104	344.1	353.6	9.5	4.50	47.3
110-671B-39X	2	1325	353.6	363.1	9.5	0.71	7.5
110-671B-40X	2	1554	363.1	372.6	9.5	5.92	62.3
110-671B-41X	2	1845	372.6	377.7	5.1	9.72	190.0
110-671B-42X	2	2125	377.7	387.2	9.5	9.69	102.0
110-671B-43X	3	0025	387.2	396.7	9.5	7.04	74.1
110-671B-44X	3	0250	396.7	406.2	9.5	8.38	88.2
110-671B-45X	3	0550	406.2	415.7	9.5	5.21	54.8
110-671B-46X	3	0830	415.7	425.2	9.5	6.43	67.7
110-671B-47X	3	1110	425.2	434.7	9.5	9.84	103.0
110-671B-48X	3	1310	434.7	444.2	9.5	9.64	101.0
110-671B-49X	3	1508	444.2	453.7	9.5	5.30	55.8
110-671B-50X	3	1715	453.7	463.2	9.5	9.04	95.1
110-671B-51X	3	2115	463.2	472.7	9.5	9.35	98.4
110-671B-52X	4	0500	472.7	482.2	9.5	5.56	58.5
110-671B-53X	4	0735	482.2	491.7	9.5	0.47	5.0
110-671B-54X	4	1000	491.7	501.2	9.5	8.84	93.0
110-671B-55X	4	1300	501.2	510.7	9.5	9.31	98.0
110-671B-56X	4	1505	510.7	520.2	9.5	9.38	98.7
110-671B-57X	4	1730	520.2	529.7	9.5	0.10	1.1
110-671B-58X	4	2000	529.7	539.2	9.5	8.34	87.8
110-671B-59X	4	2210	539.2	548.7	9.5	9.81	103.0
110-671B-60X	5	0445	548.7	558.2	9.5	2.91	30.6
110-671B-61X	5	0638	558.2	567.7	9.5	9.68	102.0
110-671B-62X	5	0921	567.7	577.2	9.5	9.43	99.2
110-671B-63X	5	1140	577.2	586.7	9.5	9.05	95.2
110-671B-64X	5	1341	586.7	596.2	9.5	8.45	88.9
110-671B-65X	5	1547	596.2	605.7	9.5	9.73	102.0
110-671B-66X	5	1758	605.7	615.2	9.5	9.64	101.0
110-671B-67X	5	2045	615.2	624.7	9.5	9.78	103.0
110-671B-68X	5	2250	624.7	634.2	9.5	0.00	0.0
110-671B-69X	6	0500	634.2	643.7	9.5	4.63	48.7
110-671B-70X	6	0655	643.7	653.2	9.5	8.92	93.9
110-671B-71X	6	0905	653.2	662.7	9.5	9.67	102.0
110-671B-72X	6	1120	662.7	672.2	9.5	9.70	102.0
110-671B-73X	6	1322	672.2	681.7	9.5	9.73	102.0
110-671B-74X	8	0740	681.7	691.2	9.5	1.30	13.7
Hole 671C							
110-671C-1X	13	0900	495.7	505.2	9.5	9.64	101.0
110-671C-2X	14	0345	505.2	514.7	9.5	7.02	73.9

2. Three KCL-inhibited mud slugs to sweep the hole of cuttings. (Lab tests on clays from the top of the hole indicated significant swelling and sloughing of the clays when subjected to fresh water or fresh water bentonite gel).
3. Reaming and circulating cuttings out of the hole.

The hole problems associated with drilling nearby sites on DSDP Leg 78A did not appear in Hole 671B. The better hole conditions are probably a result of the difference in drilling hydraulics between the rotary core barrel, used in 1979, and the APC/XCB coring system used on Leg 110. The extended cutting shoe of the XCB allows the use of higher pumping rates while coring without sacrificing core recovery. The increased pumping time generates more volume of flushing fluid for better removal of cuttings from the well bore. A second factor for better hole conditions is the larger 11-7/16-in. well bore cut by the XCB bit. The larger hole reduces the annular velocity around the 8-1/4″ drill collars and significantly reduced hole erosion.

Hole 671B coring terminated with a stuck core barrel at a total hole depth of 691.2 mbsf. Attempts to fish the barrel were unsuccessful because free-running quartz sand had invaded the well bore and flowed up around the XCB inner barrel. Two drill collars above the outer core barrel were packed with sand and required several hours to clean. The total amount of recovered core was 562.6 m, representing a 79% recovery.

The drill string was pulled until only the BHA was below the mud line. An 8-ft-diameter free-fall reentry cone with 6 ft of 13-3/8″ casing was assembled around the drill pipe and dropped to the seafloor.

The TV was lowered to the seafloor to detorque the cable and observe the free-fall reentry cone location. TV seabottom surveying revealed that the cone had sunk below cuttings, and only the two attached floats were visible above a crater washed into a featureless seafloor. The crater was judged to be about 16 ft long, 12 ft wide, and about 2 ft deep.

A logging BHA was assembled and run to the seafloor. The TV was lowered on the drill pipe and a box search pattern was used to locate the crater. After 5 hr of positioning, the pipe was stabbed between the floats for reentry. The drill string was run to 5221 m of drill-pipe depth (297 mbsf), and the pore water, temperature, and pressure (WSTP) sampling tool was lowered to the bit. The bit was subsequently positioned at 5231 m and 5241 m (307 and 317 mbsf) to give three sampling stations, and then the sampler was retrieved. The bit was run to 60 ft above total hole depth and the hole was conditioned for logging.

With the bit positioned above the décollement, the first set of Schlumberger logging tools were run to bottom. The logging tools stopped at a bridge 10 m outside the bit. The tools were recovered and the pipe was lowered to clean out the bridge; however, many firm bridges were encountered below the bit. Judging that further logging efforts in Hole 671B without the side entry logging sub would be fruitless, the hole was filled with weighted mud and operations at this hole were terminated. The total operations time on this hole was 12.4 days.

Hole 671C

Hole 671C was offset 200 m to the north of Hole 671B. This distance was the minimum offset calculated to position the drill in the unaffected formation for hydraulic purposes. The objective of this hole was to penetrate the décollement and obtain a packer test of the shear zone. If successful, the hole would be deepened and the zone below the décollement tested. A 10-1/2-in. core bit was installed and the TAM drilling packer was positioned above the outer core barrel.

The bit was positioned above PDR depth and a XCB wash barrel with modified landing shoulder was dropped. The mudline was established at 4947 m at 1300 hr, 11 July 1986. High torque and slow penetration rate lead to a decision to pull the wash barrel and drop a modified center bit at about 360 mbsf. The penetration rate improved but moderate torque remained. Hole sloughing and fill between connections was a problem throughout the lower section. Short wiper trips and mud slugs were necessary to maintain hole stability. The hole was cored from 495 to 514 mbsf to confirm stratigraphic location for the selected packer test interval. Since conditions at the bottom of the hole continued to deteriorate, the packer was positioned at 366 mbsf in a zone that had drilled tight. The total cored interval at Hole 671C was 19 m; 16.7 m were retrieved for an 87.6% core recovery.

The inflate go-devil was dropped and multiple attempts were made with the rig cementing pumps to set the packer. Several cycles of pressuring up to 1500 psi resulted in pressure bleed-off. The setting plug was sheared out at 2200 psi but still the packer did not set. The bit was pulled up the hole to 103 mbsf and the inflate go-devil retrieved with the overshot.

Another logging attempt was made; however, the tools could not be lowered beyond a few meters past the bit. Twenty-three m were logged by raising the drill string above the logging tools. The logging tools were recovered, the pipe run back to 250 mbsf, and the hole filled with weighted mud. The drill string was recovered and the work in the area of Site 671 terminated. The operations time at Hole 671C was 4.3 days. The total time spent at Site 671 was 17.9 days. The *JOIDES Resolution* was underway to proposed site LAF-0 by dead reckoning at 0830 hr, 15 July 1986.

Hole 671D

Site 671 was revisited during the Leg after attempting to drill Site 675 for a packer experiment. Poor hole conditions at Site 675 precluded the packer experiment and our previous experience indicated that the lithologic section at Site 671 was the best location to try the test again.

Hole 671D is located 200 m south of Hole 671C. The site approach was made by positioning off the beacons at Sites 675 and 671. The beacon at Site 671 was still operating after 41 days but had weakened to the point where a new beacon was needed for stationkeeping. A beacon was dropped after the location was established at 2330 hr, 6 August 1986. The location of Hole 671D is 15°31.481′N, 58°0.882′W.

The drilling packer was assembled above the core barrel of a nine-drill collar, bottom hole assembly. A 10-1/2-in.-diameter XCB bit and mechanical bit release with a flapper valve was used to drill the hole. The pipe was tripped to 3 m above the PDR depth and a center bit was attached to the bottom of an XCB inner barrel and dropped. The mudline was established by weight indicator reading at 4953 m below rig floor, and the hole was then drilled to 450 mbsf. Drilling conditions in Hole 671D were excellent, with little fill or torque.

To find a good packer seat above the décollement we decided to start coring at 450 mbsf. The first efforts to retrieve the center bit proved it was stuck; however, it was jarred free on a second wireline run. A core barrel was dropped and the first core cut at 452 m. Again, the core barrel was stuck and could not be retrieved. After three wireline trips and attempts to dislocate the barrel, we decided to conduct a packer test with the inner barrel in place.

The hole was subsequently deepened to a total depth of 519 mbsf to provide communication with the décollement. The penetration depth was limited to 519 mbsf primarily because of increased sticking and torque conditions that became quite noticeable below 452 mbsf. The pipe was pulled back to place the packer element at 439 mbsf and sea water was circulated to clean the hole. The first packer inflation cycle was normal, pressuring

up to 1500 psi. After pumping 2-1/2 barrels of fluid, the pump gage gave a sharp kick and the stand- pipe pressure dropped back to 1300 psi. After that point, an increase in flow rate was needed to maintain the pressure at 1600 psi. The pumps were turned off and the drill-pipe pressure slowly bled off after the test. The second pressuring cycle to 1600 psi required 3-1/2 barrels of fluid to achieve this pressure, which returned to zero within 2 min of pumps turnoff. The packer was moved to 432 mbsf and the inflate cycle was repeated with the same results. On the fourth cycle, the drill-pipe pressure was taken up to 2200 psi at which point the go-devil shear pin released. The drill pipe was moved several meters up and down the hole with no indication of drag, and we therefore concluded that the packer failed to seat. The inflate go-devil was retrieved, the drill string was tripped out of the hole, and the packer was disassembled from the drill string and inspected for damage. The element jacket had ripped open, the wires had been exposed, and a 2-in. slit was found in the bladder. Operations at Hole 671D were concluded at 0715 hr, 10 August 1986 after 3.3 days.

STRUCTURAL GEOLOGY

The most conspicuous structural features encountered at Site 671 are three reverse faults, or thrust faults, and the zone of detachment, or décollement, of the Lesser Antilles accretionary prism.

Proceeding from top to bottom, the drill hole intersects thrust A (Fig. 3) at 128 mbsf with a dip of approximately 50°. The fault emplaces late Miocene calcareous muds of package A upon lower Pleistocene calcareous muds of package B. The fault is a 5-mm-wide shear zone of light brown and darker brown muds with a biostratigraphic inversion constrained within a 50-cm section straddling the fault plane. The vertical throw of this fault is approximately 175 m. No pervasive wall rock deformation (scaly fabric, see Fig. 3) was recorded on either side of the fault.

The Miocene-Pleistocene section above thrust A appears to have suffered gentle folding as indicated in the bedding dip log, but the strata immediately above the fault are flat-lying. The interior of package A is crosscut by a large number of small-scale brittle faults. In Cores 110-671B-5H, -671B-6H, and -671B-7H there are exclusively high-angle normal faults, as determined by bedding offsets (Fig. 4) with dominant dips toward the east or southeast. Two conjugate sets were recognized, one of which is depicted in Figure 5. The faults encountered in Core 110-671B-8H possibly have dominant wrench characteristics, as interpreted from the steep intersection of the conjugate fault pair. Unfortunately, this core was not oriented with respect to magnetic north because of a failure of the multishot camera. Core 110-671B-10H contains one set of south-dipping faults with probable reverse displacements. Minor fault dip angles in the nonorientable Cores 110-671B-11X to -671B-13X become progressively smaller to give them thrust fault characteristics. The following bedding orientations are deduced from the oriented cores: horizontal bedding in Core 110-671B-5X, westward dips of 10° and 20° in Cores 110-671B-6H and 110-671B-10H, and north- to northeast-directed dips at 10° to 15° in Core 110-671B-7H.

A second important thrust fault (Thrust B) was intersected in Core 110-671B-41X at 375 mbsf. Here the upper Miocene to lower Pleistocene succession of calcareous mudstones in tectonic package B (Fig. 3) is emplaced upon carbonate-poor mudstones and claystones of the upper Miocene. This thrust (Fig. 3) lacks a clear-cut stratigraphic inversion. However, the thrust zone is defined structurally by two distinct horizons of scaly cleavage fabrics and intense mesoscopic brittle faulting of the core. Figure 6 shows a close-up of the deformed mudstones in the fault zone. A set of scaly cleavages is developed subparallel to steeply dipping bedding surfaces. Individual beds were dismembered by deformation to form phacoid-shaped bodies. The traces of scaly fabric can be seen particularly well in Figure 7, together with numerous polished microfault surfaces in a ripped-apart piece of Core 110-671B-41X. Visible drilling deformation superimposed onto the tectonic fabrics includes fragmentation of the rock into biscuits, and formation of a soft mud surrounding the fragments. In the interbiscuit sections the mud may acquire its own subhorizontal cleavage fabric in the course of progressive drilling (Figure 6). Probable drilling-related features within the biscuits are conjugate sets of steeply dipping microfractures related to axial compression of the core.

Another zone of scaly fabrics (Thrust C) is encountered in Cores 110-671B-49X and 110-671B-50X around 455 mbsf. Thrust C may be the locus of displacements within the unusually thick (145 m or more) upper Miocene section within Hole 671B. The lower boundary of tectonic package B may therefore be placed at 375 mbsf, as is done in Figure 3, or at 455 mbsf. Both fault zones may be taken as indications of tectonic thickening of the upper Miocene section. Supporting evidence for tectonic thickening comes from an expansion of the stratigraphic section in Cores 110-671B-38X to 110-671B-42X, which all belong to nannofossil zone CN9b (see section on biostratigraphy).

The prominent deformation features within package B are three distinct zones of scaly cleavage, and numerous small-scale brittle faults (Fig. 3). As in tectonic package A, there is a concentration of brittle faulting toward the center of the thrust unit. Where the sense of displacement is distinguishable, the faults in package B have reverse or thrust displacements. Fault dips change from shallow near the top and bottom of package B, to steep or even vertical in the center. A small-scale thrust cutting across a reverse fault in Core 110-671B-30X suggests multistage faulting at least on a local stage. Bedding dips are vertical near the top of package B, with a quick change to horizontal downsection. Horizontal bedding is maintained down to the base of the upper Pliocene. Steep dips are found in the lower Pliocene and upper Miocene sections, within a sequence in apparent proper stratigraphic succession.

The main offscraping zone, or décollement, was intersected just below 500 mbsf. Displacement appears to be taken up by an approximately 40-m-thick sequence of scaly mudstones and claystones below the décollement (Fig. 3). The dominant attitude of the scaly foliation within the drilling biscuits is at high angles to the core axis (Figure 8). In places a millimeter-scale anastomosing pattern is observed, presumably separating low-strain lenses by high-strain microshears. The orientation of the scaly fabric varies between drilling biscuits, probably owing to rotation during drilling. We observed that formation of scaly fabrics is usually restricted to carbonate-free mudstones, suggesting that carbonate content may play a vital role in strain and displacement localization, and thus in the nucleation and propagation of this particular major detachment zone.

The section between thrust B and the décollement (thrust packages C and D) is occupied by upper Miocene and undated, generally carbonate-free mudstones and claystones. Three discrete zones of scaly cleavage fabrics are found at the contact of thrust packages C and D. One of the horizons (at 455 mbsf) is probably associated with significant displacements. Intensity of small-scale faulting is generally low, and there is a predominance of thrust fault geometries. Grading in ash beds suggests package C is right-way-up, with bedding dips ranging from steep at the top towards shallow near the décollement, indicating gentle folding on a 100-m scale.

The underthrust series below the décollement shows a gradual downward decrease in the frequency of scaly fabrics. As in the décollement itself, the fabrics are localized within the carbonate-free members of the Oligocene succession. Very little evidence for brittle faulting is found within the décollement, but in the footwall a large number of horizontal and shallow dip-

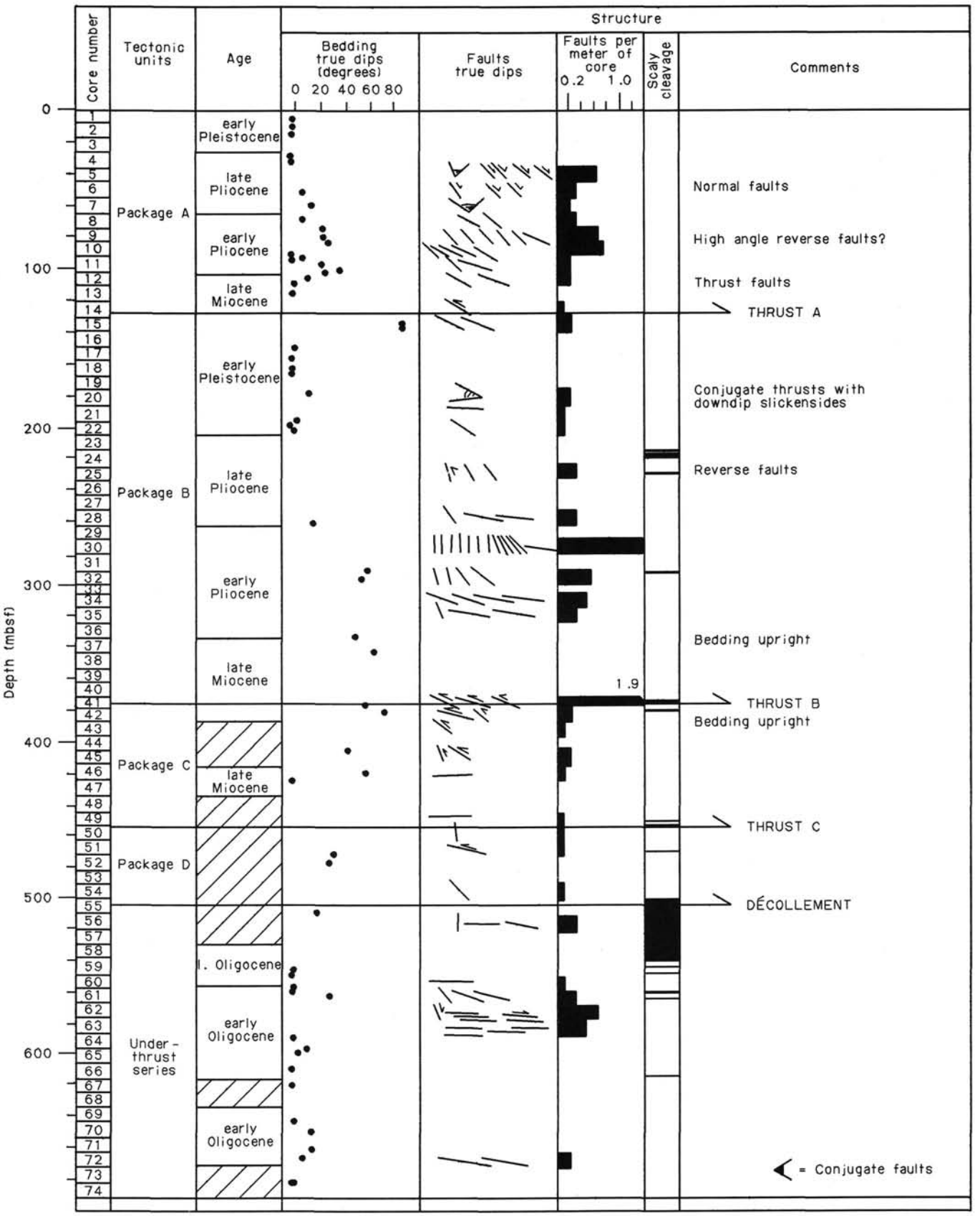

Figure 3. Structural log of Hole 671B, depicting true dips of bedding surfaces, true dips of small-scale fault surfaces, the relative intensity of brittle faulting, and the downhole distribution of scaly cleavage fabrics.

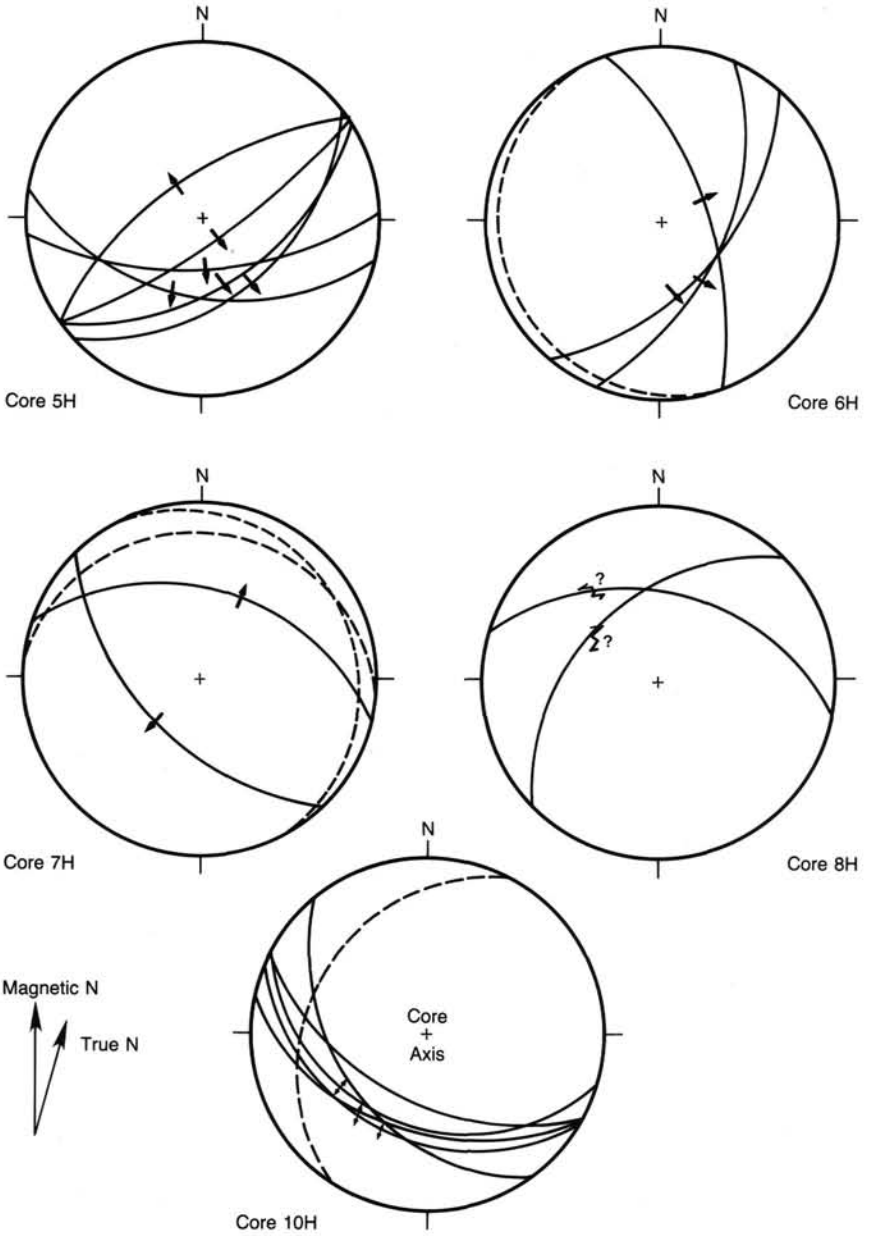

Figure 4. Oriented bedding and faults in hydraulic piston cores of Hole 671B. Solid lines are the projected intersections of fault planes with the lower hemisphere, dashed lines are those of bedding surfaces. The arrows point out the movement direction of the hanging-wall block of a fault, half-arrow pairs indicate the sense of wrenching. The orientation of the cores relative to magnetic north (N) was determined by multishot surveys of the borehole and the core in place. At Site 671, magnetic north is located at 346° (N14°W) with respect to true north.

ping faults are encountered at a depth range from 550 to 590 mbsf (Fig. 3). Deformation in the underthrust series dies out below 600 mbsf except for a thin scaly zone in Core 110-671B-66X, and two discrete flat-lying faults in Core 110-671B-72X.

In summary, Hole 671B penetrated four major thrust faults. The lowermost one probably acts as the floor detachment for the frontal thrust system of the Lesser Antilles accretionary prism. There is a downward variation of the deformation style. Thrust A is a single-fault surface with neither intense ductile nor brittle deformation of the immediate wall rocks. Thrust A was probably never more deeply buried than at present time. Thrust B is expressed by two distinct meter-scale belts of scaly cleavage, and the immediate hanging wall is heavily disturbed by brittle faulting. The décollement itself appears to be a broad belt of brittle-ductile rock flow, underlain by a zone of dominantly brittle deformation. The sediments interleaved between the thrusts show evidence of large-scale folding yielding the structural association of fold-fault packets typical for accretionary prisms.

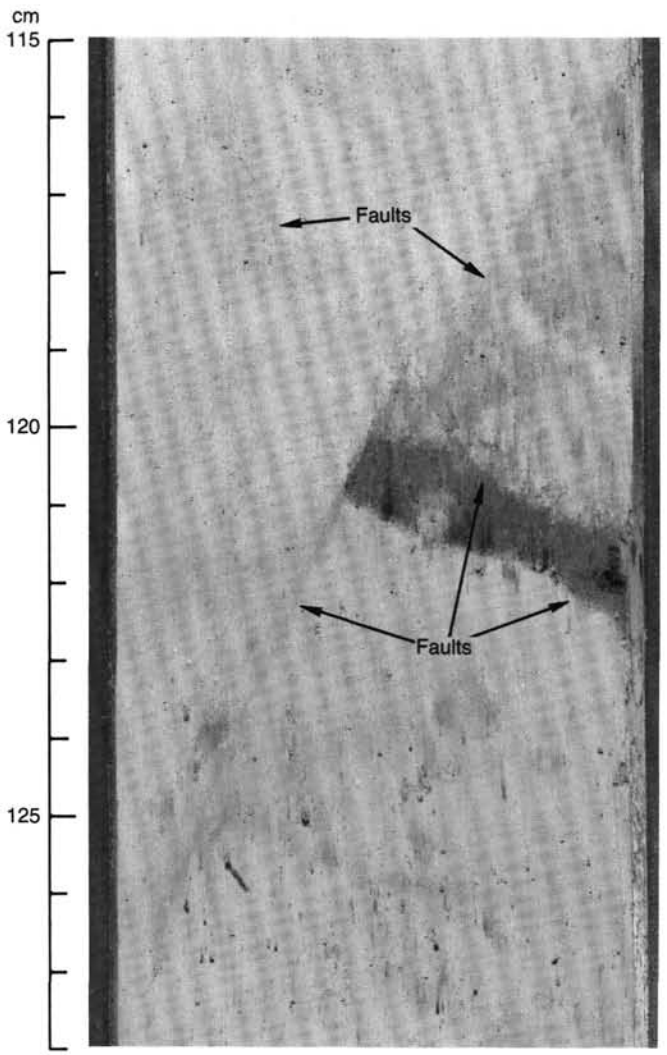

Figure 5. Conjugate set of normal faults in Sample 110-671B-7H-2, 115–128 cm. Normal displacements are visualized by the offsets on the dark bed of volcanic ash.

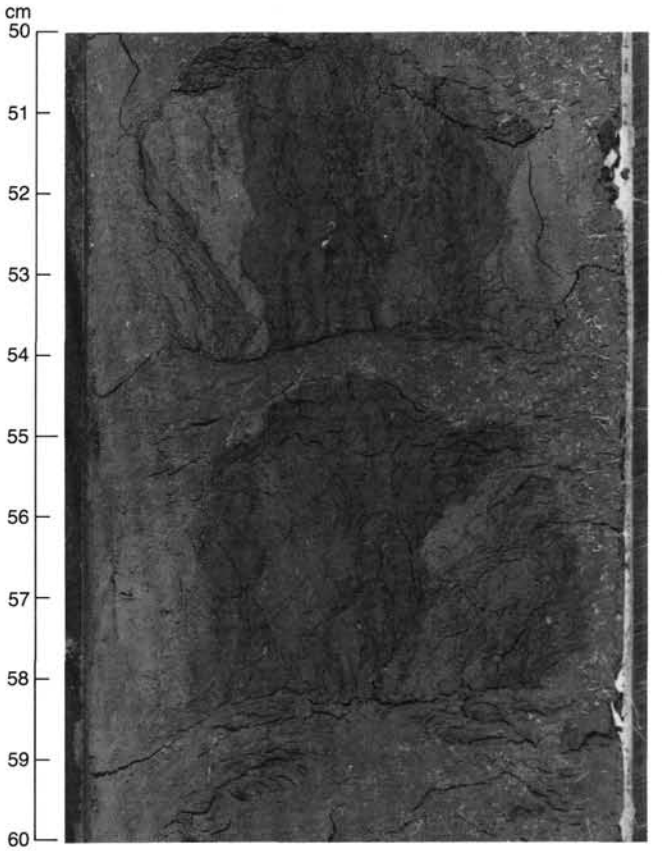

Figure 6. Deformed mudstone in Sample 110-671B-41X-4, 50–60 cm, showing stratal disruption and a steeply dipping fissility, overprinted by drilling-related biscuiting and conjugate fracturing of the core biscuits.

LITHOSTRATIGRAPHY

Sediment Lithology: Description

The sediments recovered at Site 671 are divided into four lithologic units on the basis of visual core descriptions, smear-slide analyses, and calcium carbonate data (Table 2).

Unit 1 (0–389.6 mbsf)

The unit consists of homogeneous, upper Pleistocene to upper Miocene calcareous mud/mudstone and marl/marlstone with common interbedded ash layers. Sediment color is predominantly olive-gray although several brown intervals also occur, generally in association with faults. Ash layers are typically dark gray in color and are commonly highly bioturbated. Orginal ash thickness is therefore difficult to determine in many cases. Trace amounts of sponge spicules occur locally in this unit. Carbonate content decreases markedly in the basal 45 m of Unit 1 (Fig. 9) and ash frequency decreases down section (Fig. 10).

Unit 2-A (389.6–491.7 mbsf)

The unit consists of 102 m of claystone and mudstone with a 17-m-thick interval containing calcareous mud in Cores 110-671B-46X to -671B-48X. Cores 110-671B-46X and -671B-47X are late Miocene in age, whereas the remainder of Unit 2-A is barren of microfossils and therefore of indeterminate age. Ash is relatively rare in Unit 2-A and many ash beds are intensely disturbed by bioturbation. The clays and muds are typically olive gray whereas ash beds are dark gray in color.

Unit 2-B (491.7–510.7 mbsf)

The unit is 19 m thick and consists of brown claystone of lower Miocene age. This age is based on radiolaria recovered from this interval in Hole 671C. Unit 2-B contains abundant scaly fabrics and probably corresponds to the upper portion of the décollement. Scattered pale gray 1- to 2-mm spherules and a 1-mm-thick shear vein (Core 110-671B-55X-4, 130 cm) of clinoptilolite occur in Unit 2-B. This unit is distinguished from Unit 2-A on the basis of color.

Unit 2-C (510.7–529.7 mbsf)

The unit is 19 m thick and consists of olive gray claystone of indeterminate age. This unit contains abundant scaly fabrics and is distinguished from Unit 2-B solely on the basis of color. As in Unit 2-B, common 1-mm spherules of clinoptilolite occur throughout Unit 2-C. These claystones probably represent the lower portion of the décollement (see Structural Geology section).

Unit 3 (529.7–681.7 mbsf)

The unit is a 146-m-thick sequence characterized by cyclic alternations of green claystone/mudstone, olive gray calcareous claystone/mudstone, and pale green gray marlstone. This unit is

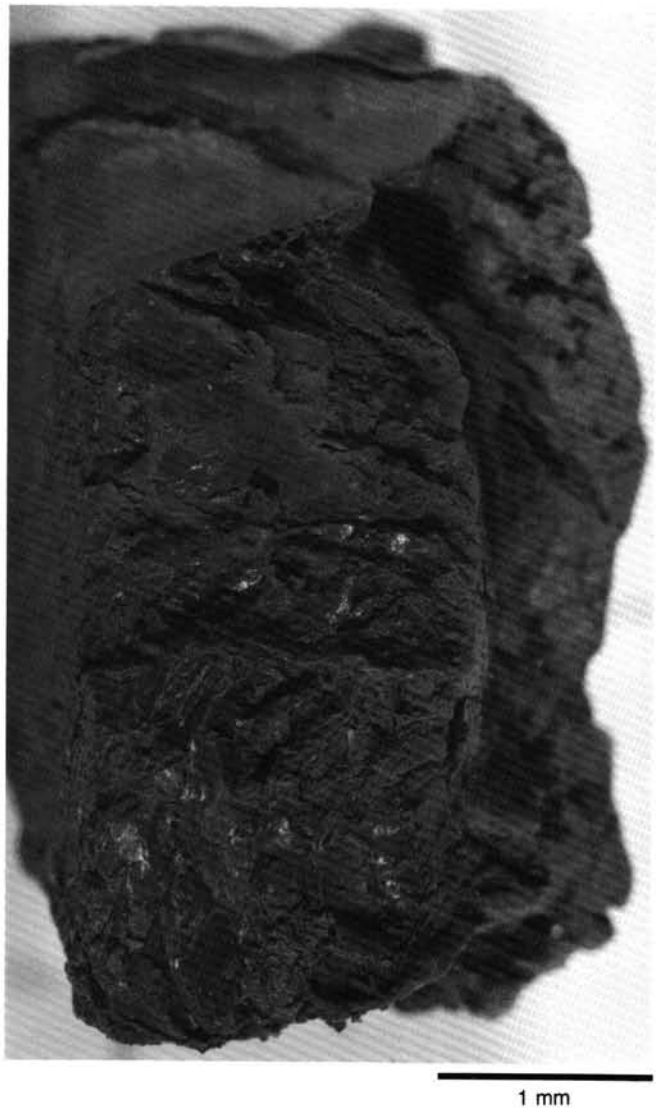

Figure 7. Scaly fabric (left half of photograph) and polished microfault surfaces in a ripped-apart portion of Sample 110-671B-41X-4, 67–70 cm.

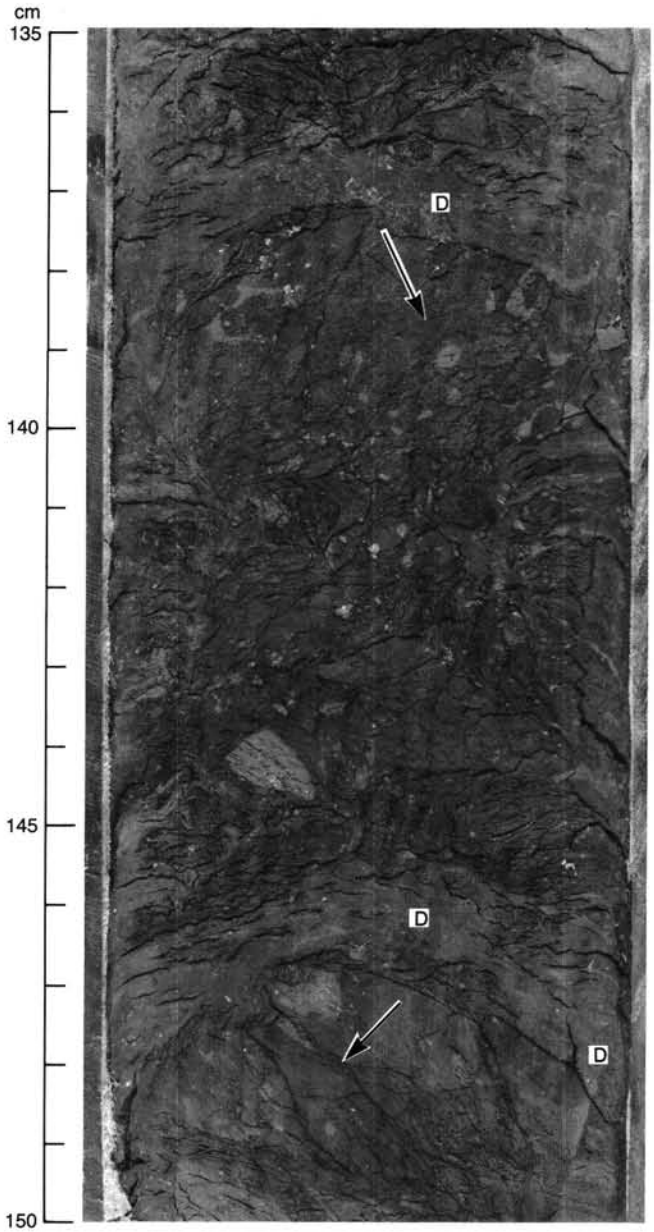

Figure 8. Tectonic and drilling fabrics in Sample 110-671B-55X-4, 135–150 cm. A prominent set of fissility planes representing scaly tectonic fabric dips left at a shallow angle in the upper core biscuit, and dips right in the lower one (arrows). Drilling-related fabrics (D) modify and overprint the tectonic fabrics.

distinguished by the common occurrence of calcareous intervals (Fig. 9). The upper 30 m of this unit is late Oligocene in age but most of the unit is early Oligocene in age. Numerous reworked microfossils, predominantly of Eocene age, occur throughout Unit 3 (see Biostratigraphy section). The claystone/mudstone and calcareous claystone/mudstone intervals typically range in thickness from 20 to 120 cm whereas the marlstones are much thinner, ranging from 5 to 30 cm in thickness. These marly intervals generally have sharp bases and consist of a lower planar laminated interval and an upper bioturbated interval. Silty intervals containing common millimeter-thick planar laminations (Fig. 11) and low-angle cross laminations occur throughout Unit 3. Some of these silty horizons exhibit probable partial Bouma sequences (Fig. 12). Smear-slide analyses reveal that the silt component of these sediments consists predominantly of subrounded-subangular quartz grains with minor amounts of plagioclase and glauconite, and local trace amounts of microcline and glaucophane. In addition, some of the silty intervals contain common pyrite-filled planktonic foraminifers and pyrite burrow casts. Pyrite-stained radiolarian fragments and sponge spicules also occur in minor amounts in Unit 3. Several probable small-scale slump horizons occur in Core 110-671B-61X and 1- to 10-cm pieces of indurated fine-grained dolomite(?) are found in Core 110-671B-59X-2, 35 to 40 cm. The lowermost 6.5 m of Unit 3 consists of brown mudstone. This interval is barren of microfossils and is consequently of indeterminate age. These sediments contain abundant green burrow mottles.

Unit 4 (681.7–683.0 mbsf)

Only 1.3 m of sediment were recovered from Unit 4. This unit consists of green gray mudstone underlain by unconsolidated, fine-medium grained, pale green gray glauconitic quartz sand (Fig. 13). Unit 4 is distinguished from Unit 3 on the basis of color and increased silt and sand content. Hole collapse prob-

Table 2. Lithologic units at Site 671.

Unit	Lithology	Cores 110-671-B	Depth (mbsf)	Age
1	Olive-gray and brown calcareous mud/mudstone and marl/ marlstone with common ash layers	1H to 43X-2, 90	0–389.6	Early Pleistocene to late Miocene
2-A	Olive-gray claystone, mudstone, and minor calcareous mudstone	43X-2, 90 to 53X-CC	389.6–491.7	Late Miocene and indeterminate
2-B	Brown radiolarian-bearing claystone	54X-1 to 55X-7, 32	491.7–510.7	Indeterminate
2-C	Olive-gray radiolarian-bearing claystone	55X-7, 32 to 57X-CC	510.7–529.7	Indeterminate
3	Alternating green claystone, olive calcareous clay/ mudstone, and pale green-gray marlstone with minor brown mudstone near base	58X-1 to 73X-2	529.7–681.7	Late Oligocene to early Oligocene
4	Olive-gray mudstone underlain by glauconitic quartz sand	73X-3 to 74X-1	681.7–691.2	Indeterminate

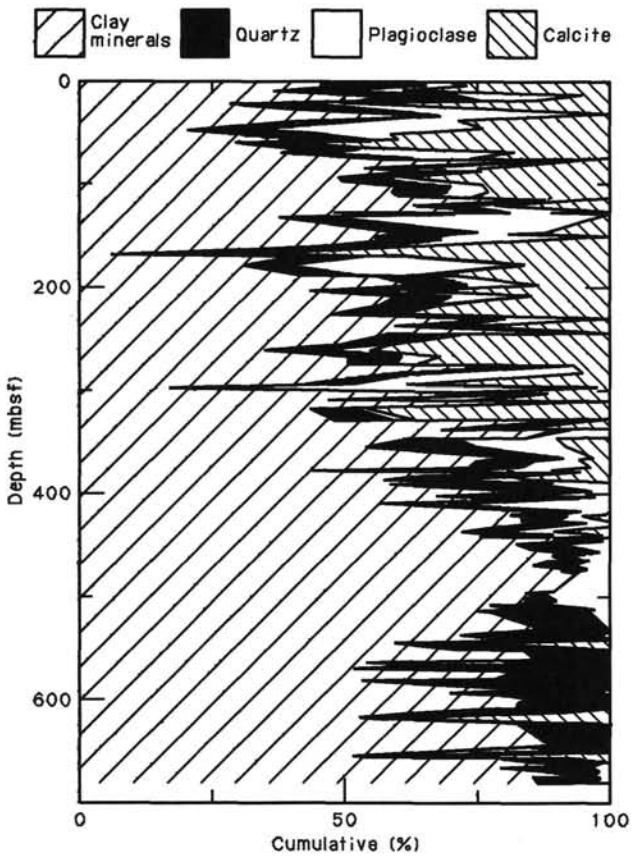

Figure 9. Bulk mineralogy of Site 671. Samples expressed as cumulative percentages of total clay minerals, quartz, plagioclase, and calcite.

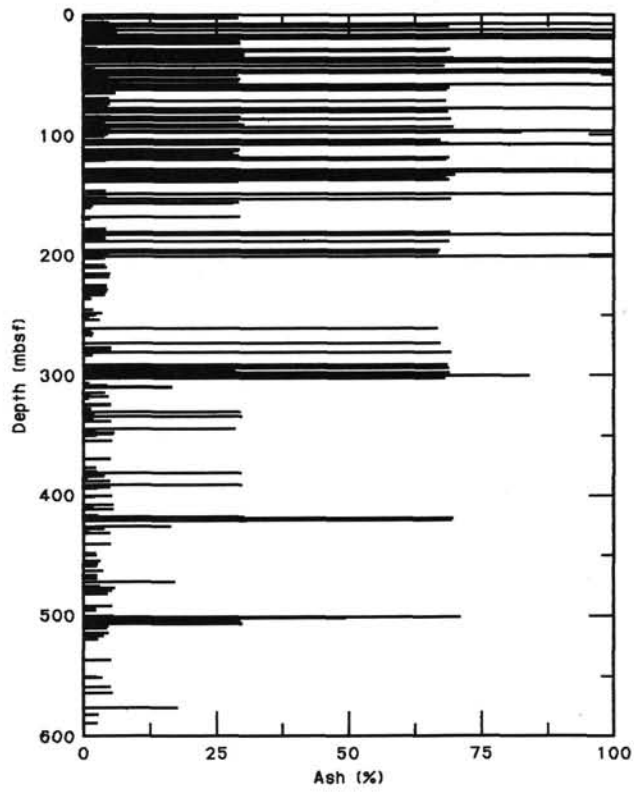

Figure 10. Plot of ash abundance in sediments from Hole 671B. Length of individual lines in the plot denotes concentration of ash, with the longest lines representing the highest ash concentrations at that interval. Ash is almost absent below the décollement (below 520 mbsf).

lems associated with the sand forced abandonment of Hole 671B at 691.2 mbsf. This sand may represent the top of a 90-m-thick, highly reflective unit that is well imaged in seismic profiles of the Site 671 area (see Seismic Stratigraphy section). Unit 4 is barren of microfossils but seismic stratigraphic correlation with DSDP Hole 543 sediments indicates that these sands are probably of early Oligocene age. Shipboard analysis of two thin sections of silt beds and a 6-mm-thick sand bed from this unit show that these layers consist of approximately 90% quartz, 3% glauconite, 3% plagioclase, 2% mudstone fragments, and 2% detrital pyrite (Fig. 14). Overall sorting in the silt layers is moderate, whereas sorting in the sand layer is moderately poor. The sand layer examined in thin section exhibits a distinct break in grain-size abundance, with a medium-grained sand component (300- to 500-μm grain diameter), little to no fine sand, and a very fine sand to coarse silt component (30- to 100-μm grain diameter). The quartz grains in the sand are subangular to subrounded, whereas grains in the silt layers range from subangular to angular. Many of the quartz grains exhibit strongly undula-

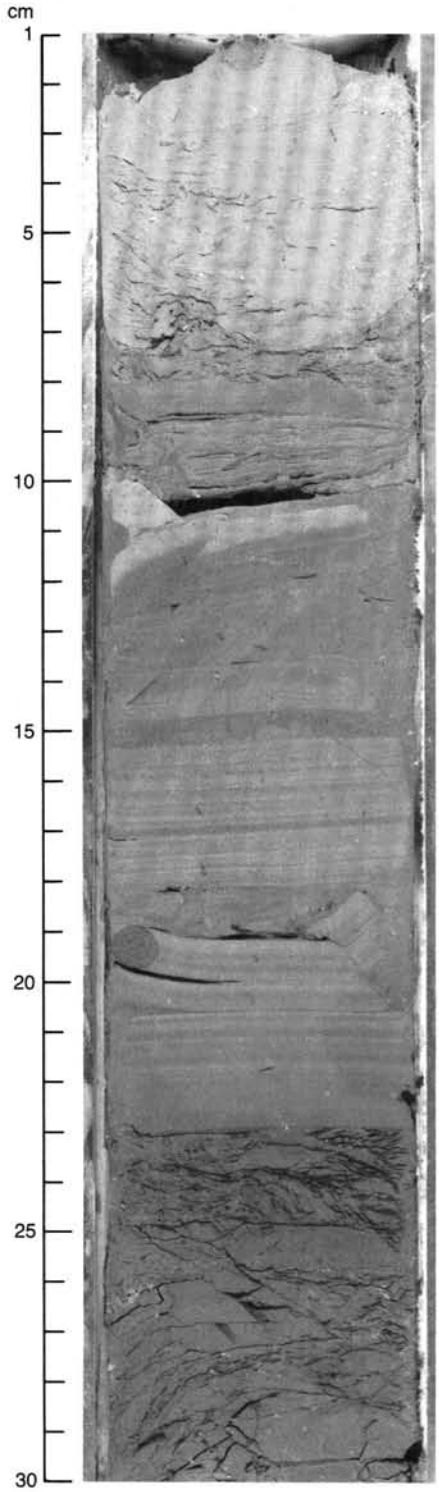

Figure 11. Well-developed interval of silty, planar-laminated sediment characteristic of lithologic Unit 3. Pronounced color variations are also typical of this unit.

tory, and locally domainal, extinction patterns under polarized light.

Thickness of Site 671 sediments vs. age is shown in Figure 15. Sedimentation rates were not calculated from these data because they were not corrected for bedding dip, compaction effects, or thickening by folding and thrust faulting.

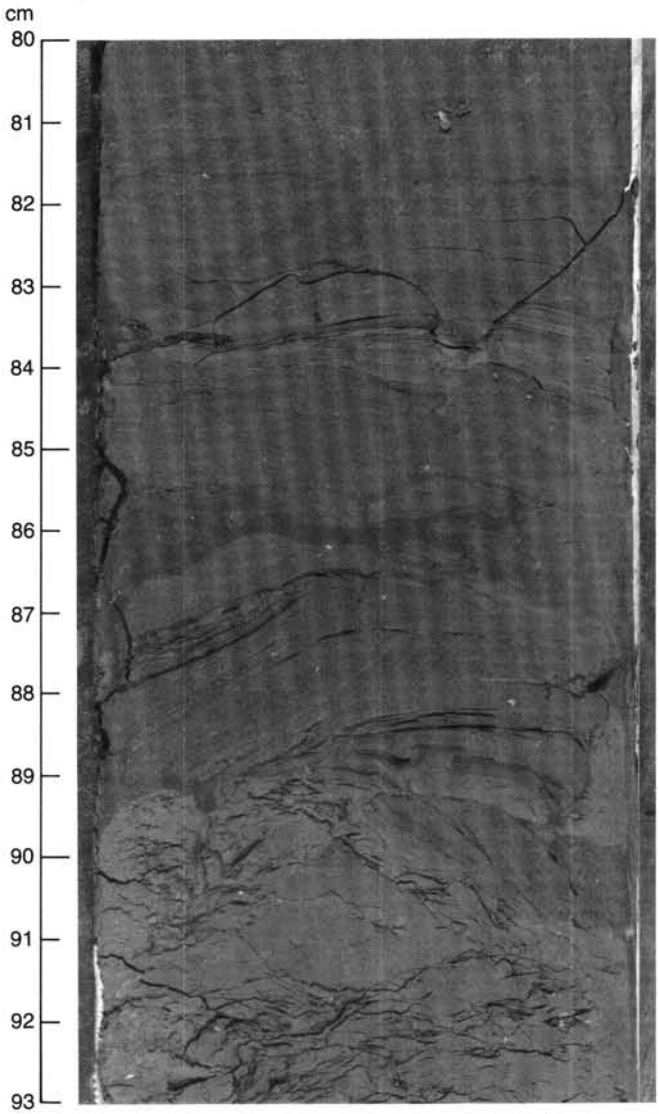

Figure 12. Possibly turbiditic silt layers showing partial Bouma sequences. An especially well-developed T_{abc} sequence is visible from 89.1 to 86.3 cm (measured along the left side of the core).

Depositional Environments and Processes

A striking change in the character of the sediments recovered at Site 671 occurs at the base of the décollement, between lithologic Units 2-C and 3. Sediments above the décollement are homogeneous, bioturbated, predominantly olive gray in color and contain abundant ash and few preserved sedimentary structures. In contrast, sediments below the décollement are characterized by cyclic color changes, common well-preserved sedimentary structures undisturbed by bioturbation, little ash, coarser overall grain size, and much more abundant detrital quartz.

Sediments above the décollement appear to have accumulated predominantly by pelagic-hemipelagic settling, showing no sedimentary structures indicative of current deposition. Ash layers in this interval probably originally reached the Site 671 area as air-fall material derived from the Lesser Antilles Arc. Carbonate content in sediments above the décollement decreases downsection (Fig. 9). Unit 1 typically contains from 10% to 40% carbonate, whereas sediments of Unit 2 generally contain less than 1% carbonate. This change in carbonate content re-

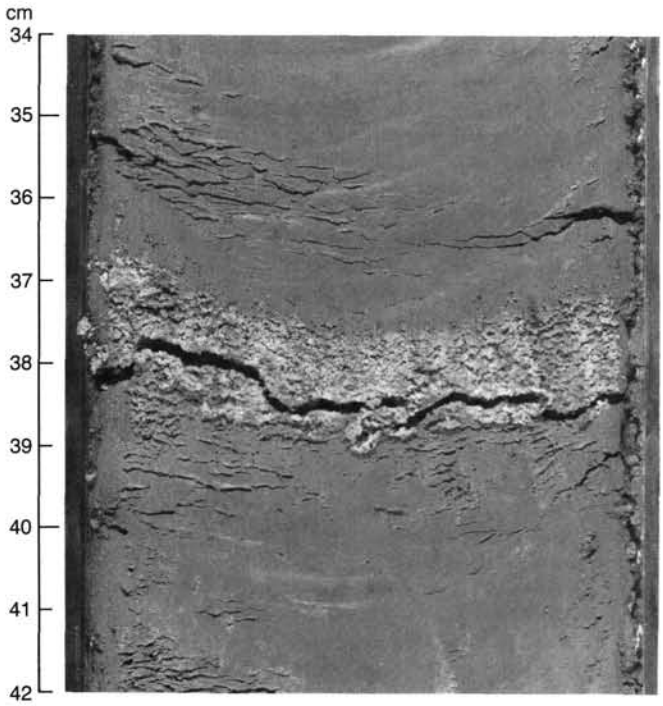

Figure 13. Thin bed of glauconitic quartz sand from upper portion of Unit 4. Sand is ungraded and exhibits sharp upper and lower boundaries.

flects the increasing importance of pelagic carbonate sedimentation at Site 671 since late Miocene time. The lack of terrigenous turbidites in this interval may reflect deposition of the Site 671 sediments on the slope of the Tiburon Rise, above the level of turbidite deposition. An abrupt decrease in water content and increase in density in Section 110-671B-2H-6, 50 cm, may represent the boundary between relatively dense, offscraped sediments and the overlying hemipelagic slope sediments.

In contrast to the sediments above the décollement, the underthrust series contains abundant sedimentary structures indicative of current reworking (Figs. 11 and 12). However, the exact nature of these currents remains unresolved. Although several examples of probable partial Bouma sequences occur in Unit 3 (Fig. 12), most silt layers from this unit exhibit no obvious turbiditic characteristics. Deposition by bottom-current activity, therefore, cannot be ruled out. The quartz-rich composition of the silts and sands of the underthrust series, combined with the occurrence of minor microcline and glaucophane in these sediments, strongly suggests that they were derived from South America, the nearest plausible source for these sediments. The greater abundance of silt and sand-sized quartz in the lithologic Units 3 and 4 clearly indicates a greater influx of relatively coarse-grained South American detritus into the Site 671 area during Oligocene time. The foraminiferal silt layers that occur in Unit 4 may represent pelagic sediments shed off the Tiburon Rise to a base-of-slope or near-slope abyssal plain depositional site. Probable slump horizons in Core 110-671B-61X and evidence of reworked Eocene microfossils throughout Unit 3 (see Biostratigraphy section) support this interpretation. The scarcity of ash in the underthrust series may reflect: (a) a period of little explosive volcanic activity in the Lesser Antilles Arc during Oligocene time; (b) removal of the ash from the Site 671 area by bottom currents, and/or (c) distance of the Site 671 area from the Lesser Antilles Arc during Oligocene time.

Bioturbation

Minor to intense bioturbation occurs in almost all cores recovered at Site 671. Four ichnogenera were observed: *Chondrites, Planolites, Zoophycos*, and a subcylindrical burrow (1-cm average diameter), steeply dipping to vertical, which could represent *Teichichnus*, although some specimens could represent large *Planolites*. Section 110-671B-35X-3 contains excellent examples of *Zoophycos* (Fig. 16). All of these ichnogenera belong to the *Zoophycos* ichnofacies defined by Seilacher (1967) and

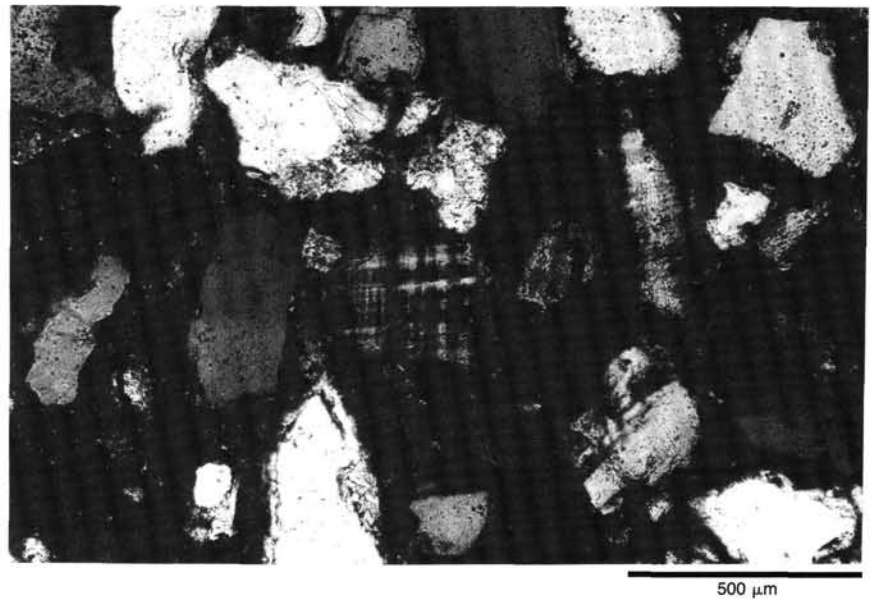

Figure 14. Thin-section photograph of quartz sand shown in Figure 13 (Section 110-74X-2, 77 cm), taken under crossed nichols. Note the microcline grain. Sand-sized grains range from subrounded to angular.

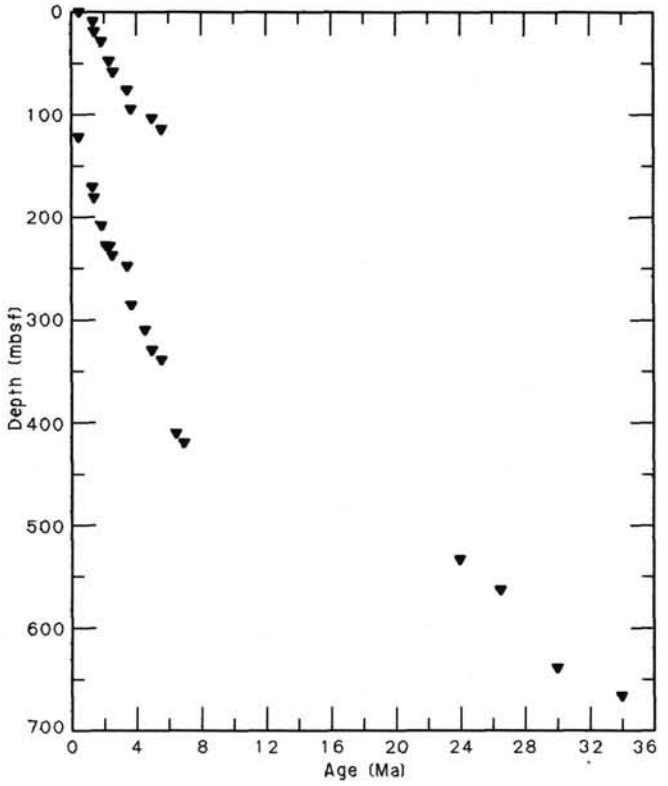

Figure 15. Sediment depth vs. sediment age for Hole 671B.

have been previously described on several Deep Sea Drilling Project cruises (e.g., Leg 15, Leg 78A). This ichnofacies is common on muddy substrates in calm, bathyal conditions where continuous sedimentation occurs.

Figure 17 illustrates downhole changes in bioturbation intensity observed in Hole 671B. Bioturbation is common and nearly continuous from Cores 110-671B-1H through -671B-57X (lithologic Units 1 and 2). In contrast, bioturbation in the underthrust series (lithologic Units 3 and 4) is discontinuous and generally restricited to pale green gray, highly calcareous intervals. In these latter sediments *Planolites* is the most common ichnogenus.

Bioturbation has extensively modified the original sediment texture of the Site 671 sediments, particularly above the décollement. This effect is especially well illustrated in and around ash layers, where sediment color contasts are generally greatest. In many examples, burrowing has completely destoyed original bedding and has redistributed ash particles for tens of centimeters up and down the core, especially in thinner ash layers. This degree of redistribution indicates locally deep, exichnia-like burrowing. Locally two, and sometimes three, burrows are superimposed on one another. The homogeneous nature of the sediments above the décollement (lithologic Units 1 and 2) may in part be caused by complete destruction of original sedimentary structures by bioturbation.

Volcanic Ash Occurrence

A semiquantitative estimate of the volume of ash deposited in the sedimentary sequence recovered at Site 671 has been determined by plotting the intervals over which ash horizons occur, and by estimating the relative ash concentration in those intervals. A graphic log of ash abundance is necessary for comparative analysis of regional sedimentation patterns and for geochemical mass balance computations. The graphic ash log

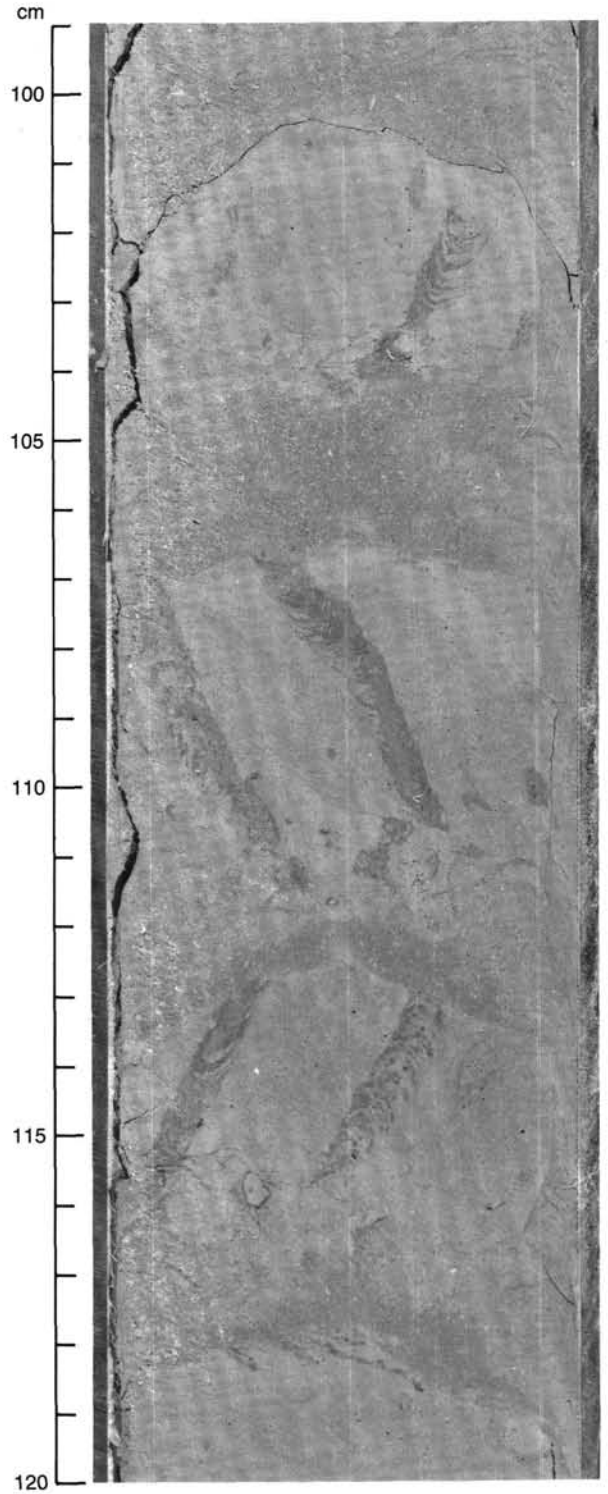

Figure 16. *Zoophycos* burrows in lithologic Unit 1. *Zoophycos* traces observed elsewhere in Site 671 sediments generally dip at shallow angles, suggesting that these examples occur in steeply dipping beds.

shown in Figure 10 results from analysis of core descriptions, core photos, and smear-slide descriptions. Steep bedding dips from 150 to 160 mbsf make accurate estimates of ash abundance in this interval difficult to determine, but the distinct ash abundance "peak" at this interval in Figure 10 is clearly an overestimate. Ash in the Site 671 sediments occurs as: (a) pure,

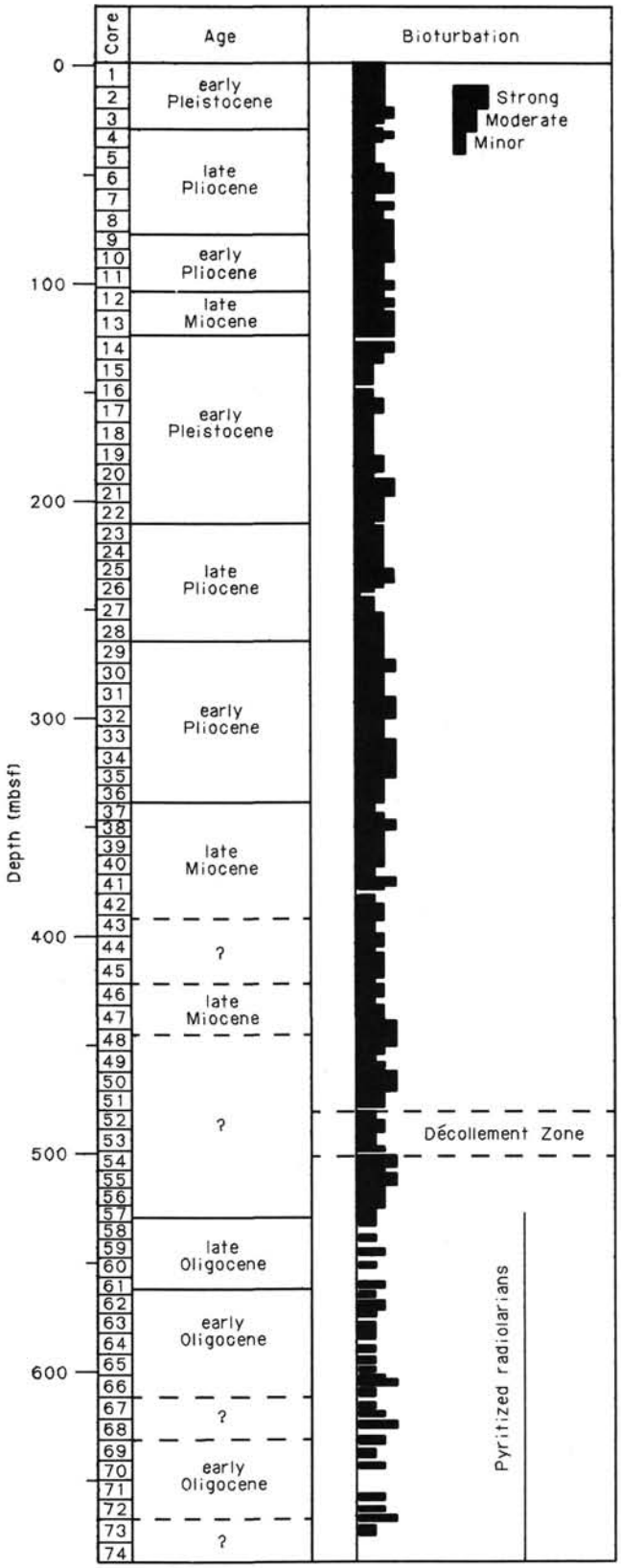

Figure 17. Frequency of bioturbation noted in visual core descriptions of Hole 671B sediments. Bioturbation is common and relatively constant above the décollement, whereas below the décollement burrowing is much more discontinuous.

relatively little-bioturbated layers (e.g., Figure 18), (b) highly bioturbated, but still recognizable ash layers, and (c) dispersed ash particles where originally layering has been completely obliterated by bioturbation. Concentrations used in Figure 10 are therefore only approximate, but are probably accurate to within 20%. Although every effort has been made to include all ash horizons, the cumulative abundance is probably underestimated owing to ambiguity in analysis of clay-sized particles and by diagenetic alteration of unstable components (e.g., volcanic glass). The presence of ash layers noted in smear slides is defined by the occurrence of plagioclase laths ± volcanic glass ± hornblende ± clinopyroxene ± orthopyroxene.

Smear slides of 18 ash layers from the lower Pleistocene and Pliocene section at Site 671 were examined in detail. Seven of these beds are composed of crystalline ash (e.g., Fig. 19-A). These layers consist of very fine to fine sand-sized grains. The other two crystalline ashes contain subequal amounts of sand- and silt-sized particles. Plagioclase is the most abundant mineral in these ashes (avg. 40%), followed in abundance by dark

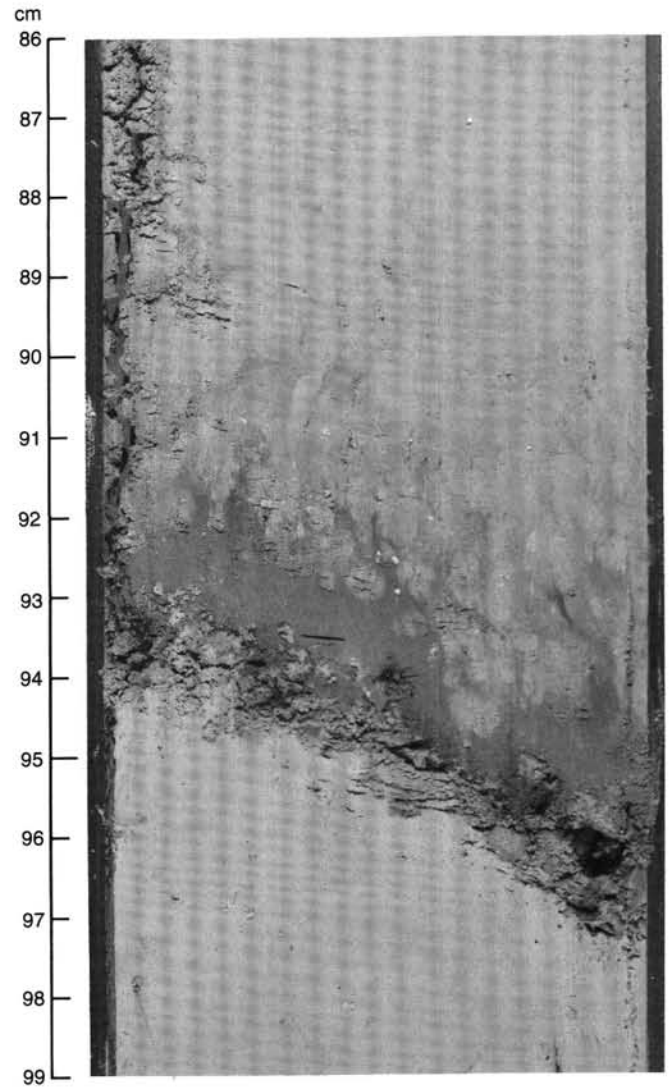

Figure 18. Typical ash layer from lithologic Unit 1. The sharp base and bioturbated top of this bed probably reflect rapid air-fall deposition. Bedding in many thinner ash layers has been completely obliterated by bioturbation.

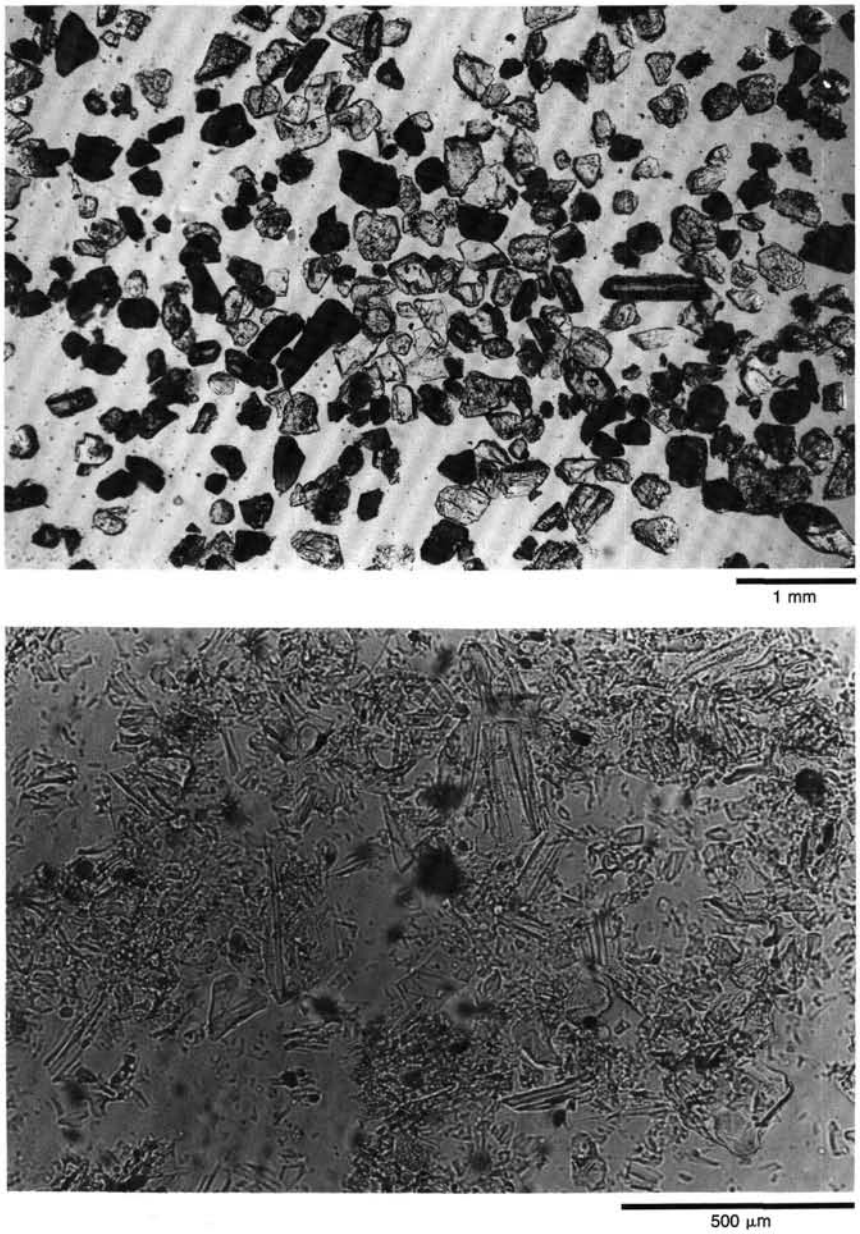

Figure 19. Smear-slide photographs of ash layers from Site 671 sediments. A. Crystalline ash from Section 110-671B-6H-1, 14 cm. B. Vitric ash from Sample 110-671B-5H, CC (10 cm) composed almost entirely of volcanic glass fragments. Note common, elongate vesicles.

greenish brown hornblende (5%–20%), pale green clinopyroxene (0%–20%), prismatic orthopyroxene (0%–5%), and primary opaque minerals (0%–5%). In most of these samples, the crystals are surrounded by thin remnants of glass. A few of the glass fragments (e.g., 110-671B-2H, CC, 9 cm), resemble andesitic mesostase. Sample 110-671B-5H, 113 cm contains minor quartz, rare mica (biotite or phlogopite), and reddish amphibole (probably kersutite).

The eighth ash layer, Sample 110-671B-5H, CC, consists of 95% glass shards (Fig. 19-B). These glass shards are silt sized and some of them exhibit numerous tubular vesicles; others show a typical scoriaceous texture.

The remaining seven ash samples consist of 40% to 60% volcanic particles and 40% to 60% clay minerals. The volcanic component of these layers is generally silt sized and consists of subequal amounts of crystals (plagioclase, hornblende, pyroxene) and glass shards (mostly nonvesicular).

The predominance of crystals over glass in the samples described probably reflects relatively proximal deposition of airfall material derived from the Lesser Antilles arc. Alternatively, the scarcity of glass in these samples may be related to current winnowing of these deposits (see discussion above) or to diagenetic alteration of much of the glass to clay minerals.

Bulk Mineralogy

Bulk mineralogy was determined for 270 samples taken from Site 671 following methods outlined in the "Explanatory Notes" chapter, this volume. In addition to the semiquantitative analysis by X-ray diffraction (XRD), total percentage carbonate was determined on many of these samples by Coulometric analysis

(precision = 0.2%). These data provide an external check on the estimate of percentage calcite by means of XRD. A plot of percentage carbonate vs. calcite (Fig. 20) shows generally good agreement between the two data sets. The two analyses agree to within +/- 10% for approximately 70% of the samples. The estimate of percentage calcite by XRD is significantly lower than that of percentage carbonate in several samples. Although this difference could reflect the presence of carbonate minerals other than calcite (e.g., dolomite, rhodochrosite) in the samples, peaks for other carbonate minerals were not noted on the XRD profiles. Despite these outlying samples, the general agreement between the two data sets is very encouraging in terms of interpretation of semiquantitative XRD results.

Results of the semiquantitative analysis for Site 671 sediments are given in Figure 9. In this figure, percentages of the four major phases (total clay minerals, quartz, plagioclase, and calcite) have been normalized to 100% and depicted on a cumulative plot. Several major trends with depth are evident. Total clay, the sum of all clay minerals, increases with depth from about 40% to 60% in the upper 330 m, to about 65% to 90% between 330 and 565 mbsf. From 565 to 675 mbsf, total clay content varies between 45% and 80% with few intermediate values. This interval corresponds to the early Oligocene age, cyclic sediments of lithologic Unit 3. The percentage of total clay is generally inversely correlated with calcite content, particularly in the Oligocene-aged sediments. The calcite content of lower Pleistocene and Pliocene sediments generally falls in the range 15% to 40%, then drops to 0% (with a few intervals containing up to 10% calcite) in the Miocene sediments. Lithologic Unit 2 is located in this interval of very low calcite content. Oligocene sediments of lithologic Unit 3 are characterized by highly variable calcite contents ranging between 0% and 40%.

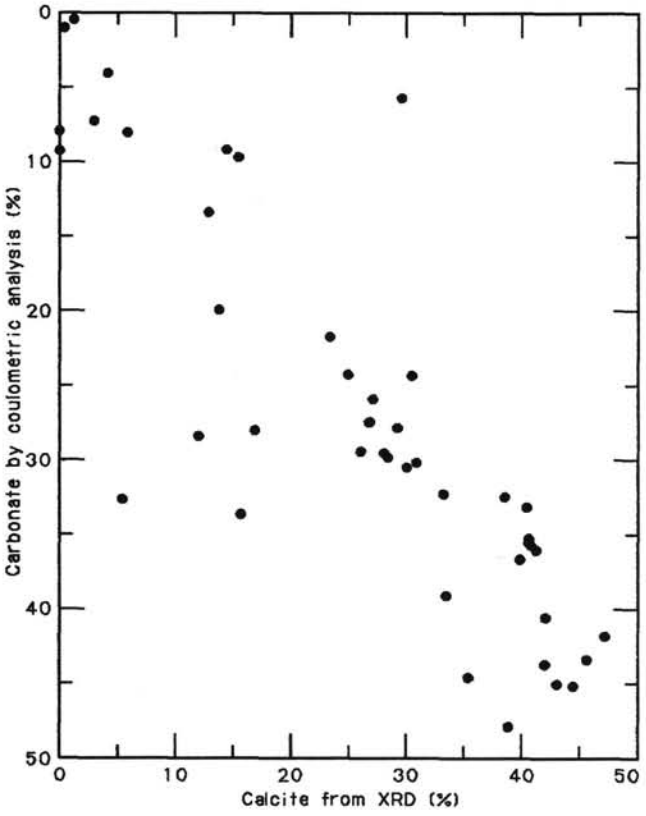

Figure 20. Plot of calcite percentage as determined by semiquantitative XRD, vs. carbonate percentage measured by coulometric analysis of the same samples.

The amount of plagioclase in Site 671 sediments varies widely between 0% and 52% but generally decreases with depth, reflecting the downsection decrease in abundance of ash beds and ash-rich sediments (Fig. 10). Sediments of lithologic Units 2-C and 3 contain at most 5% plagioclase. The quartz content of Site 671 sediments is generally uniform but decreases slightly with depth from 10% to 20% in the shallowest sediments to about 0% to 5% at approximately 500 mbsf. Below 500 mbsf depth, quartz content increases to about 5% to 25% and is highly variable throughout the lower and upper Oligocene sediments (lithologic Unit 3).

A major thrust fault (Thrust A; see Structural Geology section) was penetrated at Site 671 at about 128 mbsf. The fault is the boundary between thrust packages A (above) and B (below). It is of interest to compare the bulk mineralogy of the lower Pleistocene, Pliocene, and Miocene sediments of thrust package A to that of sediments of similar ages present below the fault in thrust package B. The major differences are summarized in Table 3.

The lower Pleistocene sediments of thrust package A are similar mineralogically to the lower portion of the lower Pleistocene sequence in thrust package B (below about 150 m depth). Nannofossil zonations support this correlation (see the Biostratigraphy section). This suggests that the upper portions of the lower Pleistocene sequence in thrust package A may be missing.

No major differences in bulk mineralogy were noted for the Pliocene sequences in thrust packages A and B.

The total clay and calcite contents of Miocene sediments of the two packages differ significantly. The higher calcite content of the Miocene sediments in thrust package A most likely reflects a greater degree of preservation, perhaps a result of deposition on a relative topographic high.

Six samples from lithologic Unit 2-B (thought to represent the décollement zone) were analyzed quantitatively for bulk mineralogy. The sediments from this zone are not different in terms of bulk mineral content from sediments immediately above or below. The entire zone is characterized by high clay mineral content (75%–90%) with most samples containing about 85% total clay minerals. No calcite was detected in any of the samples. Plagioclase content is 10% to 15% and quartz content is less than 5% in most samples, although the range is 0% to 12%.

BIOSTRATIGRAPHY

Summary

Sediments at Site 671 may be dissected by as many as four major faults associated with tectonic underthrusting of the Atlantic Plate. The largest of these faults is represented by a décollement structure between the descending Atlantic Plate and the offscraped wedge of accretionary sediments. Smaller reverse faults occur within the accretionary sediment package and are linked with tectonic movement along the décollement.

Table 3. Comparison between bulk mineralogy of sediments in thrust packages A and B.

Age	Thrust package A	Thrust package B
E. Pleist.	% calcite = 30–40 % plag = 10–12	Above 150m: % calcite = 0–10 % plag. = 10–50 Below 150m: % calcite = 25–40 % plag = 5–15
Pliocene	Bulk mineralogy similar in both packages.	
Miocene	% total clay = 40–60 % calcite = 20–30	% total clay = 70–90 % calcite = 0–10

Biostratigraphic evidence at Site 671 indicates up to four sedimentary sequences bound by thrust fault zones. A moderately complete, lower Pleistocene through upper Miocene section occurs in Cores 110-671B-1H through -14X. Near the base of Core 110-671B-14X a major biostratigraphic interruption was recognized that places upper Miocene sediments above those of lower Pleistocene. This inversion indicates that large-scale reverse faulting occurred after the early Pleistocene. A lower Pleistocene through upper Miocene section, repeated below the fault, is much thicker and more complete than the same biostratigraphic interval in the upper part of the hole. The upper Miocene CN9b Zone of Okada and Bukry (1980) and the corresponding *Neogloboquadrina humerosa* Zone of Bolli and Premoli-Silva (1973) are both slightly expanded in the lower section. This may be attributed to one of two causes: (a) the presence of a second thrust fault that forms the base of tectonic package 3 or (b) an increase in the sedimentation rate. Slightly older upper Miocene sediments occur below the expanded CN9a section. These sediments become progressively more dissolved with depth and give way to a long interval barren of calcareous populations (Samples 110-671B-48X, CC to 58X-5, 81–83 cm). The décollement structure is contained within this dissolved section and was dated as early Miocene by radiolarian fauna in the first washed core of Hole 671C. Core 110-671B-52X contains a small amount of nannofossiliferous material that was assigned to the CN9a Zone of Okada and Bukry (1980). Assuming this sample does not represent downhole contamination, another tectonic reversal of biostratigraphic sequence is indicated.

Geochemical and structural evidence suggests that the décollement was crossed within Cores 110-671B-54X and -55X. Nannofossiliferous sediments of Oligocene age were encountered in Core 110-671B-58X and provide a firm lower boundary for the décollement zone. A thick sediment section was then cored that extended just into the top of the lower Oligocene (Samples 110-671B-58X, CC to -72X, CC). Coarse sands were encountered in Core 110-671B-74X and the hole was abandoned.

Nannofossil and foraminiferal assemblages are present throughout the more calcareous portions of the sediment column. Radiolarians occur in small numbers within the décollement zone and in sediments of late Oligocene age. Calcareous populations are moderately well preserved in the Neogene sediments with the exception of increased dissolution intervals in the upper Miocene. Nannofossils are well preserved in Oligocene sediments although the foraminifers are much more dissolved. Dissolution patterns suggest that sediments at Site 671 were deposited below the foraminiferal lysocline throughout Miocene and Oligocene time. Barren intervals between Cores 110-671B-42X and -57X may be correlated with upward excursions of the Miocene CCD.

Reworking is common in all portions of the sediment column. Reworked Eocene assemblages of all three fossil groups were noted within the upper Oligocene section (Samples 110-671B-60X, CC to -63X, CC). Reworked Eocene assemblages were also observed in Pleistocene radiolarian populations. Site 671 is positioned on the flank of the Tiburon Rise and may have received sediments eroded from older sections at shallower depth.

Comparisons of nannofossil, radiolarian, and foraminifer biostratigraphies for Site 671 are presented in Figure 21. Figure 22 shows the interrelationship between the zonation schemes used for these fossil groups.

Calcareous Nannofossils

Nannofossiliferous sediments at Site 671 range from early Pleistocene to early Oligocene in age. Floras are moderately well preserved throughout the section with the exception of intervals of increased dissolution in the Miocene. Upper Miocene assemblages show marked deterioration as placcoliths become selectively dissolved. A barren interval occurs in Cores 110-671B-48X through -57X that may represent an upward excursion of the Miocene carbonate compensation depth (CCD).

Samples 110-671B-1H-1, 88–90 cm through -3H-3, 78–80 cm are placed within the early Pleistocene *Pseudoemiliania lacunosa*/small gephyrocapsa Zone of Gartner (1977) owing to the presence of *P. lacunosa* without the co-occurence of older markers. No upper Pleistocene section was observed in either Hole 671A or 671B. Samples 110-671B-3H-4, 78–80 cm through 5H-1, 80–82 cm are also early Pleistocene in age and are assigned to the *Calcidiscus macintyrei* Zone of Gartner (1977) occurs between Samples 110-671B-4H-3, 80–82 cm and -5H-1, 80–82 cm. *Helicosphaera sellii*, in the absence of *Calcidiscus macintyrei*, indicates the *Helicosphaera sellii* Zone between Samples 110-671B-3H-4, 78–80 cm and -4H-2, 80–82 cm. Gephyrocapsids are perhaps the most prolific forms encountered in the Pleistocene section. The abundance of this group is strongly affected by changes in dissolution and can be used as a reliable gage of overall sample preservation.

Rare specimens of *Discoaster brouweri* mark the top of the Pliocene in Sample 110-671B-5H-2, 80–82 cm. Samples 110-671B-5H-1, 80–82 cm through -10H-1,79–81 cm are assigned to the *Discoaster brouweri* Zone of Okada and Bukry (1980) that spans the entire upper Pliocene. This zone is divided into four subzones based on the last appearance datums of *D. brouweri, D. pentaradiatus, D. surculus*, and *D. tamalis*. Sediments in Cores 110-671B-5H through -10H-1, 79–81 cm are partitioned as follows:

110-671B-5H-1, 80–82 cm to -6H-1, 80–82 cm *Calcidiscus macintyrei* Subzone CN12d.

110-671B-6H-2, 80–82 cm to -6H-5, 80–82 cm *Discoaster pentaraditus* Subzone CN12c

110-671B-6H-6, 80–82 cm to -7H-2, 79–81 cm *Discoaster surculus* Subzone CN12b.

110-671B-7H-3, 79–81 cm to -10H-1, 79–81 cm *D. tamalis* Subzone CN12a.

Sphenolithus abies and *Reticulofenestra pseudoumbilica* are first encountered in Sample 110-671B-10H-2, 79–81 cm. These species mark the top of the early Pliocene *R. pseudoumbilica* Zone (CN11) of Okada and Bukry (1980).

The *Amaurolithus tricorniculatus* Zone (CN10) of Okada and Bukry (1980) is observed in Sections 110-671B-11X, CC through -12X, CC. Owing to the inconsistent occurrence of the marker species *Amaurolithus primus*, Subzone CN10c is recognized in Samples 110-671B-11X, CC through -12X-1, 80–82 cm by the presence of *Amaurolithus tricorniculatus* without *Ceratolithus acutus*. The LAD of *A. tricorniculatus* was observed to be a more reliable datum in this geographic location than *A. primus* (Bergen, 1984). The *Ceratolithus acutus* Subzone 10b occurs in Samples 673B-12X-2, 80–82 cm through -12X-5, 80–82 cm. The Miocene boundary is placed within the Sample interval 110-671B-12, CC because of an increase of *Triquetrorhabdulus rugosus* below the FAD of *Ceratolithus acutus*.

Discoaster quinqueramus is first noted in Section 110-671B-13X-1, 80–82 cm, where it exists concurrently with *Amaurolithus primus*. Samples 110-671B-13X-1, 80–82 cm through -14X-6, 74–76 cm are placed within the upper Miocene *A. primus* Subzone (CN9b) of Okada and Bukry (1980).

A major biostratigraphic inversion is noted in Core 110-671B-14X-6; yellow brown clay of Miocene age directly overlies lower Pleistocene green marl. This reversal of sedimentary sequence indicates that large-scale thrust faulting has occurred. The lower Pleistocene to upper Miocene section below the fault is thicker and more complete than the same interval in the upper part of the hole.

Sections 110-671B-14X, CC to -19X, CC belong to the *Pseudoemiliania lacunosa* Zone of early Pleistocene age. The co-occurrence of *Helicosphaera sellii* and *Calcidiscus macintyrei* indi-

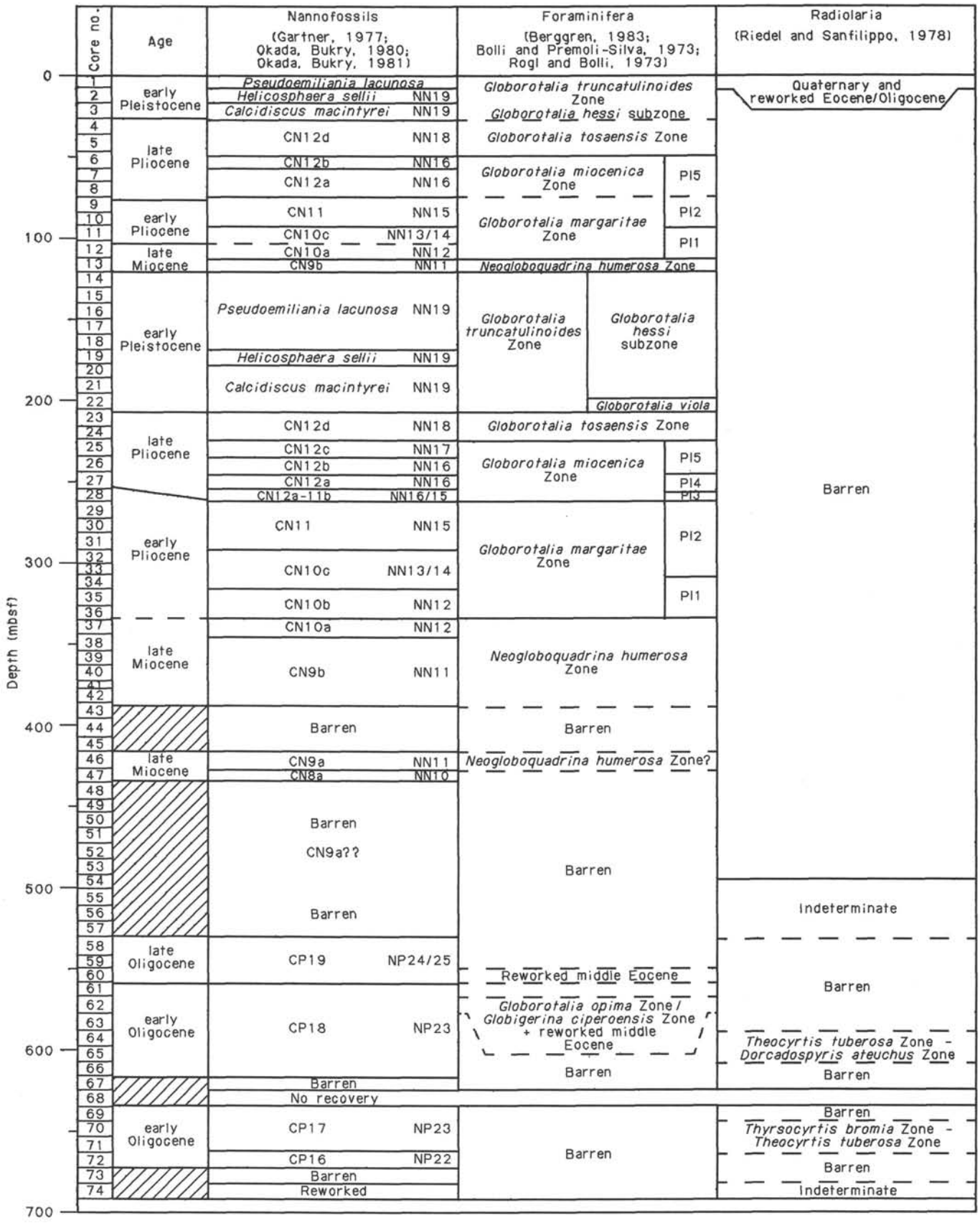

Figure 21. Hole 671B biostratigraphic summary.

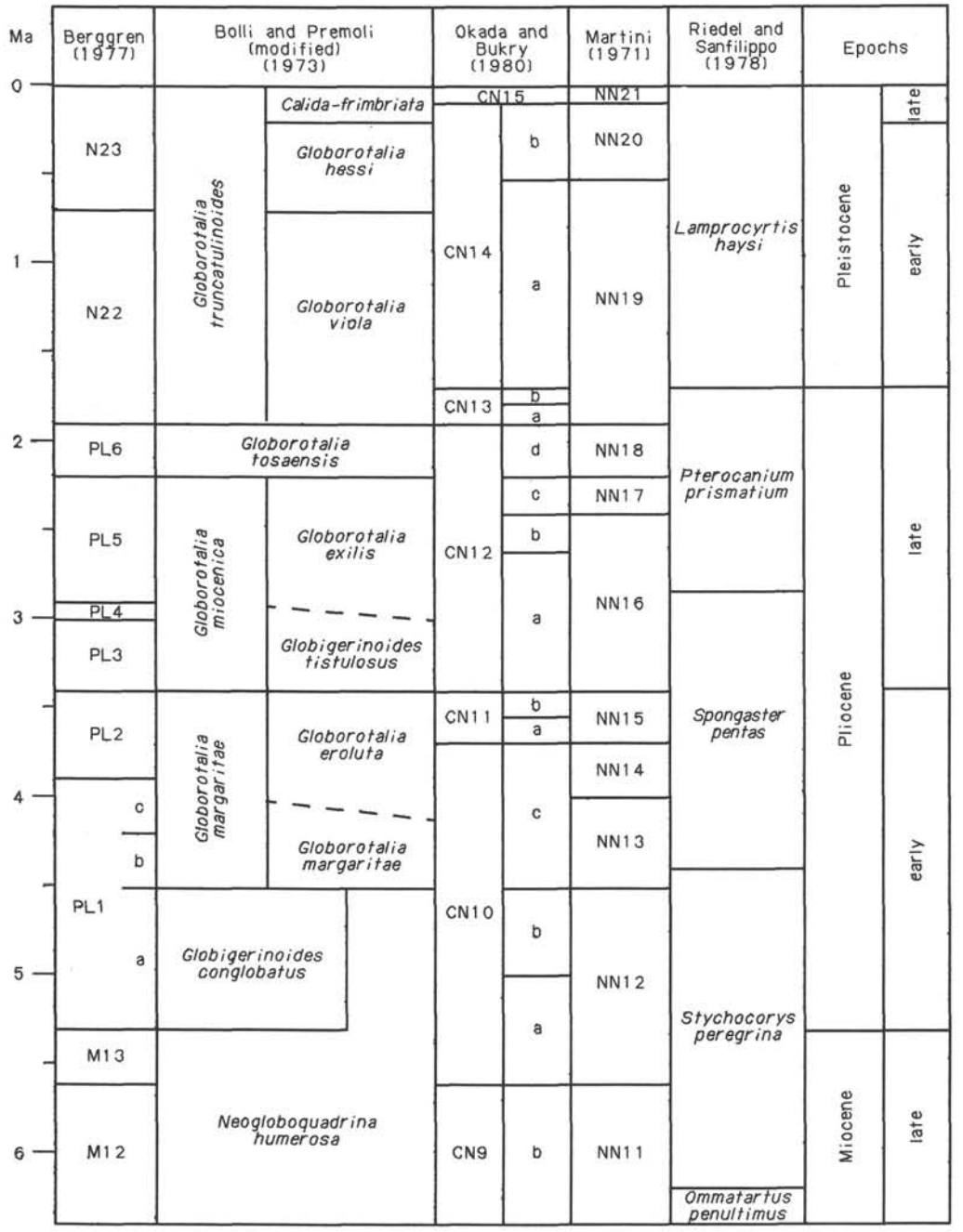

Figure 22. Upper Miocene through Pleistocene comparison between zonal schemes of foraminifers, nannofossils, and radiolarians. Nannofossils are zoned according to Gartner (1977) in the Pleistocene and Okada and Bukry (1980) in the Tertiary.

cates the *C. macintyrei* Zone of Gartner (1977) in Sample 110-671B-19X, CC. The *Helicosphaera Sellii* Zone of Gartner (1977) was not observed in the section.

Discoaster brouweri appears in Sample 110-671B-22X-3, 79–81 cm and signals the beginning of the Pliocene in the reversed section below the fault. Secondary reversals noted in Samples 110-671B-22X-3, 79–81 cm to -29X-3, 80–82 cm are partitioned between the upper Pliocene *D. brouweri* Zone of Okada and Bukry (1980) and the *Calcidiscus macintyrei* Zone of Gartner (1977) in the following manner:

110-671B-22X-3, 79–81 cm to -22X-6, 79–81 cm *Calcidiscus macintyrei* Subzone CN12d.

110-671B-22X, CC to 23X, CC *Calcidiscus macintyrei* Zone (Gartner, 1977).

110-671B-24X-1, 80–82 cm to -25X-1, 80–82 cm *Calcidiscus macintyrei* Subzone CN12d.

110-671B-25X-2, 80–82 cm to 25X, CC *Discoaster pentaradiatus* Subzone CN12c.

110-671B-26X-1, 79–81 cm to 26X, CC *D. surculus* Subzone CN12b.

110-671B-27X-1, 80–82 cm to 29X-3, 80–82 cm *D. tamalis* Subzone CN12a.

Section 110-671B-29X, CC is placed just within the lower Pliocene boundary. *Sphenolithus abies* and *Reticulofenestra*

pseudoumbilica are both present in Sections 110-671B-29X, CC through -33X, CC and indicate the top of the CN11 Zone of Okada and Bukry (1980).

Samples 110-671B-34X-1, 79–81 cm through 35X-6, 79–81 cm are placed within the CN10c Subzone of the *Amaurolithus Tricorniculatus* Zone (CN10) of Okada and Bukry (1980). Zone (CN10c) is designated by the LAD of *Amaurolithus tricorniculatus* above the LAD of *Ceratolithus acutus*.

Ceratolithus acutus occurs in Samples 110-671B-35X, CC and -37X-1, 79–81 cm and is the range marker for the *C. acutus* Zone CN10b.

The Pliocene/Miocene boundary is defined in Samples 110-671B-37X-2,79–81 cm through -37X, CC by the presence of *Triquetrorhabdulus rugosus* without *Ceratolithus acutus*.

The *Amaurolithus primus* Subzone of the *Discoaster quinqueramus* Zone occurs in Samples 110-671B-38X-1, 78–80 cm to -42X, CC. This zone is slightly expanded and may indicate the presence of a low-angle thrust fault in this part of the section. Below Section 110-671B-42X, CC, barren sediments are encountered which may be the result of increased levels of dissolution. Core 110-671B-46X contains nannofossils and is placed into the *Discoaster berggrenii* Subzone CN9a based on the disappearance of amauroliths from the assemblage. The last fossiliferous interval above the décollement contains *Discoaster neohamatus*. The presence of *D. hamatus* places Samples 110-671B-48X-1, 80–82 cm through 48X-6, 80–82 cm within the *D. hamatus* Zone (CN7) of Okada and Bukry (1980). Calcareous material in Core 110-671B-48X is fairly dissolved and few placcoliths remain in this interval. Below this point sediments are barren of carbonate microfossils until Core 110-671B-52X, where a small pocket of nannofossiliferous sediment is found. This sparce assemblage belongs to Subzone CN9a of the *D. quinqueramus* Zone. The younger age of this material represents weak evidence for another reverse thrust fault.

A long barren interval persists from Cores 110-671B-52X through -57X. The décollement is contained within this zone and could not be precisely dated owing to the dissolved nature of the sediments. Below the décollement zone a thick, upper Oligocene section was cored. Sections 110-671B-58X, CC to -60X, CC were assigned to the upper Oligocene *Sphenolithus ciperoensis* Zone (CP19) of Okada and Bukry (1980) because of the presence of the range marker *Sphenolithus ciperoensis*. Zone CP18/17 was not well differentiated below the FAD of *S. ciperoensis* in Samples 110-671B-61X-4 to -71X-4 owing to the persistence of rare *S. distentus* downhole.

No biostratigraphic information was discernable from Cores 110-671B-67X or -68X. The absence of *S. distentus* in Sample 110-671B-71X, CC designates the *S. predistentus* Zone (CP 17) of Okada and Bukry (1980). Core 110-671B-72X is placed into the lower Oligocene CP16b Subzone based on the presence of *Reticulofenestra umbilica* and *Coccolithus formasus*. Below Core 110-671B-72X, loose sand was encountered and the hole was abandoned.

Planktonic Foraminifers

The sediments drilled at Site 671 are rich in planktonic foraminifers from the lower Pliocene to the Pleistocene. Preservation is generally good, but dissolution has affected some samples and may have removed some species in the more dissolved intervals. Sediments belonging to the uppermost Miocene have been severely affected by dissolution and provided only scarce microfaunas of highly resistant species. The older sediments seem to have been deposited close to the CCD and are mostly barren of planktonic foraminifers. The biostratigraphic results given here are mainly based on core-catcher samples.

Sections 110-671A-1H, CC through -671B-3H, CC belong to the lower Pleistocene, *Globorotalia hessi* subzone of the *Globorotalia truncatulinoides* Zone (Bolli & Premoli-Silva, 1973). The assemblages are dominated by *G. truncatulinoides, G. hessi, G. crassaformis, Sphaeroidinella dehiscens, Pulleniatina obliquelo-culata, Neogloboquadrina dutertrei, Globigerinoides ruber, G. trilobus*, and *G. sacculifer*. The *Globorotalia menardii- G. tumida* complex is represented only in Sections 110-671A-1H, CC (which includes the subspecies *G. tumida flexuosa*) and 110-671B-3H, CC.

The Pleistocene/Pliocene boundary, as defined by the last downhole occurrence, i.e., first appearance datum (FAD) of *G. truncatulinoides* is between Sections 110-671B-3H, CC and -671B-4H, CC.

Sections 110-671B-4H, CC through -671B-7H, CC are assigned to the upper Pliocene. *Globorotalia tosaensis* is identified in Section 110-671B-4H, CC which thus belongs to the *G. tosaensis* Zone, equivalent to Zone PL6 (Berggren, 1977). The first down hole occurrence of *Globigerinoides extremus* was found in Section 110-671B-6H, CC. In the Caribbean, this species definitely became extinct in the upper part (*Globorotalia exilis* subzone) of the *Globorotalia miocenica* Zone, which is broadly equivalent to Berggren's Zone PL5. Based on this useful event, this section can be assigned to the *G. exilis* Subzone although the delicate thin-shelled zonal markers have been removed by dissolution. On the other hand, *G. exilis* and *G. miocenica* occur together in Section 110-671B-7H, CC, which belongs to the same biostratigraphic unit. The lower part of the *G. miocenica* Zone (*Globigerinoides fistulosus* Subzone) has not been identified but should be represented in Core 110-671B-8H.

The upper Pliocene/lower Pliocene boundary, as defined by the first downhole occurrence (i.e., last appearance datum, LAD) of *G. margaritae* is between Sections 110-671B-7H, CC and -671B-8H, CC. Sections 110-671B-8H, CC through -671B-10H, CC belong to the upper part of the *G. margaritae* zone (= PL 2). The assemblages are dominated by *Globorotalia multicamerata, G. limbata, G. crassaformis, Sphaeroidinellopsis sphaeroides, Globigerinoides extremus, G. ruber, Neogloboquadrina humerosa, Globoquadrina altispira. G. margaritae* is rare and the genus *Sphaeroidinella* (as *S. immatura*) becomes extinct in Section 110-671B-10H, CC.

The lower part of the *G. margaritae* zone (= PL1) is marked by the LAD of *Globigerina nepenthes*, which occurs in Section 110-671B-11X, CC.

Below this last sample depth, the dissolution increases rapidly, the foraminifers become sparse, and are represented only by resistant species, such as *Globigerina nepenthes, Globigerinoides conglobatus*, and *Sphaeroidinellopsis sphaeroides*.

The Pliocene/Miocene boundary is tentatively determined on the basis of the FAD of *Globigerinoides conglobatus*, the estimated age of which is 5.3 Ma (Berggren, Kent & Van Couvering, 1985). The absence of this resistant species in Section 110-671B-13X, CC is not considered here to be an artifact of dissolution.

At the level of Core 110-671B-13X, a major fault occurs, leading to a stratigraphic repetition. Sections 110-671B-14X, CC through 110-671B-21X, CC belong to the lower Pleistocene, *Globorotalia hessi* Subzone of the *G. truncatulinoides* Zone. Section 110-671B-22X, CC, which contains the first specimens of the *Globorotalia tosaensis* group (including *G. tenuitheka*) together with *G. truncatulinoides*, is assigned to the lowermost Pleistocene *Globorotalia viola* Subzone.

The Pleistocene/Pliocene boundary (FAD of *G. truncatulinoides*) is found between Sections 110-671B-22X, CC and -671B-23X, CC. Sections 110-671B-23X, CC and -671B-24X, CC, which yield common specimens of *G.* gr. *tosaensis* (including *G. tenuitheka*) and *G. viola* (including *G.* cf. *viola* of Bolli, 1970) belong to the uppermost Pliocene *Globorotalia tosaensis* Zone (PL6).

The *Globorotalia miocenica* Zone is identified from Section 110-671B-25X, CC (LADs of *G. miocenica* and *G. exilis*) through 110-671B-28, CC. Several planktonic foraminifer events occur within this interval: the LAD of *Globigerinoides extremus* in Section 110-671B-26X, CC shows that this sample and the previous one belong to the upper part of the Zone (PL5); LAD of *Globoquadrina altispira* in Section 110-671B-27X, CC determines the top of the lower part of the zone (PL4); LADs of *Globorotalia multicamerata* and *Sphaeroidinellopsis* ssp. in Section 110-671B-28X, CC indicate the lowermost part of the Zone (PL3).

Although the zonal marker is virtually absent, Sections 110-671B-29X, CC through -671B-36X, CC are assigned to the lower Pliocene *Globorotalia margaritae* Zone on the basis of occurrences of alternative markers, such as *Pulleniatina primalis* and *Globorotalia plesiotumida*. The LAD of *Globigerina nepenthes* in Section 110-671B-33X, CC provides the same bipartite subdivision of the zone as observed in the above tectonic unit. Section 110-671B-36X, CC contains *Globorotalia cibaoensis* and thus belongs to the lowermost part of Berggren's (1977) Subzone PL1a of the lower Pliocene.

Strong dissolution of foraminifer tests starts at the same stratigraphic level in tectonic package 3 as in the upper tectonic unit, i.e. near the Pliocene/Miocene boundary. Sections 110-671B-38X, CC through -671B-42X, CC are dated from the late Miocene on the basis of the downhole extinction of *Globigerinoides conglobatus*. Below this last core, the samples are mostly barren of foraminifers.

Core 110-671B-62X, however, contains scarce planktonic foraminifers belonging to the upper Oligocene *Globorotalia opima* Zone or *Globigerina ciperoensis* Zone: *Globigerina angulisuturalis, G. angustiumbilicata, G.* gr. *praebulloides, G. prasaepis, Globorotalia permicra*, occur in Sample 110-671B-62X-2, 38–40 cm. The core catcher from this same core yields a mixed microfauna including *Globigerina* gr. *ciperoensis, G.* gr. *eocaena, Globorotalia obesa, G. nana* (late Oligocene) and *Acarinina broedermanni, A. bullbrooki, Morozovella* cf. *spinulosa*, reworked from middle Eocene strata. Finally, very rare *Globorotalia* gr. *cerroazulensis* and *Truncorotaloides* sp. have been identified in Section 110-671B-60X, CC; they are considered here as reworked from the middle Eocene.

Radiolarians

Hole 671A

Radiolarians and sponge spicules are found in Section 110-671A-1X, CC. Sponge spicules are few and broken. Radiolarians are very rare. Some radiolarians with fine, thin skeletons are well preserved, and most of the others with stout ones are considerably dissolved. The former are common in the Quaternary, though none of them indicate age. In the latter, *Dictyoprora* (= *Theocampe*) *mongolfieri, Lithocyclia ocellus, Tristylospyris* sp., and such Eocene and/or Oligocene radiolarians are contained as reworked fossils.

Hole 671B

In Section 110-671B-1H, CC, few and broken radiolarians and sponge spicules are found. Cores 110-671B-2H through -671B-53X are barren of radiolarians. Radiolarians are rare in Cores 110-671B-54X and -55X, and few to common in Cores 110-671B-56X and -57X. The specimens found are conspicuously dissolved and slightly crystallized, and no speciation is possible.

Radiolarians do not occur in Cores 110-671B-58X through -63X, except in Sections 110-671B-60X, CC and -671B-62X, CC. In Section 110-671B-60X, CC, where the specimens are rare and poorly preserved, *Cyrtocapsella tetrapera* and *Cyrtocapsella* cf. *C. cornuta* are found. In Section 110-671B-62,CC, only four specimens (*Calocycletta* sp. and *Tholospyris* sp.) were found.

In Cores 110-671B-64X and -65X radiolarians are rare, and the specimens are opaque (replaced with pyrite(?)). Coexistence of *Tristylospyris triceros* and *Dorcadospyris* cf. *D. ateuchus* may assign these cores to the Oligocene *Theocyrtis tuberosa* Zone or *Dorcadospyris ateuchus* Zone (Riedel and Sanfilippo, 1978). Cores 110-671B-66X through -69X are barren of radiolarians.

In Cores 110-671B-70X and -71X, a few and opaque radiolarians are found. *T. triceros* alone is specified. *T. triceros* ranges from *Carpocanistrum azyx* Zone (Saunders *et al.*, 1984: = lower part of *Thyrsocyrtis bromia* Zone of Riedel and Sanfilippo (op. cit.)) to *D. ateuchus* Zone.

Cores 110-671B-72X and -73X are barren of radiolarians. In Core 110-671B-74X, radiolarians are common and very poorly preserved (considerably dissolved), and no conclusions are drawn from these specimens.

Ichthyoliths are found throughout the cores from Hole 671B, and they are common in Cores 110-671B-58X through -73X.

Hole 671C

Core 110-671C-1X contains abundant and poorly to moderately preserved radiolarians. Radiolarians are present in Core 110-671C-2X but in a considerably dissolved state.

Samples 110-671C-1X-1, 64–66 cm through -671C-1X-5, 99–100 cm are assigned to the *Stichocorys wolffii* Zone. *Calocycletta virginis, Carpocanopsis cingulata, Cyrtocapsella cornuta, Cyrtocapsella tetrapera, Lychnocanoma elongata, Stichocorys delmontensis* and *Stichocorys wolffii* occur throughout the samples, and *Calocycletta costata* and *Siphostichoartus* (= *Phormostichoartus*) *corona* are not found.

Samples 110-671C-1X-5, 132–133 cm through 110-671C-1X, CC, 29–30 cm are assigned to the *Cyrtocapsella tetrapera* Zone, owing to the appearance of *C. tetrapera, C. cornuta* and *Dorcadospyris ateuchus*, and the disappearance of *C. costata, S. wolffii* and *S. delmontensis*.

The *Stichocorys delmontensis* Zone, which is defined between the *C. tetrapera* and *S. wolffii* Zones, was not detected.

PALEOMAGNETICS

Paleomagnetic measurements on samples from accretionary prisms provide several problems not encountered with normal paleomagnetic measurements in undisturbed marine sediments. These problems are a result of tectonic disturbance that may reset the primary magnetization to one acquired at the time of deformation, and tilt the bedding so that a correction has to be applied to the remanence measurements to determine the polarity stratigraphy. Previous paleomagnetic measurements from areas of active deformation have generally been restricted to parts of core where bedding is visible and so provide the necessary information to perform the correction for tilt (Niitsuma, 1981; Gose, 1982; Wilson, 1984). This approach is limited by the availability of bedding planes in areas of core showing no drilling deformation. Magnetic fabric measurements provide a way of defining the bedding plane that is independent of whether any bedding is visible or not. The measurement of magnetic fabric is performed on the same sample that is used for remanence measurement so that the two can be uniquely related. From these two measurements the true bedding dips at a large number of points and the directions of these dips relative to present day north, can be defined.

This information can then be used as a constraint on the structural model of the accretionary prism. The magnetic fabric measurements may also indicate the degree to which tectonism has disturbed the sedimentary grain fabric. These measurements

from Leg 110 will provide the first magnetic fabric measurements of sediments undergoing initial tectonic deformation.

The principal objectives of paleomagnetic measurements on samples from Hole 671B and, more generally, Leg 110 are to: (a) provide a magnetostratigraphy to compliment the biostratigraphy; (b) determine geographic orientation information for piston cores and drilling biscuits from XCB cores to orient structural features; (c) measure the ash stratigraphy by means of whole-core susceptibility measurements and hence provide a means of detailed stratigraphic correlations between cores. The magnetic fabric measurements will be performed after the cruise, in laboratories at Sheffield and Southampton in England.

Remanence Measurements

The methodology of sampling and remanence measurements are outlined in Chapter 1, this volume. In the piston-cored section (Cores 110-671B-1H to -671B-10H) samples were preferentially taken from the more ash-rich horizons, whereas in the XCB-cored section (110-671B-11X to -671B-73X) samples were taken in undisturbed drilling biscuits with no preference for lithology.

Results

The natural remanent magnetization (NRM) intensity and inclination of all samples is shown in Figure 23. The NRM inclination of most samples to 350 mbsf is positive, reflecting a downward-directed, drilling-induced remanence (Fig. 23). This effect largely dominates the remanence of these samples, typically comprising over 70% of the NRM intensity. The samples with NRM intensities above 10mA/m have comparatively low coercivities with median destructive fields of typically 5 mT. The low coercivity nature of these samples created problems with demagnetization at fields much above 40 mT, resulting in erratic directional movement and increases in intensity. This type of behavior is thought to be a result of the acquisition of spurious magnetizations in the demagnetizer. Sample behavior during demagnetization generally consists of four types of responses:

1. Consistent directional movement between the NRM direction and a high-coercivity component indicating strongly overlapping coercivites of these two components. The stable endpoint is generally reached by about 35 mT, although samples may not reach a stable direction, just show an increase in scatter at larger demagnetization fields. These samples frequently have strongly curved magnetization paths on a Zijderveld diagram which may not show convergence to the origin on the last demagnetization steps. The primary component of this type of sample was determined either by averaging at least two datum points or, if the sample had not reached a stable endpoint, by selecting the projected end of the demagnetization path swept out by the datum points on a stereonet (Figs. 24 and 25).
2. The stable endpoint is reached after removal of the drilling remanence by 5 to 15 mT and the sample then shows no appreciable consistent directional movement up to fields of 50 mT, just an increase in scatter. The primary component is determined by averaging the points at the stable endpoint, or if the Zijderveld plot was linear a least-squares line was fitted to it and this measurement used (Fig. 26).
3. Little directional movement from the NRM direction, just an increase in scatter (Fig. 27). This type of sample behavior may be indicative of a primary component that is not appreciably different from the NRM direction.
4. Erratic directional movements, possibly as a result of spurious magnetization acquisition at low demagnetization fields (Fig. 28). Alternatively, these samples may be displaying large directional responses to demagnetization that could not be assertained because of the large demagnetization steps used.

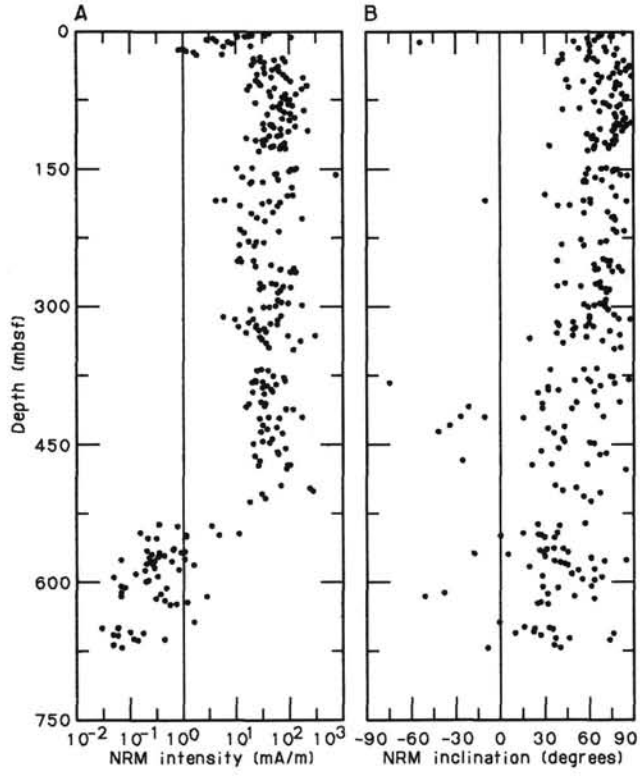

Figure 23. NRM intensity (A) and inclination data (B) from Site 671 sediments.

In addition, a number of samples below a depth of 500 mbsf have low NRM intensities, which make these samples infeasible to demagnetize. A high proportion of the samples to a depth of 500 mbsf have demagnetization behavior types 1 and 2. Demagnetization behavior 3 is fairly typical of samples below about 500 mbsf.

Normal and reversed intervals within the same APC core should be indicated by opposite inclinations and declinations. This is not the case for many of the samples from Cores 110-671B-1H to -671B-10H, which may show opposite inclinations but the same relative declination. This type of behavior is considered to result from both reversed and normal components being present, with completely overlapping coercivities, so that the resulting stable end point may not be indicative of the primary component at the time of deposition. However, the inclination is approximately the expected 28° for the latitude of Site 671. Bleil (1985) noted similar behavior in northwest Pacific calcareous oozes and attributed it to an "artificial overprinting." However, with these reservations in mind, the geographic orientation of the double line on core liners for Cores 110-671B-1H to -671B-10H is indicated in Table 4, along with a reliability estimate.

The inclination of the primary component in samples to a depth of 100 mbsf is reasonably close to the predicted inclination, and a reversal stratigraphy has been drawn (Fig. 29). Although the polarity boundaries are poorly defined, and there are several anomalous samples, there is general agreement of the reversal stratigraphy with the polarity chrons. In the section of the hole between 100 and 200 mbsf, the inclinations are scattered, with many inclinations greater than 40°. Many samples are not sufficiently stable to determine a primary component.

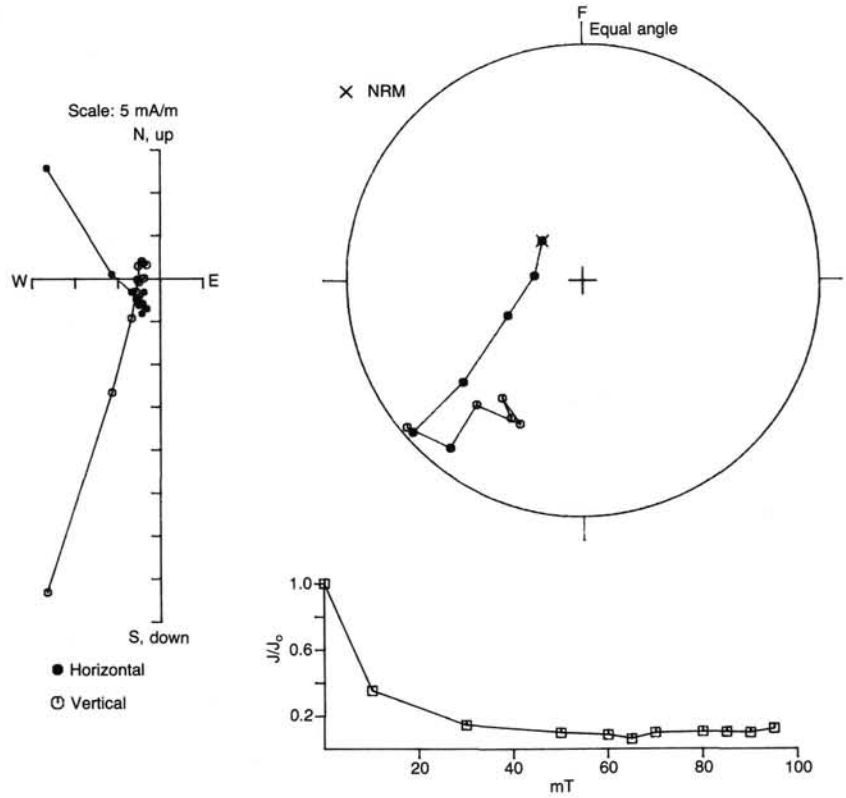

Figure 24. The directions represented on the following diagrams are with reference to the sample fiducial (F or N). A Zijderveld diagram, equal-angle stereographic projection and normalized intensity (NRM intensity/demagnetization step intensity, J/J_o) plot for Section 110-671B-13X-2, 120 cm is shown. The Zijderveld diagram represents the measured magnetic vector (both intensity and direction) in two planes, which share a common axis that is horizontal (in this diagram this common axis is E–W). The movement of the magnetic vector is projected onto the horizontal plane (N, E, S, W) and the vertical plane containing up (upcore), E, down (downcore) and W. The scale represents the magnitude of intensity between two ticks on the axes. A line connects consecutive demagnetization steps, where the NRM measurement is usually of the highest intensity. In the stereographic projection the open symbols are negative inclinations (corresponding to an upward-directed component), and filled symbols are positive inclinations (downward directed). This diagram represents the directional movement of the magnetic vector during demagnetization steps, where the NRM measurement is marked with a cross. This sample displays progressive movement in the stereonet along a planar path (the movement of the magnetic vector in three-dimensional space defines a plane) indicating that this sample has at least two overlapping magnetic components. The sample appears to reach a negative-inclination stable end point.

Some of the scatter is undoubtedly owing to tectonic tilting. The section below 250 mbsf has many more samples with stable behavior and may yield a reversal stratigraphy when these have been corrected for tectonic tilt.

The magnetic behavior of samples from Site 671 is quite unlike that reported by Wilson (1984) from the nearby Site 541. The samples reported here have much larger intensities, generally above 10 mA/m, compared to values below 10 mA/m reported by Wilson. Samples from Site 541 did not show the large drilling-induced remanence, which may be in part owing to the rotary drilling used on Site 541 or the different drill string. Otherwise, the generally poor-quality magnetic record noted at Site 541 does appear to be present in these samples, although when the tectonic tilt correction has been applied the interpretation of the record may become clearer.

Magnetic Susceptibility

Methods used in the whole-core susceptibility measurements are outlined in Chapter 1. Five-centimeter measurement spacing was generally used in the piston cores, whereas 10 cm was used in the XCB-cored interval.

Results

The peaks in susceptibility values in the Pleistocene to upper Miocene section are a result of the ash beds and marls with a high ash content. However, some of the ash beds that are dominated by crystal fragments do not necessarily give a larger susceptibility than the surrounding lithology, and rarely some ash beds give a lower reading. The higher readings in the ash beds are thought to be largely owing to the presence of titanomagnetite, pyroxene, and hornblende. The section from 0 to 128 mbsf shows a broad low that is matched in equivalent age sediments from 128 to 380 mbsf. Below 500 mbsf there is a dramatic change, a drop in susceptibility, that corresponds closely to the position of the décollement. In the Oligocene section the fluctuations in susceptibility are approximately related to lithology, the more calcareous parts showing a lower susceptibility. These two distinct susceptibility units (from 0 to 500 mbsf, and 500 to

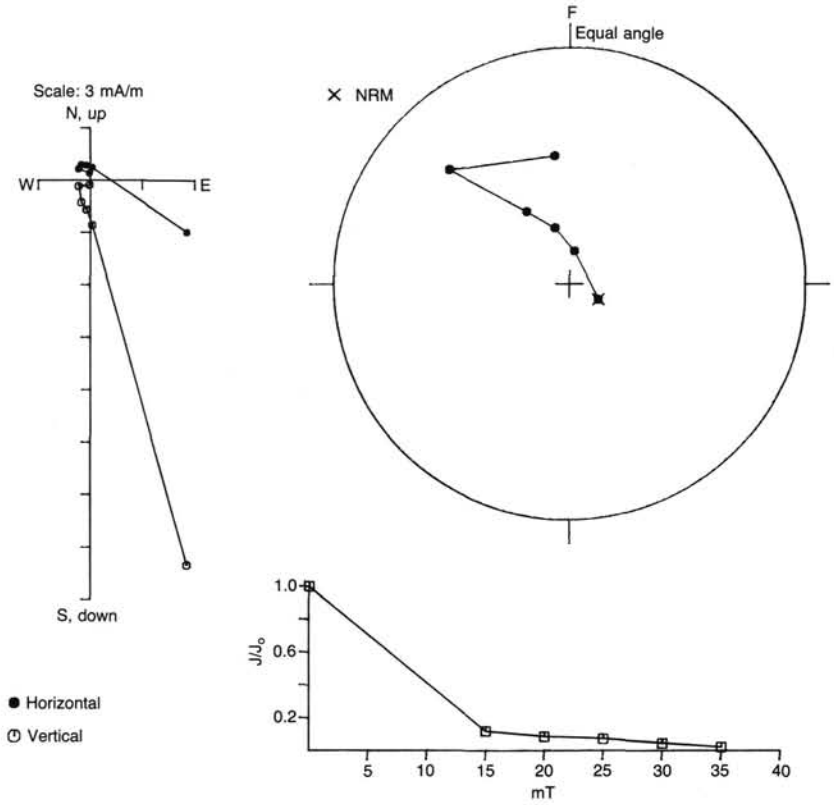

Figure 25. Demagnetization data for Section 110-671B-28X-2, 98 cm. This section shows no well-defined stable end point, which is seen on the Zijderveld plot by the strongly curved paths which do not converge on the origin. The last measurement at 35 mT shows considerable divergence from the demagnetization path shown by the other points, probably as a result of acquisition of spurious magnetizations.

670 mbsf) correspond to the coarse fraction divisions (Lithostratigraphy, this chapter) and a change from an igneous source (volcanic ash) in the Pleistocene–Miocene to a metamorphic source in the Oligocene (clastics from South America), with a corresponding change in the abundance of types of magnetic minerals.

A correlation was attempted between the susceptibility fluctuations in the repeated Pleistocene-Pliocene sections (Fig. 30). The obvious correlations between these repeated sections are the two peaks in susceptibility at 97 and 299 mbsf (Fig. 30) which are in nannofossil Zone 10c. A correlation between Cores 110-671B-7H to -671B-11X and 110-671B-27X to -671B-32X is shown in Figure 31. The correlations are complicated by the missing core material, the different coring processes, the steep bedding dips in Cores 110-671B-29X to -671B-32X, and the assignment of partially recovered cores to the top of the cored interval, when they correspond more closely to the bottom of the cored interval. A correlation between the Pleistocene and upper Pliocene sections was attempted without success. There is a good correlation between Cores 110-671B-1H and -671A-1H (Fig. 32).

GEOCHEMISTRY

Introduction

A major aim of the geochemistry program at Site 671 was to study the chemical composition of the pore waters. Studies on samples collected above the zone of décollement during Leg 78A of the Deep Sea Drilling Project (Gieskes et al., 1984) have indicated that alteration reactions involving volcanic matter have a pronounced effect on the composition of the interstitial waters. This is particularly evident from the pore-water $^{87}Sr/^{86}Sr$ ratio. This ratio is substantially less than that of contemporaneous seawater, as is also evident from the data reproduced in Figure 33. In addition, dissolved calcium increases directly below the sediment-seawater interface, even in the presence of sulfate reduction. In the absence of ash alteration, sulfate reduction leads to substantial increases in alkalinity, precipitation of calcium carbonate, and decreased dissolved calcium concentration (Gieskes, 1983). Concentrations of magnesium and potassium decrease with depth below seafloor in Leg 78 samples, again as a result of uptake in clay minerals produced during the alteration of volcanic matter. Unfortunately, during DSDP Leg 78A no hole penetrated below the zone of décollement. A major goal of ODP Leg 110 was to penetrate through the décollement zone. This was achieved at Site 671.

Interstitial Water

Methods

Interstitial water methodologies are essentially the same as those described by Gieskes and Peretsman (1986). Samples were obtained at frequent intervals to follow any changes with depth in interstitial water constituents in as great detail as possible.

Chloride determinations were also carried out by means of a potentiometric titration. The Gran method was used to evaluate the equivalence volume (Jagner and Aren, 1970).

Carbonate was determined by the standard shipboard Coulometric method, which yields accurate results to about 1%.

Dissolved gas concentrations were determined from head space samples after equilibration with He-degassed seawater. This sam-

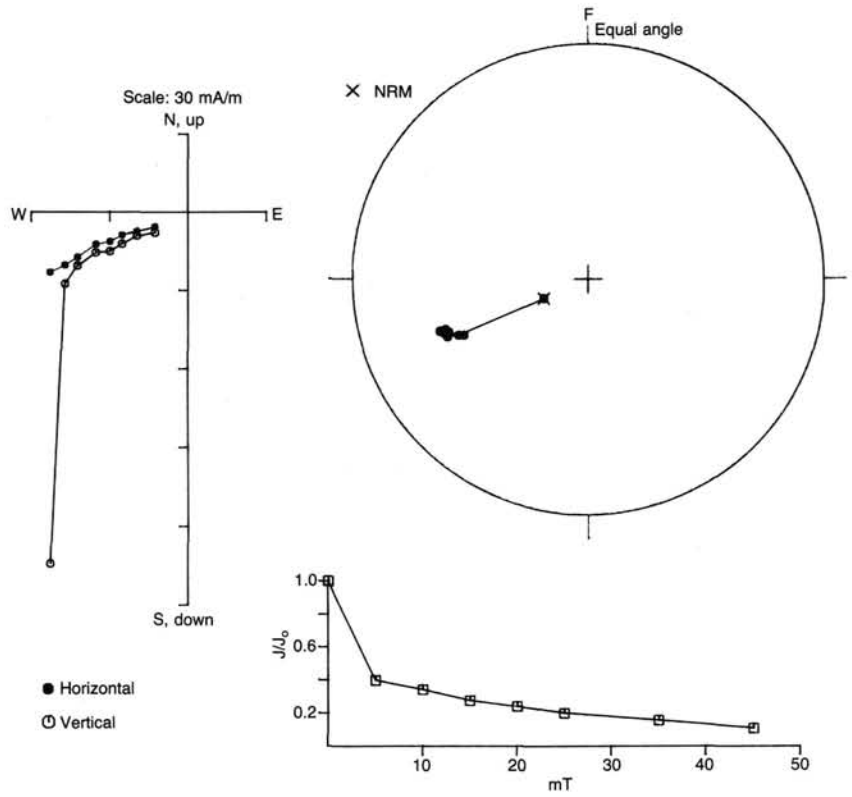

Figure 26. Demagnetization data for Section 110-671B-1H-3, 94 cm. This section shows removal of a steeply dipping positive component on the first 5-mT step, after which the section indicates an essentially stable component, with nearly linear convergence to the origin in the Zijderveld diagram.

pling method has been improved recently during an expedition to the Atlantis-2 deep (Blanc et al., 1986).

Results

The results obtained on the composition of the interstitial waters are presented in Table 5. Other analyses will be carried out in shore-based laboratories (e.g., Sr, $^{87}Sr/^{86}Sr$, Mn, trace metals, oxygen, and hydrogen isotopes). The shipboard data are also presented in Figure 34.

Chloride

In most open ocean drill sites, dissolved chloride concentrations are nearly constant with depth, which reflects the relatively small variations in the dissolved chloride concentrations of the world ocean during the last few hundreds of million years. However, the concentration-depth profile of dissolved chloride at Hole 671B (Fig. 34) shows a very distinct minimum in the décollement zone at 505 mbsf. Both above and below the décollement, gradients of gradually increasing chloride concentrations occur, with the upward gradient extending over 200 m. This gradient pattern in the accreted sequence is an important observation. If this low-chloride water in the décollement originates by the dewatering of the underthrust sediments, then this dewatering process appears to be accompanied by membrane filtration or at least some phenomenon involving ion exclusion, in which ions are retained preferentially in the formation and relatively fresh water is released. These processes have also been invoked to explain observed low salinities in overpressurized zones sandwiched between sediment layers containing oil field brines (Fertl, 1976; Hanshaw and Coplen, 1973; Fritz and Marine, 1983; Marine and Fritz, 1981).

Injections of low chloride concentrations into the décollement zone must have occurred at least as early as 1 to 1.5 Ma based on the observed chloride gradient (extending over 200 m) and assuming a diffusion coefficient of 5.0×10^{-6} cm^2/s (diffusive path length about equal to $(2Dt)^{1/2}$, where D = diffusion coefficient and t = time). Presumably these injections have been frequent enough to maintain low chloride concentrations over a fairly narrow range of the sediment column.

The chloride gradient below the décollement is about three times stronger than that above the décollement. This gradient difference may be the result of lower diffusion coefficients in the less porous deeper clays. Data on dissolved magnesium and calcium (see below) rule out the importance of upward advection.

The substantially lower chloride concentrations in Cores 110-671B-73X and -671B-74X are intriguing. The underlying sand layers may act as additional aquifers in the dewatering process. This dewatering process may also be episodic, with the expulsed waters varying in composition, as is suggested by the gradients in calcium and magnesium.

Calcium and Magnesium

The concentration-depth profiles of Ca and Mg are complex (Fig. 34). For this reason we discuss the observations over various depth intervals. In the upper 450 m of sediment, and especially in the upper 125 m, increases in Ca and decreases in Mg can be related to the *in-situ* alteration of volcanic matter. Volcanic components and ash layers are plentiful in these sediments (see Lithostratigraphy section, this chapter). The profiles, especially in the upper 125 m, are similar to those at Site 541 (Gieskes et al., 1984). The increase in Ca at Site 541 is greater in the upper part of the hole, presumably because the substantially

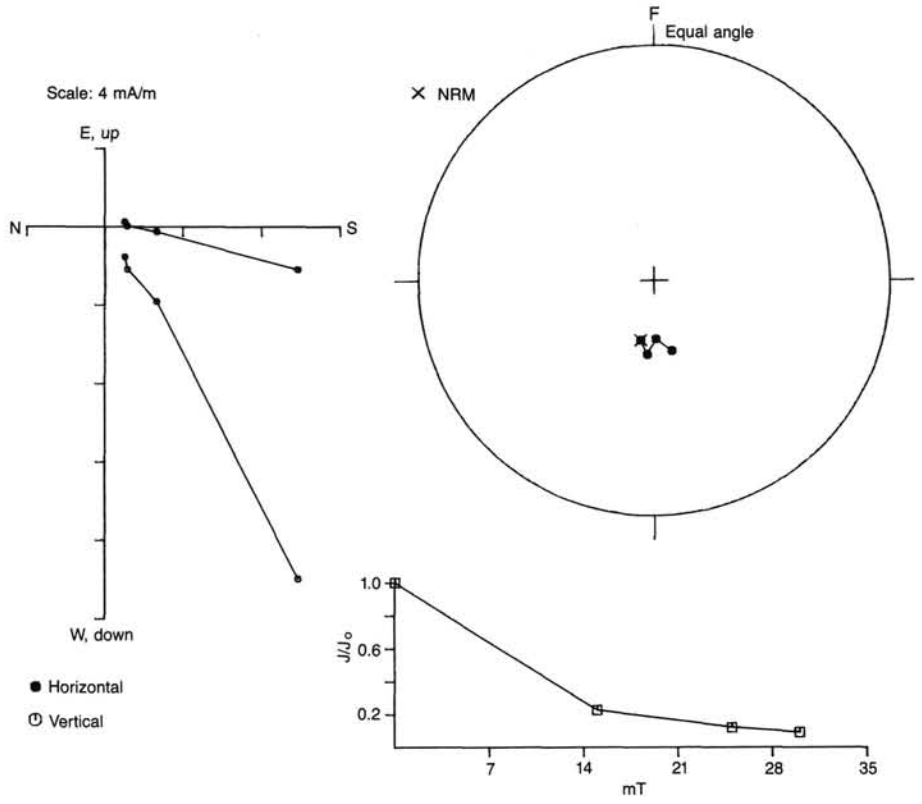

Figure 27. Demagnetization data for Section 110-671B-34X-5H, 17 cm. This section shows essentially one component, with perhaps some indication of a second component by the slight planar movement in the stereo-projection.

higher Pleistocene sedimentation rate at Site 541 decreases the loss of Ca by diffusion into the overlying ocean. One could argue that the increase in Ca may be caused by the dissolution of calcium carbonate; however, no significant increases in alkalinity are observed (Table 5) and, indeed, with an almost constant pH, the content of CO_2 also remains low. We suggest that the increase in Ca is caused by the release of Ca by alteration of volcanic matter.

The Ca and Mg concentration profiles reverse below 125 mbsf, at the first major thrust fault drilled in Hole 671B. We postulate that the Pleistocene sediments penetrated below 125 mbsf had lower Ca and higher Mg concentrations at the time of emplacement. The emplacement of tectonic package 3 occurred recently enough to prevent the reestablishment of a normal, smooth concentration gradient by diffusive exchange. With a formation factor of about 4 (see Physical Properties section) we expect the diffusion coefficient of dissolved Ca, D, to be about 2.0×10^{-6} cm^2/s. Using this diffusion coefficient we can estimate the diffusive path length for different time intervals. If the calculated pathlengths are less than the range over which the concentration anomaly persists, it can be concluded that steady state has not been reached. The results of this calculation are given below.

Time Interval	Diffusive Pathlength
t = 100,000 yr	$(2Dt)^{1/2}$ = 35 m
200,000	50
300,000	60
500,000	78
1,000,000	110
5,000,000	245

Thus, if emplacement of tectonic package 3 occurred less than 1 Ma ($(2Dt)^{1/2} \leq 110$ m), the observed concentration-depth profiles would be transient. The calculations ignore reaction, and the diffusive path length estimates above can be reduced since alteration reactions involving volcanic ash do tend to increase Ca and to reduce Mg. Another fault, perhaps marking the lower boundary of the underthrust sediment section, may occur between 320 and 380 mbsf. The low Cl concentration at about 325 mbsf may be related to this fault.

Dissolved Ca concentrations below 375 mbsf closely match those in the deeper parts of Site 541 (Fig. 33), but the Mg concentrations in Site 541 are somewhat lower than at Site 671. Unfortunately, Site 541 did not penetrate through the décollement so that the reversal in the Mg concentration gradient observed at Site 671 was not seen at Site 541.

A maximum in the Mg concentration occurs approximately 20 m below the décollement zone. We suggest that this, in part, is a remnant of a concentration depth profile that existed in the subducting slab about 1 Ma, i.e., prior to its subduction. This will indeed be shown to be the case for Site 672. The rapid increase in dissolved calcium and the decrease in magnesium is then owing to exchange between sediments and basement rocks, as has been described for other geologic settings (Gieskes and Johnston, 1984). This exchange, limited to depths below the décollement, is constrained by the reduced porosities and thus lower diffusivities of the subducted sediments, and by a boundary condition maintained by periodic water advection along the décollement. Whereas Mg diffuses across the décollement zone along a sharp gradient, calcium does not show any signs of diffusion across this zone, notwithstanding the steep concentration gradient below it. We suggest that replacement of waters in the

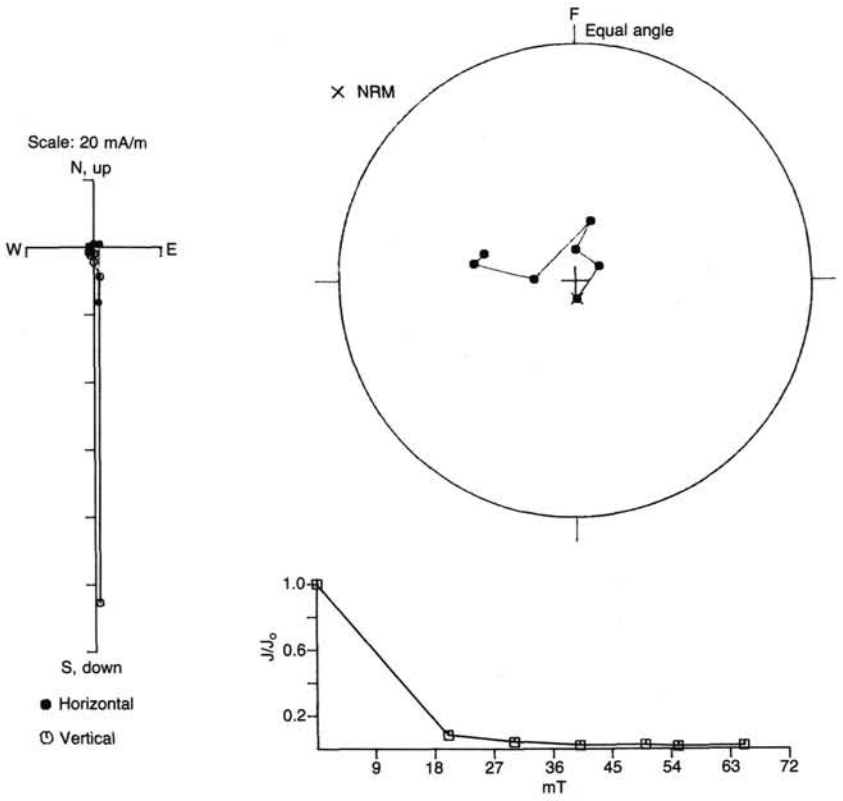

Figure 28. Demagnetization data for Section 110-671B-9H-6, 27 cm. This section shows removal of the vertical positive component on the first step after which there is rather erratic movement, perhaps indicating further unresolved components.

Table 4. Paleomagnetically determined orientation of piston cores from Hole 671B. Reliability estimates are as follows: 1 = consistent orientation from samples; 2 = declinations less consistent and dominantly do not flip over at inclination changes, the orientation estimate being based on dominant inclination; 3 = declinations scattered.

Core number 110-671B-	Orientation (degrees)	Reliability estimate
1H	120	1
2H	100	1
3H	110	2
4H	080	2
5H	230	1
6H	080	2
7H	210	2
8H	057 (or 237)	2
9H	180	3
10H	067	3

décollement must occur at least every 50,000 yr $(2Dt)^{1/2} = 12$ m, with $D = 1.0 \times 10^{-6}$ cm^2/s.

The shape of the calcium and magnesium concentration depth profiles below the décollement suggests that diffusive processes characterize the gradients. Any advection would cause a noticeable curvature in the concentration gradients. Thus, if upward advection does occur below the décollement, it must be slow enough for diffusive processes to dominate.

A complex set of processes effects the distributions of Ca and Mg at Site 671. If a geochemical steady state exists within these sediments the concentration depth profiles, particularly below the décollement, will change from the open ocean side (Site 672) towards the west, as the accretionary prism thickens and the subducted sediments get older.

Future studies of the oxygen and hydrogen isotopic composition of the interstitial waters and of the $^{87}Sr/^{86}Sr$ ratio of the dissolved Sr will help unravel the causes of the observed concentration changes of Ca and Mg.

Sodium and Potassium

We have no shipboard estimates of dissolved K, but we have been able to estimate the sum of the K and Na concentrations from charge balance considerations (Fig. 34).

Often, when concentration changes in Ca exceed those of Mg, depletions in Na are observed. These depletions usually have been related to processes involving the alteration of basalts (McDuff, 1981; Gieskes, 1983).

The (Na + K) concentration profile at Site 671 undergoes some subtle changes in the upper 300 m, probably related to decreases in K (cf., Site 541, Fig. 33). Below 300 m, however, a rapid decrease in Na occurs, with a slight minimum in the zone of décollement. The main sink for Na appears to be located below the drilled sections, a feature also observed in the (Na + K)/Cl profiles. This is consistent with the idea that the main sink for Na in the underlying basalts.

The Na minimum in the décollement is of some interest. Although the higher Na concentrations below the décollement may be an older, inherited signal (similar to the one postulated for Mg), the décollement minimum may also be transient, i.e., it

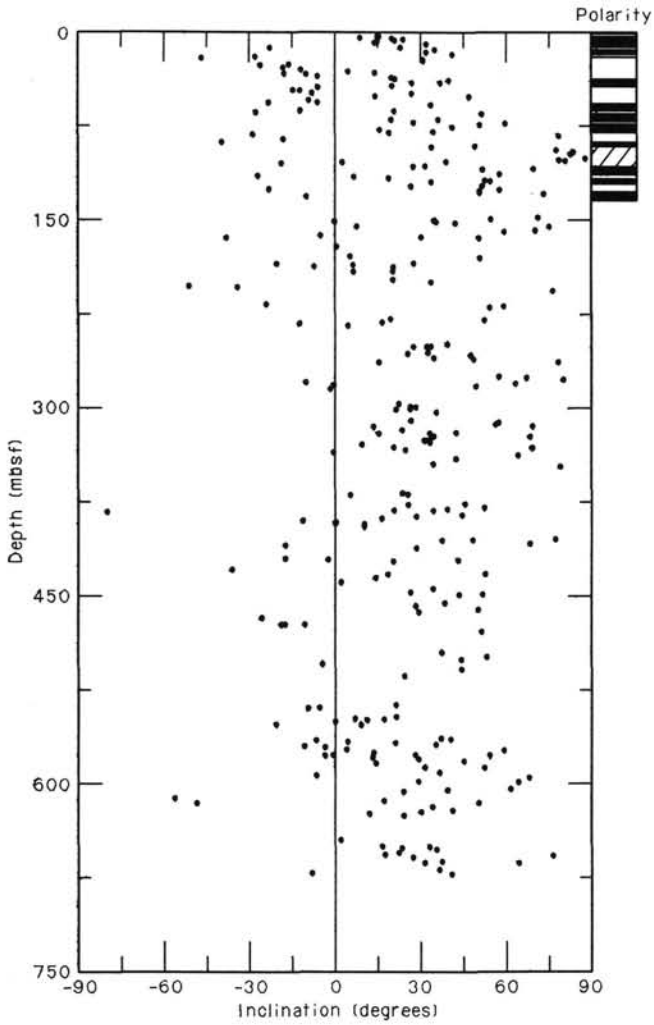

Figure 29. The high-coercivity component inclinations for the upper part of Hole 671B, with the suggested polarity events indicated. Black is normal polarity, white is reversed polarity, and hatched is indeterminate.

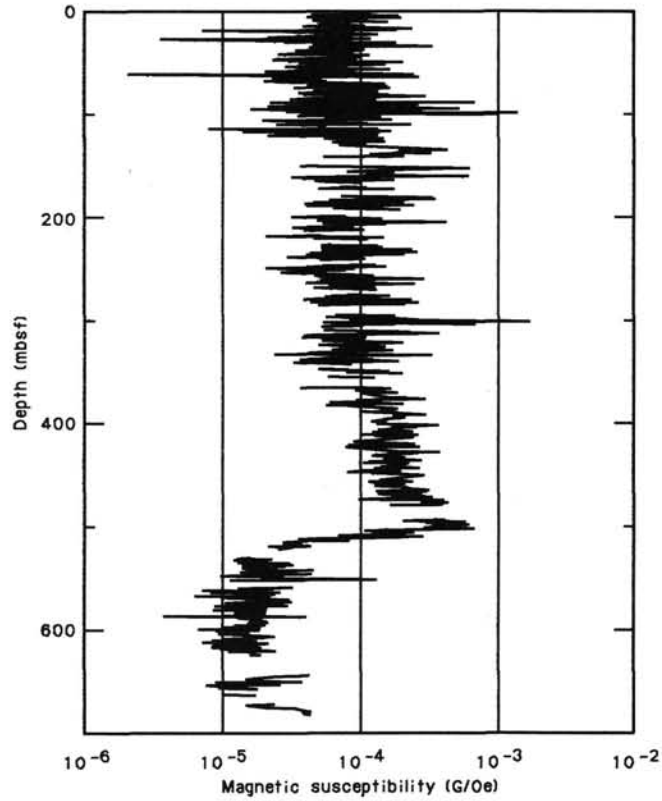

Figure 30. Downhole susceptibility plot for Hole 671B.

will disappear periodically, thus allowing a continuous drop in Na below 300 mbsf. We speculate that when the fresher advected waters intrude into the décollement, the minimum will last only for a limited time, and diffusion from above and below will tend to eliminate this minimum.

Sulfate and Ammonia

The concentration depth profile of dissolved sulfate (Fig. 34) reveals a clearly established minimum at about 150 mbsf. Such minima are often observed in situations where recent sedimentation rates and associated higher organic carbon contents have been greater than those in earlier time epochs (Gieskes, 1983). However, we suggest that the tectonic emplacement of surface sediments below the fault at 125 mbsf resulted in the burial of more reactive organic carbon, thus causing enhanced sulfate reduction. Sulfate reduction continues to be important below the décollement zone.

The dissolved ammonia profile is essentially a mirror image of the sulfate profile (Fig. 34), with the exception of a fairly high amount of ammonia at 125 mbsf, i.e., associated with the upper fault. Why more bacterial activity should be associated with this zone is not clear, unless the top of the Pleistocene section was indeed close to the sediment surface prior to its movement. The dissolved silica data discussed below support this concept.

Silica

Dissolved silica concentrations (Fig. 34) generally range between 200 and 300 μmol/L, which is expected in sediment with little or no biogenic silica. No interpretation of the absolute concentrations can be made, particularly in view of the "temperature of squeezing effect" (Gieskes, 1973; 1974). However, relative silica concentration changes can indicate mineralogical changes.

Noticeable changes in the silica concentrations occur in the upper 20 m, and are also repeated in the sediment section directly below the fault at 125 mbsf. We postulate that the enhanced silica concentrations reflect higher plagioclase contents in these sediments (see Lithostratigraphy, this chapter).

Another important feature is the large increase in dissolved silica in the décollement zone. The cause for this localized silica concentration is not clear. The presence of radiolarians in the décollement zone is rare, yet in the underlying sediments which do contain radiolarians, silica concentrations remain low. A combination of silica dissolution and precipitation as well as clinoptilolite formation may cause these increased silica values. Just above the basal sands at Hole 671B, higher silica values again occur.

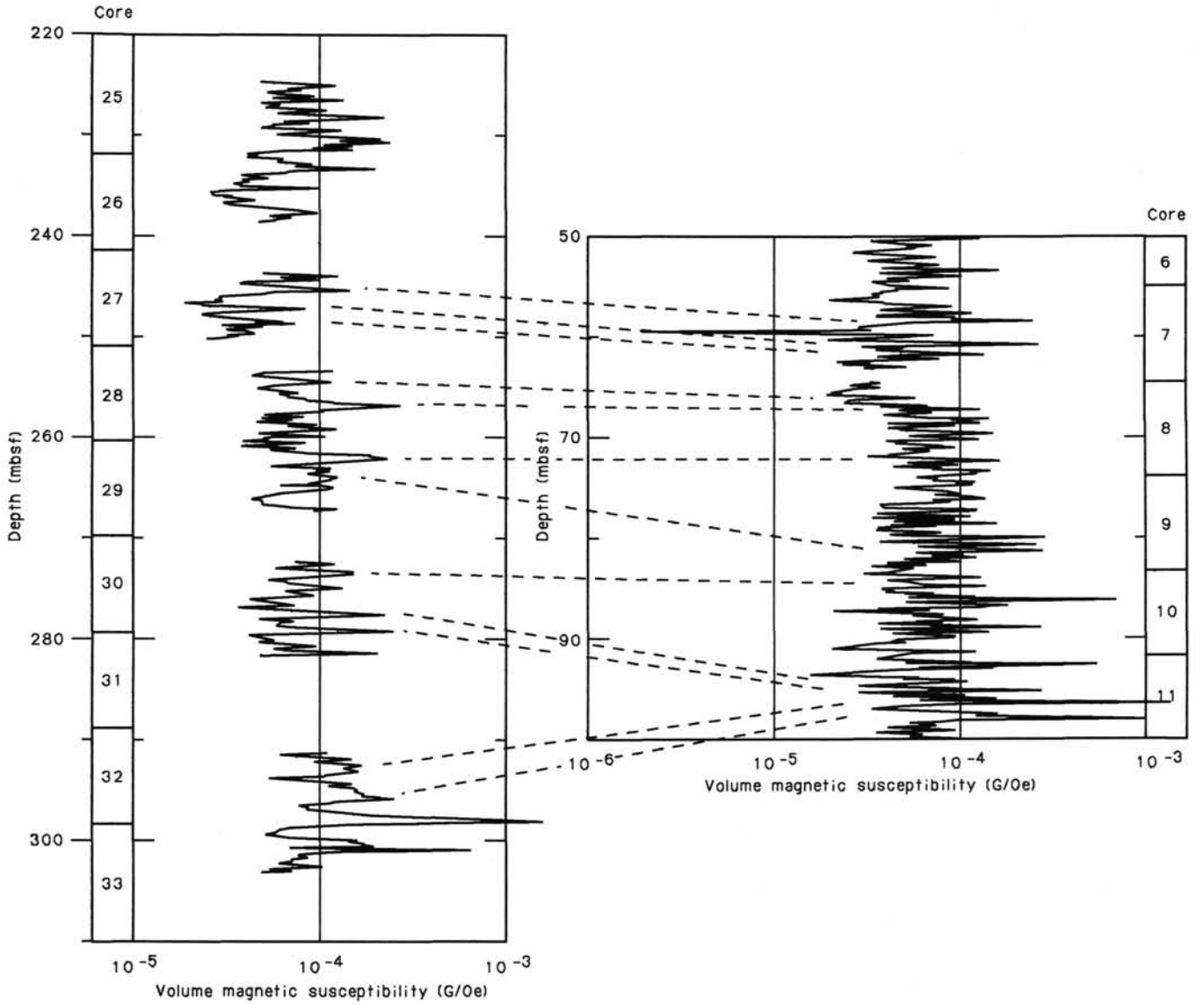

Figure 31. Susceptibility log correlations between Cores 110-671B-7H to -671B-11X and Cores 110-671B-27X to -671B-32X in the upper to lower Pliocene sections of packages A and B.

Some Observations in Hole 671C

In Hole 671C we obtained further information on geochemical processes operating in the décollement zone. Preliminary results are presented below.

Leg 110, Hole 671C Cores	Cl mmol/L	Ca mmol/L	Mg mmol/L
1X-5, 140/150 (505 m)	548	39.6	32.0
Do.	532	38.7	31.3
2X-1, 145/150 (507 m)	542	37.1	32.1
2X-3, 145/150 (510 m)	546	37.7	31.6
2X-4, 145/150 (511 m)	543	35.4	34.6
2X-CC (514.5 m)	522	37.6	30.9

The sediments in Core 110-671C-2X showed evidence of core disturbance and possible seawater contamination except for the core-catcher sample. Typically, the core-catcher sample showed the lowest chlorosity. Nonetheless, the data indicate that low chloride concentrations occur in the décollement zone, thus confirming the observations in Hole 671B.

In all the samples of Hole 671C we encountered difficulties with the Eriochrome Black-T indicator in the EDTA titration for Ca + Mg. This could be traced back to a complex of the indicator with manganese ions. Laboratory experiments indicated that dissolved Mn may reach concentrations between 1 and 2 mmol/L. Presumably these high concentrations stem from the dissolution of manganese oxides which occur abundantly in these sediments.

Conclusions

The interstitial water chemistry data of Site 671 have revealed the following features:

1. Increases in Ca and decreases in Mg in the upper sedimentary sections are mainly caused by reactions involving the alteration of volcanic ash;
2. Below 125 mbsf changes in the concentration-depth profiles of Ca and Mg indicate a transient condition, resulting from

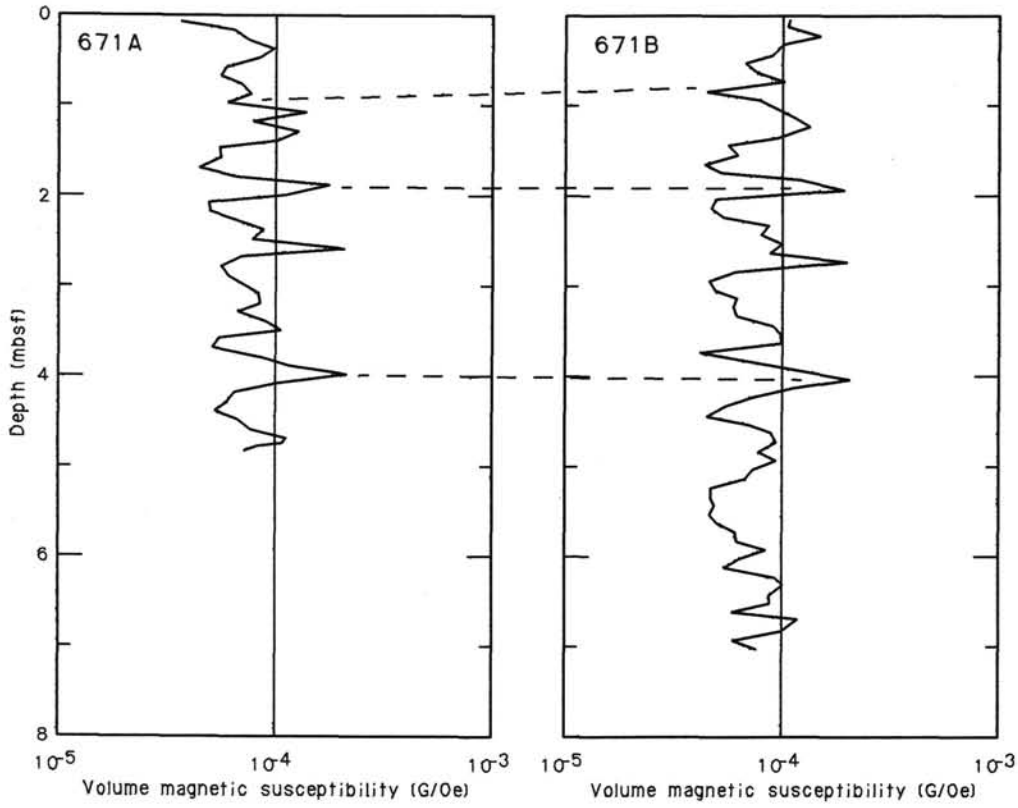

Figure 32. Cross-correlations of Cores 110-671B-1H and -671A-1H, from the lower Pleistocene.

a recent emplacement of a younger sediment section below a Miocene section;

3. The décollement is clearly marked by a minimum in chloride, most likely caused by advection of relatively fresh water along the décollement. This fresh water probably results from the dewatering of the subducting plate and is probably owing to membrane filtration or other ion exclusion processes;

4. Below the décollement, concentration-depth profiles of Ca and Mg indicate a changing pattern, in which older established profiles are being modified by diffusive processes;

5. The principal sink for Na appears to lie below the cored section of the hole, presumably in the underlying basalts of the oceanic crustal layer 2.

Calcium Carbonate

The data on carbonate content are reported in Table 6.

Dissolved Gases and Organic Carbon

Methane

Methane analyses were carried out by a head-space method (Bernard, 1976; Bernard et al., 1978). In this method sediment is mixed with He-degassed seawater, and after equilibration methane gas is analyzed with a Hewlett-Packard 5890 Gas Chromatograph. From dry weight of sediment and sediment-water contents (see Physical Properties section), concentrations can be expressed in micromoles per kilogram of interstitial water.

The concentration-depth profile of dissolved methane (Fig. 35) shows low and fairly uniform values from the mudline to 450 mbsf. The amount of methane is fairly constant, ranging between 3 and 35 μmol/kg (Table 6). Below this upper part we notice three maxima in the methane concentrations:

1. The first peak correlates with a reverse thrust in upper Miocene sediments between 455 and 470 mbsf.

2. The highest methane measured in this hole occurs at the décollement.

3. From 580 to 650 mbsf, we notice a linear increase of methane with depth.

Unfortunately, we were unable to determine the methane contents in the sand layer at the base of Hole 671B. However, the last six values measured show a linear trend suggesting a source in the sands. Extrapolation of the trend suggests that methane concentrations in the underlying sand layer reach levels comparable to those found in the décollement. Elevated methane concentrations are confined to narrow zones around the maxima. We conclude that both in the décollement and in the sandy zone, methane is advected with low-chlorine waters, originating from the west. Diffusion into the sediments combined with consumption by micro-organisms could explain the depletions in methane in the surrounding sediments.

Unfortunately, we were unable to determine the light hydrocarbons C2 and C3. However, we propose a thermogenic origin for the methane at Site 671, based on Rock-Eval results discussed below. Thermogenic methane originating in accretionary wedges has been documented by the Kaiko program off Nankai Trough and Japan Trench (Boulegue et al., in preparation) and by DSDP off northern Japan (Whelan et al., 1980). These petrologically produced hydrocarbons occur at temperatures higher than 60°C (Schoell, 1984). The thermal gradient found in the Hole 671B is 43°C/km (see Heat Flow section). Assuming that this gradient is constant with depth, thermogenic methane could be produced at a depth of 1200 to 1500 m, farther onto the prism.

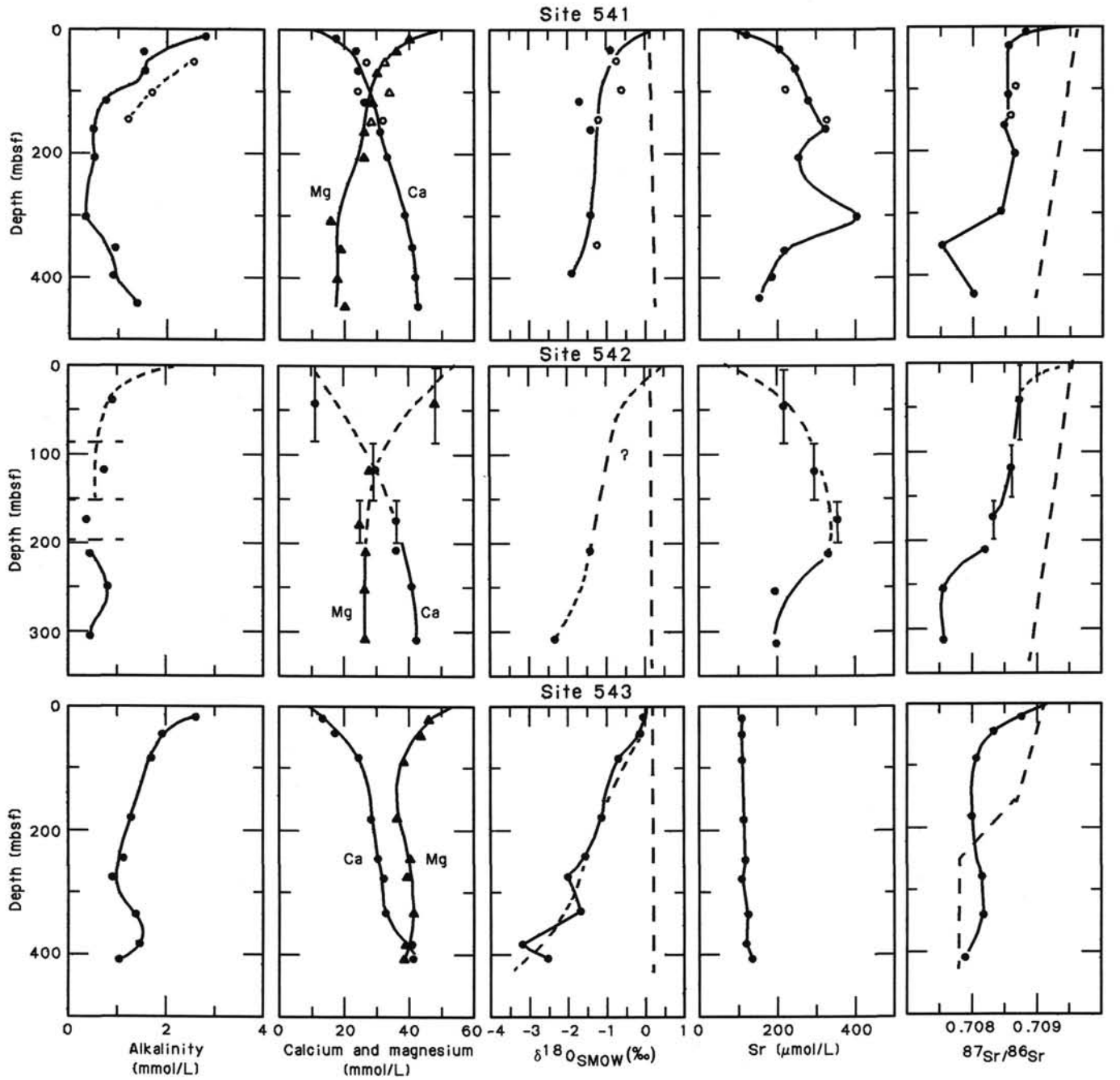

Figure 33. Interstitial water chemistry of Sites 541, 542, and 543, DSDP Leg 78A. Dashed lines represent contemporaneous seawater curves of $^{87}Sr/^{86}Sr$.

Studies on the biological communities located at the front of the subduction zones off Japan suggest that methane is utilized as a food source by species such as clams (Boulegue et al., in preparation).

Organic Matter

A rapid method developed (Barker, 1974; Claypool and Reed, 1976; Espitalié et al., 1977a, b; Espitalié et al., 1986) for investigating petroleum source rocks and sediments in general involves the use of temperature program pyrolysis under an inert atmosphere, and subsequent analysis of the product gas. The instrument employed is a Rock-Eval that Espitalié et al. (1977a, b) designed to operate on rock samples requiring no demineralization or other preparation except grinding. Pyrolysis equipment was first used on board the *GLOMAR Challenger* during Leg 48 (Deroo et al., 1976). The main aim of this method is to determine the quantity and character of the hydrocarbons that have been produced; depending on the character of the organic matter originally deposited in the source rocks as well as on subsequent thermal evolution (Espitalié et al., 1977a, b). We used this method to determine the content and origin of organic matter in offscraped and underscraped sedimentary series of Barbados Accretionary Complex.

Site 671 analytical data are presented in Table 7(a). Each parameter in this table is defined in the accompanying Table 8. We first present the principle of the Rock-Eval method with its ap-

Table 5. Data on interstitial water chemistry.

Core	Sec.	Interval (cm)	Depth (mbsf)	pH	Alkalinity (mmol/L)	Salinity (‰)	Cl (mmol/L)	Ca (mmol/L)	Mg (mmol/L)	NH_4 (μmol/L)	Si (μmol/L)	SO_4 (mmol/L)
Hole 671A												
1	2	145/150	3	7.43	2.95	35	570	11.4	51.5	25	450	27.8
Hole 671B												
1	3	145/150	4.5	7.89	3.09	35	559	11.9	50.6	35	530	27.6
2	5	145/150	16	7.69	4.10	35	564	12.8	49.9	55	480	27.8
3	4	145/150	22	7.68	2.67	35.5	570	16.0	45.1	115	212	25.0
4	5	145/150	33	7.70	2.13	[a]n.d.	574	18.0	42.3	160	228	22.8
6	4	145/150	50.5	7.74	1.56	34.7	570	20.7	39.6	180	220	20.8
8	4	145/150	68.5	7.76	1.41	34.4	568	23.5	34.6	210	184	18.0
10	3	145/150	86	7.89	0.85	34.2	571	25.2	32.9	220	240	16.6
13	3	145/150	113	n.d.	n.d.	n.d.	559	28.0	30.8	240	240	14.8
14	6	84/89	125	n.d.	n.d.	n.d.	570	30.2	27.0	270	510	13.0
15	1	59/65	127	n.d.	n.d.	n.d.	572	28.1	24.4	540	520	13.6
17	4	145/150	153	n.d.	n.d.	n.d.	573	27.3	27.1	520	640	13.2
[b]I.S.			164	n.d.	n.d.	n.d.	567	26.5	32.8	230	132	15.8
19	1	145/150	171	7.62	1.05	34.0	569	26.2	26.9	390	250	12.8
22	5	145/150	200	7.69	0.92	n.d.	570	27.6	26.1	325	250	13.2
25	4	145/150	230	7.74	1.02	n.d.	570	28.6	26.5	260	228	14.6
28	5	140/150	260	7.72	0.71	34.2	564	30.7	24.8	240	275	15.0
31	1	140/150	290	7.38	0.64	n.d.	560	30.7	25.0	230	230	16.2
33	2	16/22	310	n.d.	n.d.	n.d.	554	33.0	22.9	320	200	16.2
34	3	140/150	320	7.54	0.70	32.3	533	36.0	22.9	215	230	15.6
37	2	140/150	348	7.43	1.85	33.0	539	36.1	24.3	195	240	18.0
40	3	140/150	368	7.65	1.05	n.d.	539	39.1	22.6	185	252	16.6
41	4	93/101	380	n.d.	n.d.	n.d.	n.d.	39.5	20.4	265	180	16.6
43	3	140/150	397	8.11	1.02	32.7	536	37.1	25.4	210	170	19.1
46	3	140/150	420	n.d.	n.d.	32.4	526	40.2	22.7	215	175	15.0
49	3	140/150	450	7.86	1.70	n.d.	523	40.7	25.5	195	300	19.0
52	2	140/150	477	7.63	2.24	32.5	520	40.2	27.0	235	260	17.0
55	5	140/150	508	n.d.	n.d.	n.d.	505	37.2	28.1	225	815	13.9
56	2	139/150	516	n.d.	n.d.	n.d.	508	36.3	30.9	260	650	14.0
58	6	140/150	535	n.d.	n.d.	n.d.	552	39.9	37.1	240	250	13.0
61	5	140/150	566	7.73	2.78	37.2	556	43.6	38.8	315	220	11.2
63	5	140/150	580	7.52	2.47	n.d.	560	46.0	38.0	320	280	9.5
65	5	140/150	600	n.d.	n.d.	n.d.	547	49.6	39.3	330	240	8.6
67	5	140/150	620	n.d.	n.d.	n.d.	564	55.7	37.6	355	230	7.8
70	5	140/150	650	7.23	2.80	34.3	563	64.9	36.6	355	275	6.6
73	5	140/150	675	n.d.	n.d.	n.d.	508	66.1	33.6	340	440	6.0
74		special	685	n.d.	n.d.	n.d.	523	35.4	26.9	210	n.d.	16.8
74	1	16/22	685	n.d.	n.d.	n.d.	542	72.4	34.0	n.d.	375	8.7

[a] n.d. = not determined.
[b] I.S. = *in-situ* water sample.

plications. Then we discuss the total organic carbon (TOC) contents, followed by a discussion of the Rock-Eval results.

Principle and Applications of the Rock-Eval Method

The Rock-Eval method is based on the pyrolysis of small rock samples (ca. 100 mg). From the parameters given by the apparatus, it enables the determination of: (a) various types of source rocks, (b) their degree of evolution, and (c) their petroleum potential.

a—Types of organic matter

Three types of organic matter can be defined directly from the rock samples:

1. High hydrocarbon index (HI) and low oxygen index (OI): characterize excellent source rocks containing algal organic matter (Kerogen type I).
2. High OI and Low HI: characterize low source rock potential with terrestrial organic matter (Kerogen type III). This organic matter is generally more favorable for gas than for oil.
3. Between these two types, we have good source rocks. The organic matter is of marine origin (Kerogen type II).

b—Maturation stage

Three factors indicate the maturation stage of source rocks:

1. The position of samples on their specific evolution path in the HI/OI diagram. At the beginning of maturation of immature matter, a rapid decrease of the OI appears while the HI remains quite constant. When the main maturation zone (oil zone) is reached, only the HI will increase.
2. The temperature increases with the degree of evolution. Temperatures from 400 to 435°C indicate an immature zone. Temperatures from 400 to 460 °C indicate an oil zone. Temperatures up to 460 °C indicate a gas zone.
3. Production Index: PI = S1/(S1 + S2). PI increases regularly with depth. A rapid increase of PI indicates an oil accumulation zone.

c—Petroleum Potential (PP)

PP represents the maximum quantity of hydrocarbon compounds (oil + gas) that can be provided in nature by a rock.

PP = (S1 + S2) kg of hydrocarbon/metric ton of rock

S1 gives the quantity of hydrocarbons (oil + gas) currently generated in the rock. S2 gives the quantity of hydrocarbons that the rock could still produce should burial and maturation continue.

TOC (Total Organic Carbon)

Total organic carbon of analyzed Hole 671B squeezecakes shows great variations (Fig. 35). From the mudline to 450 mbsf,

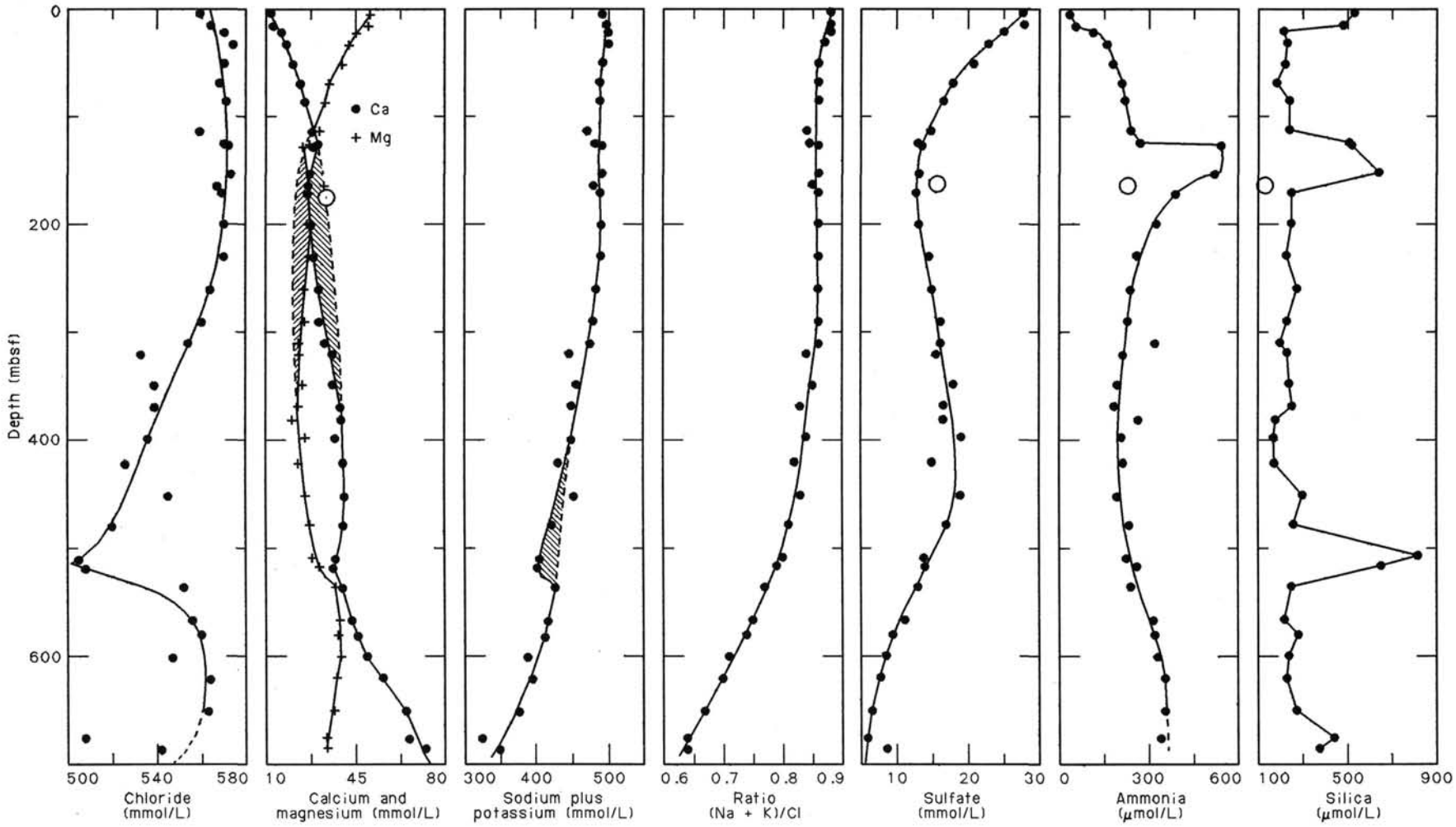

Figure 34. Interstitial water Cl, Ca, Mg, (Na + K), (Na + K)/Cl, SO_4, NH_4, and $Si(OH_4)$ in Hole 671B.

Table 6. Organic carbon, inorganic carbon, and methane in Hole 671B.

Core 110-671B-	Sec.	Interval (cm)	Depth (mbsf)	Organic carbon (%)	Inorganic carbon (%)	CH_4 (μmole/L)
1	3	145-150	4.5	0.03	1.81	19.1
2	5	145-150	16	0.01	0.49	[a]n.d.
3	4	145-150	22	0.03	3.74	n.d.
4	5	145-150	33	0.02	4.14	n.d.
5	5	145-150	43	n.d.	n.d.	27.4
6	4	145-150	50.5	0.02	2.47	n.d.
8	4	145-150	68.5	0.01	3.85	n.d.
10	3	145-150	86	0.01	4.31	n.d.
13	3	145-150	113	0.08	0.34	23.5
15	1	145-150	127	n.d.	n.d.	5.2
17	4	145-150	153	0.09	0.87	3.5
19	1	145-150	171	0.05	4.61	12.9
22	5	145-150	200	0.03	4.51	28.5
25	4	145-150	230	0.02	2.98	7.0
28	5	145-150	260	0.07	5.47	26.5
31	1	140-150	290	0.34	5.63	n.d.
32	5	140-150	300	n.d.	n.d.	25.4
34	3	140-150	320	0.28	2.57	16.6
37	2	140-150	348	0.26	1.53	34.5
40	3	140-150	368	0.16	0.84	13.6
43	3	140-150	397	n.d.	0.01	26.1
46	3	140-150	420	0.13	0.36	n.d.
48	5	140-150	442	n.d.	n.d.	15.1
49	2	140-150	450	0.04	0.02	15.0
50	3	140-150	458	n.d.	n.d.	286
51	4	140-150	470	n.d.	n.d.	258.2
52	1	140-150	477	0.16	0.04	151.8
55	5	140-150	508	0.07	0.01	550.2
58	6	140-150	535	0.25	0.02	n.d.
59	5	140-150	546	n.d.	n.d.	259
61	5	140-150	566	0.12	0.02	76.1
63	5	140-150	580	0.26	0.99	147.0
65	5	140-150	600	0.16	0.02	238.9
67	5	140-150	620	0.92	0.08	356.5
70	4	140-150	650	0.32	0.68	450.4
73	4	140-150	675	0.01	0.02	535.0

[a] n.d. = not determined.

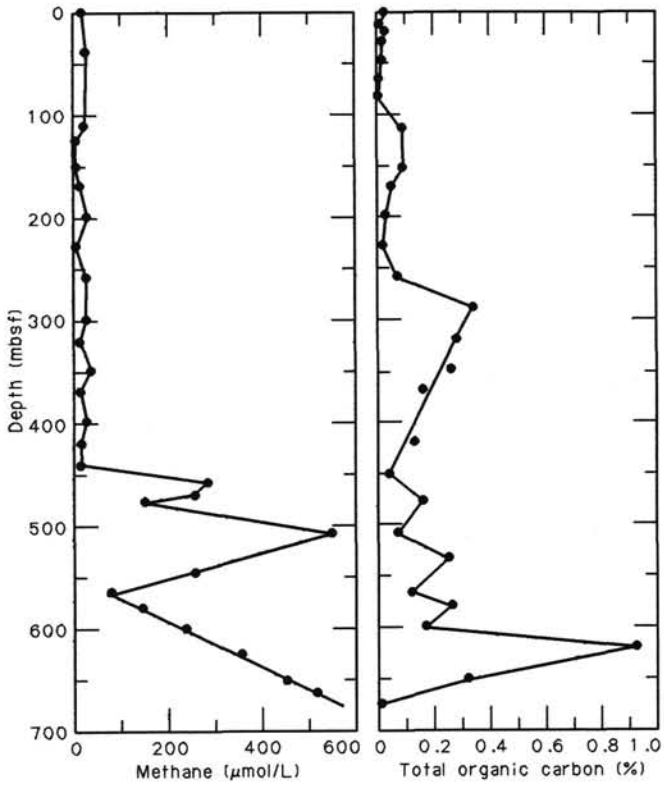

Figure 35. Plots of methane and organic carbon vs. burial depth in Hole 671B.

the TOC are low (<0.4%) as already pointed out for Leg 78A sediments (<0.3%; Claypool, 1984). But in Leg 78A, a trend of decreasing carbon content with increasing depth beneath the seafloor is apparent at each drilling site (Fig. 36). In Hole 671B, the results show quite different variations, which can be divided into four parts:

1. From 0 to 100 mbsf, TOC is very low (<0.03%) but with a decreasing trend with burial depth (from lower Pleistocene to upper Miocene).

2. From 100 to 230 mbsf, we notice the same trend of decreasing carbon contents with increasing depth (from lower Pleistocene to upper Pliocene). The TOC average (x = 0.06%) is slightly larger than in the upper 100 m. As discussed for Leg 78A results (Claypool, 1984), these observed decreasing trends with burial depth in part 1 and 2 could be the result of a constant deposition rate of organic matter and slow decomposition (oxidation) over time or increasing depth. The data suggest that relatively more organic carbon has been oxidized in the upper layer than below 120 mbsf. Two postulates to explain this difference are: (a) The diffusion efficiency of oxygen from overlying seawater could be greater in the upper part since the underlying layer was in less contact with seawater, and (b) more probably, the oxidation of organic matter is caused by sulfate reduction. The sulfate concentrations decrease from 28 to 13 mmole in this layer.

3. Below 230 m, the increase in TOC could result from a change in organic matter deposition rates. From 260 to 450 mbsf, the observed regular decrease in carbon content with increasing burial depth could be caused by a regular increase in the deposition rate of organic matter with time (from deeper to upper levels). This, in turn, could be related to the formation of the "Orinoco" deep-sea fan during the late Miocene. In addition, the sulfate concentration gradient in Hole 671B does not support the idea of organic matter oxidation to explain the decrease in carbon content.

4. Below 450 mbsf, the TOC data are variable. The observed increasing trend with a maximum at 620 mbsf (0.92%) could be caused by more important terrigenous inputs during this sedimentary period of late Oligocene, also suggested by the presence of silt layers (see Lithology section, this chapter) or richer organic matter inputs. Below the décollement, the sulfate profile indicates that reducing conditions become more and more important. From these results, we can conclude that only upper Oligocene sediment could act as hydrocarbon source rock.

Rock Eval Results

Rock Eval analysis was used to characterize the nature of deposited organic matter as well as its source potential for oil and gas. In general, Rock Eval data cannot be interpreted for TOC data <0.25% (J. P. Herbin, pers. commun., 1987). In Hole 671B, we can give an interpretation for only six samples (Table 7(B)). These samples were measured between 290 and 348 mbsf (from the base of upper Pliocene to the top of lower Pliocene), and between 600 and 650 mbsf (in upper Oligocene series). The plot of HI versus OI allows determination and classification of organic matter. This diagram is similar to a van Krevelen diagram, where H/C and O/C atomic ratios obtained by elementary analysis of kerogen isolated from rock are plotted. The position of these samples in the HI/OI diagram (Fig. 37) suggests that terrestrial organic matter is the major component of organic matter in the Pliocene and Oligocene sedimentary series.

Table 7. A and B, Rock Eval geochemistry data for Hole 671B.

A

Core 110-671B-	Sec.	Interval (cm)	Depth (mbsf)	Temp. (°C)	S_1	S_2	S_3	PI	S_2/S_3	PC	TC	HI	OI
1	3	145–150	4.5	420	0.18	0.21	1.63	0.47	0.12	0.03	0.03	700	5433
2	5	145–150	16	288	0.07	0.17	0.90	0.29	0.18	0.02	0.01	1700	9000
3	4	145–150	22	425	0.11	0.29	1.57	0.27	0.18	0.03	0.03	966	5233
4	5	145–150	33	356	0.09	0.21	1.47	0.30	0.14	0.02	0.02	1050	7350
6	4	145–150	51	432	0.08	0.21	1.07	0.29	0.19	0.02	0.02	1050	5350
8	4	145–150	69	422	0.08	0.15	1.44	0.36	0.10	0.01	0.01	1500	14400
10	3	145–150	86	473	0.05	0.09	1.05	0.36	0.08	0.01	0.01	900	10500
13	3	145–150	113	478	0.07	0.10	0.51	0.44	0.19	0.01	0.08	125	637
17	4	145–150	153	386	0.08	0.06	0.92	0.57	0.06	0.01	0.09	66	1022
19	1	145–150	171	436	0.05	0.04	1.42	0.62	0.02	0.00	0.05	80	2840
22	5	145–150	200	449	0.09	0.22	1.42	0.30	0.15	0.02	0.03	733	4733
25	4	140–150	230	486	0.09	0.19	1.24	0.32	0.15	0.02	0.02	950	6200
28	5	140–150	260	471	0.08	0.19	0.96	0.31	0.19	0.02	0.07	271	1371
31	1	140–150	290	434	0.07	0.21	0.97	0.25	0.21	0.02	0.34	61	285
34	5	140–150	320	539	0.16	0.23	1.03	0.42	0.22	0.03	0.28	82	367
37	2	140–150	348	593	0.06	0.21	0.96	0.23	0.21	0.02	0.26	80	369
40	3	140–150	368	527	0.05	0.11	0.68	0.31	0.16	0.01	0.16	68	425
46	3	140–150	420	604	0.12	1.02	0.28	0.11	3.64	0.09	0.13	784	215
49	2	140–150	450	484	0.04	0.08	0.50	0.33	0.16	0.01	0.04	200	1250
52	2	140–150	477	506	0.04	1.91	0.27	0.02	7.07	0.16	0.16	1193	168
55	5	140–150	508	582	0.13	0.76	0.59	0.15	1.28	0.07	0.07	1085	842
58	6	140–150	535	524	0.08	0.27	0.33	0.24	0.81	0.02	0.25	108	132
61	5	140–150	566	605	0.04	0.34	0.28	0.11	1.21	0.03	0.12	283	233
63	5	140–150	580	360	0.06	0.00	0.67	1.00	0.00	0.00	0.26	0	257
65	5	140–150	600	536	0.04	0.06	0.36	0.40	0.16	0.00	0.16	37	225
67	5	140–150	620	400	0.05	0.23	1.39	0.18	0.16	0.02	0.92	25	151
70	4	140–150	650	337	0.05	0.05	1.68	0.50	0.02	0.00	0.32	15	525
73	5	140–150	675	609	0.02	0.17	0.23	0.11	0.73	0.01	0.01	1700	2300

B

Core 110-671B-	Sec.	Interval (cm)	Depth (mbsf)	Temp. (°C)	S_1	S_2	S_3	PI	S_2/S_3	PC	TC	HI	OI
31	1	140–150	290	434	0.07	0.21	0.97	0.25	0.21	0.02	0.34	61	285
34	5	140–150	320		0.16	0.23	1.03	0.42	0.22	0.03	0.28	82	367
37	2	140–150	348		0.06	0.21	0.96	0.23	0.21	0.02	0.26	80	369
65	5	140–150	600		0.04	0.06	0.36	0.40	0.16	0.00	0.16	37	225
67	5	140–150	620	400	0.05	0.23	1.39	0.18	0.16	0.02	0.92	25	151
70	4	140–150	650		0.05	0.05	1.68	0.50	0.02	0.00	0.32	15	525

Table 8. Explanatory note to Table 7.

S1 (mg hydrocarbon/g rock): the quantity of free hydrocarbons present in the rock and which are volatilized below 300°C.
S2 (mg hydrocarbon/g rock): the amount of hydrocarbon-type compounds produced by cracking of kerogen as the temperature increases to 550°C.
S3 (mg CO_2/g rock): quantity of CO_2 produced from pyrolysis of the organic matter in the rock.
S2/S3 : A means of determining the type of organic matter in the rock.
— from 0.0 to 2.5: gas, type III
— from 2.5 to 5.0: oil/gas, type III
— from 5.0 to 10.0: oil, types I and II
Temperature (°C): maximum temperature at which maximum generation of hydrocarbon from kerogen occurs.
PI (Productivity Index): PI = S1/(S1 + S2).
PI characterizes the evolution level of the organic matter.
PC "Pyrolysized carbon": PC = k(S1 + S2) where k = 0.083 mg C/g rock.
PC corresponds to the maximum quantity of hydrocarbons capable of being produced from the source rock given sufficient burial and time.
TOC: Total Organic Carbon
HI "Hydrogen index": HI = (100 × S2)/TOC
OI "Oxygen index": OI = (100 × S3)/TOC

The temperatures obtained (430°C at 290 mbsf and 400°C at 620 mbsf) could indicate an immature zone. The petroleum potential of these samples is very low (about 0.28 kg hydrocarbons/metric ton of sediments).

Conclusion

The dissolved methane in pore water and organic matter chemical data reveal the following features:

1. The décollement and the reverse thrust just above the décollement are clearly marked by maxima in pore water methane concentrations.
2. The methane is carried from deeper horizons by advection of fluids along the décollement and probably along underthrust porous layers such as sand layers.
3. The observed variations of TOC are most likely the result of differences between the rates of deposition and preservation of organic matter rather than reactivity of organic matter.
4. The underthrust sediments at Site 671 were the main zone of accumulation of organic matter. The upper Oligocene sediments contain significant terrestrial input from the South American continent.
5. The maturation of that terrestrial organic matter could produce gas at depths of 1200 to 1500 m according to the heat flow data.

PHYSICAL PROPERTIES

Several measurement programs were carried out during the process of coring Hole 671B. They were:

1. Index Properties—Gravimetric determinations of density, porosity, and water content.
2. Vane Shear Strength—A measure of the resistance of the sediment to loads.
3. Compressional Wave Velocity—The speed of sound in the sediments.

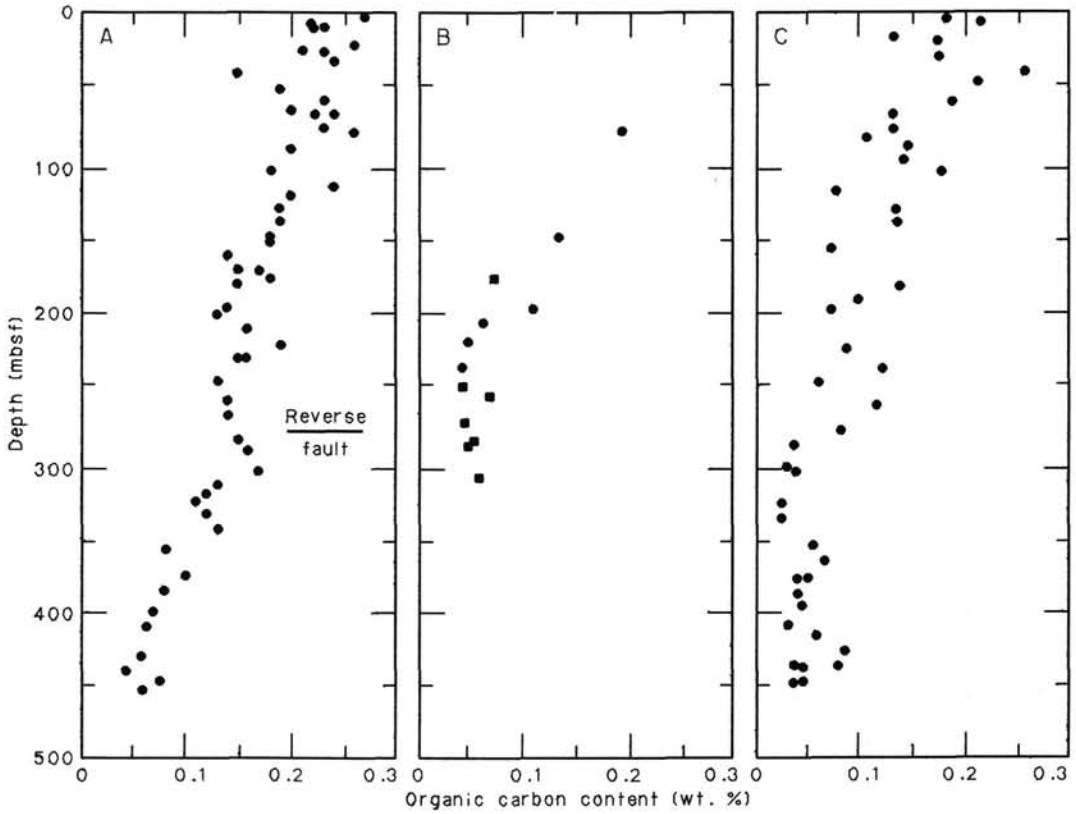

Figure 36. Plot of organic carbon (carbonate-free basis) vs. depth in Holes (A) 541, (B) 542, and (C) 543 (from Claypool, 1984).

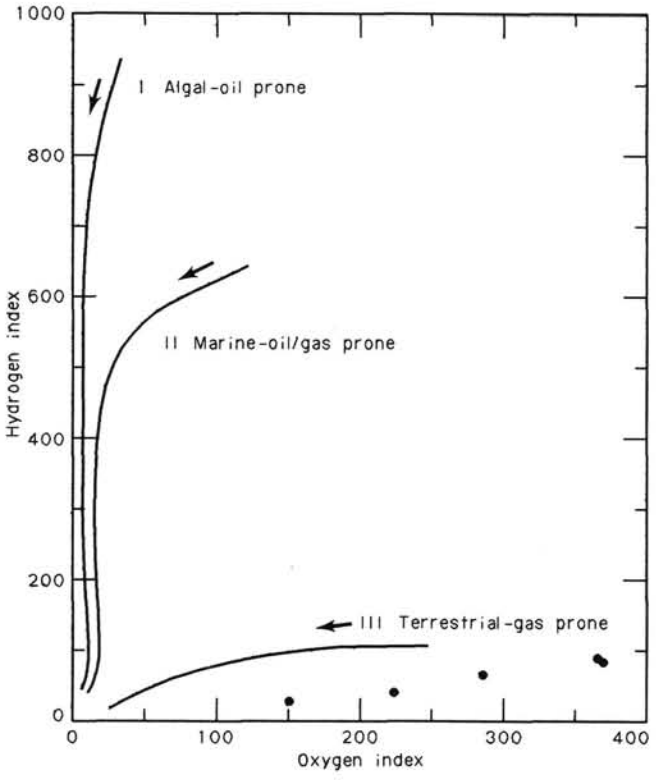

Figure 37. Plot of hydrogen index (HI) vs. oxygen index (OI) in Hole 671B. Arrows left indicate increasing maturation.

4. Thermal Conductivity—The ability of the sediment to transport heat.

5. Formation Factor—An electrical measurement that is linked to pore geometry.

Wherever possible these measurements were made on the same interval of core or on immediately adjacent positions. Hole 671B was cored using the APC to Core 110-671B-10H and the XCB to the bottom of the hole. A second hole (671C) was drilled and partially cored at the site for packer experiments. Two surface cores were collected. Table 9 lists the index property data for Hole 671C. No other physical-property measurements were made on this hole.

Index Properties

Methods

Index properties were measured at Site 671 following the procedures outlined in the "Explanatory Notes" chapter, this volume. Index properties were measured on samples selected from the most intact portions of cores and are listed in Table 10. The bulk densities and porosities calculated on the basis of dry volumetric measurements are not used in this discussion, but are presented in the table for the sake of completeness. Profiles of water content (wet and dry calculated basis), porosity, bulk density (GRAPE and samples), the density of solid matrix (grain density), and the compressional wave velocity are illustrated in Figure 38.

Results

The sediment section from Hole 671B exhibits a rapid change of index properties in the uppermost 100 m, a characteristic of

Table 9. Index properties summary, Hole 671C.

Core 110-671C-	Sect	Int (cm)	Depth (mbsf)	Water (% Wet)	Water (% Dry)	Porosity[a] (%)	Bulk density[a] (g/cm^3)	Grain density (g/cm^3)	Bulk density[b] (g/cm^3)	Porosity[b] (%)
1	2	4	1.54	32.8714	48.9679	58.4042	1.82028	2.66196	1.7407	56.262
1	2	14	1.64	32.3893	47.9055	58.3214	1.84475	2.73637	1.7710	56.394
1	2	23	1.73	36.3018	56.9902	62.9867	1.77760	2.72631	1.6961	60.535
1	2	32	1.82	35.9983	56.2459	61.5905	1.75284	2.66602	1.6863	59.687
1	2	48	1.98	36.1570	56.6342	61.9454	1.75521	2.65730	1.6813	59.775
1	2	55	2.05	33.6891	50.8049	59.0882	1.79690	2.74530	1.7486	57.917
1	2	68	2.18	34.0316	51.5876	58.9170	1.77360	2.71081	1.7330	57.985
1	2	84	2.34	33.6902	50.8072	58.3004	1.77288	2.66630	1.7270	57.201

[a] Calculated on basis of wet and dry measurements.
[b] Calculated on basis of dry volumetric measurements.

most marine sediments. A porosity decrease from nearly 80% at the mudline to 56% at 128 mbsf is matched by a water content loss (dry calculated basis) from 137% to 45%. Lithologic Unit 1, an olive gray and brown calcareous mudstone and marlstone, has consistent index properties. Bulk density increases within this unit from 1.5 to 1.8 g/cm^3. The only exception to this consistency occurs at a major thrust fault (A), located at 128 mbsf, which separates the overlying units (Tectonic Package A from the underthrust section, Package B). A sharp increase in water content and porosity occurs across this thrust (Fig. 38). Tectonic Package A is a repeated section of the underlying Package B. The reversed trend in physical properties (Fig. 38) at 132 mbsf reflects this sedimentary stacking associated with thrusting. Water content decreases within the second major physical properties trend from a high of 75% at 135 mbsf to under 40% at 335 mbsf. This dewatering process is not as accentuated as in the upper tectonic package, and can be viewed as a portion of a larger scale trend together with the uppermost units. The bulk density of lithologic Unit 3 increases within the second trend from 1.65 to about 1.9 g/cm^3. A comparison of the low bulk density in Tectonic Package B with those found in Tectonic Package A shows equivalent values of density are offset between 70 to 90 m. Porosities below thrust A decrease from 69.5% at 135.4 mbsf to values near 50% below 300 mbsf. A disruption of the second trend in physical properties takes place between 285 and 310 mbsf. This interval is marked by increased water contents and porosities, and slightly decreased bulk densities.

The span between 335 and 370 mbsf does not conform to any particular trend; however, few samples were taken from this portion of the hole because of core disturbance. The index properties within this interval are only transitional between the series above and below it. The third major trend in index properties is associated with the relatively carbonate-free sediments of lithologic Unit 2-A. Lithologic Unit 2-A is structurally bound by a major thrust (B) fault centered around 375 mbsf, and by the sheared material tied to the décollement zone near 500 mbsf. The overall downhole trend of index properties at Site 671 is disrupted by the properties of these apparently less-consolidated sediments. The material between 370 and 505 mbsf falls into two distinct groups; one group extending from 370 to about 450 mbsf, the other from 450 to 505 mbsf. The top of lithologic Unit 2-A marks the base of the general trend of decreasing porosity and water content developed in the overlying lithologic Unit 1 (Fig. 38). Unit 2-A exhibits an increase of water contents from low values near 30% at 381 mbsf to between 35% and 70% in the lower section of Unit 2-A. Bulk densities in the interval from 370 to 505 mbsf show, as do other index properties, two cycles of local maxima and minima. Bulk densities decrease from 1.9 g/cm^3 (370 mbsf) to 1.7 g/cm^3 (400 mbsf), and increase again to 1.9 g/cm^3 (458 mbsf). A decrease of bulk density to approximately 1.6 g/cm^3 (476 mbsf), followed by another increase, mimics the sediment behavior from 370 to 460 mbsf.

Lithologic Units 2-B through 4 make up the remainder of the cored section below 505 mbsf at Site 671. The index properties of the sediment units below the 500–510 mbsf interval once again develop the regular pattern of consolidating sediments, with decreasing porosity and water content matched by increasing bulk densities. The base of the cored sequence at Site 671 has a porosity of approximately 48%, water content 30%–33% and bulk density near 2.0 g/cm^3. The apparent "normal" consolidation of the lowermost sediments at this site is possibly complicated by diagenetic effects yielding higher velocities than previously observed for sediments of similar porosities.

Compressional Wave Velocity

Methods

The compressional wave velocity measurements at Site 671 were made following the methods described in the "Explanatory Notes" chapter. The V_p logger was used on all of the recovered cores at Site 671 and constitutes the only velocity record for the upper 90 m of the hole. Beginning with Core 110-671B-10H, discrete velocity determinations were made on chunk samples removed from the core using the Hamilton Frame Velocimeter, generally with one measurement from every other section, or three per core. V_p was measured in two directions, horizontal propagation (normal to the axis of the core) and vertical propagation (parallel to the axis of the core). In intervals of severe core disturbance, measurements were made only on competent "biscuits" or were not made at all.

Results

Determinations of V_p in both the vertical and horizontal propagation directions are presented in Table 11. The V_p in the horizontal direction vs. depth is plotted with index properties in Figure 38. Only the horizontal data were used, owing to core disturbance that opened cracks in the horizontal plane, yielding somewhat slower, as well as questionable, results for velocity measured in the vertical direction. Velocities from the V_p Logger have not been processed, so the following discussion will deal primarily with the data acquired using the Hamilton Frame. Cursory examination of the V_p logger records suggests a fairly normal compaction-dominated velocity gradient over the first 90 m of core, with near-seafloor values of approximately 1.50 km/s increasing gradually to 1.55 km/s at 100 mbsf.

The velocity vs. depth data displayed in Figure 38 can be examined at several different scales. In general terms, there appear to be three distinct sections; two marked by velocity gradients (at the top and bottom of the hole), separated by a third zone of relatively constant velocity. The uppermost zone extends from the seafloor to a depth of approximately 200 mbsf. Within this interval the average velocity increases from about 1.50 km/s (V_p Logger data) to a little more than 1.60 km/s. The increase in velocity within this zone represents what is normally seen in shal-

Table 10. Index properties summary, Hole 671B.

Core 110-671B-	Sect	Int (cm)	Depth (mbsf)	Water (% wet)	Water (% dry)	Porosity[a] (%)	Bulk density[a] (g/cm^3)	Grain density (g/cm^3)	Bulk density[b] (g/cm^3)	Porosity[b] (%)
1	2	70	2.20	53.0007	112.7690	77.4029	1.4962	2.7652	1.4500	75.5546
1	3	70	3.70	50.9706	103.9590	74.9627	1.5067	2.7211	1.4707	73.7009
1	4	70	5.20	57.8409	137.1970	79.2748	1.4042	2.6890	1.3814	78.5599
1	5	15	6.15	50.2038	100.8190	75.2021	1.5346	2.7869	1.4905	73.5607
2	2	70	9.60	51.0484	104.2840	73.3462	1.4720	2.5553	1.4449	72.5392
2	4	73	12.63	52.9069	112.3450	76.3612	1.4787	2.7358	1.4474	75.2876
2	6	30	15.20	45.5211	83.5574	71.2262	1.6030	2.8001	1.5603	69.8234
2	6	70	15.60	48.1313	92.7945	72.3999	1.5411	2.6752	1.5019	71.0780
3	2	70	19.10	44.3981	79.8501	70.3042	1.6223	2.7537	1.5692	68.4963
3	4	120	22.60	41.1504	69.9247	66.8298	1.6638	2.7504	1.6196	65.5216
3	6	20	24.60	43.6245	77.3819	68.6778	1.6129	2.8148	1.5923	68.2845
4	2	70	28.60	49.2640	97.0986	73.6447	1.5315	2.7306	1.4951	72.4155
4	4	70	31.60	42.7217	74.5861	68.3544	1.6392	2.7028	1.5853	66.5876
4	6	70	34.60	39.1030	64.2118	64.8117	1.6981	2.7902	1.6621	63.8920
5	2	70	38.10	44.6797	80.7656	70.2537	1.6109	2.7650	1.5670	68.8309
5	4	70	41.10	42.3632	73.5003	68.0316	1.6453	2.7047	1.5912	66.2744
5	6	70	44.10	42.8269	74.9073	67.6017	1.6172	2.6545	1.5740	66.2848
6	2	90	47.80	35.9631	56.1599	59.4165	1.6926	2.5061	1.6443	58.1634
6	4	90	50.80	38.5298	62.6803	63.0423	1.6763	2.7101	1.6540	62.6556
6	6	90	53.80	42.4651	73.8075	67.6803	1.6328	2.7406	1.5967	66.6592
7	2	70	57.10	36.9335	58.5627	68.8173	1.9089	2.7531	1.6915	61.4173
7	3	130	59.20	34.2279	52.0401	58.9153	1.7634	2.7867	1.7494	58.8649
7	4	130	60.70	36.6710	57.9055	61.9292	1.7301	2.7247	1.6892	60.9029
7	6	70	63.10	33.6428	50.6995	58.9743	1.7959	2.6969	1.7364	57.4352
8	2	70	66.60	35.7161	55.5599	61.2065	1.7557	2.7574	1.7143	60.1941
8	4	70	69.60	38.3778	62.2792	63.3887	1.6922	2.7271	1.6604	62.6503
8	6	70	72.60	37.5934	60.2394	61.9256	1.6876	2.7252	1.6733	61.8483
9	2	90	76.30	36.9668	58.6465	63.3216	1.7549	2.8506	1.7136	62.2670
9	4	70	79.10	33.2867	49.8951	58.6963	1.8066	2.7234	1.7503	57.2802
9	6	65	82.05	33.6933	50.8143	58.4865	1.7784	2.6353	1.7183	56.9292
10	2	106	85.96	37.2536	59.3718	61.7353	1.6978	2.7094	1.6754	61.3672
10	3	1	86.41	35.9282	56.0749	61.4161	1.7513	2.7575	1.7105	60.4170
10	4	114	89.04	34.2808	52.1626	58.7637	1.7562	2.7200	1.7309	58.3376
11	2	64	93.74	38.0158	61.3316	63.5338	1.7122	2.7105	1.6627	62.1470
11	4	69	96.79	39.7552	65.9895	65.2094	1.6805	2.7143	1.6346	63.8929
11	6	70	99.80	33.1339	49.5527	57.2613	1.7705	2.7561	1.7622	57.4015
12	2	9	102.69	32.9481	49.1381	58.0761	1.8058	2.8170	1.7823	57.7259
12	3	8	104.18	32.0013	47.0616	56.3647	1.8045	2.7582	1.7847	56.1498
12	4	8	105.68	35.0880	54.0546	59.8205	1.7466	2.7341	1.7198	59.3286
13	2	7	112.17	45.5677	83.7145	71.2083	1.6010	2.6888	1.5403	69.0096
13	3	8	113.68	33.3033	49.9326	58.3200	1.7941	2.8021	1.7713	57.9901
13	4	10	115.20	37.8732	60.9611	62.8660	1.7006	2.7392	1.6718	62.2497
13	6	18	118.28	31.1853	45.3177	55.8597	1.8351	2.7222	1.7903	54.8914
14	2	9	121.69	35.3211	54.6100	61.1437	1.7735	2.7395	1.7170	59.6228
14	3	9	123.19	32.2984	47.7070	56.1675	1.7812	2.7385	1.7733	56.3107
14	4	18	124.78	31.1534	45.2505	55.8107	1.8354	2.7705	1.8052	55.2874
14	6	17	127.77	31.2674	45.4914	56.5305	1.8523	2.6783	1.7756	54.5868
15	2	112	132.22	33.5828	50.5634	58.4193	1.7822	2.6441	1.7227	56.8884
15	3	120	133.80	40.6340	68.4466	67.9562	1.7134	2.7020	1.6178	64.6333
15	4	130	135.40	42.9399	75.2538	69.5243	1.6588	2.7510	1.5912	67.1746
15	6	21	137.31	35.8403	55.8611	61.8383	1.7677	2.7480	1.7097	60.2433
15	6	76	137.86	39.5767	65.4990	65.8430	1.7044	2.7743	1.6506	64.2199
16	6	130	147.90	32.4508	48.0403	58.0750	1.8335	2.7548	1.7750	56.6275
17	2	137	151.47	39.8732	66.3152	66.1441	1.6995	2.7356	1.6373	64.1854
17	4	70	153.80	41.6145	71.2754	67.1025	1.6520	2.7569	1.6134	66.0070
17	6	66	156.76	36.3508	57.1112	61.0931	1.7218	2.6933	1.6871	60.2973
18	2	60	160.20	34.9383	53.7002	59.9791	1.7588	2.7167	1.7180	59.0155
18	4	60	163.20	32.6906	48.5676	57.8029	1.8115	2.7679	1.7740	57.0119
19	2	45	169.55	31.8017	46.6312	56.9032	1.8332	2.6625	1.7607	55.0558
20	2	37	178.97	33.8565	51.1863	59.8396	1.8108	2.7338	1.7424	57.9983
20	2	37	178.97	33.8565	51.1863	59.8396	1.8108	2.7338	1.7424	57.9983
21	2	81	188.91	31.4693	45.9200	55.6692	1.8123	2.7795	1.8014	55.7308
22	2	125	198.85	32.9362	49.1118	57.8822	1.8005	2.7492	1.7641	57.1210
22	4	29	200.89	33.3064	49.9394	59.2052	1.8211	2.7669	1.7618	57.6867
22	7	33	205.43	29.8556	42.5630	54.1710	1.8589	2.7257	1.8179	53.3614
23	3	3	208.63	31.4666	45.9143	55.9135	1.8204	2.6850	1.7738	54.8785
23	4	47	210.27	36.2021	56.7451	61.3092	1.7350	2.7144	1.6949	60.3280
24	1	78	215.88	28.6825	40.2180	52.7153	1.8829	2.6909	1.8306	51.6255
24	2	125	217.85	26.1372	35.3861	50.0450	1.9616	2.7548	1.9069	49.0013
24	3	47	218.57	28.7075	40.2671	53.0712	1.8940	2.7577	1.8519	52.2646
25	2	58	226.68	29.6912	42.2298	54.6990	1.8874	2.8554	1.8610	54.3141
25	4	99	230.09	32.1259	47.3316	57.3463	1.8288	2.7205	1.7715	55.9545
25	6	40	232.50	28.5720	40.0012	53.2216	1.9083	2.7294	1.8455	51.8432
26	3	69	237.79	28.7213	40.2944	53.0931	1.8938	2.7947	1.8634	52.6117
27	2	70	245.80	29.4229	41.6891	54.2641	1.8895	2.8484	1.8647	53.9326
27	4	70	248.80	28.4359	39.7348	52.5317	1.8926	2.7514	1.8556	51.8746
28	2	70	255.30	28.5623	39.9821	52.5956	1.8865	2.8146	1.8731	52.5935

Table 10 (continued).

Core 110-671B-	Sect	Int (cm)	Depth (mbsf)	Water (% wet)	Water (% dry)	Porosity[a] (%)	Bulk density[a] (g/cm^3)	Grain density (g/cm^3)	Bulk density[b] (g/cm^3)	Porosity[b] (%)
28	4	70	258.30	26.6469	36.3269	49.7804	1.9139	2.7217	1.8840	49.3584
28	6	67	261.27	26.1583	35.4248	50.1448	1.9640	2.7493	1.9045	48.9787
29	3	63	266.23	25.7176	34.6215	49.2820	1.9632	2.7514	1.9152	48.4233
30	2	53	274.13	26.0861	35.2925	48.9943	1.9242	2.8073	1.9265	49.4036
30	4	74	277.34	28.2109	39.2969	52.7238	1.9147	2.7573	1.8623	51.6506
30	6	65	280.25	25.3486	33.9560	48.5338	1.9616	2.7131	1.9095	47.5896
31	10	10	283.81	26.5110	36.0748	50.4261	1.9487	2.7165	1.8851	49.1357
32	2	66	293.26	30.7401	44.3836	55.2479	1.8413	2.7660	1.8122	54.7674
32	4	67	296.27	34.8556	53.5052	60.0790	1.7659	2.7531	1.7290	59.2472
32	6	67	299.27	26.7133	36.4504	50.1624	1.9238	2.7555	1.8943	49.7494
33	1	65	301.25	31.7170	46.4492	57.5809	1.8599	2.6798	1.7674	55.1179
33	2	68	302.78	25.1148	33.5378	48.6830	1.9859	2.6934	1.9073	47.0988
34	2	84	308.44	31.5838	46.1643	55.1673	1.7895	2.5859	1.7414	54.0874
34	4	70	311.30	30.6974	44.2947	55.5590	1.8542	2.7890	1.8199	54.9207
34	6	72	314.32	23.7198	31.0956	46.6451	2.0147	2.7888	1.9759	46.0749
35	2	70	317.80	25.9067	34.9650	49.2112	1.9461	2.7210	1.9000	48.3947
35	4	68	320.78	25.0953	33.5030	47.8527	1.9536	2.7163	1.9164	47.2834
35	6	71	323.81	25.4847	34.2006	49.1284	1.9750	2.7321	1.9134	47.9419
36	2	70	327.30	25.7870	34.7472	49.5376	1.9681	2.7186	1.9018	48.2162
36	4	75	330.35	32.4588	48.0578	57.9627	1.8295	2.6508	1.7450	55.6950
36	6	64	333.24	25.3226	33.9094	48.6445	1.9681	2.7657	1.9294	48.0320
37	3	5	337.65	29.8778	42.6083	54.4322	1.8665	2.7396	1.8218	53.5137
37	3	100	338.60	26.6126	36.2632	49.8159	1.9178	2.6971	1.8760	49.0883
38	2	71	346.31	37.3227	59.5473	64.1551	1.7610	2.6791	1.6669	61.1719
38	3	65	347.75	28.0372	38.9606	51.0984	1.8672	2.7410	1.8606	51.2877
40	2	136	365.96	30.2419	43.3525	55.1385	1.8679	2.7296	1.8113	53.8550
40	4	74	368.34	26.5173	36.0865	49.8528	1.9261	2.7356	1.8917	49.3183
41	2	51	374.61	29.0741	40.9923	54.7026	1.9276	2.7747	1.8495	52.8630
41	4	39	377.49	29.1571	41.1574	53.7106	1.8872	2.6681	1.8136	51.9930
42	2	69	379.89	25.1235	33.5533	48.6214	1.9827	2.7068	1.9122	47.2334
41	6	57	380.67	23.3996	30.5477	45.8477	2.0073	2.7341	1.9623	45.1445
42	4	64	382.84	29.3497	41.5422	53.8026	1.8781	2.7565	1.8380	53.0331
42	6	51	385.71	28.4138	39.6918	53.4827	1.9284	2.7345	1.8505	51.6947
43	2	84	389.54	33.5153	50.4106	58.7477	1.7958	2.7308	1.7480	57.5984
43	4	70	392.40	34.4014	52.4424	60.3630	1.7976	2.7037	1.7243	58.3232
44	2	62	398.82	29.7364	42.3213	53.9998	1.8604	2.6860	1.8078	52.8561
44	4	68	401.88	34.8659	53.5294	59.9163	1.7606	2.7119	1.7181	58.8955
45	3	52	409.72	37.0529	58.8636	64.5085	1.7836	2.7781	1.6952	61.7509
46	2	42	417.62	33.6473	50.7097	60.1880	1.8326	2.7924	1.7620	58.2835
46	3	101	419.71	37.5669	60.1714	63.7849	1.7395	2.7505	1.6797	62.0376
46	4	87	421.07	30.1983	43.2630	55.2798	1.8754	2.7062	1.8049	53.5907
46	5	12	421.82	24.9158	33.1838	49.5975	2.0394	2.7932	1.9489	47.7357
47	2	56	427.26	35.0583	53.9842	60.7859	1.7763	2.7386	1.7215	59.3366
47	4	75	430.45	30.8710	44.6571	56.8260	1.8858	2.7817	1.8142	55.0586
47	6	77	433.47	30.9507	44.8240	55.2613	1.8292	2.7754	1.8107	55.0955
48	1	94	435.64	32.4893	48.1246	57.3104	1.8072	2.6804	1.7531	56.0013
48	2	98	437.18	30.3261	43.5258	55.4202	1.8722	2.7307	1.8099	53.9647
48	4	24	439.44	34.9108	53.6352	60.1321	1.7646	2.6780	1.7084	58.6415
48	6	95	443.15	30.1166	43.0954	54.8368	1.8654	2.6927	1.8024	53.3710
49	2	70	446.40	31.8909	46.8232	58.1099	1.8668	2.7637	1.7885	56.0731
49	3	16	447.36	30.7700	44.4461	55.4634	1.8467	2.8362	1.8322	55.4184
49	4	28	448.98	29.3172	41.4771	53.3938	1.8659	2.6855	1.8160	52.3473
50	2	109	456.29	28.0370	38.9603	52.1405	1.9053	2.7974	1.8792	51.7934
50	4	76	458.96	28.6918	40.2362	53.2511	1.9014	2.7750	1.8577	52.4005
50	6	35	461.55	32.1005	47.2765	57.0438	1.8206	2.6859	1.7620	55.6119
51	2	70	465.40	36.2518	56.8671	62.1010	1.7550	2.7447	1.7015	60.6428
51	4	68	468.38	31.4021	45.7771	56.6789	1.8492	2.6644	1.7688	54.6146
51	6	69	471.39	38.6461	62.9888	63.8154	1.6917	2.7489	1.6608	63.1004
52	2	3	474.23	32.8315	48.8793	58.3078	1.8195	2.7594	1.7689	57.0945
52	2	69	474.89	41.1696	69.9802	65.8340	1.6383	2.7183	1.6127	65.2763
52	4	58	477.78	36.9120	58.5087	62.0686	1.7227	2.6037	1.6550	60.0745
54	2	100	494.20	33.8766	51.2323	59.9406	1.8127	2.7608	1.7493	58.2586
54	4	20	496.40	32.3834	47.8927	57.7547	1.8272	2.6951	1.7593	56.0157
54	6	57	499.77	36.3285	57.0562	61.4194	1.7321	2.5939	1.6620	59.3765
55	2	72	503.42	31.8283	46.6884	56.2439	1.8104	2.6930	1.7692	55.3664
55	4	50	506.20	27.9778	38.8461	52.0445	1.9058	2.7238	1.8562	51.0577
55	6	40	509.10	27.1353	37.2407	50.8977	1.9217	2.7392	1.8795	50.1402
56	2	40	512.60	30.6205	44.1347	55.8803	1.8696	2.6976	1.7940	54.0101
56	4	68	515.88	24.2211	31.9628	47.6692	2.0163	2.7758	1.9589	46.6449
56	6	69	518.89	25.7920	34.7564	50.2987	1.9979	2.7599	1.9166	48.5971
58	2	54	531.74	32.2458	47.5923	57.2652	1.8194	2.6888	1.7601	55.8031
58	4	38	534.58	28.6896	40.2319	53.0056	1.8928	2.6919	1.8308	51.6432
58	6	15	537.35	27.9483	38.7892	51.4690	1.8867	2.7207	1.8558	50.9932
59	2	65	541.35	29.8983	42.6498	54.3592	1.8627	2.6922	1.8066	53.1064
59	6	70	547.40	25.2264	33.7370	48.5982	1.9737	2.6945	1.9053	47.2575

Table 10 (continued).

Core 110-671B-	Sect	Int (cm)	Depth (mbsf)	Water (% wet)	Water (% dry)	Porosity[a] (%)	Bulk density[a] (g/cm^3)	Grain density (g/cm^3)	Bulk density[b] (g/cm^3)	Porosity[b] (%)
60	2	56	550.76	26.4484	35.9590	49.9277	1.9340	2.7315	1.8918	49.1922
61	2	66	560.36	33.1292	49.5421	58.6491	1.8137	2.7583	1.7628	57.4150
61	4	76	563.46	26.5009	36.0561	49.7435	1.9230	2.7115	1.8836	49.0774
61	6	68	566.38	27.4580	37.8512	51.1816	1.9097	2.7618	1.8801	50.7522
62	2	40	569.60	23.5245	30.7609	46.9084	2.0429	2.8229	1.9937	46.1052
62	4	66	572.86	25.5112	34.2484	48.3374	1.9412	2.7513	1.9198	48.1511
62	6	145	576.65	25.8377	34.8393	48.3508	1.9172	2.7041	1.8954	48.1495
63	2	70	579.40	27.7635	38.4342	51.0885	1.8852	2.7372	1.8652	50.9124
63	4	85	582.55	31.1421	45.2267	56.1802	1.8482	2.7465	1.7984	55.0603
63	6	53	585.23	27.3335	37.6150	51.4580	1.9287	2.7652	1.8840	50.6254
64	2	90	589.10	29.5053	41.8547	53.6478	1.8628	2.7212	1.8236	52.9015
64	4	74	591.94	26.3859	35.8435	49.7019	1.9298	2.6720	1.8719	48.5648
64	6	31	594.51	26.2395	35.5739	48.9773	1.9123	2.7019	1.8858	48.6518
65	2	51	598.21	28.2270	39.3281	51.2106	1.8587	2.6715	1.8334	50.8851
65	4	34	601.04	25.1006	33.5124	47.5670	1.9415	2.7170	1.9165	47.2967
65	6	59	604.29	27.7992	38.5026	51.4402	1.8958	2.6738	1.8429	50.3746
66	2	60	607.80	29.3654	41.5737	54.4193	1.8986	2.8063	1.8531	53.4953
66	4	69	610.89	27.6758	38.2663	51.7656	1.9162	2.7224	1.8621	50.6682
66	6	63	613.83	27.1312	37.2329	50.3115	1.8998	2.6897	1.8624	49.6817
67	2	31	617.01	24.6932	32.7901	47.0553	1.9523	2.6933	1.9167	46.5358
67	4	94	620.64	22.2669	28.6454	44.0672	2.0275	2.6948	1.9732	43.2000
67	6	65	623.35	26.5651	36.1749	49.7121	1.9172	2.7264	1.8874	49.2958
70	2	65	645.85	24.3705	32.2235	47.0849	1.9794	2.6971	1.9254	46.1365
70	4	70	648.90	24.3746	32.2307	47.8213	2.0100	2.7671	1.9520	46.7752
70	6	35	651.55	22.4525	28.9532	44.6461	2.0372	2.7209	1.9796	43.6987
71	2	75	655.45	24.2112	31.9455	46.7520	1.9783	2.6680	1.9177	45.6524
71	4	61	658.31	26.3287	35.7380	50.3478	1.9591	2.7633	1.9056	49.3253
71	6	70	661.40	24.9340	33.2161	47.5176	1.9524	2.6379	1.8902	46.3441
72	2	106	665.26	26.1320	35.3766	50.2639	1.9706	2.7573	1.9079	49.0163
72	4	77	667.97	23.7218	31.0991	45.9405	1.9841	2.6842	1.9351	45.1347
72	6	96	671.16	23.4038	30.5548	45.9709	2.0124	2.7356	1.9628	45.1635
73	2	62	674.32	25.8087	34.7867	49.2671	1.9557	2.6986	1.8940	48.0615
73	4	60	677.30	24.9547	33.2529	48.2773	1.9820	2.6343	1.8884	46.3373
73	6	77	680.47	25.2236	33.7320	48.7301	1.9793	2.6878	1.9029	47.1922

[a] Calculated on basis of wet and dry measurements.
[b] Calculated on basis of dry volumetric measurements.

low marine sediments and generally is the result of porosity reduction from compaction of the sediments. It is perhaps surprising, however, that the presence of the fault at 128 mbsf does not have the same effect on velocity that it appears to have on gravimetric properties (such as density and porosity; Fig. 38). Velocities below this boundary are generally greater than those measured above the boundary, even though the density profiles are similar. The single "fast" datum point is attributed to a hard ash layer at approximately 135 mbsf.

From 200 to 550 mbsf, the velocity is variable about a mean of approximately 1.70 km/s. As several intervals of core within this depth range were disturbed, it is difficult to decide if the local variation seen is real or induced by recovery. At a depth of about 390 m (Unit 1/Unit 2 boundary) there is an increase in porosity (Fig. 38) that may correspond to slightly lower velocities within most of Unit 2-A when compared to the overlying unit. It should be kept in mind that there are small (thin) intervals within each of these lithologies that have anomalous properties. These properties are illustrated by both the ash layer already mentioned and by the marl velocity recorded at 300 mbsf. Neither of these rock types represent major components of their respective units, but they may give rise to "fast" logging velocities.

Below the décollement zone a second velocity gradient is observed, beginning at approximately 550 mbsf and a velocity near 1.70 km/s, and extending to the bottom of the hole, where velocities of 1.95 km/s were measured. The increase over this interval corresponds to the reappearance of carbonate in the sediments and may be a reflection of some amount of recrystallization as well as a porosity reduction on the order of 5%.

Formation Factor

Methods

Formation factor measurements made on core recovered from Site 671 followed the procedures outlined in the "Explanatory Notes" chapter. Measurements were made on every other section until the recovered core began to exhibit drilling disturbance.

Results

Values of the formation factor at Hole 671B are displayed vs. depth below seafloor in Figure 39 and listed in Table 12. Below Thrust A very few intervals were considered intact enough to measure resistance over a 3-cm distance. The increase in formation factor (F) with depth is typical of a compacting sedimentary section and is related primarily to the water content (porosity) of the sediments. Formation factor and water content are compared in Figure 40. The relationship agrees well with previous studies that have shown an exponential relationship between porosity and formation factor. The preliminary sedimentologic description suggests that sediment compositions are such that grain densities are fairly uniform throughout the column, allowing the use of water content and porosity almost interchangeably.

Formation factor is perhaps most useful as a comparative tool, and determinations made on cored material are most useful in conjunction with well logs. It is interesting to note, however, that the behavior of the electrical properties of the clay-rich sediments at Site 671 is markedly different than what has been observed at pelagic sediment sites in the Pacific (Wilkens and Handyside, 1985). Values of formation factor increase over

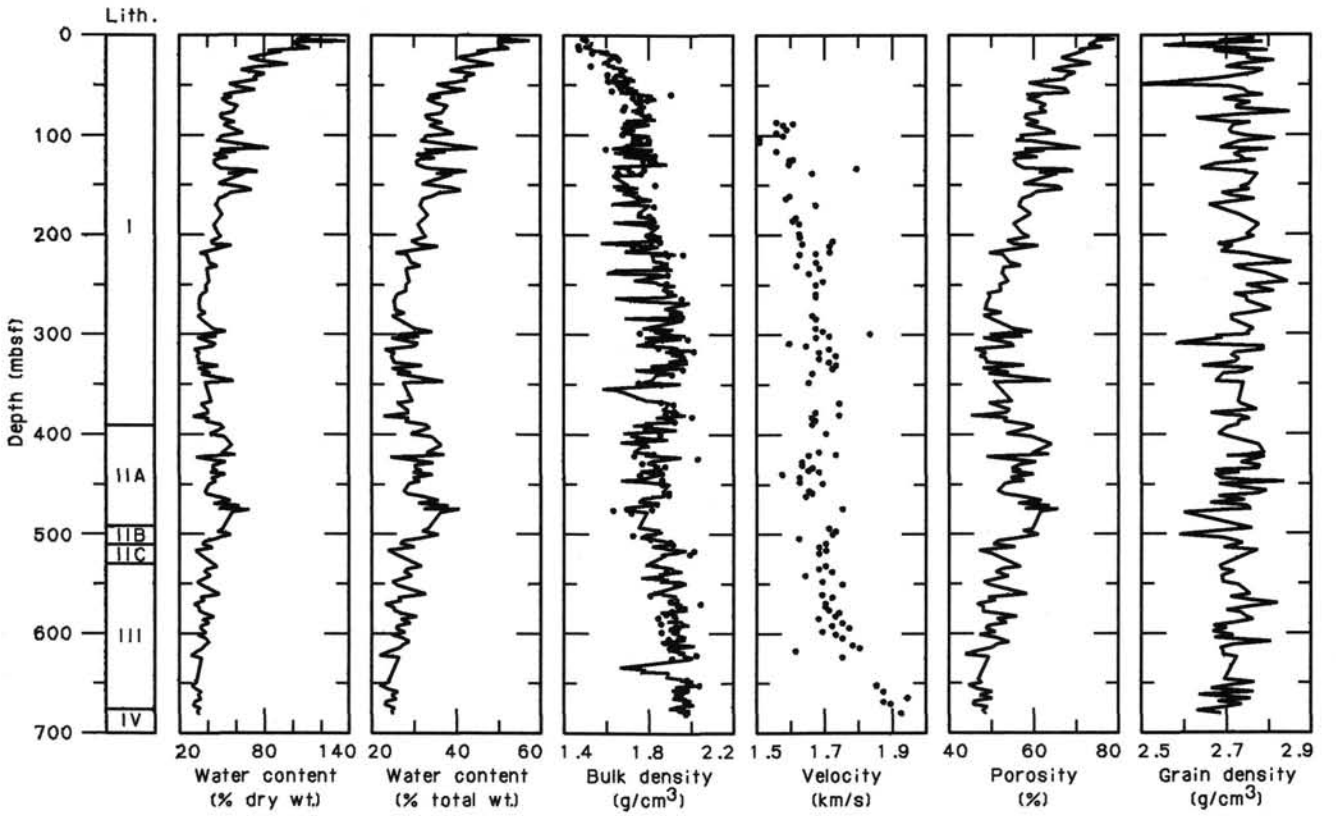

Figure 38. Summary of index properties and compressional wave velocity plotted against depth below seafloor at Hole 671B. Bulk density figure includes data from samples taken from core (points) and GRAPE data smoothed at 1.0-m intervals.

the first 100 m of core at about the same rate in both regimes, but the pelagic sediments maintain values of formation factor less than four to depths greater than 330 m. Formation factor exceeds four at Site 671 below the first major thrust fault and increases considerably below this boundary. This may result from the ability of microfossils in pelagic sediments to maintain a more open sediment framework to far greater depths than is allowed by the clay grains of Site 671.

Shear Strength

Methods

The undrained shear-strength measurements were primarily made at Site 671 using the miniature vane shear device and following procedures outlined in the "Explanatory Notes." Measurements were primarily made in the APC cores, where sample disturbance was minimal. However, some measurements were made on XCB cored samples using both the miniature vane device and the torvane.

Results

The undrained shear-strength was measured within lithologic Unit 1. Data are listed in Table 13. In the upper portion of Unit 1, the peak strength has a range of 14 to 23 kPa and no consistent trend with depth (Fig. 41). The residual strength range is small, but increases with depth from 6 to 12 kPa (Fig. 41). Assuming that the residual and the remolded strengths are equivalent (Pyles, 1984), the sediment sensitivity can be estimated. Sensitivity is defined as the ratio of peak, undrained shear strength to the remolded shear strength. In upper lithologic Unit 1, the sensitivity is low with an average value of 2. The shear-strength profile defines a break near 15 mbsf where the strength increases from 23 kPa to 39 kPa. This break in properties is also seen in the water content and density profiles.

The strength increases from 39 to 150 kPa between 15.6 and 89 mbsf and can be approximated as a linear increase with depth (Fig. 41). The residual shear strength is consistent with the peak measurements. The range of residual strengths is from 15 to 69 kPa (Fig. 41). In sediments sampled with the extended core barrel (XCB), the peak strengths decrease from 150 kPa in the APC-sampled sediments to 50 kPa over a depth of 4 m. Within the XCB-sampled zones, the peak strength increases to a maximum of 189 kPa. Above the APC/XCB sampling break, the approximate sensitivity of the sediments is between 2 and 3.

Drilling disturbance in the XCB cores limited the measurement of undrained shear strength to one vane test and four estimates of undrained strength using a Soiltest pocket penetrometer. The strength, based on the limited data, has a range of 70 to 160 kPa. However, disturbance caused by drilling procedures probably reduced the strength, yielding the low measurement values.

The total overburden (lithostatic), the hydrostatic, and the effective stress (P′) were determined for Site 671. The density of the pore fluid was assumed to be 1.025 g/cm^3. Total overburden (P) and hydrostatic stress are plotted vs. sub-bottom depth in Figure 42. The ratio of the undrained shear strength (C_u) to effective overburden stress (C_u/P') can be used as an indication of strength deviations from that expected of a normally consolidated sediment. Figure 41 has a plot of C_u/P' with sub-bottom depth for Unit 1. The deepest tests have low C_u/P' ratios (<0.2) which suggest reduced shear strengths, either from *in situ* modifications of the stress conditions (e.g., excess pore pressure) or, more probably, disturbance due to drilling.

Table 11. Compressional wave velocity in Hole 671B.

Core 110-671B-	Sec	Int (cm)	Depth (mbsf)	Vel(A)[a] (km/s)	Vel(B-C)[b] (km/s)
10	2	106	85.96	1.5700	1.5600
10	3	111	87.51	1.6000	1.6100
10	4	114	89.04	1.6000	1.5800
11	2	64	93.74	1.5800	1.5900
11	4	69	96.79	1.5300	1.5600
11	6	70	99.80	1.5400	1.5800
12	2	9	102.69	1.5700	1.5100
12	3	8	104.18	1.5500	
12	4	8	105.68	1.5400	1.5100
13	3	8	113.68	1.5600	
13	4	10	115.20	1.5500	1.5600
14	3	9	123.19	1.5900	1.6100
14	4	18	124.78	1.6000	1.6000
14	6	17	127.77	1.6000	1.6000
15	2	112	132.22	1.6100	1.8000
15	6	76	137.86		1.6700
18	2	60	160.20	1.6200	1.6000
18	4	60	163.20	1.5800	1.5900
19	2	44	169.54	1.6400	1.6800
20	4	68	182.28	1.6300	1.6200
20	6	53	185.13	1.5900	1.6100
21	2	81	188.91	1.6400	1.6300
22	2	125	198.85	1.6400	1.6300
22	4	29	200.89	1.6400	1.6300
22	7	33	205.43	1.7100	1.7300
23	3	3	208.63	1.5900	1.6400
23	4	47	210.27		1.7200
24	1	78	215.88	1.7500	1.7200
24	2	125	217.85		1.6800
24	3	47	218.57		1.6300
25	2	58	226.68	1.6900	1.6800
25	4	99	230.09	1.6400	1.6200
25	6	40	232.50	1.7100	1.6900
26	3	71	237.81	1.6300	1.6600
27	2	70	245.80	1.6800	1.7000
27	4	70	248.80	1.6800	1.6800
28	2	79	255.39	1.7100	1.5600
28	4	85	258.45	1.7100	1.6800
28	6	45	261.05	1.7000	1.6800
29	3	63	266.23	1.6400	1.5600
30	2	53	274.13	1.5700	
30	4	74	277.34	1.5800	
30	6	65	280.25	1.6600	1.6700
31	10	10	283.81	1.6900	1.6800
32	2	66	293.26	1.6700	1.6800
32	4	67	296.27	1.6900	1.7000
32	6	66	299.26	1.7800	1.8400
33	1	65	301.25	1.6900	1.7200
33	2	68	302.78	1.4500	1.6800
34	2	84	308.44		1.6000
34	4	70	311.30	1.6500	1.6500
34	6	70	314.30	1.7300	1.7200
35	2	70	317.80	1.6700	1.6900
35	4	70	320.80	1.7500	1.7400
35	6	71	323.81		1.6900
36	2	70	327.30	1.7200	1.7200
36	4	75	330.35	1.7400	1.7400
36	6	64	333.24	1.7300	1.7300
37	3	5	337.65	1.6700	
37	3	100	338.60	1.7200	1.6700
38	3	65	347.75	1.7200	1.6600
40	2	136	365.96	1.6700	
40	4	74	368.34	1.7600	1.7500
41	4	40	377.50		1.6800
42	2	69	379.89	1.7500	1.7500
41	6	58	380.68	1.7500	1.7500
42	4	64	382.84		1.6700
42	6	51	385.71	1.7000	1.6800
43	2	84	389.54		1.6700
44	2	62	398.82	1.7400	1.7100
46	2	42	417.62		1.6900
46	3	101	419.71	1.7400	
46	4	87	421.07		1.6600
46	5	12	421.82		1.5300
47	2	56	427.26		1.6400
47	4	75	430.45		1.6400
47	6	77	433.47		1.6700
48	1	94	435.64		1.6600
48	2	98	437.18		1.6900
48	4	24	439.44		1.5800
48	6	95	443.15		1.6300
49	3	16	447.36		1.6300
49	4	28	448.98		1.7000
50	2	109	456.29		1.6600
50	4	76	458.96		1.6700
50	6	55	461.75		1.6500
52	2	3	474.23	1.7500	1.7600
52	4	58	477.78	1.7200	
54	2	100	494.20		1.7200
54	4	20	496.40	1.7400	1.7400
54	6	57	499.77	1.7200	1.7300
55	2	72	503.42		1.6300
55	6	40	509.10		1.7100
56	2	40	512.60	1.7300	1.6900
56	4	68	515.88		1.7100
56	6	69	518.89		1.6900
58	2	54	531.74	1.6200	1.7100
58	4	38	534.58		1.6900
58	6	15	537.35		1.7300
59	2	65	541.35	1.6200	1.6500
59	6	70	547.40	1.6900	1.7000
60	2	56	550.76	1.7000	1.7600
61	2	66	560.36	1.6300	1.7000
61	4	76	563.46	1.7300	1.7300
62	2	40	569.60	1.6900	1.7100
62	4	66	572.86	1.6700	1.7100
62	6	145	576.65	1.6800	1.7200
63	2	70	579.40	1.7500	1.7500
63	4	85	582.55	1.6900	1.7400
63	6	53	585.23		1.6900
64	2	90	589.10	1.6400	1.7600
64	4	74	591.94	1.5900	1.7300
64	6	31	594.51	1.6700	1.7800
65	2	51	598.21	1.6500	1.7000
65	4	34	601.04	1.6600	1.7400
65	6	59	604.29	1.6700	1.7600
66	4	69	610.89	1.6900	1.7900
66	6	63	613.83	1.6800	1.8100
67	2	31	617.01	1.6700	1.6200
67	6	65	623.35	1.6900	1.7600
70	6	35	651.55	1.7500	1.8600
71	2	70	655.40	1.7300	2.5000
71	4	61	658.31	1.7200	1.8800
72	2	106	665.26		1.9500
72	4	77	667.97		1.8800
72	6	96	671.16		1.9000
73	2	62	674.32	1.7500	
73	4	60	677.30	1.7600	
73	6	77	680.47	1.7600	1.9300

[a] Calculated on basis of wet and dry measurements.
[b] Calculated on basis of dry volumetric measurements.

Thermal Conductivity

Methods

The thermal conductivity measurements for Site 671 were carried out according to the procedures outlined in the "Explanatory Notes."

Results

The thermal conductivity increases within the upper 100 m of Hole 671B from 1.0 to 1.5 W/m/°C (Table 14). The data scatter is large, with maximum changes of 0.27 W/m/°C over a depth interval of 3 m (Fig. 43). The thermal conductivity increase correlates with a decrease in water content (Fig. 44), and the trend is similar to that observed by Bullard (1980) in red clays, ooze, and mud.

The thermal conductivity between 100 mbsf and 127 mbsf decreases significantly with values as low as 0.95 W/m/°C. This

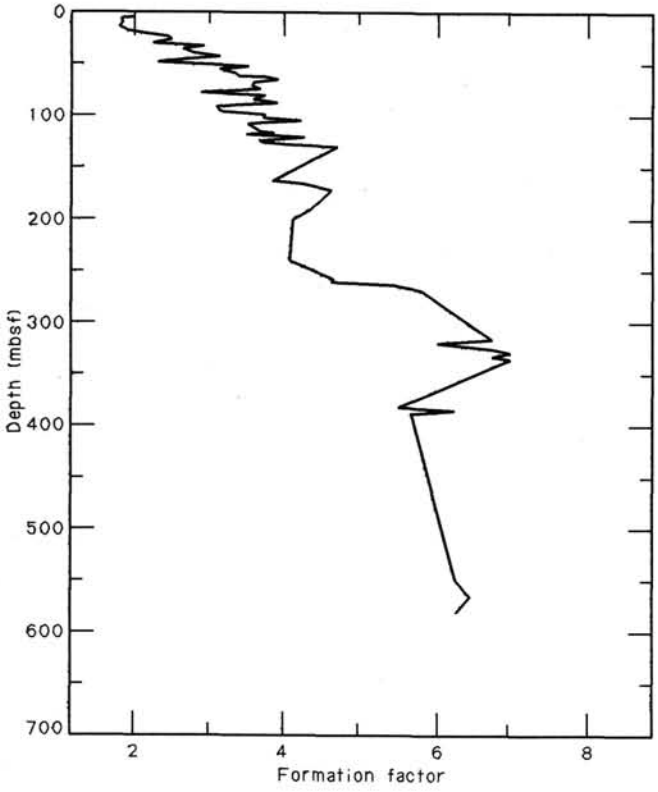

Figure 39. Formation factor vs. depth at Hole 671B. The plot represents measurements made with electrical flow parallel to the axis of the core.

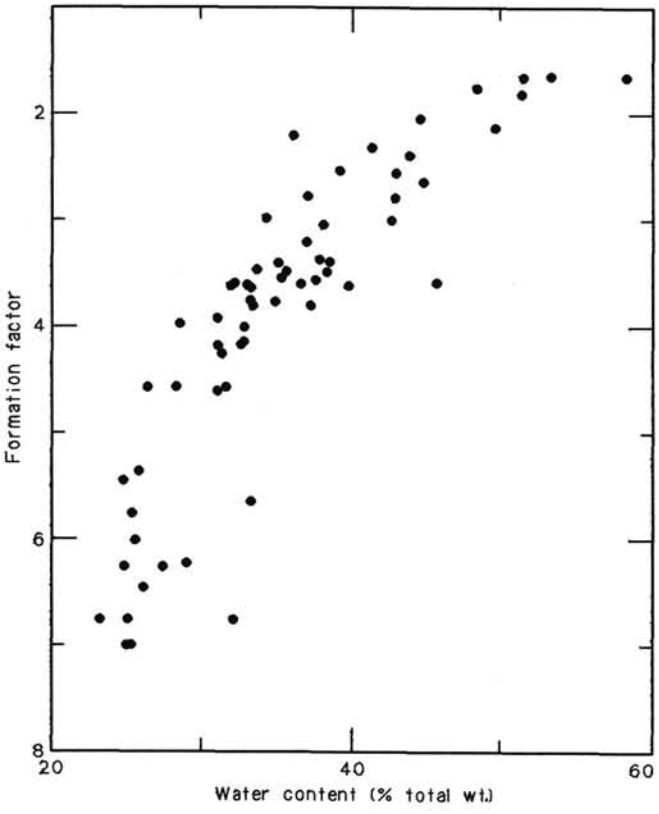

Figure 40. Water content (% wet weight) plotted vs. formation factor at Hole 671B. Measurements were made with electrical flow parallel to the axis of the core.

Table 12. Sediment formation factor in Hole 671B.

Core 110-671B-	Sect	Int (cm)	Depth (mbsf)	F-horiz	F-vert
1	3	65	3.65	1.7000	1.8100
1	4	65	5.15	1.5200	1.6500
2	2	65	9.55	1.5300	1.6500
2	4	65	12.55	1.5200	1.6400
2	6	65	15.55	1.5900	1.7600
3	2	65	19.05	1.9900	2.0400
3	3	130	21.20	2.1900	2.3300
3	4	110	22.50	2.1800	2.3200
3	6	20	24.60	2.2700	2.3900
4	2	65	28.55	1.9700	2.1300
4	4	65	31.55	2.7500	2.7900
4	6	65	34.55	2.5000	2.5300
5	2	65	38.05	2.4000	2.6400
5	4	65	41.05	2.7100	3.0000
5	6	65	44.05	2.4400	2.5600
6	2	85	47.75	2.1300	2.2000
6	4	85	50.75	3.1500	3.3800
6	6	85	53.75	2.8300	3.0000
7	2	65	57.05	3.0000	3.2000
7	4	65	60.05	3.1200	3.2800
7	4	133	60.73	3.2800	3.6000
7	6	75	63.15	3.4000	3.8000
8	2	65	66.55	3.3600	3.4800
8	4	65	69.55	3.2000	3.4800
8	6	65	72.55	3.2000	3.5600
9	2	85	76.25	2.5800	2.7700
9	4	65	79.05	3.4400	3.6300
9	6	60	82.00	3.2000	3.4600
10	2	100	85.90	3.4000	3.8000
10	3	100	87.40	3.1800	3.2400
10	4	110	89.00	2.7800	2.9800
11	2	65	93.75	2.8000	3.0400
11	4	68	96.78	3.6000	3.6100
11	6	68	99.78	3.6000	3.6100
12	2	6	102.66	3.6500	4.1300
12	3	23	104.33	3.4100	3.6100
12	4	17	105.77	3.2000	3.4000
13	2	3	112.13	3.3700	3.5800
13	3	20	113.80	3.3500	3.7500
13	4	5	115.15	3.2500	3.3700
13	6	26	118.36	3.4400	4.1700
14	2	26	121.86	3.3400	3.5400
14	3	25	123.35	3.3900	3.5900
14	4	27	124.87	3.7600	3.9200
14	6	23	127.83	4.2000	4.6000
18	2	65	160.25	3.6000	3.7600
18	4	65	163.25	3.8000	4.1600
19	2	47	169.57	4.4400	4.5600
21	2	70	188.80	3.5900	4.2500
22	2	110	198.70	3.4200	4.0000
26	3	70	237.80	3.7700	3.9700
28	2	74	255.34	4.4400	4.5600
28	4	65	258.25	4.5600	4.5600
28	6	70	261.30	4.7800	5.3500
28	6	70	261.30	4.7800	5.3500
29	3	60	266.20	4.3700	5.7500
29	3	60	266.20	4.3700	5.7500
34	6	70	314.30	6.8000	6.7500
34	6	70	314.30	6.8000	6.7500
35	2	65	317.75	5.9000	6.0000
35	2	65	317.75	5.9000	6.0000
35	6	63	323.73	6.4000	6.7500
35	6	63	323.73	6.4000	6.7500
36	2	72	327.32	6.5000	7.0000
36	2	72	327.32	6.5000	7.0000
36	4	69	330.29	6.5000	6.7500
36	4	69	330.29	6.5000	6.7500
36	6	70	333.30	6.5000	7.0000
36	6	70	333.30	6.5000	7.0000
42	2	74	379.94	5.1600	5.4400
42	2	74	379.94	5.1600	5.4400
42	4	70	382.90	4.9600	6.2200
42	4	70	382.90	4.9600	6.2200
42	6	80	386.00	6.4300	5.6300
43	2	70	389.40	4.7200	5.6400
59	6	70	547.40	6.2500	6.2500
61	4	77	563.47	1.0000	6.4500
63	2	70	579.40	4.5600	6.2500

Table 13. Vane shear strength at Hole 671B.

Core 110-671B-	Sect	Int (cm)	Depth (mbsf)	Peak (kPa)	Residual (kPa)
1	3	70	3.70	14.5200	6.4400
1	4	70	5.20	20.2900	8.9900
1	5	15	6.15	19.8300	7.9700
2	2	70	9.60	14.5200	8.0800
2	4	73	12.63	20.6300	9.1900
2	6	30	15.20	22.6000	12.9100
2	6	70	15.60	39.4400	14.7500
3	2	70	19.10	32.2700	13.8400
3	4	115	22.55	28.8200	18.4300
3	6	20	24.60	48.4300	17.2900
4	2	70	28.60	55.3200	11.5300
4	4	70	31.60	57.6400	29.9700
4	6	70	34.60	78.3800	36.9000
5	2	90	38.30	71.4800	39.1900
5	4	70	41.10	59.9500	18.4500
5	6	70	44.10	76.0900	29.9800
6	2	90	47.80	103.8000	29.9800
6	4	90	50.80	87.6200	36.9000
6	6	90	53.80	110.7000	39.1900
7	2	70	57.10	50.7200	29.9800
7	4	70	60.10	117.6000	41.5000
7	4	130	60.70	145.3000	47.2700
7	6	70	63.10	106.1000	46.1100
8	2	70	66.60	78.3800	38.0300
8	4	70	69.60	99.1400	40.3500
8	6	70	72.60	129.1000	124.5000
9	2	90	76.30	96.8200	23.0500
9	4	70	79.10	136.0000	53.0300
9	6	65	82.05	108.4000	62.2500
10	2	110	86.00	156.8000	10.0000
10	3	115	87.55	147.5000	
10	4	114	89.04	149.9000	69.1700
11	2	70	93.80	50.7200	32.2700
11	4	75	96.85	83.0100	11.0000
11	6	75	99.85	96.8300	
12	2	15	102.75	147.5100	12.0000
12	3	14	104.24	131.4000	
12	4	15	105.75	106.1000	13.0000
13	2	15	112.25	54.1900	
13	3	15	113.75	122.7000	13.0000
13	4	15	115.25	99.6000	
13	6	15	118.25	166.0000	14.0000
14	2	15	121.75	142.9000	
14	3	15	123.25	157.9000	14.0000
14	4	15	124.75	162.5000	
14	6	15	127.75	189.1000	18.0000
18	2	70	160.30	88.7700	
18	4	70	163.30	96.8300	21.0000
21	2	80	188.90	169.5000	

zone is immediately above the upper major fault zone. The measurements may have also been influenced by drilling disturbance induced by XCB coring.

Thermal conductivity increases below 127 mbsf to a maximum of 1.71 W/m/°C at 218 mbsf (Fig. 43). The conductivity measurements are greatly scattered within this interval. Below 220 mbsf, the conductivity decreases, with less scatter, to the base of Unit 2-A. Within Tectonic Package B the conductivity shows a higher sensitivity to changes in water content than in the overlying package (Fig. 44).

Thermal conductivity increases from 503 mbsf to a maximum of 2.14 W/m/°C at 532 mbsf (Fig. 43). Below this maximum, the conductivity shows very little change with depth below the seafloor to the bottom of the hole. The correlation with water content within the lower tectonic packages is different from that of the upper packages and shows the largest variation in conductivity over small changes in water content (Figure 43).

Summary

The results of physical-property measurements at Site 671 are perhaps as interesting for their lack of extraordinary revelations as for any positive conclusion that can be drawn from them. A plot of compressional wave velocity vs. water content is presented in Figure 45. In general, the shallowest sediments measured by the Hamilton Frame are the highest in water content and lowest in velocity. At the bottom of the hole, samples from Units 3 and 4 exhibit the highest velocities, although they do not have considerably lower water contents than other sediments that overlie them. Most of the samples from 100 mbsf to almost the base of Unit 3, seem to be fairly homogeneous in both velocity and water content and are most remarkable in the fact that they do not have a more well-defined velocity-water content trend.

A second noncorrelation considers compressional wave velocity and composition. A plot of carbonate content vs. V_p (Fig. 46) demonstrates that both carbonate-rich and non-carbonate-rich units appear to have the same span of velocity values. Barring water content as a strong velocity control (Fig. 45) it remains to be seen exactly what systematics will be revealed during further examination of the data.

An interesting comparison can be made between the water content and composition of the Pliocene sections above and below Thrust A. These data are shown in Figure 47. The loss of water in the buried section can clearly be seen when compared to sediments above which both have the same age and composition. Still, it remains somewhat of a surprise that so much of the integrity of the lower section of Pliocene sediments has been maintained during the thrusting process.

Finally, in terms of seismic discontinuities, there would appear to be two areas which should definitely produce reflections, one at Thrust A, owing to the rather abrupt change in density as the section is repeated, and the other in the lower part of Unit 3, where the density perhaps shows some slight increase and the velocity exhibits a substantial jump. At the décollement, there is a decrease in porosity (and increase in density) that might also produce a reflector, and several excursions of density values at approximately 300, 400, and 450 mbsf are likely candidates. Perhaps the most interesting observation is that, with the exception of the base of Unit 3, the reflection record is dominated by density contrasts rather than velocity changes.

LOGGING RESULTS

After logging efforts in Hole 671B failed because of an impenetrable hole restriction just above the décollement, operations to measure *in situ* physical properties of the Barbados accretionary wedge moved to Hole 671C, which was drilled to 522 mbsf specifically for packer and logging experiments. Logging measurements discussed below indicate that the true mudline depth for Hole 671C was 4940 m rather than 4947 m as indicated by the drilling records, so sub-bottom depths throughout this section are referred to a water depth of 4940 m. Before logging, the pipe was set at 138 mbsf, but after the first tool string encountered a bridge just below the drill pipe, the pipe was raised 28 m, which allowed 23 m of measurements in the open hole. A continuous log was made from the bridge up through the pipe to the mudline. Poor hole conditions precluded any further experimentation.

The logging tool string run in Hole 671C was the standard Schlumberger Ocean Drilling Program first logging run, the DIL-LSS-GR-CAL, which provides measurements of formation resistivity (DIL), sonic velocity (LSS), and natural radioactivity (GR), along with a measurement of hole diameter (CAL). The dual induction log (DIL) combination includes the simultaneous recording of three focused resistivity measurements, each with a different diameter of investigation. Two of the measurements are obtained from induction devices (induction log Deep or ILD and induction log Medium or ILM) and the third from a

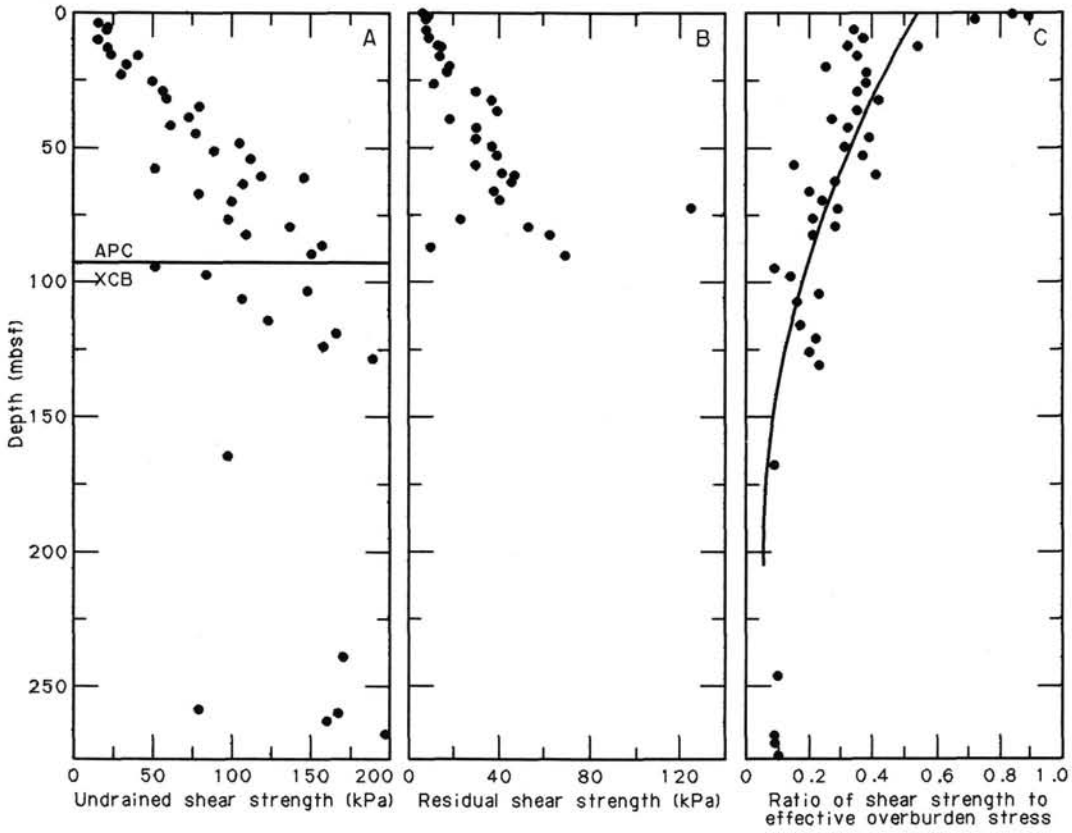

Figure 41. Undrained and residual shear strengths, and ratio of shear strength to effective overburden stress, vs. depth for Hole 671B.

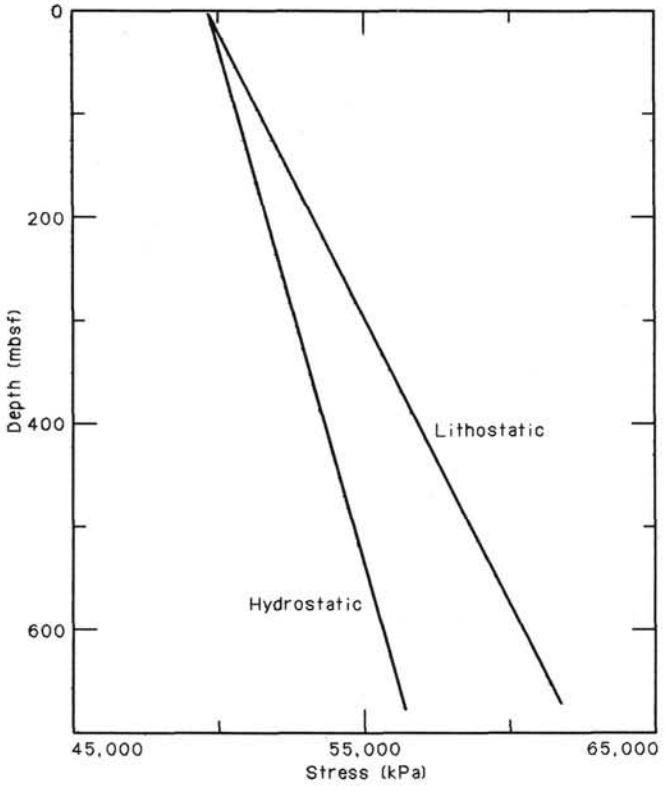

Figure 42. Total lithostatic and hydrostatic stress calculated from bulk density determinations vs. depth for the sediment column at Hole 671B.

shallow investigating focused device (spherical focused log or SFL). The long spacing sonic (LSS) utilizes a two-source-two-receiver combination to yield two estimates of sonic travel time over distance of 8, 10, and 12 ft. Two logs are generated, the DT-log (short-spacing slowness) and DTL-log (long-spacing slowness), each measuring the travel time for 2 ft of formation but with different depths of investigation. Complete sonic waveforms can also be recorded during an LSS run. The gamma-ray tool (GR) makes an integrated measurement of the natural radioactivity (mainly K, Th, U) of the formation, and the three-arm caliper (CAL) measures hole size up to a diameter of 15 in. The logging curves are listed in Table 15. A full description of the operating principles of these tools can be found in the downhole measurement report of the Leg 102 *Proceedings*, Volume A, or in any standard logging reference.

Results

Figure 48 displays the results of the logging run. The gamma-ray and caliper curves are in track 1. (Tracks are numbered from left to right.) The deep induction curve (ILD), the medium induction curve (ILM), and the spherically focused curve (SFLU) are in track 2, and the DT and DTL curves of the long spacing sonic are in track 3. As noted previously, only the interval between 110 and 132 mbsf (5050 and 5072 m) was logged in open hole. Some of the curves fail to cover the entire open hole interval because of offsets in the position of various tools on the string. The upper part of the hole, between 110 and 0 mbsf (5050 and 4940 m) was logged through the drill pipe, in which the resistivity and sonic tools cannot measure formation properties. Except for the cores retrieved for stratigraphic position, Hole 671C was not cored; the only core correlations available are those from Hole 671B. The water depth of Hole 671B was

Table 14. Thermal conductivity, Hole 671B.

Core 110-671B-	Sec	Int (cm)	Depth (mbsf)	Cal/cm·°C·s ($\times 10^{-4}$)	W/m °C
1	2	70	2.20	25.5100	1.0680
1	3	70	3.70	25.2100	1.0550
2	2	70	9.60	25.7300	1.0770
2	4	70	12.60	24.2800	1.0160
3	2	70	19.10	27.3500	1.1450
3	4	120	22.60	28.3000	1.1850
3	6	20	24.60	27.7700	1.1620
4	2	70	28.60	25.2400	1.0560
4	4	70	31.60	28.5700	1.1960
4	6	70	34.60	28.9500	1.2120
5	2	70	38.10	28.7500	1.2030
5	4	70	41.10	28.1600	1.1790
6	2	90	47.80	24.4700	1.0240
6	4	90	50.80	28.7200	1.2020
6	6	90	53.80	27.5000	1.1510
7	2	70	57.10	30.1200	1.2610
7	4	70	60.10	28.9300	1.2110
7	6	70	63.10	32.1000	1.3430
8	2	70	66.60	29.9700	1.2540
8	4	70	69.60	30.5200	1.2770
8	6	70	72.60	25.4600	1.0660
9	4	70	79.10	32.1900	1.3480
9	6	70	82.10	31.7200	1.3280
10	2	115	86.05	24.5100	1.0260
10	3	115	87.55	27.4700	1.1500
10	4	115	89.05	29.3800	1.2300
11	2	70	93.80	35.9600	1.5050
11	4	70	96.80	32.7600	1.3710
11	6	70	99.80	32.7500	1.3710
12	2	15	102.75	28.5500	1.1950
12	3	15	104.25	25.2700	1.0580
12	4	15	105.75	27.0100	1.1310
13	2	15	112.25	22.7900	0.9540
13	3	15	113.75	22.7300	0.9520
13	4	15	115.25	24.9500	1.0450
13	6	15	118.25	22.7700	0.9530
14	2	15	121.75	28.3100	1.1850
14	3	15	123.25	27.8300	1.1650
14	4	15	124.75	27.4800	1.1500
14	6	15	127.75	26.0000	1.0890
15	2	70	131.80	40.2700	1.6860
17	2	70	150.80	24.8900	1.0420
17	4	70	153.80	21.4900	0.8990
17	6	70	156.80	26.9500	1.1280
18	2	70	160.30	33.7400	1.4120
18	4	110	163.70	33.3100	1.3940
20	2	70	179.30	31.0900	1.3010
20	4	70	182.30	25.3800	1.0620
20	6	70	185.30	33.2500	1.3920
21	2	75	188.85	38.0800	1.5940
22	2	125	198.85	33.3100	1.3940
22	4	125	201.85	35.7900	1.4980
23	3	40	209.00	25.6000	1.0720
23	4	40	210.20	25.2400	1.0560
24	1	120	216.30	33.5700	1.4050
24	2	100	217.60	38.4900	1.6110
24	3	40	218.50	40.9900	1.7160
25	2	50	226.60	39.4400	1.6510
25	4	100	230.10	37.6700	1.5770
25	6	40	232.50	38.8800	1.6280
27	1	80	244.40	29.3000	1.2270
27	2	70	245.80	31.8200	1.3320
27	3	70	247.30	30.8100	1.2900
28	2	70	255.30	34.6500	1.4500
28	4	70	258.30	37.7700	1.5810
29	3	70	266.30	34.4700	1.4430
30	2	55	274.15	35.9800	1.5060
30	4	70	277.30	38.7700	1.6230
30	6	70	280.30	37.5700	1.5730
32	2	70	293.30	33.3100	1.3940
32	4	70	296.30	29.6900	1.2430
32	6	70	299.30	35.8900	1.5020
33	2	70	302.80	37.4200	1.5660
34	2	70	308.30	30.4800	1.2760
34	4	70	311.30	34.5800	1.4480
34	6	70	314.30	37.2000	1.5570
35	2	70	317.80	34.7100	1.4530
35	4	112	321.22	37.2600	1.5600
35	6	70	323.80	36.0600	1.5090
36	2	70	327.30	37.2600	1.5600

Table 14 (continued).

Core 110-671B-	Sec	Int (cm)	Depth (mbsf)	Cal/cm·°C·s ($\times 10^{-4}$)	W/m °C
36	4	70	330.30	32.8000	1.3730
36	6	73	333.33	37.0100	1.5490
38	1	60	344.70	31.1100	1.3020
38	2	57	346.17	29.2900	1.2260
38	3	60	347.70	32.2300	1.3490
40	2	118	365.78	31.7200	1.3280
40	3	63	366.73	29.3000	1.2260
40	4	50	368.10	32.4500	1.3580
41	2	50	374.60	31.1000	1.3020
41	4	40	377.50	36.3000	1.5190
42	2	68	379.88	32.5600	1.3630
41	6	60	380.70	30.9000	1.2930
42	4	68	382.88	33.8600	1.4170
42	6	68	385.88	31.8200	1.3320
43	2	70	389.40	30.5600	1.2790
43	4	70	392.40	29.8400	1.2490
44	2	65	398.85	30.1200	1.2610
44	4	70	401.90	30.2500	1.2660
45	2	70	408.40	29.1600	1.2210
46	2	70	417.90	30.0700	1.2590
47	2	70	427.40	31.7800	1.3300
47	4	90	430.60	30.7800	1.2890
48	2	92	437.12	29.2400	1.2240
48	4	111	440.31	31.0000	1.3020
48	6	68	442.88	32.6700	1.3670
49	2	31	446.01	24.9000	1.0420
49	2	83	446.53	31.8900	1.3350
49	4	41	449.11	31.4000	1.3140
50	2	115	456.35	32.9500	1.3790
50	4	75	458.95	32.7300	1.3700
50	6	35	461.55	30.6900	1.2850
51	2	128	465.98	30.2800	1.2670
51	4	116	468.86	31.1400	1.3030
51	6	73	471.43	27.9900	1.0450
52	2	75	474.95	29.0600	1.2160
52	3	70	476.40	30.0200	1.2570
54	2	60	493.80	30.6400	1.2820
54	4	60	496.80	31.8300	1.3320
54	6	60	499.80	30.4700	1.2760
55	2	70	503.40	28.7400	1.2030
55	4	70	506.40	31.0800	1.3010
55	6	40	509.10	32.8800	1.3760
56	2	70	512.90	35.6500	1.4920
56	4	70	515.90	42.1900	1.7660
56	6	70	518.90	34.7700	1.4550
58	2	87	532.07	51.0200	2.1360
58	4	66	534.86	45.1700	1.8910
58	6	20	537.40	45.2500	1.8940
59	2	75	541.45	30.9200	1.2940
59	4	68	544.38	29.7500	1.2450
59	6	70	547.40	37.5600	1.5720
61	2	70	560.40	30.7400	1.2870
61	4	70	563.40	36.2100	1.5160
61	6	70	566.40	31.5300	1.3200
62	2	70	569.90	31.2000	1.3060
62	4	70	572.90	32.2300	1.3490
62	6	70	575.90	29.9500	1.2540
63	2	60	579.30	37.4600	1.5680
63	4	60	582.30	35.9400	1.5040
63	6	80	585.50	29.8500	1.2490
64	2	70	588.90	23.2200	0.9720
64	4	70	591.90	26.4400	1.1070
64	6	40	594.60	28.8900	1.2090
65	2	50	598.20	26.7100	1.1180
65	4	70	601.40	31.6400	1.3240
65	6	70	604.40	32.5400	1.3620
66	2	60	607.80	32.2900	1.3510
66	4	60	610.80	30.4200	1.2730
67	2	70	617.40	32.5300	1.3620
67	4	70	620.40	41.9800	1.7570
67	6	70	623.40	31.3000	1.3100
70	2	65	645.85	36.0500	1.5090
70	4	70	648.90	33.8100	1.4150
71	2	75	655.45	33.3000	1.3940
71	4	60	658.30	31.6600	1.3250
71	6	70	661.40	33.3100	1.3940
72	2	60	664.80	31.7800	1.3300
72	4	60	667.80	33.6900	1.4100
72	6	60	670.80	36.4000	1.5230
73	2	70	674.40	34.7600	1.4550
73	4	70	677.40	34.1200	1.4280

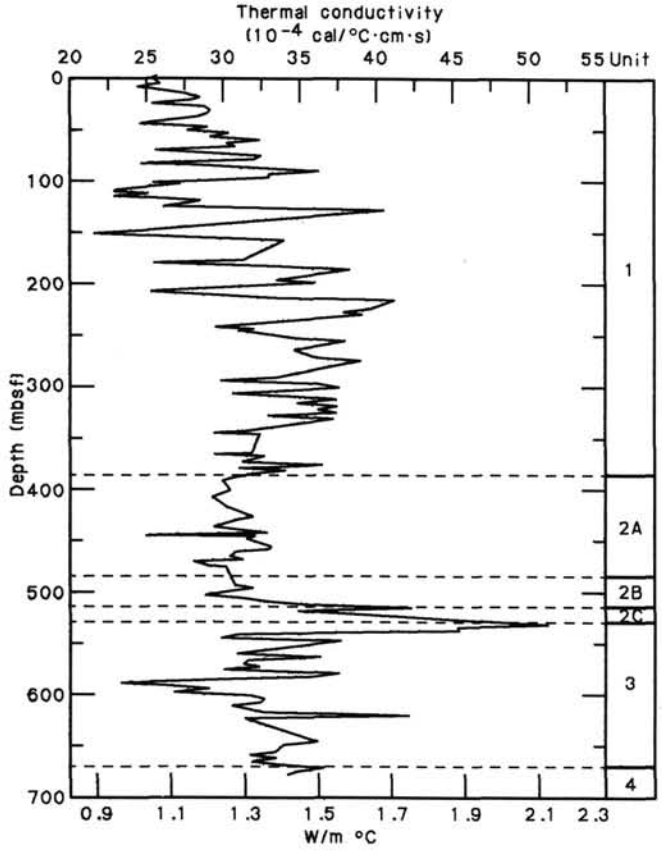

Figure 43. Thermal conductivity vs. depth at Hole 671B.

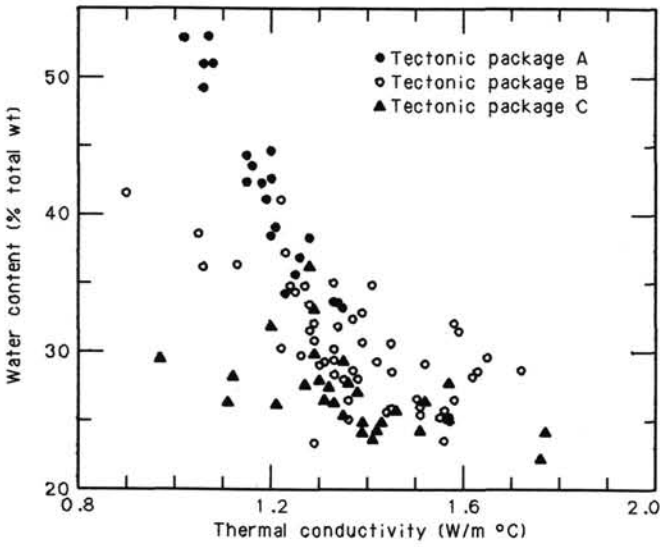

Figure 44. Thermal conductivity vs. water content at Hole 671B.

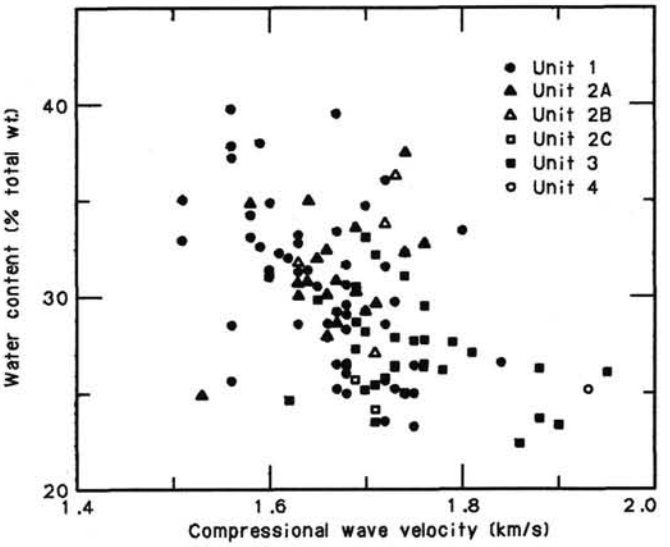

Figure 45. Compressional wave velocity vs. water content at Hole 671B.

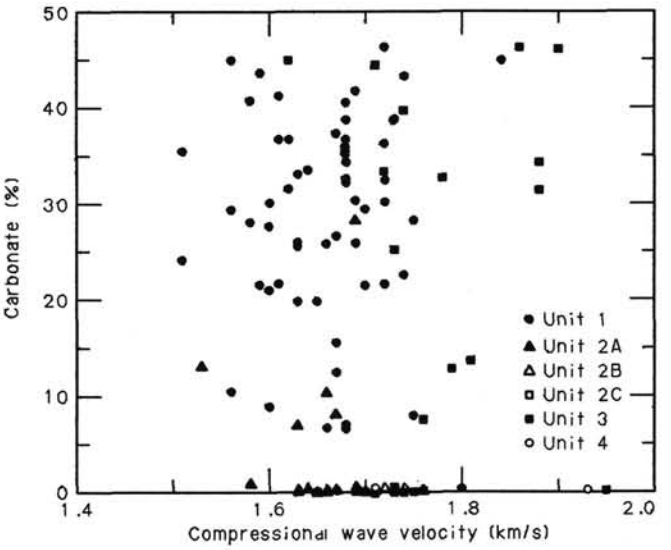

Figure 46. Compressional wave velocity vs. carbonate content at Hole 671B. Many intervals were almost totally lacking in carbonate.

4942 m, which is close to the 4940 m found from logging of Hole 671C. Assuming that the cores from Hole 671B are representative of Hole 671C, the logged interval would correspond to Cores 110-671B-13X through 110-671B-15X. The relative depths and recoveries of these cores are indicated on Figure 48. Note that this interval includes a thrust fault juxtaposing upper Miocene on lower Pleistocene sediments (see "Biostratigraphy" section, this chapter). The Caliper trace shows that, except for one 9-in. constriction, the hole diameter was close to the bit size (10.5 in.) and the amount of background radiation, shown in the gamma-ray trace, falls between 30 and 50 American Petroleum Institute (API) units, a value somewhat low for the large clay content of the formation.

Of the three resistivity logs, ILM and ILD match closely in value between 1 and 3 ohm-m, but SFLU reads approximately a factor of 3 lower. This is owing to the limited depth of investigation of the SFL (more of the signal comes from the low resistivity of the borehole fluid). The induction logs are usually best suited to drilling fluids of high resistivity (e.g., fresh-water muds or mud with moderate conductivity), but in this case the low resistivity of the formation (owing to high porosity) compensates for the use of seawater as a drilling fluid. The accuracy of the ILM and ILD measurements is confirmed by a quick comparison of log-derived formation factors ($F = R_o/R_w$ where F = formation factor, R_o is the resistivity of the fully saturated formation, and R_w is the resistivity of the formation fluid. Note that this expression neglects the conductivity of excess mobile

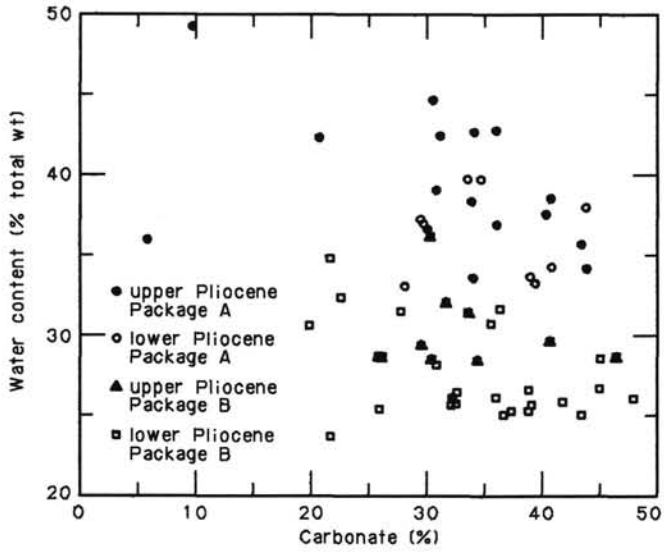

Figure 47. Water content–carbonate content relationship for the repeated Pliocene section at Site 671B.

Table 15. Summary of logged curves.

Run-1 (LLS-DIL-GR)		
Acronym	Designation	Units
Cali	3-arm caliper	inches
GR	gamma ray	GAPI
ILD	deep induction log	ohm*m
ILM	medium induction Log	ohm*m
SFL	spherically focused log	ohm*m
DT	delay time (sonic)	μs/ft
DTL	delay time long spacing (sonic)	μs/ft

ions held in solution near the surface of the clay particles) with the shipboard measurements at this depth in Hole 671B. According to the physical properties laboratory measurements, the formation factor varies in the range from 4.5 to 6.5 (see "Physical Properties" section, this chapter). Using an estimated seawater resistivity of 0.4 ohm-m, F determined from the SFL ranged from 1 to 2.5, whereas F determined from the ILD ranged from 3 to 7, confirming the accuracy of the ILD.

In Figure 48, the DT curve indicates slowness values of approximately 215 μs/ft (velocity = 1.42 km/s). Since the slowness of water at this temperature and depth is approximately 195 μs/ft (velocity = 1.56 km/s), the DT values are clearly erroneous. The error results from the narrowness of the logging interval, because the short-spacing measurement geometry has not begun to record actual arrivals before entering the drill pipe. For the large-spacing slowness measurement (DTL), most of the readings vary between 192 μs/ft (velocity = 1.60 km/s) and 170 μs/ft (velocity = 1.79 km/s), results that are consistent with physical-properties measurements.

Little else can be said about the logging results from this hole because of the lack of a significant amount of data. However, if we assume that all the depths are correct and that few variations occur between Holes 671B and 671C, then the thrust fault observed in Hole 671B corresponds to a sub-bottom depth of about 128 m in Hole 671C (about 5068 m on the log, see Fig. 48). The general decrease in the resistivity, recorded at about 5063 m (see Fig. 48), could correspond to this fault, but the question cannot be resolved because the dual induction log was the only tool operating at this depth. A large wash-out in the borehole is a more likely explanation.

SEISMIC STRATIGRAPHY

The IFP-IFREMER site survey of DSDP Leg 78A and ODP Leg 110 was shot in 1976 and partly processed in 1980 (Lines A1A to A1F, Figure 6, Chapter 1, this volume; Ngokwey et al., 1984). The quality of the processed data was good but only very few reflectors, and of uncertain origin, were recorded in the accretionary complex. Furthermore, the location of the lines was bad as very few satellite fixes were available at that time. As a result of navigation limitations, errors up to 1.5 mi were noted once more accurate data became available. The seismic correlations and hole projections on lines A1A to A1F must thus be considered with caution. Lines A1A to A1F were shot near line A3 that was part of an earlier CEPM 1973 survey of the Lesser Antilles forearc. Reprocessing of line A3 in 1986 greatly improved the quality of this profile; for the first time arcward dipping reflectors were clearly defined in the accretionary complex. This realization led to the reprocessing of the line CRV 128, a high-resolution seismic profile shot in 1982 by IFP and ELF-Aquitaine as part of a large research program that also included the Seabeam coverage shown on Figure 1 and the profile CRV 001 shot in 1980 (Valery et al., 1985). The reprocessed line CRV 128 also shows clear evidence of arcward dipping reflectors in the accretionary complex and its relatively good positioning allows correlations with the nearby DSDP Sites 541 and 542 as well as with the ODP Site 671 that was drilled close to shotpoint 450.

Site 542 is located 1.5 km west of the deformation front and about 1.3 km south of line CRV 128, where it would project to shotpoint 350 (if we assume that the structural trends are North–South, i.e., parallel to the deformation front) (Figs. 1, 2 and 49, this chapter). Although no significant change in the physical properties was encountered in the Hole 542 cores, a few weak westward dipping reflectors appear on the seismic section. Their apparent dip is about 12 degrees when an interval velocity of 1700 m/s is used for the depth conversion. This dip is quite similar to the average bedding dip of 16–17 degrees measured in the cores. Thus the dip of the westward dipping reflectors is close to the true dip of accreted sequences and probably to one of the bounding faults. Site 542 ended in a major thrust zone that correlates fairly well with the first dipping reflector outcropping at the morphologic expression of the deformation front. This fault represents the presently active frontal thrust (T1) at the base of the youngest accreted package (P1). Other dipping reflectors can be observed at a shallower depth that originate from the foot of a prominent scarp on the seabottom topography. We interpret the shallower reflectors as the trace of thrust fault T2 located at the base of the second accreted package P2. A fault, inferred from stratigraphic evidence to be between 183 and 202 mbsf (Bergen, 1984), could be correlated with T2, although it appears to be slightly deeper than the corresponding reflectors. Alternatively, T2 could be located somewhere in the uncored section between 100 and 150 mbsf. In such a case, the fault observed in the core would be a secondary one.

Site 541 is located 3.5 km west of the deformation front and about 1 km south of line CRV 128, where it would project to shotpoint 430 (Figs. 1 and 2, this chapter, and Fig. 50). The average dip of seismic reflectors in this area is about 13–15° while the average bedding dip in Hole 541 is 20°. Hole 541 ended at 459 mbsf in what is obviously the main décollement, D, on the seismic records. The conspicuous thrust fault at 276 mbsf can be correlated with a set of dipping reflectors that outcrop on the seafloor close to the foot of a small scarp. These reflectors are therefore interpreted as the trace of the thrust T3 over which the tectonic package P3 has been accreted.

Site 671 is located 4 km west of the deformation front and at shotpoint 465 on line CRV 128. Figure 51 shows the correlation

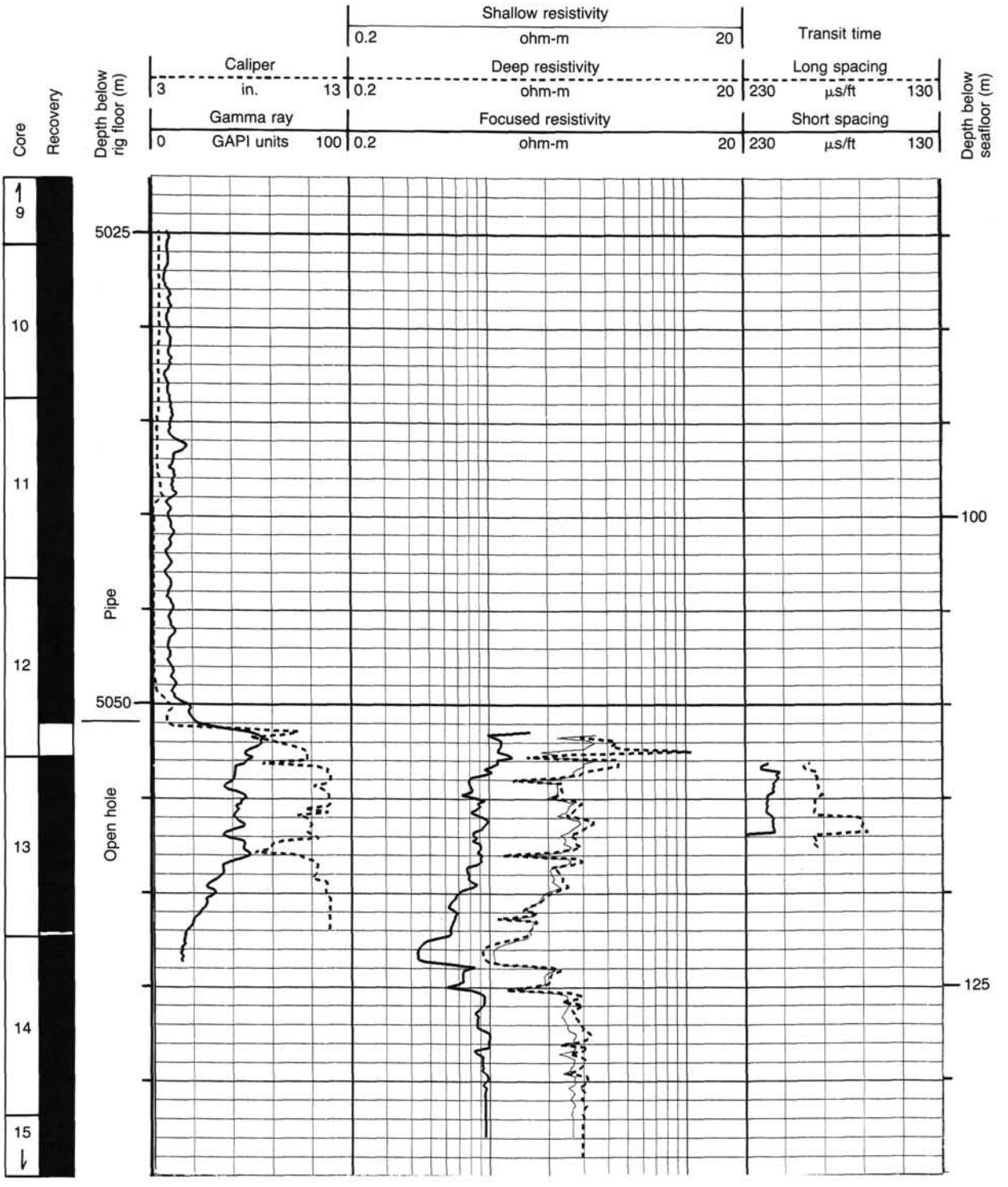

Figure 48. Results of the logging run in Hole 671C. The gamma-ray (GR) and caliper curves are in track 1. The deep induction curve (ILD), the medium induction curve (ILM), and the spherical focused curve (SFL) are in track 2. The DT and DTL curves of the long spacing sonic are in track 3. The position of the drill pipe and the location of cores are also recorded on the figure.

of the seismic record with the bulk density and velocity diagrams. Hole 671B successfully drilled through the décollement (D) that separates the accreted sequence (above) from the underthrust one (below). The décollement appears as a major reflector probably related to the observed increase in density between the overlying and underlying beds. A few discontinous, westward dipping reflectors are recorded in the accreted sequence. Thrust A corresponds to a decrease of the average density and is correlated with the strongest of these reflectors. Thrust A, however, is steeply dipping (50°) at Hole 671B. This dip is in contradiction with the average dip of seismic reflectors (15°). We maintain our initial interpretation that these reflectors are the expres-

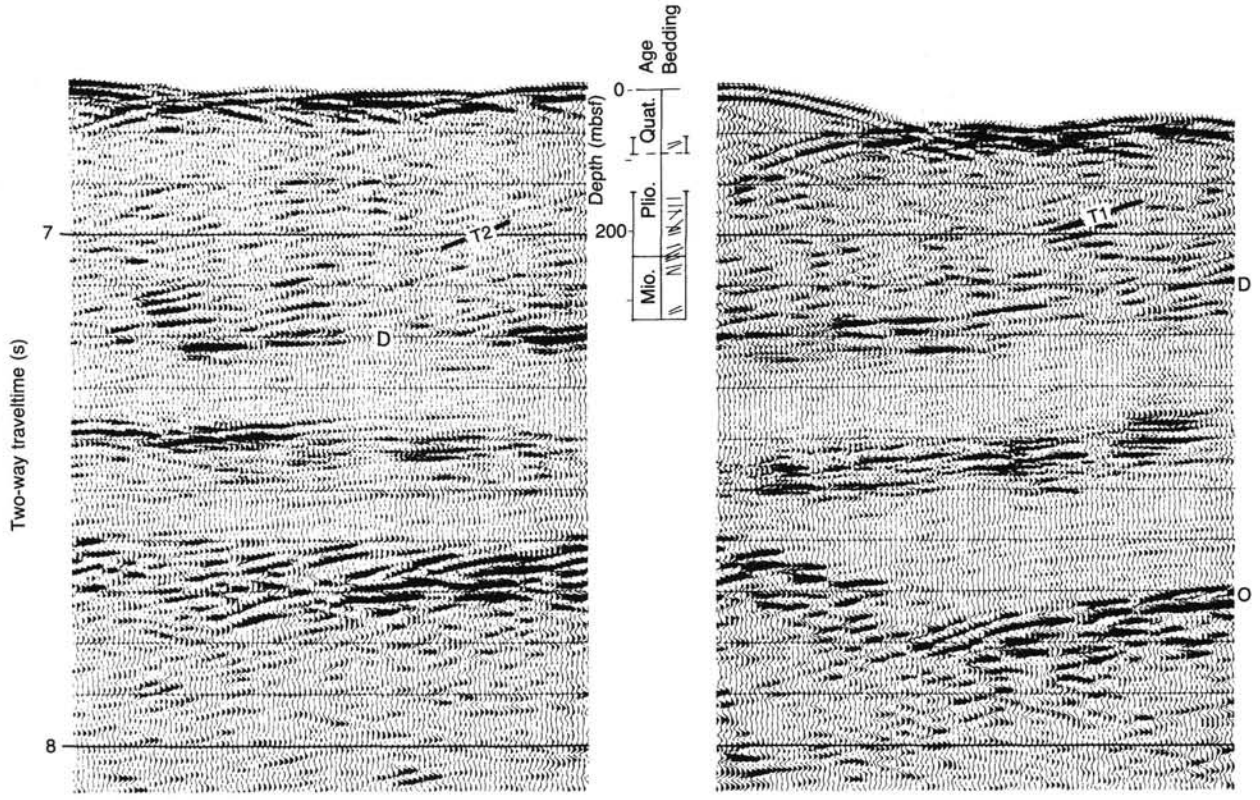

Figure 49. Seismic reflection line CRV 128 (shotpoints 290 to 390) and projection of DSDP Hole 542 (from Biju-Duval, B., Moore, J. C. et al., 1984). T1: Thrust; T2: Thrust; D: Décollement; O: Top of oceanic crust.

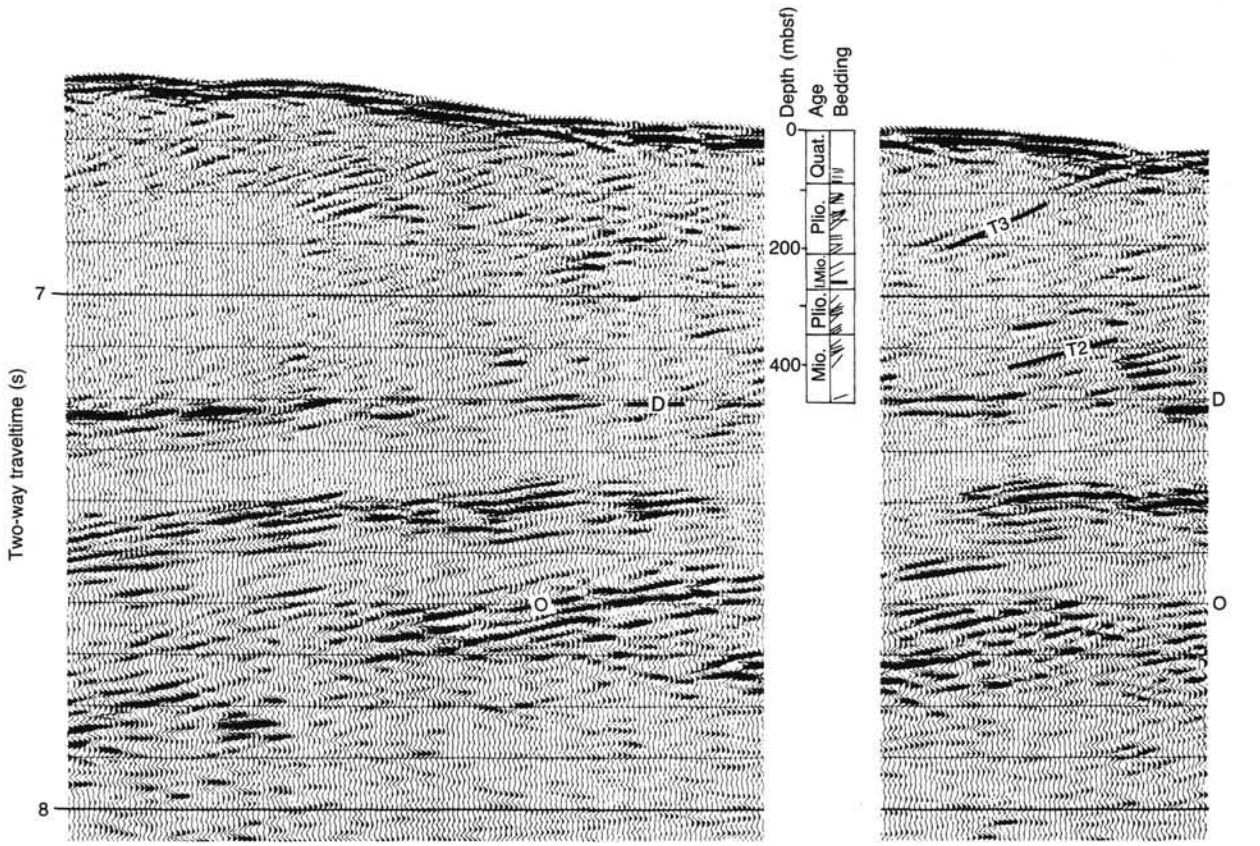

Figure 50. Seismic reflection line CRV 128 (shotpoints 350 to 450) and projection of DSDP Hole 541 (from Biju-Duval, B., Moore, J. C. et al., 1984). T2: Thrust; T3: Thrust; D: Décollement; O: Top of oceanic crust.

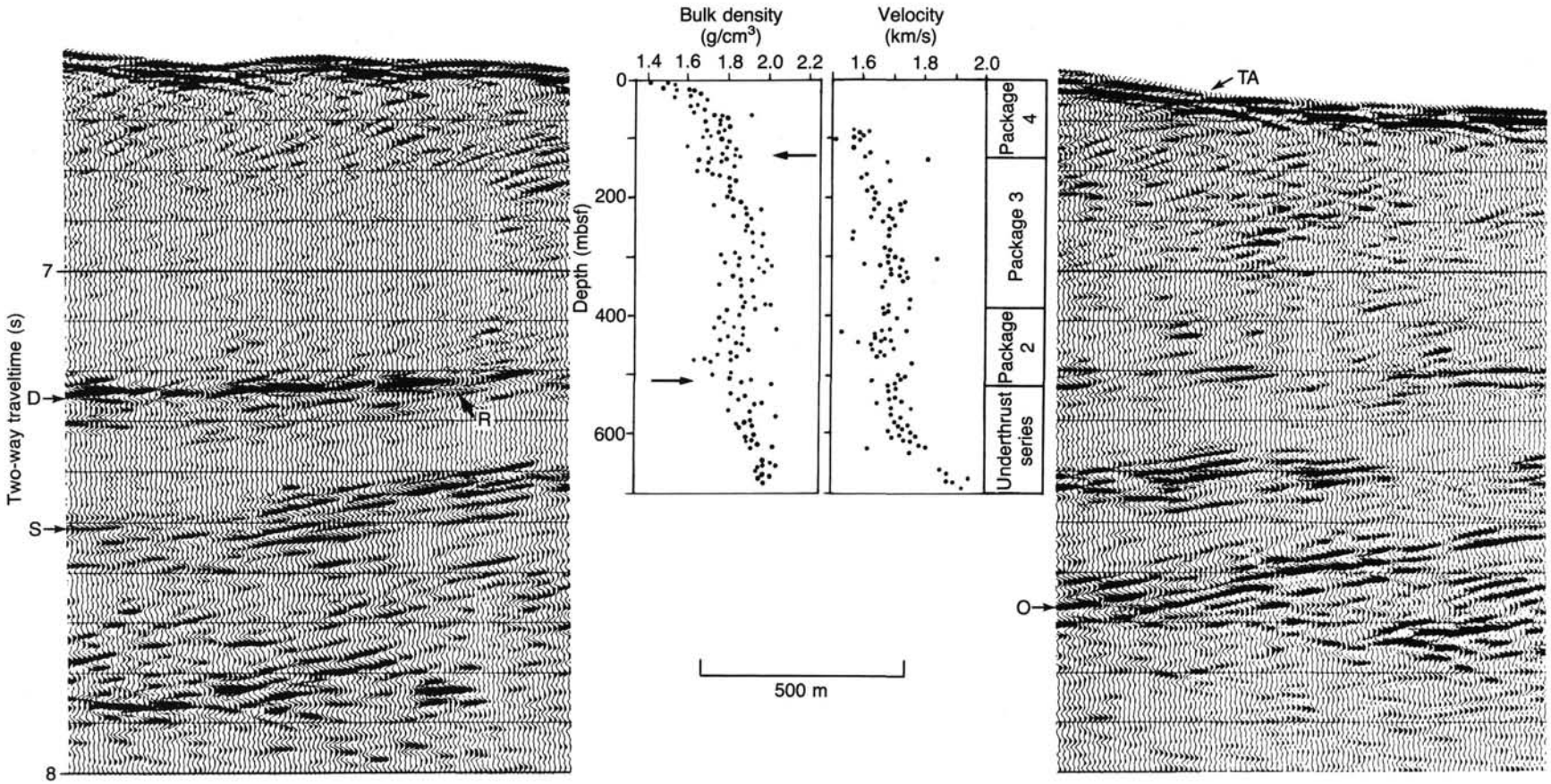

Figure 51. Seismic reflection line CRV 128 (shotpoints 430 to 490) and ODP Site 671, including the density and velocity diagrams. TA: Thrust A; D: Décollement; S: Top of the sand layer; O: Top of the oceanic crust. R: Truncated reflector.

sion of the average thrust faults and bedding dips in the accreted packages. We explain this apparent inconsistency as follows: (a) the steep dip of Thrust A measured in the core could be owing to local steps or ramps as the fault is progressing seaward, or (b) alternatively it could be related to subsequent small-scale folding of the fault plane when younger packages are accreted below.

The calcareous and noncalcareous muds which constitute most of the accreted sequences (lithologic Units 1 to 2-A in Tectonic Packages A, B, C, and D) have a quite homogenous velocity (1600 to 1700 m/s) as well as smooth density variations (with the exception of the Thrust A). This absence of pronounced velocity and density changes, plus the locally high dip structure (more than 40° between 40 to 110 mbsf and 290 to 480 mbsf) accounts for the lack of continuous and strong reflectors.

The underthrust unit encompasses three seismic sequences. An upper transparent sequence, about 180 ms thick, lies just below the décollement and corresponds to lithologic Units 2-C and 3. These units consist of lower to upper Oligocene clays and alternating clays, mudstones, and marls. These sedimentary units show a regular increase of velocity with depth (from 1700 to 1950 m/s) that correlates with a small increase of density and a small decrease in porosity (Fig. 51). One hundred meters west of the hole this sequence is overlain by a single reflector R that is apparently truncated by the décollement, thus suggesting that the décollement is not always parallel to the bedding but may occasionally cut through it to an older (but not deeper) level. Hole 671B ended in sand (Unit 4) that correlates with the top of a highly reflective sequence. This sand exhibits little cementation and presumably has a high porosity and permeability. The sands should have a slightly lower density than the overlying clays, explaining their high reflectivity. This reflective sequence is 100 ms thick (about 90 m) and is probably composed of alternating sands and clays. This unit could be either of early Oligocene or late Eocene age, or both. The underlying semitransparent seismic unit has a thickness of about 150 ms (150 m) and is tentatively correlated with the 200-m-thick Campanian to Eocene series drilled at Site 543 (Biju-Duval, Moore et al., 1984). Reflector O is interpreted as the top of the oceanic crust.

HEAT FLOW

Introduction

The return to the Lesser Antilles forearc, 5 yr after Deep Sea Drilling Project Leg 78A (Biju-Duval et al., 1984), provided another opportunity to core into and through an accretionary complex and conduct a series of downhole experiments. Although many models of convergent margins offer predictions of large-scale thermal structure (e.g., Hsui and Toksoz, 1979), few actual measurements have been made (e.g., Langseth and Burch, 1981; Uyeda and Horai, 1982; Davis and Hussong, 1984; Langseth et al., 1986). Fluid transport, sedimentation, and sediment accretion influence heat flow through accretionary prisms. Temperature measurements should provide a better understanding of heat conduction and advection, and accretion, in these systems.

Heat Flow at Active Margins

Langseth and Birch (1981) and Shipley and Shephard (1982) reported geothermal gradients of 25 to 50 °C/km for the Japanese and southwest Mexican accretionary complexes, respectively. These temperature gradients are in general agreement with thermal models of accretionary margins (e.g., Toksoz et al., 1971; Hsui and Toksoz, 1979) in which large quantities of heat are removed with the subducting slab. This heat is transported downward by the underthrust plate more quickly than it can be conducted upwards, owing to accretion of "cold" sediments into the accretionary wedge and a lack of thermal coupling between the two plates (Langseth et al., 1986).

Assuming 90 Ma crust is underthrust beneath the Barbados Ridge, the expected heat flow based on theoretical crustal cooling models is 48 to 53 mW/m^2 (Anderson and Skilbeck, 1982; Lister, 1977). Birch (1970) and Schubert and Peter (1974) reported surface measurements of heat flow east of the deformation front averaging 52 mW/m^2, with the lowest values (<12 mW/m^2) northeast of the Barracuda Ridge. The mean of all heat flow measurements recorded in the vicinity of the Barracuda Ridge (from Speed et al., 1984), is 43.4 mW/m^2 (standard deviation, 19.0 mW/m^2). This value is slightly lower than that theoretically expected. The one previous heat flow measurement reported just south of the Tiburon Rise is 30.2 mW/m^2 (Speed et al., 1984).

Davis and Hussong (1984) estimated a geothermal gradient of 30 to 50 °C/km at reference Site 543 on DSDP Leg 78A and a heat flow of 35 mW/m^2, significantly lower than the mean of earlier measurements. Their estimate was based on measurements made with a Gearhart-Owen downhole temperature logging device and a temperature sensor included in a downhole seismometer package. Davis and Hussong (1984) provided no information on the accuracy of these sensors, nor details of how corrections for the major drilling disturbances were applied; their estimate must be viewed as a rough lower bound.

Method and Results

See the Explanatory Notes chapter of this volume for a discussion of experimental methods, intertool calibration, and data reduction. The vital tool properties are summarized in Table 16 and temperatures measured at Site 671 are summarized in Table 17.

Table 16. Temperature measurement instruments used at Site 671.

Tool	Thermistor housing	Thermistor resolution	Recorder program
APC tool	steel annular cylinder ID: 0.0617 m OD: 0.0786 m	0.02°C	variable recording interval
T-probe	steel cylindrical probe 0.0125 m dia	0.05°C	5.12 s recording interval

Table 17. Temperature measurement summary for Hole 671B.

Depth (mbsf)	Tool	Equilibrium T (est. error) (°C)	Sediment/Water Temperature
0	APC-tool #6	2.29 (±0.05)	water
17.4	APC-tool #6	4.29 (±0.05)	sediment
36.4	APC-tool #6	5.95 (±0.10)	sediment
45.4	T-probe #12	none	sediment
55.5	APC-tool #6	none	sediment
74.4	APC-tool #6	none	sediment
167.6	T-probe #14	10.7 (±0.5)	sediment
288.6	T-probe #14	13.2 (±1.0?)	water

Hole 671B

Site 671 is located 3.5 km arcward of the deformation front. The APC tool was first deployed at a depth of 17.4 mbsf, just before taking Core 110-671B-2H. Before firing the hydraulic piston core mechanism, the shoe was exposed to bottom water 5 m above the mudline. The shoe was held in this position for 15 min, reaching an equilibrium temperature of 2.29°C (±0.05°C) (Figs. 52A and 52B). Later runs with the APC tool and the corrected T-probe gave nearly identical bottom-water temperatures. After we measured bottom water, we fired the APC tool into the sediment, producing a good penetration record (Figs. 52A and 52C), from which a sediment temperature was extrapolated to an equilibrium value of 4.29°C (± 0.05°C).

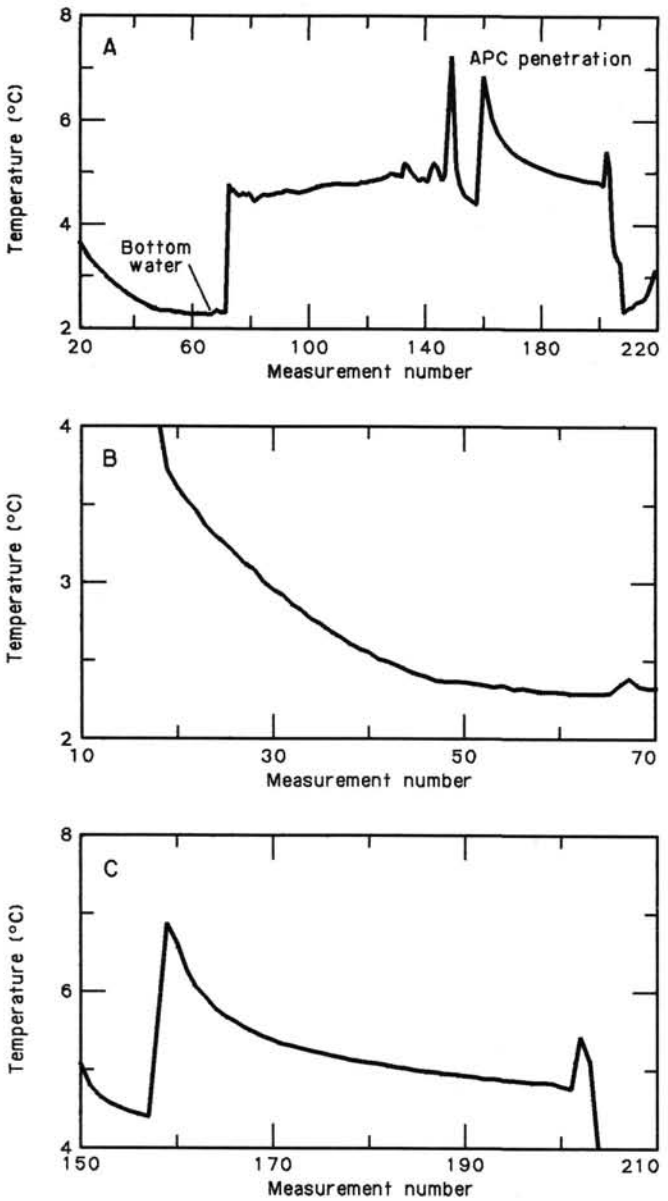

Figure 52. A. Temperature vs. time record for first deployment of APC-tool. B. Detail of record of first APC-tool deployment, showing bottom-water temperature, and C. Detail of record of first APC-tool deployment, showing sediment temperature, in Core 110-671B-2H. All measurement intervals 15 s at 17.4 mbsf.

The APC tool was also run during the collecting of Cores 110-671B-4H, -671B-6H, and -671B-8H, to depths of 36.4, 55.5, and 74.4 mbsf, respectively. While the record from Core 110-671B-4H is clear (Figs. 53A and 53B) and produced a good equilibration temperature of 5.95°C (± 0.10°C), it became difficult to dump data from the APC tool after Core 110-671B-6H. When data were finally extracted, they contained no record of coring shoe penetration into sediment (Fig. 54) although a full core liner was returned. It is assumed that low battery power during this run prevented accurate recording. It is believed that the same power supply problem prevented all data recording when the tool was run with Core 110-671B-8H.

The T-probe was run after Core 110-671B-5H to a depth of 45.5 mbsf. We lowered the WSTP tool by wireline to avoid damaging the instrument during freefall. The tool is designed to be latched into position, where it protrudes 0.5 m past the end of the bit, and then pushed into the sediment. Once in position, the bit was placed on the hole bottom, and the tool left in position for 15 minutes with the heave compensator on, to measure temperature, collect a water sample, and measure pressure in the sediment and in the water column above the bit. The temperature record from this first run (Fig. 55) suggests that full penetration was not achieved. While there is a good record of the tool leaving the end of the drill pipe, there is no frictional or subsequent heating during penetration. Furthermore, the pressure traces (not pictured) show little or no difference between the sediment and water transducers over the same time period. The water sampler returned full of distilled water and it is assumed that the valve did not open.

The second run with the T-probe, after Core 110-671B-18X, to 167.6 mbsf, was much more successful, as can be seen from

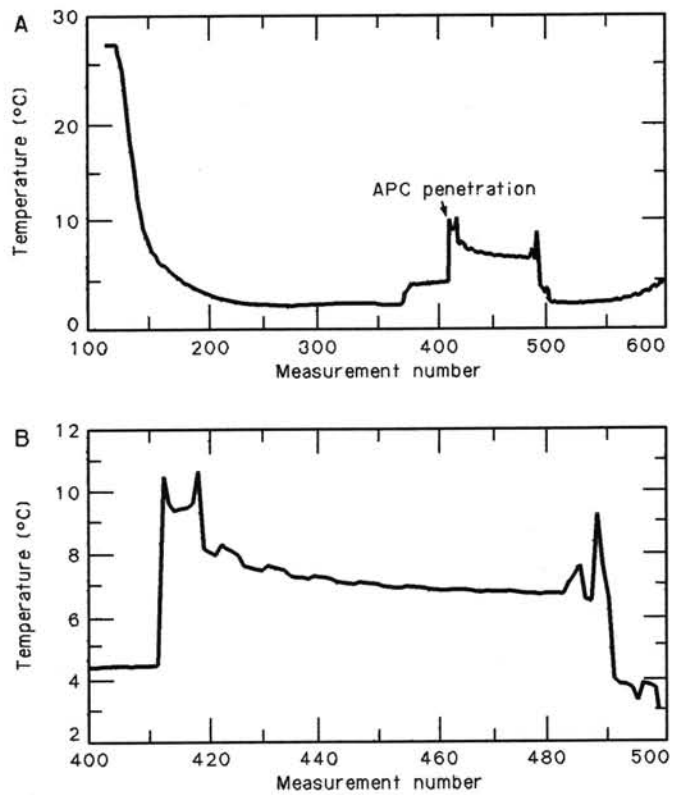

Figure 53. A. Temperature vs. time record for second deployment of APC-tool, and B. Detail of record of second deployment of APC-tool, showing sediment temperature, in Core 110-671B-4H. Measurement intervals 10 s at 36.4 mbsf.

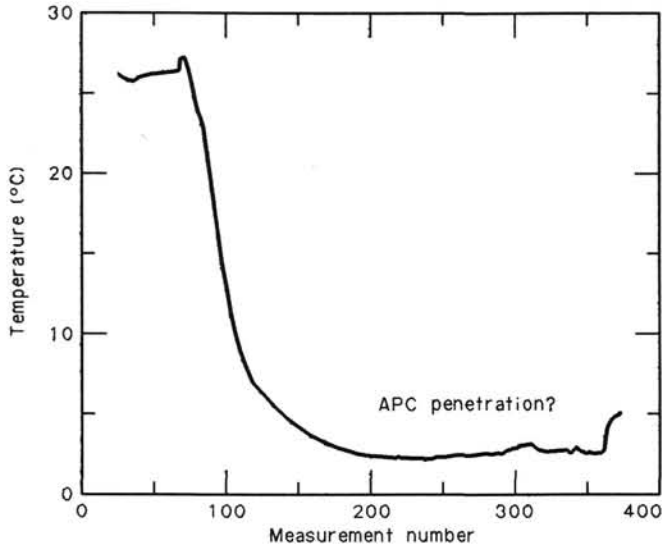

Figure 54. Temperature vs. time record for third deployment of APC-tool, Core 110-671B-6H. Measurement interval 15 s at 55.5 mbsf.

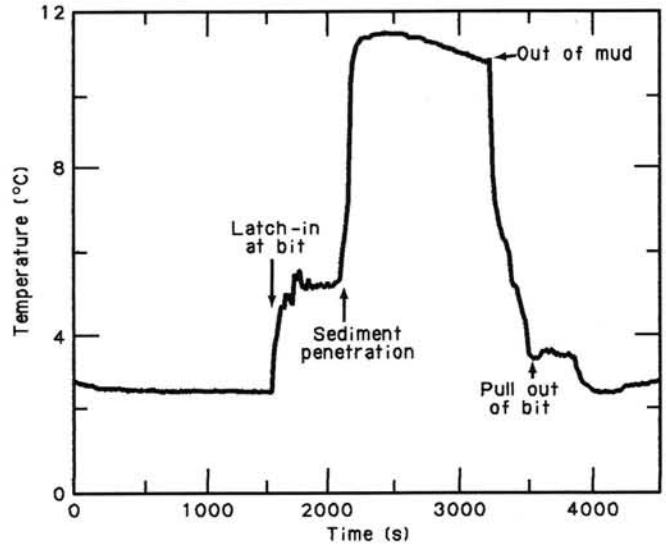

Figure 56. Temperature vs. time record for second deployment of T-probe, after Core 110-671B-18X. Hole depth 167.6 mbsf.

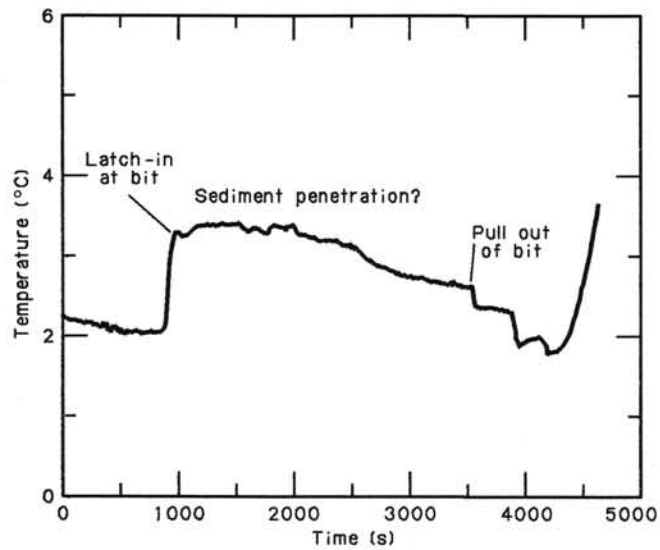

Figure 55. Temperature vs. time record for first deployment of T-probe, after Core 110-671B-5H. Hole depth 45.4 mbsf.

Fig. 56. There is clear evidence of penetration and subsequent cooling of the temperature tool, as well as differential water column and sediment pressure. The pressure traces also record the opening of the sampler valve and collection of sediment pore fluid. The calculated equilibrium temperature for this run is 10.7°C (± 0.5°C).

A third run was made with the T-probe prior to logging Hole 671B. After coring was stopped owing to bit-sticking problems, a freefall cone was dropped and the pipe was tripped. The hole equilibrated for 63 hr before reentry. Upon reentry, pipe was run to a depth of 278 mbsf, encountering little resistance. The APC tool was attached to the WSTP tool and the two were lowered down the drillpipe to the bit by wireline, without pumping. The wireline lowering limited the depth range of this experiment to 20 m, the length of pipe that could be drawn up into the derrick beneath the top-drive before the tools were run. After we paused at 278 m for 15 min, one tool joint was lowered into the drillhole and the test procedure was repeated at a bit depth of 288 mbsf. One more measurement was attempted at 298 mbsf. Unfortunately, the APC tool produced no record of the lowering. A T-probe log was produced but is of questionable quality owing to abundant recorder noise. There is evidence of probe equilibration to a temperature of 13.2°C at 288 mbsf. This value has an estimated error of 1.0°C owing to the previously mentioned recorder problem. In addition, we need to estimate the correction that must be applied to this measurement to account for the temperature disturbance in the hole due to drilling.

Interpretations

From the three APC temperatures, a best-fitting linear temperature gradient forced through the bottom-water temperature is found to be 103 °C/km for the upper 36.4 m (Fig. 57). This value results in a calculated heat flow of nearly twice the theoretical value for crust of 90 Ma (Langseth et al., 1986). The calculated thermal gradient is significantly lower when temperatures at 167.6 and 288 mbsf are included. A best-fitting linear thermal gradient forced through bottom-water temperature including these points is 43 °C/km, although there is some curvature of the gradient over this interval. Thermal conductivity increases downhole over this same interval (Fig. 58; Physical Properties section, this chapter), necessitating an adjustment using the integrated thermal resistance (Bullard, 1939) to calculate heat flow. Reliable interpretation is not possible unless a temperature correction owing to drilling disturbance can be applied to the value at 288 mbsf. However, if the low temperature measured at 288 mbsf is correct, there has been no upward migration of warm water through the drill hole from an over-pressured zone at depth. After making the borehole measurements, a sediment bridge was encountered at 450 mbsf; thus, any flow in the hole may have been blocked by sediment flow-in. Thus the temperature data from Site 671 neither supports nor refutes the presence of over-pressures at the décollement.

PACKER EXPERIMENTS

Introduction

A major goal of Leg 110 was to determine fluid pressures and permeabilities at several locations within the accretionary complex of the Lesser Antilles convergent margin. Theoretical

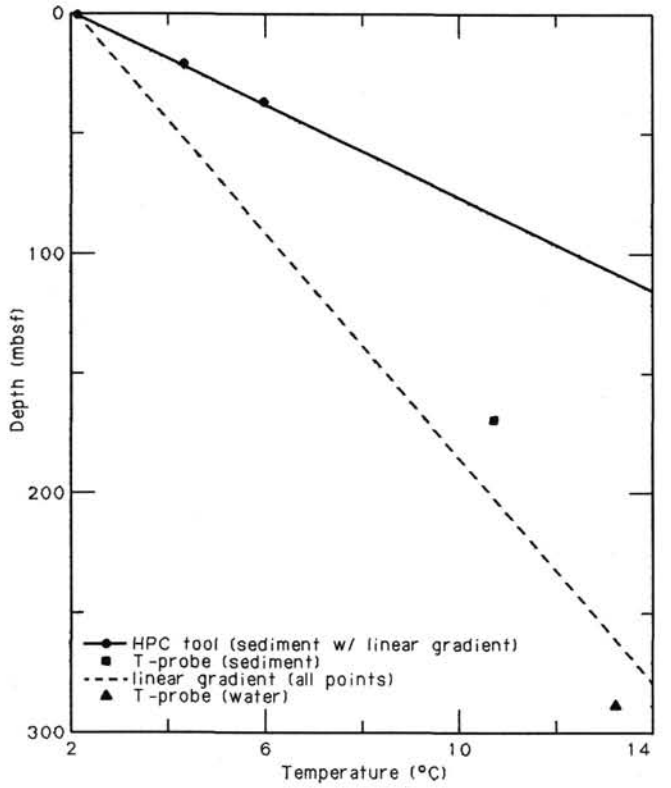

Figure 57. Plot of temperature vs. depth for Hole 671B.

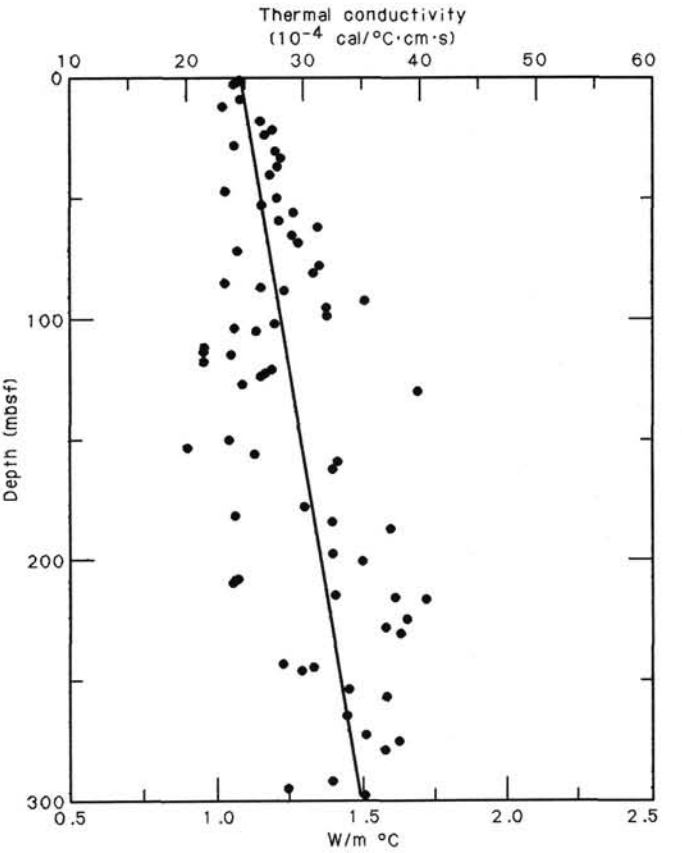

Figure 58. Plot of thermal conductivity vs. depth, including linear least-squares best fit for the data, to 300 mbsf in Hole 671B.

studies of active margins (Zhao, et al., 1986; Bray and Karig, 1985; Shi and Wang, 1985; Von Huene and Lee, 1983; and many others) suggest that near-lithostatic fluid pressures strongly influence accretionary wedge evolution. While observations during Deep Sea Drilling Project Leg 78A indirectly support this concept (e.g., Biju-Duval, Moore, et al., 1984; Davis and Hussong, 1984), direct observations of high fluid pressure and formation permeability are difficult to obtain under controlled conditions. Permeability and porosity measurements of core samples from prisms provide vital information, but may not be representative of conditions at depth where lithostatic loading, fracture permeability, and other factors alter bulk properties. In fact, estimates of bulk properties, and the models upon which these estimates are based, vary widely (e.g., Marlow et al., 1984; Ngokwey, 1984).

Packer experiments, along with careful heat-flow and pore-water chemistry analyses and logging, were to provide reasonable estimates of fluid pressure and permeability over several zones through the accretionary complex of the Lesser Antilles.

Method

A packer is a wireline or drill string tool that hydraulically seals an interval of a drill hole. Once in place, the isolated formation may be tested by altering fluid pressure in the test zone and monitoring the response. The formation properties which may be determined include fluid pressure, transmissivity (closely related to permeability), and storage coefficient (related to bulk porosity). These properties may be determined through a series of three tests:

Static Pressure Measurements

Once the packer is set in position and downhole shut-in is achieved, pressure gages located just beneath the level of isolation monitor fluid pressure. After any initial disturbance has decayed, fluid pressure within the packed zone should approach that of the surrounding formation.

Pulse Tests

Short, effectively instantaneous, pulses of pressure are applied by surface pumps. The decay of such a pulse will be long relative to the length of the pulse itself, assuming the formation is relatively impermeable. Tests are run at different pulse intensities, and transmissivity and a storage coefficient (along with their related properties) are determined from analyses of fluid pressure decay curves.

Flow Tests

Fluid is pumped into the isolated zone at a constant rate for 20 to 30 min. Downhole gages monitor pressure, which should approach a constant value. Tests are run at several flow rates to correct for frictional and other losses to the system. If steady-state is obtained, bulk permeability may be estimated through a form of Darcy's Law. After flow is stopped, the decay of fluid pressure in the test interval provides a second estimate of formation fluid pressure. Flow tests work best in relatively permeable formations.

These tests and their interpretation are discussed in Cooper et al. (1967), Papadopulos et al. (1973), and Bredehoeft and Papadopulos (1980). Previous packer experiments utilizing the above-described tests on Deep Sea Drilling Project and Ocean Drilling Program cruises are documented in Anderson and Zoback (1982), Hickman et al. (1984), Anderson et al. (1985), and Becker (1986).

Packer Tests on the JOIDES Resolution

Two packers were available for use on Leg 110: a nonrotatable, double-element, straddle packer (described in Becker, 1986) and a drill-in, single-element packer; both tools were built by TAM International specifically for use by the Ocean Drilling Program. The straddle packer was first deployed during Ocean Drilling Program Legs 102 and 109; the drill-in packer is a new tool and its operation is described below.

Once the drill-in packer is positioned in the hole, an inflation go-devil is dropped down the drill pipe; it seats above the packer inflation element. Increasing pressure on the go-devil then shifts a control sleeve, opening inflation ports in the element. After inflation, pressure is increased further to blow out a shear plug in the go-devil. When the shear plug blows, pressure is equalized on either side of the control sleeve. A coil spring then shifts the sleeve back to its original position, locking pressure in the packer element. Deflation is accomplished by retrieving the inflation go-devil and dropping a deflation go-devil, or by dropping a weighted overshot onto the inflation go-devil.

The straddle packer offers the advantage that a specific zone within a previously drilled hole may be isolated. The drill-in packer always isolates the entire interval from the packer seat to the bottom of the hole. In addition, a maximum inflation diameter of 12-1/4 in. limits the drill-in packer to use with a 10-1/2 in. or smaller bit (unless in extremely competent rock). Also, the drill-in packer is not currently compatible with the APC system. However, the drill-in packer does have rotating, washing and drilling capabilities; the straddle packer is limited in use to extremely stable (generally basalt) holes. In addition, the 3/8-in. stainless-steel tubing which allows communication between the two straddle-packer elements is vulnerable to damage upon reentry.

Pressure pulses are generated with Halliburton cement pumps. Flow rate is monitored with a stopwatch and a volumetric counter (estimated error, 20 gal.). This volumetric error is insignificant over the length of a flow test (when 1000 to 2000 gal. may be pumped in 30 min) and has little or no effect on slug test accuracy. The downhole gages used to monitor fluid pressure are accurate to within 1/4% of their pressure range, resulting in a gage error of 2.5 to 3.5 psi.

After reaching Site 671, the hydraulics system was pressurized from the cement pumps to the rig floor to 3200 psi and shut-in to test the integrity of the pipes and joints; no leaks were detected.

Hole 671C

In the original operational plans, casing was to be cemented in position through the décollement at Site 671. After perforating or opening ports in the casing, the straddle packer was to be set across the open interval to measure formation fluid pressure. Drilling through the décollement without casing was successful, however. It appeared it would be possible to deploy the straddle packer in the open hole across the décollement zone. Unfortunately, hole conditions deteriorated prior to logging and Hole 671B was abandoned.

The pipe was tripped and a new bottom hole assembly was rigged with the drill-in packer in position. The packer was placed one drill collar above the bit with an additional five collars placed above it to add weight for drilling. The pipe was tripped back down and Hole 671C was spudded-in just 200 m north of Hole 671B.

After washing down to 320 m beneath the seafloor, drilling was slowed owing to increasing flow-in. Drilling was halted at 505 mbsf to take a core and confirm the location of the décollement zone in the hole (see Lithostratigraphy section, this chapter). Hole conditions continued to deteriorate, even after two wiper trips. A core taken at 515 mbsf contained mostly flow, but also a small section of lower Miocene mudstone (see Lithostratigraphy section, this chapter), suggesting that the base of the décollement zone had been penetrated. After another wiper trip, the bit was pulled to 479 mbsf for the first packer experiment.

An inflation go-devil with two Kuster pressure gages mounted beneath was dropped into the pipe and pumped into position in the packer. After allowing time for a hydrostatic base line to be drawn on the Kuster records, tests began. A total of 11 sets were attempted; the location of each attempt, maximum pressures, and flowrates are presented in Table 18.

Pressure was increased to 1500 psi and shut-in at the cement pumps to measure formation fluid pressure. The system immediately lost pressure. A second attempt at this depth produced the same result. Additional sets were attempted at packer depths of 470, 471, 457, and 418 mbsf. The pipe was pulled to a bit depth of 320 mbsf where physical-properties measurements from cores in Hole 671B (Physical Properties section, this chapter) indicated an increase in bulk density and a drop in porosity.

Additional sets were attempted at packer depths of 307, 310, and 314 mbsf with no success. Finally, fluid was pumped continuously to bring pressure above 2200 psi in an attempt to blow the shear plug in the go-devil and lock pressure in the packer element. After blowing the plug, the packer would still not hold weight nor provide resistance when the pipe was pulled up the hole.

An overshot was sent down to retrieve the go-devil and Kusters. Logging in Hole 671C was then abandoned after hole conditions continued to deteriorate and a sediment bridge blocked the pipe. The pipe was tripped, and the packer was returned to the surface for inspection.

Upon return, the packer element was near fully compressed against the upper portion of the tool (see Fig. 59). Approximately 95% of the rubber had been stripped away from the element, exposing frayed aircraft cable and a ripped bladder beneath.

The tool was disassembled and we determined that a metal stop-ring had been left out of the packer assembly. This stop-ring normally prevents telescoping of the element. Without the ring in position, there was nothing to keep the element extended

Table 18. Locations, test pressures, and flow rates for attempted packer seats at Site 671.

Depth (mbsf)		Maximum pressure obtained	Flow rate
Bit	Packer	(psi)	(gpm)
Hole 671C			
479	466	1500	35
479	466	1500	35
470	457	1500	45
483	470	1400	45
484	471	1300	40
431	418	950	55
431	418	900	40
320	307	1000	40
323	310	1400	45
327	314	1400	35
327	314	2200	60
		blew shear plug	
Hole 671D			
452	439	1600	45
452	439	1500	55
433	420	1500	60
433	420	2200	65
		blew shear plug	

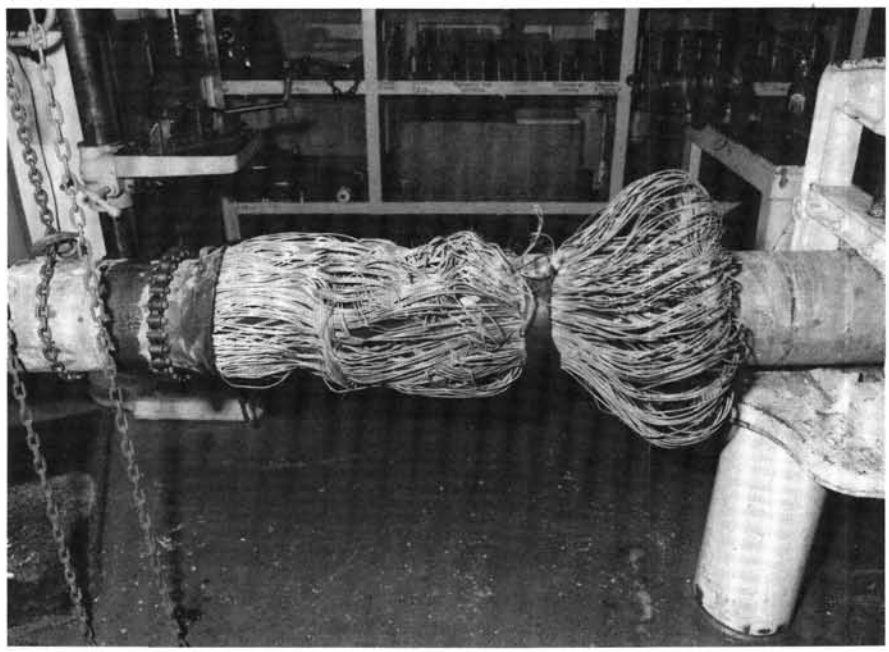

Figure 59. Photograph of TAM drill-in packer after deployment in Hole 671C. Note that most of the rubber that originally covered the braided metal cable was stripped away during drilling.

(in tension) during drilling except the coil spring. This spring has a resistance of less than 250 lb. Apparently, the element became compressed from the weight of five drill collars (15,000 lb), abraded against the side of the hole, and began to disintegrate during the first 320 m of drilling (see Operations section, this chapter). Moreover, the damaged packer element probably contributed to poor drilling conditions in Hole 671C.

Hole 671D

A second packer hole was drilled 200 m offset from Hole 671B. The drill-in packer was once again made up as part of the bottom-hole assembly and run in. Hole 671D was washed down to 450 mbsf with good hole conditions and rapid penetration.

Hole conditions began to deteriorate when drilling was halted at 450 mbsf to retrieve the washdown center-bit. This bit was finally retrieved and the first and only core (with the exception of a 20-cm mudline core) was taken. This core became wedged into the bit and could not be loosened. In addition, increased torque on the bit indicated a worsening of the hole conditions. Additional coring was abandoned, and the hole was washed down, with the XCB core still in the bit. Drilling was finally halted when the bit became stuck at 519 mbsf.

After a short wiper trip, the hole conditions appeared to stabilize and the packer was moved to 439 mbsf (bit at 452) for the first test (see Table 18 for a summary of test locations). The inflation go-devil was then dropped down the pipe with one Kuster pressure gage. Only one gage was used because the XCB inner barrel stuck in the bit and did not allow enough room for two gages in the pipe.

The cement pumps were activated and the system was pressurized. The pressure was increased to 1600 psi but would not hold. It was determined that the pipe had been rotating during this first test; the pipe was then held steady for the remainder of the tests. A second attempt was made at this depth with the same result. The packer was then raised to 420 mbsf and pressured, with no improvement. Finally, the pressure was increased to 2200 psi to blow the shear plug in the go-devil in an attempt to lock pressure into the packer element. The drill pipe was then moved up and down the hole with no resistance, indicating that the element was not inflated.

The go-devil was retrieved with all seals intact, indicating that a blown go-devil seal could not be responsible for the leak observed in the system. The pipe was tripped and the packer returned to the surface. The packer element was ripped completely down one side with a flap of rubber hanging free, although all the rubber was found to be present. The braided wire element was in good condition, but the inner rubber bladder had a 2-in. vertical tear.

We believe that the element became ruptured either during attempts to free the stuck core barrel at 460 mbsf (when the element may have inflated prematurely) or when the pipe was rotated during the first attempt to set. In any case, once the system was compromised, there was no chance to test the fluid pressure or the permeability of the formation. It is important to note, however, that 450-m depth was drilled successfully with the packer in place, confirming the tool's drill-in capability.

SUMMARY AND CONCLUSIONS

Site 671 drilling penetrated about 500 m of offscraped Neogene sediment, through a décollement zone separating the latter from a subjacent underthrust sequence, and about 190 m into Oligocene deposits of the underthrusting plate. Site 671 records the first complete penetration of the boundary between two converging plates and provides the most extensive sampling to date of the processes operating at such an active plate boundary.

Offscraped sediments above the décollement zone are subdivided into two lithologic Units (1 and 2-A) consisting of calcareous mud, mud, and local chalk ranging from early Pleistocene to late–middle(?) Miocene in age (Fig. 60). The décollement zone is composed of a 19-m-thick lower Miocene brown clay (Unit 2-B) overlying 19 m of green clays of indeterminate age (Unit 2-C). Unit 2-C and the lower part of Unit 2-B show a well-developed scaly fabric. Below the décollement zone drilling penetrated a section of Oligocene clay with local calcareous interlayers and silty beds. The beds contained quartz probably derived from South America (Unit 3). The deepest unit (4) encountered at Site 671 consists of a green mud grading down to a glauconitic quartz sand that could not be penetrated by the drill.

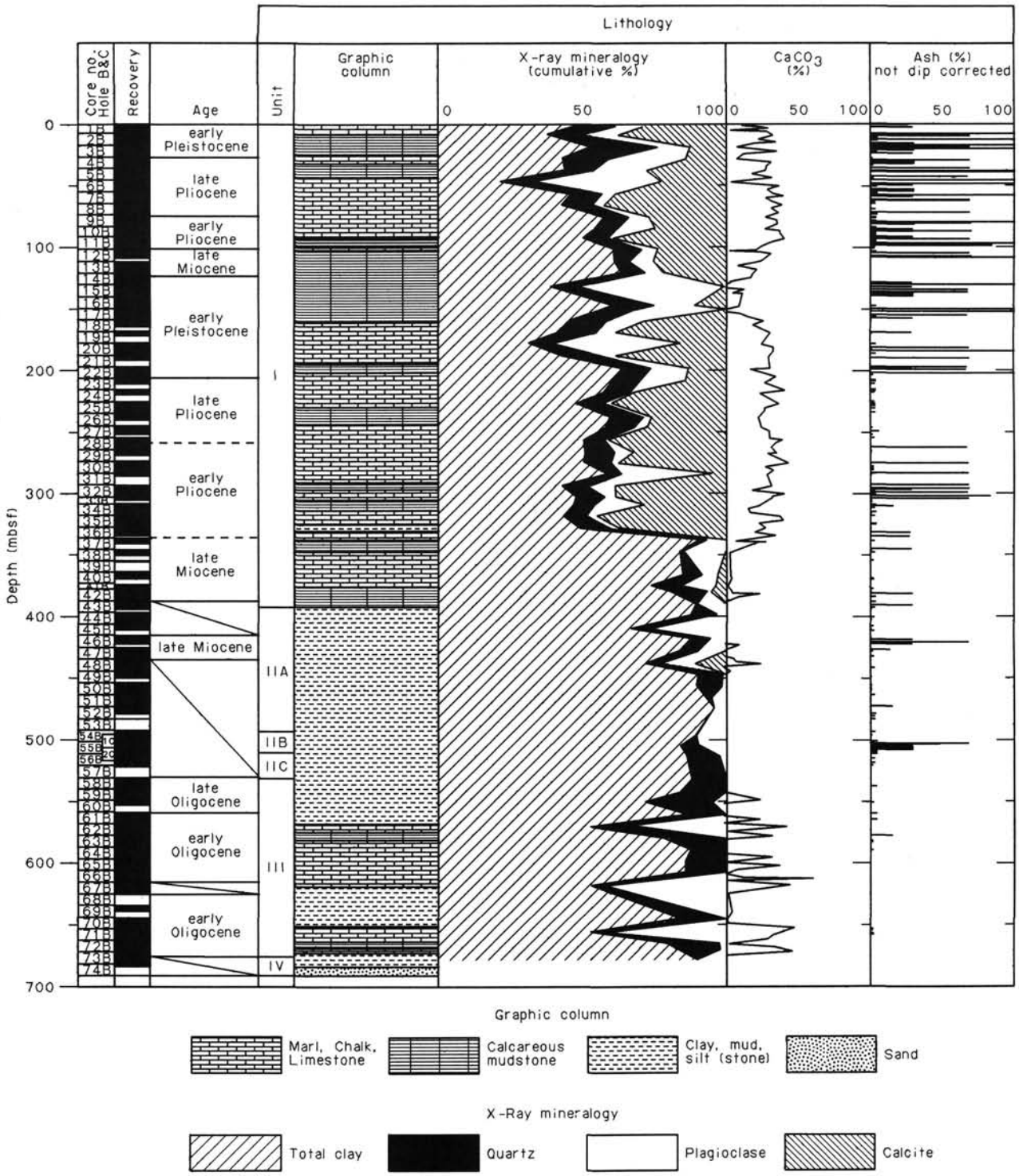

Figure 60. Site summary diagram. Thrust fault symbol in décollement zone indicates interval of most intense deformation in lower Miocene radiolarian mudstone. However, décollement zone is actually a broad interval of deformation, shown by pattern, that extends for approximately 40 m downhole.

Offscraped sediments overlying the décollement represent a hemipelagic sequence that apparently accumulated on the Tiburon Rise above the influence of terrigenous flow from South America or the Lesser Antilles magmatic arc. The abundance of terrigenous sand and silt in the underthrust Oligocene sequence is surprising as these materials accumulated on the Tiburon Rise, about 500 km from South America. The Oligocene underthrust sequence is almost ash-free whereas the overlying Neogene sequence shows increasing abundance of ash content (crystals and glass) with decreasing age. The increase in ash content upsection could result from either increased magmatic activity in Lesser Antilles and/or the progressive approach of this magmatic arc from the west. The 250-m-thick undrilled section below Unit 4 is presumed to be of Campanian to late Eocene or

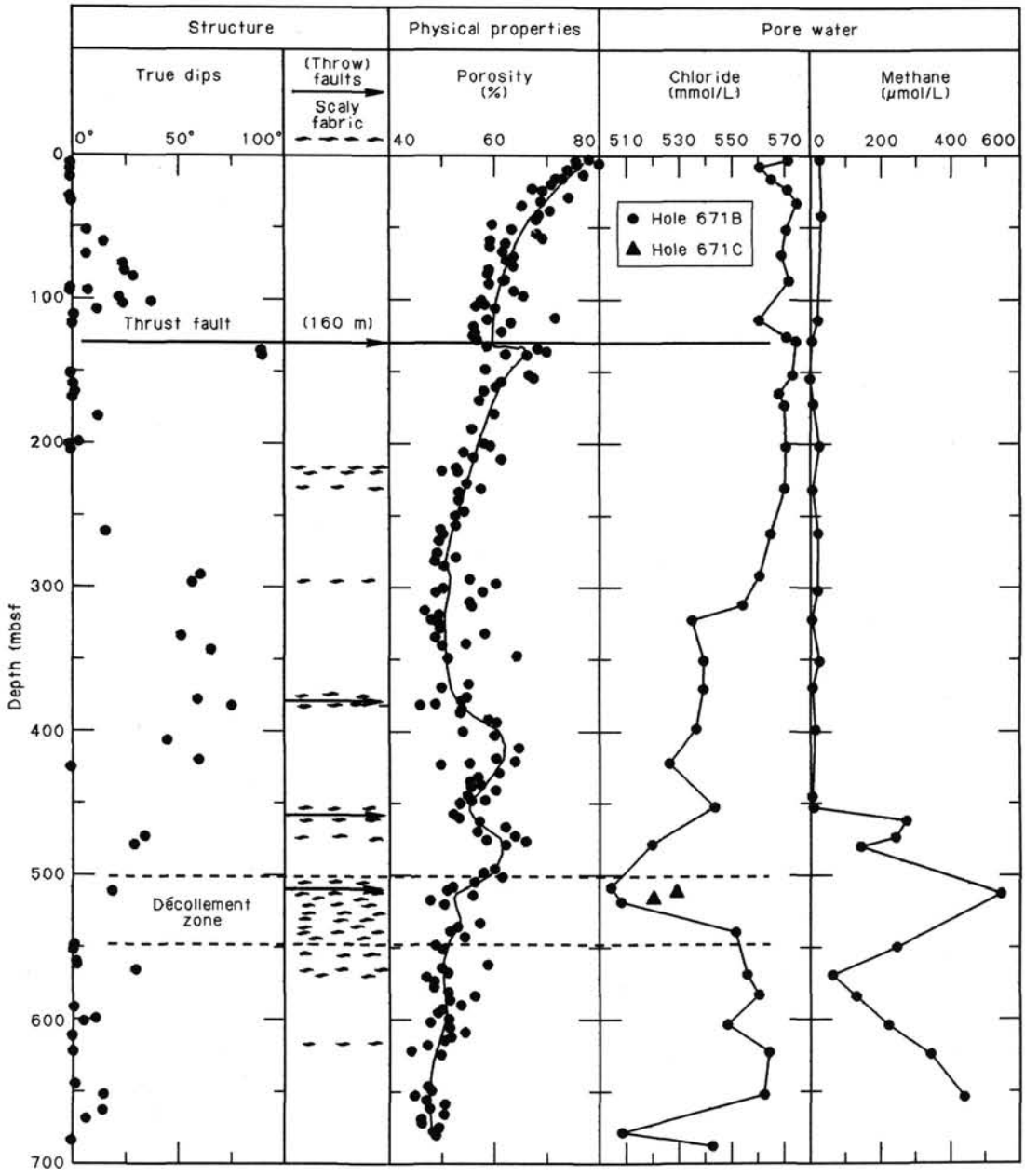

Figure 60 (continued.)

early Oligocene age based on extrapolation to DSDP Site 543; the top of the oceanic crust is estimated to be at a depth of 950 mbsf.

The structural geometry of Site 671 is very well defined by a combination of seismic, biostratigraphic, and structural data. At 128 mbsf a biostratigraphic inversion of upper Miocene over lower Pleistocene sediments defines a low-angle reverse fault with a throw of 160 m (Fig. 60). Owing to its substantial throw and its correlation with an arcward dipping reflector, the fault at 128 mbsf is interpreted as a major package-bounding thrust. An unusually thick nannofossil zone and an interval of scaly fabric at 375 mbsf suggest reverse faulting. A possible biostratigraphic inversion occurs over an interval from 435 to 482 m and may be related to a scaly zone at about 447 m. This possible fault is correlated well with some seismic reflectors and it can be carried to a biostratigraphically defined fault in Site 541. It is thus interpreted as a major package-bounding thrust. The décollement zone is not defined by a biostratigraphic inversion but by a strongly developed zone of scaly fabric just below 500 m depth. The intensity of the scaly fabric dies off with depth and encompasses a deformation zone about 30 to 40 m thick. Below the décollement zone the bedding dips are shallow; faults are also shallow but decrease in frequency with depth. By the termination of the hole at 690 mbsf all the obvious structural effects of the décollement zone are lost.

Although moderate to shallow bedding dips predominate above the décollement, locally steep patterns of bedding dips in the thrust packages suggest internal folding. Minor thrust faults were also recognized in the cores although they are often overprinted by drilling disturbance. These minor faults are particularly common in the lower Pliocene. The range of bedding dips is greater at Site 671 as compared to Sites 541 and 542, suggesting progressive internal deformation of the thrust packages. Although composed of the same stratigraphic units, the individual

packages (P_1-P_3) are each progressively thicker, also suggesting internal deformation.

The package bounding fault at 128 mbsf is unique in that it is not associated with a scaly fabric; in fact, adjacent deformation is restricted to a 5-mm-thick zone of laminar flow and steep dips of underlying beds that may be a drag feature. In contrast, all other biostratigraphically defined faults and the décollement zone are associated with scaly fabrics. The lack of obviously distributed deformation associated with the fault at 128 m may be owing to the shallow depth of deformation (low effective stresses) or the relatively carbonate-rich nature of superimposed lithologies.

Although the décollement zone can be identified structurally, the pore-water chemistry provides insights on the processes operating along this fault surface. Pore-water chemistry studies from samples across the décollement zone clearly indicate anomalies in calcium, magnesium, chloride, and silica. The chloride minimum in the décollement zone (Fig. 60) may be generated by a membrane filtration effect resulting from driving fluid down a hydraulic gradient (e.g., p. 292, Freeze and Cherry, 1979). The decrease in chloride values closer to the sand layer at the base of the hole also suggests a similar effect. Membrane filtration (Kharaka et al., 1985) is likely at Site 671 because the mudstones adjacent to the décollement zone are subject to significant effective stresses, accelerated dewatering, have sufficiently low water contents, and are of appropriate smectitic composition (Pudsey, 1984). In contrast to the décollement zone, the absence of anomalies in methane and chloride across the faults cutting the offscraped deposits suggests that they presently are not zones of significant water flow.

Overall trends in physical properties reflect a downhole consolidation punctuated by the effects of faults (Fig. 60). Sediments below the thrust at 128 mbsf show an anomalous increase in porosity related to the underthrusting of Pleistocene sediment. Neither of the possible faults at 375 or 447 mbsf are clearly expressed in the profiles of physical properties; however, the two symmetrical positive excursions in porosity between 400 and 500 mbsf could be interpreted as a stratigraphic repetition at 447 msbf. The décollement zone is marked by a sharp decrease in porosity from Miocene to Oligocene mudstones. This change in physical properties may be depositional and/or reflect selective consolidation of material below the décollement zone. A progressive increase in horizontal velocity is observed in the last 130 m of the hole where the underthrust sequence is not disturbed by the décollement zone.

REFERENCES

Anderson, R. N., Zoback, M. D., Hickman, S. H., and Newmark, R. L., 1985. Permeability versus depth in the upper oceanic crust: in situ measurements in Deep Sea Drilling project hole 504B, eastern equatorial Pacific, *In* Anderson, R. N., Honnorez, J., Becker, K., et al., *Init. Repts. DSDP*, 83: Washington (U.S. Govt. Printing Office), 429–442.

Anderson, R. N., and Skilbeck, J. N., 1982. Oceanic heat flow. *In* Emiliani, C. (Ed.), *The Sea* (Vol. 7) *The Oceanic Lithosphere*: New York (Wiley), 489–524.

Barker, C., 1974. Pyrolysis techniques for source rock evaluation. *Am. Assoc. Pet. Geol. Bull.*, 58:2347–2361.

Becker, K., 1986. Drillstring packers in the Ocean Drilling Program, *JOIDES Journal*, June, 1986.

Bergen, J. A., 1984. Calcareous nannoplankton from Deep Sea Drilling Project Leg 78A: evidence for imbricate underthrusting at the Lesser Antillian active margin. *In* Biju-Duval, B., Moore, C., et al., *Init. Repts. DSDP*, 78: Washington (U.S. Govt. Printing Office), 411–445.

Berggren, W. A., 1977. Late Neogene planktonic foraminiferal biostratigraphy of the Rio Grande Rise (South Atlantic). *Mar. Micropaleontogy*, 2, 3:265–313.

Bernard, B. B., Brooks, J. M., and Sackett, W. M., 1978. Light hydrocarbon in recent Texas continental shelf and slope sediments. *J. Geophys. Res.*, 83:4053–4061.

Biju-Duval, B., Le Quellec, P., Mascle, A., Renard, V., and Valery, P., 1982. Multibeam bathymetric survey and high resolution seismic investigations of the Barbados Ridge complex (Eastern Caribbean): A key to the knowledge and interpretation of an accretionary wedge. *In* Le Pichon, X., Augustithis, S. S., and Mascle, J. (Eds.), Geodynamics of the Hellenic Arc and Trench: *Tectonophys.*, 86:275–304.

Biju-Duval, B., Moore, J. C., et al., 1984. *Init. Repts. DSDP*, 78A: Washington (U.S. Govt. Printing Office).

Birch, F. S., 1970. The Barracuda Fault zone in the western North Atlantic: geological and geophysical studies. *Deep Sea Res.*, 17:847–859.

Blanc, G., Boulegue, J., Badaut, D., and Stouff, P., 1986. Premier resultats de la campagne oceanographique Hydrotherm (Mai, 1985) du Marion-Dufresne sur la fosse Atlantis II (Mer Rouge). *Compt. Rend. Acad. Sci. Paris*, 302:175–180.

Bleil, U., 1985. The magnetostratigraphy of northwest Pacific sediments, Deep Sea Drilling Project Leg 86. *In* Heath, G. R., Burkle, L. H. et al., *Init. Repts. DSDP* 86: Washington (U.S. Govt. Printing Office), 441–458.

Bolli, H. M., 1970. The foraminifera of Sites 23-31, Leg 4. *In* Bader, R. G., et al., *Init. Repts. DSDP*, 4: Washington (U.S. Govt. printing Office), 577–643.

Bolli, H. M., and Premoli-Silva, I., 1973. Oligocene to Recent planktonic foraminifera and stratigraphy of the Leg 15 Sites in the Caribbean Sea. *In* Edgar, N. T., Saunders, J. B., et al., *Init. Repts. DSDP*, 15: Washington (U.S. Govt. Printing Office), 475–497.

Boulegue, J., Iiyama, J. T., Charlou, J. L., Wakita, H., and Jedwab, J. (in press) Nankai Trough and Japan Trench preliminary geochemistry of fluids. *Earth Planet. Sci. Lett.*

Bray, C. J., and Karig, D. E., 1985. Porosity of sediments in accretionary prisms and some implications for dewatering processes. *J. Geophys. Res.*, 90:768–778.

Bredehoeft, J. D., and Papadopulos, S.S., 1980. A method for determining the hydraulic properties of tight formations. *Water Resour. Res.*, 16:233–238.

Bullard, E. C., 1939. Heat flow in South Africa. *Proc. Roy. Soc. London*, A173:474–502.

Chase, R. L., and Bunce, E. T., 1969. Underthrusting of the eastern margin of the Antilles by the floor of the western North Atlantic Ocean, and the origin of the Barbados Ridge. *J. Geophys. Res.*, 74: 1413–1420.

Claypool, G. E., 1984. Diagenesis of organic matter, isotopic composition of calcite veins in basement basalt and pore water in sediments—Barbados Ridge complex. *In* Biju-Duval, B. Moore, J. C., et al., *Init. Repts. DSDP*, 78A: Washington (U.S. Govt. Printing Office), 385–391.

Claypool, G. E., and Reed, P. R., 1976. Thermal analysis technique for source-rock evaluation: quantative estimate of organic richness and effects of lithologic variation. *Am. Assoc. Pet. Geol. Bull.*, 60:608–612.

Cooper, H. H., Bredehoeft, J. D., and Papadopulos, I. S., 1967. Response of a finite diameter well to an instantaneous charge of water, *Water Resour. Res.*, 3:263–269.

Davis, D., and Hussong, D., 1984, Geothermal observations during Deep Sea Drilling project Leg 78A, *In* Biju-Duval, B., Moore, J. C., et al., *Init. Repts. DSDP*, 78A: Washington (U.S. Govt. Printing Office), 593–598.

Deroo, G., Herbin, J. P., Roucaché, J., and Tissot, B., 1978. Organic geochemistry of Cretaceous mudstones and marly limestones from DSDP Sites 400 and 402, Leg 48, Eastern North Atlantic. *In* Montadert, L., Roberts, D. G., et al., *Init. Repts. DSDP*, 48: Washington (U.S. Govt. Printing Office), 921–930.

Espitalié, J., Deroo, G., and Marquis, F., 1986. La pyrolyse Rock-Eval et ses applications. *Rev. Inst. Fr. Pétrole*, 41(1)73–89.

Espitalié, J., Laporte, J. L., Madec, M., Marquis, F., Leplat, P., Poulet, J., and Boutefeu, A., 1977a. Methode rapide de caracterisation des roches méres de leur potentiel petrolier et de leur degré d'évolution. *Rev. Inst. Fr. Pétrole*, 32:32–42.

Espitalié, J., Madec, M., Tissot, B., Menning, J. J., and Leplat, P., 1977b. Source rock characterization method for petroleum exploration. *9th Annual Offshore Technology Conference Proceedings*, 439–444 (OTC paper 2935).

Fertl, W. N., 1976. Abnormal formation pressures: implications to exploration, drilling, and oil and gas resources. *In Developments in Petroleum Science*: New York (Elsevier), 190–196.

Freeze, R. A., and Cherry, J. A., 1979. *Groundwater*: Englewood Cliffs, New Jersey (Prentice-Hall).

Fritz, S. J., and Marine, I. W., 1983. Experimental support for a predictive osmotic model of clay membranes. *Geochim. Cosmochim. Acta*, 47:1515.

Gartner, S., 1977. Calcareous nannofossil biostratigraphy and revised zonation of the Pleistocene. *Mar. Micropaleontolgy*, 2:1–25.

Gieskes, J. M., 1973. Interstitial water studies, Leg 15, alkalinity, pH, Mg, Ca, Si, PO_4 and NH_4. *In* Heezen, B. C., MacGregor, I. D., et al., *Init. Repts. DSDP*, 20: Washington (U.S. Govt. Printing Office), 813–829.

Gieskes, J. M., 1974. Interstitial water studies, Leg 25. *In* Simpson, E. S., Schlich, R., et al., *Init. Repts. DSDP*, 25: Washington (U.S. Govt. Printing Office), 361–394.

Gieskes, J. M., 1983. The chemistry of interstitial waters of deep sea sediments: interpretation of Deep Sea Drilling data. *Chem. Oceanogr.*, 8:221–269.

Gieskes, J. M., and Johnston, K., 1984. Interstitial water studies Leg 81. *In* Roberts, D. G., Schnitker, D., et al., *Init. Repts. DSDP*, 81: Washington (U.S. Govt. Printing Office), 829–836.

Gieskes, J. M., and Peretsman, G., 1986. Procedures of interstitial water analysis. *ODP Technical Report*.

Gose, W. A., 1982. Some paleomagnetic results from Deep Sea Drilling Project Leg 67 off Guatemala. *In* Aubouin, J., von Huene, R., et al. *Init. Repts. DSDP*, 67: Washington (U.S. Govt. Printing Office), 669–673.

Hanshaw, B. B., and Coplen, T. B., 1973. Ultrafiltration by a compacted clay membrane-II. Sodium ion exclusion at various ionic strengths. *Geochim. Cosmochim. Acta*, 47:2311.

Hickman, S. H., Langseth, M. G., and Svitek, J. F., 1984. *In situ* permeability and pore-pressure measurements near the mid-Atlantic Ridge, Deep Sea Drilling Project Hole 395A. *In* Hyndman, R. D., Salisbury, M. H., et al., *Init. Repts. DSDP*, 78B: Washington (U.S. Govt. Printing Office), 699–708.

Hsui, A. T., and Toksoz, M. N., 1979. The evolution of thermal structures beneath a subduction zone. *Tectonophysics*, 60:43–60.

Jagner, D., and Aren, K., 1970. A rapid automatic method for the determination of the total halide concentration in sea water by means of a potentiometric titration. *Anal. Chim. Acta*, 52:491.

Kharaka, Y. K., Hull, R. W., and Carothers, W. W., 1985. Water-rock interactions in sedimentary basins. *In* Relationship of organic matter and mineral diagenesis. *SEPM Short Course* No. 17:74–176.

Langseth, M., and Burch, T., 1981. Geothermal observations on the Japan trench transect. *In* Langseth, M., Okada, H., et al., *Init. Repts. DSDP*, 56, Pt. 2: Washington (U.S. Govt. Printing Office), 1207–1210.

Langseth, M., Westbrook, G., and Hobart, M., 1986. Geothermal transects of the lower trench slope of the Brabados accretionary prism. [paper presented at the 11th Annual Caribbean Geological Conference, Bridgetown, Barbados].

Lister, C. R. B., 1977. Estimates for heat flow and deep rock properties based on boundary layer theory. *Tectonophys.*, 41:157–171.

Marine, I. W., and Fritz, S. J., 1981. Osmotic model to explain anomalous hydraulic heads. *Water Resour. Res.*, 17:73.

Marlow, M., Lee, H., and Wright, A., 1984. Physical properties of sediment from the Lesser Antilles margin along the Barbados Ridge: results from Deep Sea Drilling Project Leg 78A. *In* Biju-Duval, B., Moore, J. C., et al., 1984. *Init. Repts. DSDP*, 78A: Washington (U.S. Govt. Printing Office), 549–558.

McDuff, E., 1981. Major cation gradients in DSDP interstitial waters: the role of diffusive exchange between sea water upper ocean crust. *Geochim. Cosmochim. Acta*, 45:1705.

Minster, J. B., and Jordan, T. H., 1978. Present-day plate motions. *J. Geophys. Res.*, 83:5331–5354.

Moore, J. C., and Biju-Duval, B., 1984. Tectonic synthesis, Deep Sea Drilling Project Leg 78A: Structural evolution of offscraped and underthrust sediment, northern Barbados Ridge complex. *In* Biju-Duval, B. and Moore, J. C., et al., *Init. Repts. DSDP*, 78A: Washington (U.S. Govt. Printing Office), 601–621.

Ngokwey, K., Mascle, A., and Biju-Duval B., 1984. Geophysical setting of DSDP Sites 541, 542, and 543, Leg 78A, Barbados accretionary prism. *In* Biju-Duval, B., Moore, J. C., et al., *Init. Repts. DSDP*, 78A: Washington (U.S. Govt. Printing Office), 39–48.

Niitsuma, N., 1981. Paleomagnetic results, Middle America trench off Mexico, Deep Sea Drilling Project Leg 66. *In* Watkins, J. S., Moore, J. C. et al., *Init. Repts. DSDP*, 66: Washington (U.S. Govt. Printing Office), 737–770.

Okada, H., and Bukry, D., 1980. Supplementary modification and introduction of code numbers to the low latitude coccolith biostratigraphic zonation (Bukry, 1973, 1975). *Mar. Micropaleontolog*, 5: 321–325.

Papadopulos, I. S., Bredehoeft, J. D., and Cooper, H. H., 1973. On the analysis of 'slug test' data. *Water Resour. Res.*, 9:1087–1089.

Pudsey, C. J., 1984. X-ray mineralogy of Miocene and older sediments from Deep Sea Drilling Project leg 78A. *In* Biju-Duval, B., and Moore, J. C., et al., *Init. Repts. DSDP*, 78A: Washington (U.S. Govt. Printing Office), 325–341.

Pyles, M. R., 1984. Vane shear data on undrained residual strength. *J. Geotech. Div., Am. Soc. Civ. Eng.*, 110:543–547.

Riedel, W. R., and Sanfilippo, A., 1978. Stratigraphy and evolution of tropical Cenozoic radiolarians. *Micropaleontology*, 24:61–96.

Rögl, F., and Bolli, H. M., 1973. Holocene to Pleistocene planktonic foraminifera of Leg 15, Site 147 (Cariaco Basin (Trench), Carribean Sea) and their climatic interpretation. *In* Edgar, T. N., Saunders, J. B., *Init. Repts. DSDP*, 15: Washington (U.S. Govt. Printing Office), 553–615.

Sanders, J. B., Bernoulli, D., Müller-Merz, E., Oberhänsli, H., Perch-Nielsen, K., Riedel, W. R., Sanfilippo, A., and Torrini, R., Jr., 1984. Stratigraphy of later Middle Eocene to Early Oligocene in Bath Cliff section Barbados, West Indies. *Micropaleontology.*, 30: 390–425.

Schoell, M., 1984. Recent advances in petroleum isotope geochemistry. *Organic Geochem.*, 6:645–663.

Schubert, C. E., and Peter, G., 1974. Heat flow northeast of Guadeloupe Island, Lesser Antilles. *J. Geophys. Res.*, 79:2139–2140.

Seilacher, A., 1967. Bathymetry of trace fossils. *Mar. Geol.*, 5:413–428.

Shi, Y., and Wang, C. -Y., 1985. High pore pressure generation in sediments in front of the Barbados Ridge complex. *Geophys. Res. Lett.*, 12:773–776.

Shipley, T. H., and Shephard, L. E., 1982. Temperature data from the Mexico drilling area: Report on logging and inhole temperature experiments. *In* Watkins, J. S., Moore, J. C., et al., *Init. Repts. DSDP*, 66: Washington (U.S. Govt. Printing Office), 771–774.

Speed, R., Westbrook, G., Mascle, A., Biju-Duval, B., Ladd, J., Saunders, J., Stein, S., Schoonmaker, J., and Moore, J., 1984. *Lesser Antilles Arc and adjacent terranes*. Ocean Margin Drilling Program, Regional Atlas Series, *Atlas 10*: Woods Hole (Marine Science International) 27 sheets.

Sykes, L. R., McCann, W. R., and Kafka, A. L., 1983. Motion of Caribbean Plate during last 7 million years and implications for earlier Cenozoic movements. *J. Geophys. Res.*, 87:10656–10676.

Toksoz, M. N., Minear, J. W., and Junan, B. R., 1971. Temperature field and geophysical effects of a downgoing slab, *J. Geophys. Res.*, 76:1113–1138.

Uyeda, S., and Horai, K., 1982. Heat flow measurements on Deep Sea Drilling Project Leg 60. *In* Hussong, D., Uyeda, S., et al., *Init. Repts. DSDP*, 60: Washington (U.S. Govt. Printing Office), 789–800.

Valery, P., Nely, G., Mascle, A., Biju-Duval, B., Le Quellec, P., and Berthon, J. L., 1985. Structure et croissance d'un prisme d'accretion tectonique proche d'un continent: la ride de la Barbade au sud de l'arc Antillais. *In*: Mascle, A. (Ed.), *Symposium Geodynamique des Caraibes*, 27:173–186 Edition TECHNIP.

Von Huene, R., and Lee, H., 1983, The possible significance of pore fluid pressures in subduction zones. *In* Watkins, J. S., and Drake, C. L. (Eds.), *Studies in Continental Margin Geology, Am. Asso. Pet. Geol. Memoir* 34:781–791.

Westbrook, G. K., 1982. The Barbados Ridge complex: tectonics of a mature forearc system. *In* Leggett, J. K. (Ed.), *Trench-Forearc Geology*, Sp. Publ. Geol. Soc. London, No. 10: London (Blackwells), pp. 275–290.

Whelan, J. K., and Sato, S., 1980. C_1-C_5 hydrocarbons from core gas pockets, DSDP Legs 56 and 57, Japan Trench Transect. *Init. Repts. DSDP*, 56, 57, Pt 2: Washington (U.S. Govt. Printing Office), 1335–1347.

Wilkens, R. H., and Handyside, T., 1985. Physical properties of equatorial Pacific sediments. *In* Mayer, L., Theyer, F., et al., *Initial Repts. DSDP*, 85:Washington (U.S. Govt. Printing Office), 839–847.

Wilson, D. S., 1984. Paleomagnetic results from Deep Sea Drilling Project Leg 78A. *In* Biju-Duval, B., Moore, J. C. et al., *Init. Repts. DSDP*, 78A: Washington (U.S. Govt. Printing Office), 583–591.

Ms 110A-105

SITE 671 HOLE A CORE 1 H CORED INTERVAL 4931.6-4936.6 mbsl; 0-5 mbsf

TIME-ROCK UNIT	BIOSTRAT. ZONE/ FOSSIL CHARACTER: FORAMINIFERS	NANNOFOSSILS	RADIOLARIANS	DIATOMS	PALEOMAGNETICS	PHYS. PROPERTIES	CHEMISTRY	SECTION	METERS	GRAPHIC LITHOLOGY	DRILLING DISTURB.	SED. STRUCTURES	SAMPLES	LITHOLOGIC DESCRIPTION
LOWER PLEISTOCENE	*Globorotalia truncatulinoides* Zone/ (*G. hessi* subzone)	R/P	vR/vP	indet.				1	0.5				*	CLAY-BEARING, FORAMINIFER-BEARING, VOLCANIC COMPONENT-BEARING NANNOFOSSIL-BEARING MUD
		Pseudoemiliania lacunosa Zone							1.0				*	CLAY-BEARING, FORAMINIFER-BEARING, VOLCANIC COMPONENT-BEARING NANNOFOSSIL-BEARING MUD, generally yellow-brown (10YR5/4), moderate to strong bioturbation, little drilling disturbance.
								2					*	Minor lithology: several cm-scale beds of volcanic ash.
								3					IW ** *	SMEAR SLIDE SUMMARY (%):
								4					PP	
								CC					*	

	1, 78 M	1, 110 D	2, 40 D	3, 5 D	3, 19 D	CC D
TEXTURE:						
Sand	5	—	27	18	10	5
Silt	93	10	10	10	50	15
Clay	2	90	63	72	40	80
COMPOSITION:						
Feldspar	10	5	15	5	20	1
Mica	—	—	—	2	—	—
Clay	—	85	24	20	44	17
Volcanic glass	86	—	5	—	—	3
Accessory minerals						
Clinopyroxene	2	Tr	—	—	—	2
Opaques	Tr	—	—	—	25	Tr
Hornblende	—	—	5	—	Tr	—
Foraminifers	—	—	7	10	—	—
Nannofossils	2	10	30	45	10	70
Diatoms	—	Tr	6	5	Tr	2
Radiolarians	Tr	Tr	5	10	—	1
Sponge spicules	—	Tr	3	3	Tr	3
Silicoflagellates	—	Tr	—	—	Tr	1

Information on Core Description Forms, for ALL sites, represents field notes taken aboard ship. Some of this information has been refined in accord with post-cruise findings, but production schedules prohibit definitive correlation of these forms with subsequent findings. Thus the reader should be alerted to the occasional ambiguity or discrepancy.

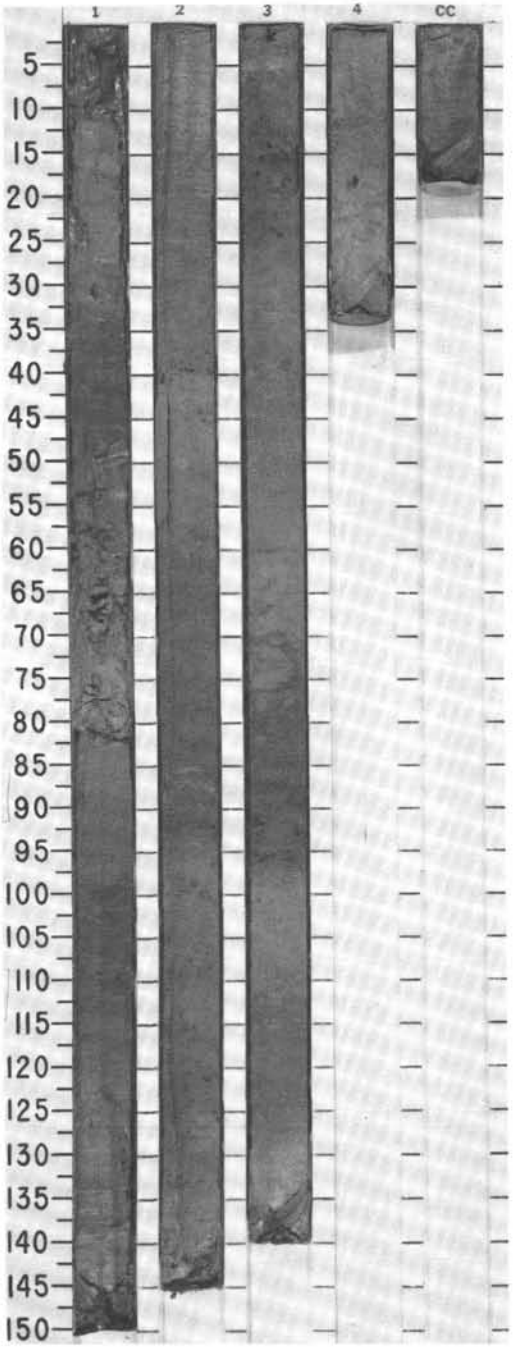

SITE 671 HOLE B CORE 1 H CORED INTERVAL 4931.7-4939.1 mbsl; 0.0-7.4 mbsf

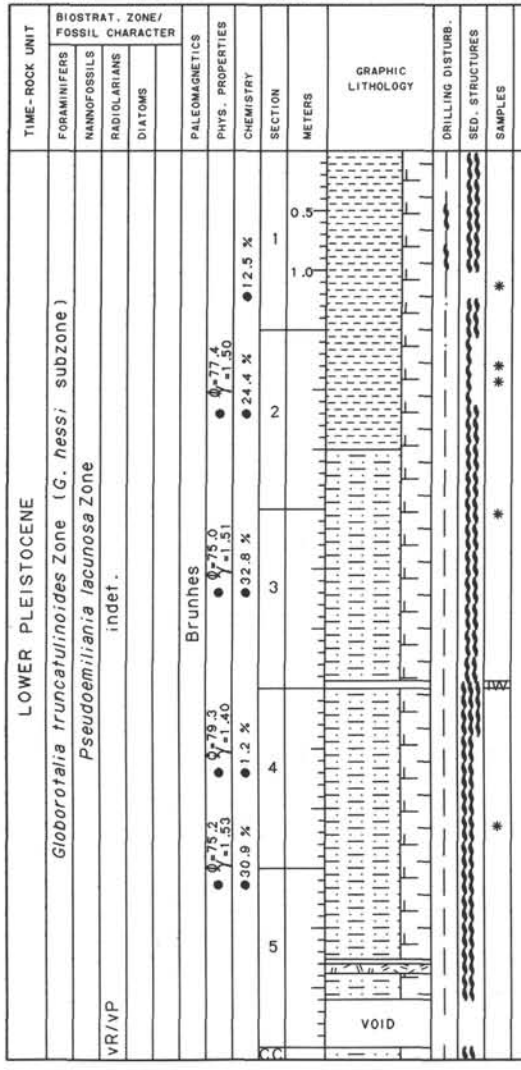

LITHOLOGIC DESCRIPTION

CALCAREOUS MUD

CALCAREOUS MUD, generally yellow-brown (10YR5/4), mild to moderate bioturbation with large non-systematic variations in clay content, little drilling disturbance.

Minor lithology: blebs of volcanic ash in main lithology, one distinct layer of volcanic ash.

SMEAR SLIDE SUMMARY (%):

	1, 120 D	2, 37 D	2, 50 D	3, 3 D	4, 115 D
TEXTURE:					
Sand	Tr	1	Tr	5	Tr
Silt	7	4	15	25	10
Clay	93	95	85	70	90
COMPOSITION:					
Feldspar	Tr	5	Tr	—	Tr
Clay	74	69	50	58	86
Volcanic glass	Tr	—	30	2	12
Accessory minerals					
Clinopyroxene	Tr	—	—	Tr	—
Fe/Mn oxides	—	1	—	20	—
Foraminifers	—	—	Tr	—	—
Nannofossils	25	25	20	20	2
Radiolarians	—	—	Tr	—	Tr
Sponge spicules	Tr	—	Tr	Tr	Tr

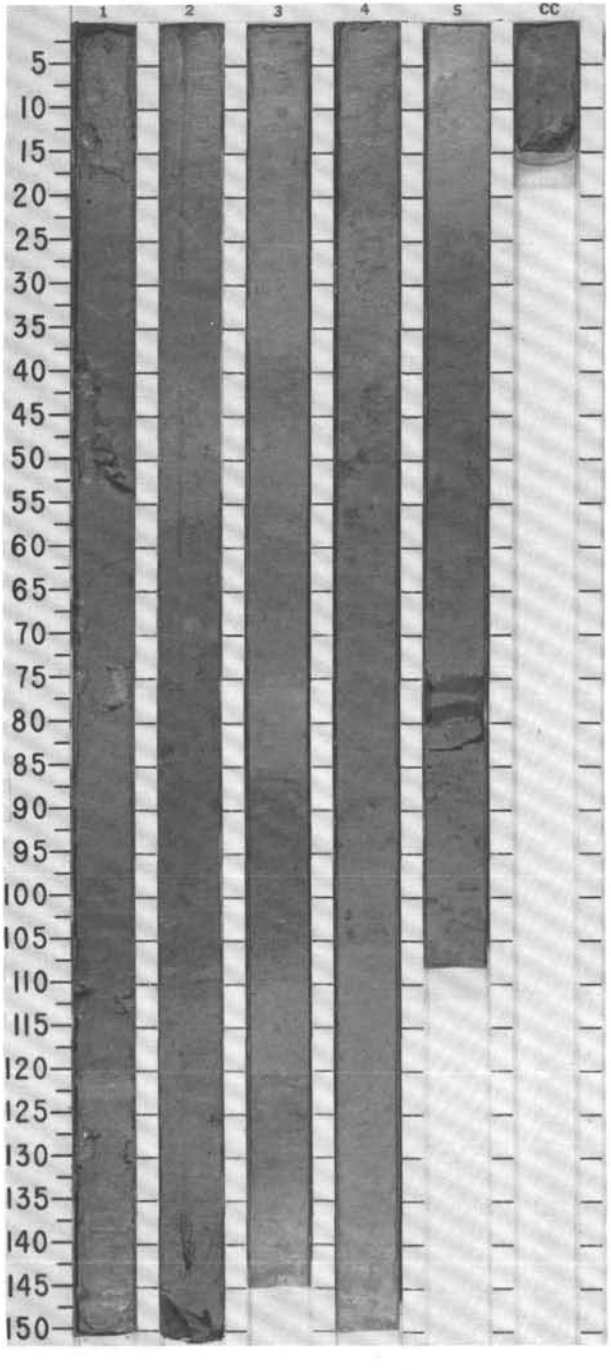

SITE 671 HOLE B CORE 2 H CORED INTERVAL 4939.1-4948.6 mbsl; 7.4-16.9 mbsf

TIME-ROCK UNIT: LOWER PLEISTOCENE
BIOSTRAT. ZONE/FOSSIL CHARACTER: *Globorotalia truncatulinoides* Zone (*G. hessi* subzone); *Helicoportosphaera sellii* Zone; Barren
FORAMINIFERS
NANNOFOSSILS
RADIOLARIANS
DIATOMS
PALEOMAGNETICS: Brunhes
PHYS. PROPERTIES: Φ=72.4, ρ=1.54; Φ=71.2, ρ=1.60; Φ=78.4, ρ=1.48; Φ=73.3, ρ=1.47
CHEMISTRY: 22.5 %; 38.4 %; 24.3 %; 35.6 %
SECTION: 1, 2, 3, 4, 5, 6, 7, CC
METERS: 0.5, 1.0
GRAPHIC LITHOLOGY
DRILLING DISTURB.
SED. STRUCTURES
SAMPLES: TW, OG

LITHOLOGIC DESCRIPTION

CALCAREOUS MUD

Dominantly yellow-brown CALCAREOUS MUD showing moderate bioturbation. Little drilling disturbance apart from strong drilling features in Section 7. Occasional blebs of lithic crystal ash in main lithology.

Minor lithology: three distinct layers of glass-crystal volcanic ash.

SMEAR SLIDE SUMMARY (%):

	1, 130 M	4, 10 M	4, 110 D	6, 70 D	CC, 9 M	CC, 28 D
TEXTURE:						
Sand	80	20	Tr	—	30	—
Silt	10	70	1	10	20	10
Clay	10	10	99	90	50	90
COMPOSITION:						
Feldspar	10	3	—	2	20	—
Clay	10	10	65	72	15	81
Volcanic glass	20	85	—	—	60	1
Accessory minerals	—	—	Tr	—	—	—
Clinopyroxene	—	2	—	—	5	—
Hornblende	60	—	—	—	—	1
Foraminifers	—	—	—	—	—	2
Nannofossils	—	—	35	25	—	15
Sponge spicules	—	—	—	1	—	—

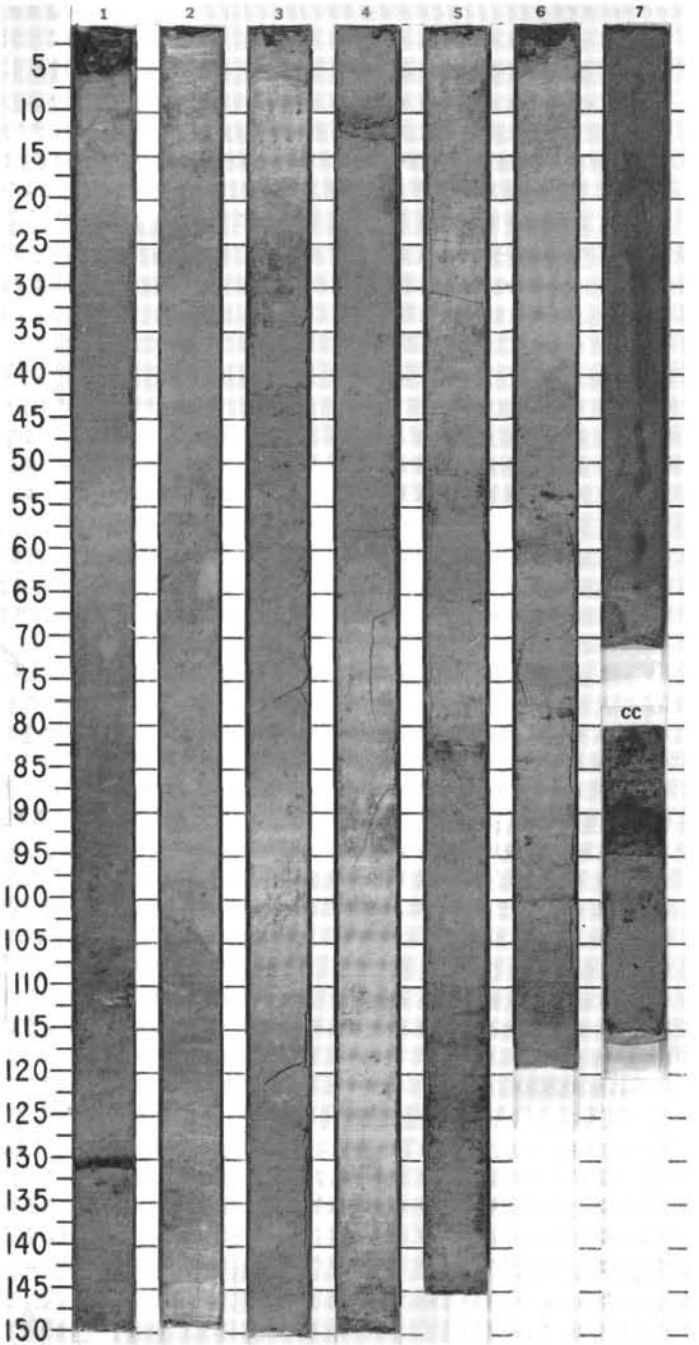

SITE 671 HOLE B CORE 3 H CORED INTERVAL 4948.6-4958.1 mbsl; 16.9-26.4 mbsf

TIME-ROCK UNIT	BIOSTRAT. ZONE/ FOSSIL CHARACTER: FORAMINIFERS	NANNOFOSSILS	RADIOLARIANS	DIATOMS	PALEOMAGNETICS	PHYS. PROPERTIES	CHEMISTRY	SECTION	METERS	GRAPHIC LITHOLOGY	DRILLING DISTURB.	SED. STRUCTURES	SAMPLES
LOWER PLEISTOCENE	*Globorotalia truncatulinoides* Zone (*G. hessi* subzone)	*Calcidiscus macintyrei* Zone	Barren	B		Φ 70.2 ρ 1.82	9.2 %	1	0.5				
								1	1.0				
								2					*
								3		VOID			IW
						Φ 66.8 ρ 1.66	38.7 %	4					
								5					PP
						Φ 68.7 ρ 1.61	14.9 %	6		VOID			
								7					
								CC					

LITHOLOGIC DESCRIPTION

MUD, CALCAREOUS MUD, and MARL

MUD, CALCAREOUS MUD, and MARL, olive-brown to olive-gray (5Y5/2, 5Y6/2, 5Y7/1), with moderate to strong bioturbation. Apart from 20 cm interval at beginning of core, there is only very minor drilling disturbance.

Minor lithology: one distinct layer of glassy volcanic ash.

SMEAR SLIDE SUMMARY (%):

	2, 36 M
TEXTURE:	
Sand	6
Silt	25
Clay	69
COMPOSITION:	
Feldspar	15
Clay	10
Volcanic glass	70
Accessory minerals	
Clinopyroxene	5

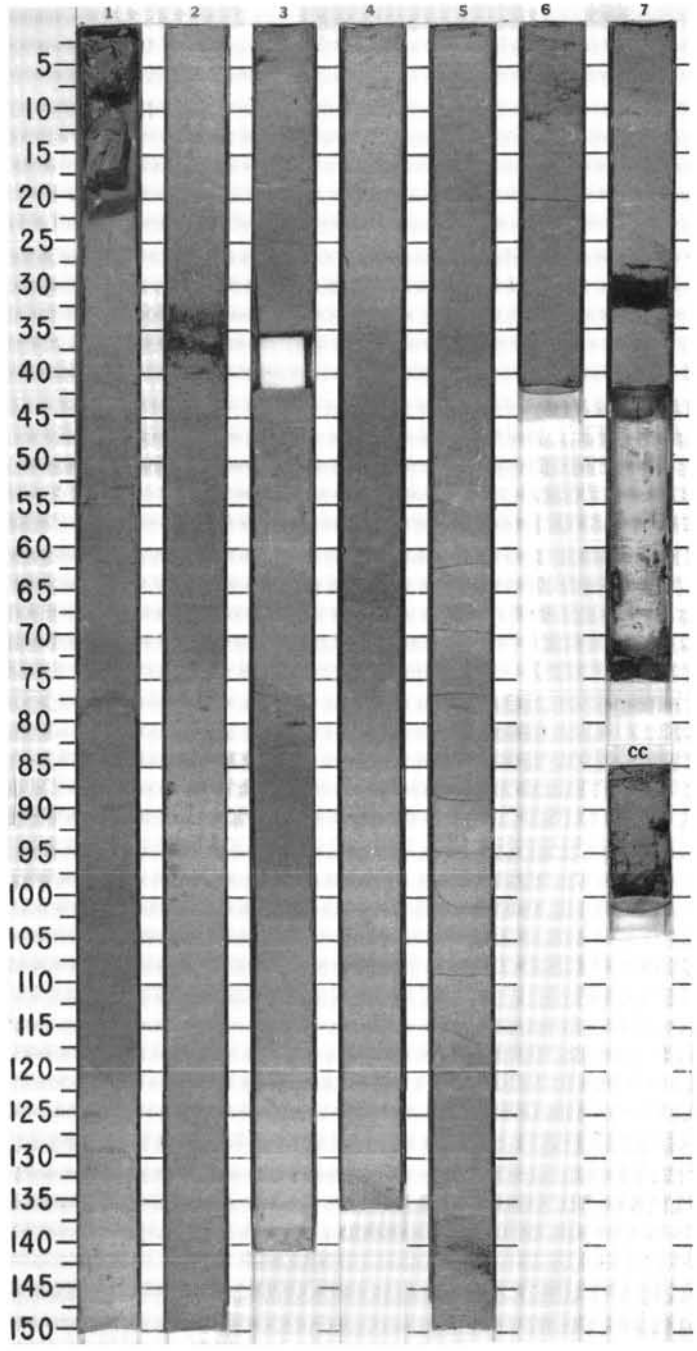

SITE 671 HOLE B CORE 4 H CORED INTERVAL 4958.1-4967.6 mbsl; 26.4-35.9 mbsf

TIME-ROCK UNIT	BIOSTRAT. ZONE/ FOSSIL CHARACTER: FORAMINIFERS	NANNOFOSSILS	RADIOLARIANS	DIATOMS	PALEOMAGNETICS	PHYS. PROPERTIES	CHEMISTRY	SECTION	METERS	GRAPHIC LITHOLOGY	DRILLING DISTURB.	SED. STRUCTURES	SAMPLES
UPPER PLIOCENE	*Globorotalia truncatulinoides* Zone (PL6)	CN12 d	Barren		Olduvai / Matuyama	● ϕ_r=64.8 / χ=1.70	● 30.8 %	6					
						● ϕ_r=68.4 / χ=1.64	● 34.1 %	5					
						● ϕ_r=73.6 / χ=1.53	● 9.7 %	4					
								3					
								2					
								1	0.5 / 1.0				
								7					
								CC					

LITHOLOGIC DESCRIPTION

CALCAREOUS MUD

Variegated CALCAREOUS MUD, Sections 1 and 2 dominantly gray (10YR6/2, 10Y6/1), Section 3 contains mostly olive (5Y6/4) mud rich in foraminifers, Sections 4 to 7 are dominantly gray (10Y6/1, 5Y5/1, 5GY6/1, 5Y6/2) muds, containing scattered sand-sized foraminifers. Patchy, but strong bioturbation in Sections 3 to 7.

Minor lithology: one gray (5Y4/1) ashy bed at the base of Section 3 with burrows of *Teichinus* type. One distinct gray layer of volcanic ash in Section 6.

SMEAR SLIDE SUMMARY (%):

	3, 8 D	4, 122 D	5, 93 D
TEXTURE:			
Sand	5	20	3
Silt	20	30	12
Clay	75	50	85
COMPOSITION:			
Feldspar	Tr	25	—
Mica	2	—	—
Clay	28	10	49
Volcanic glass	Tr	—	3
Accessory minerals			
Glauconite	—	Tr	—
Pyrite	Tr	—	—
Zeolite	—	—	Tr
Opaques	—	—	3
Foraminifers	25	25	2
Nannofossils	45	40	40
Chitinozoa	—	—	Tr
Bioclasts	—	—	2

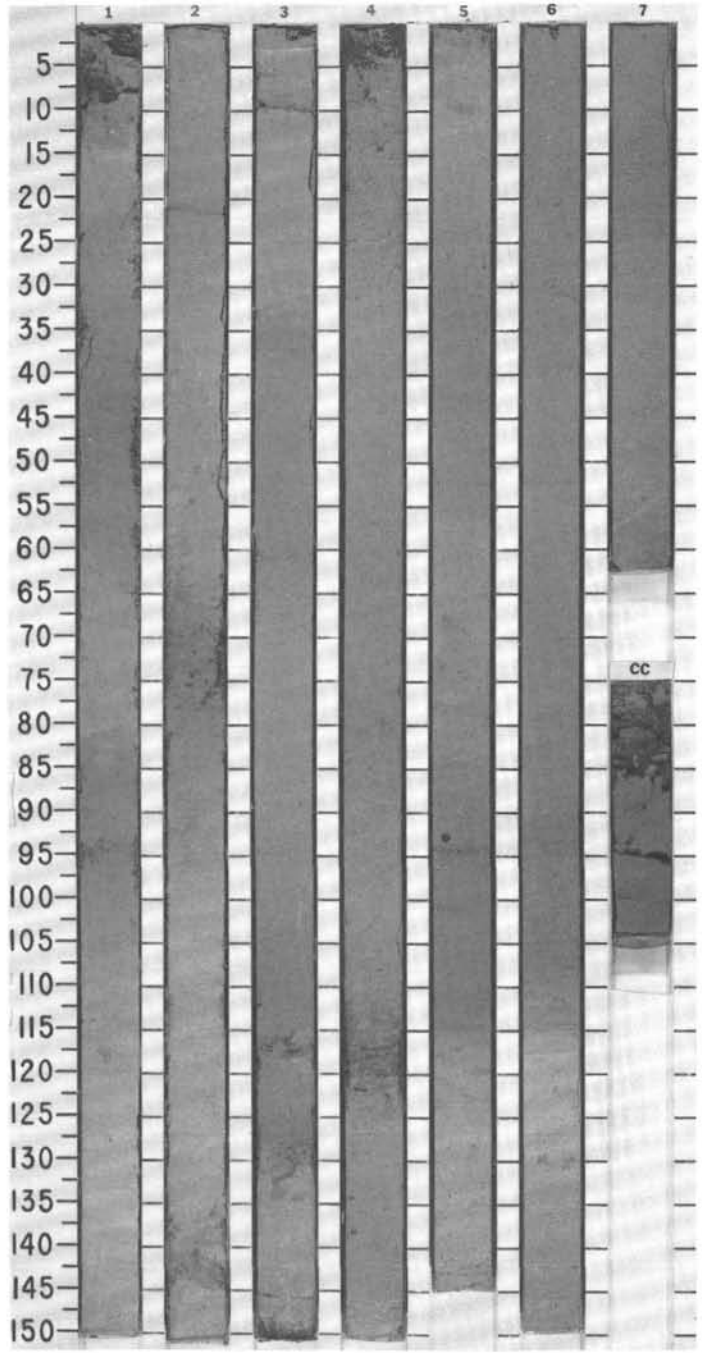

SITE 671 HOLE B CORE 5 H CORED INTERVAL 4967.6-4977.1 mbsl; 35.9-45.4 mbsf

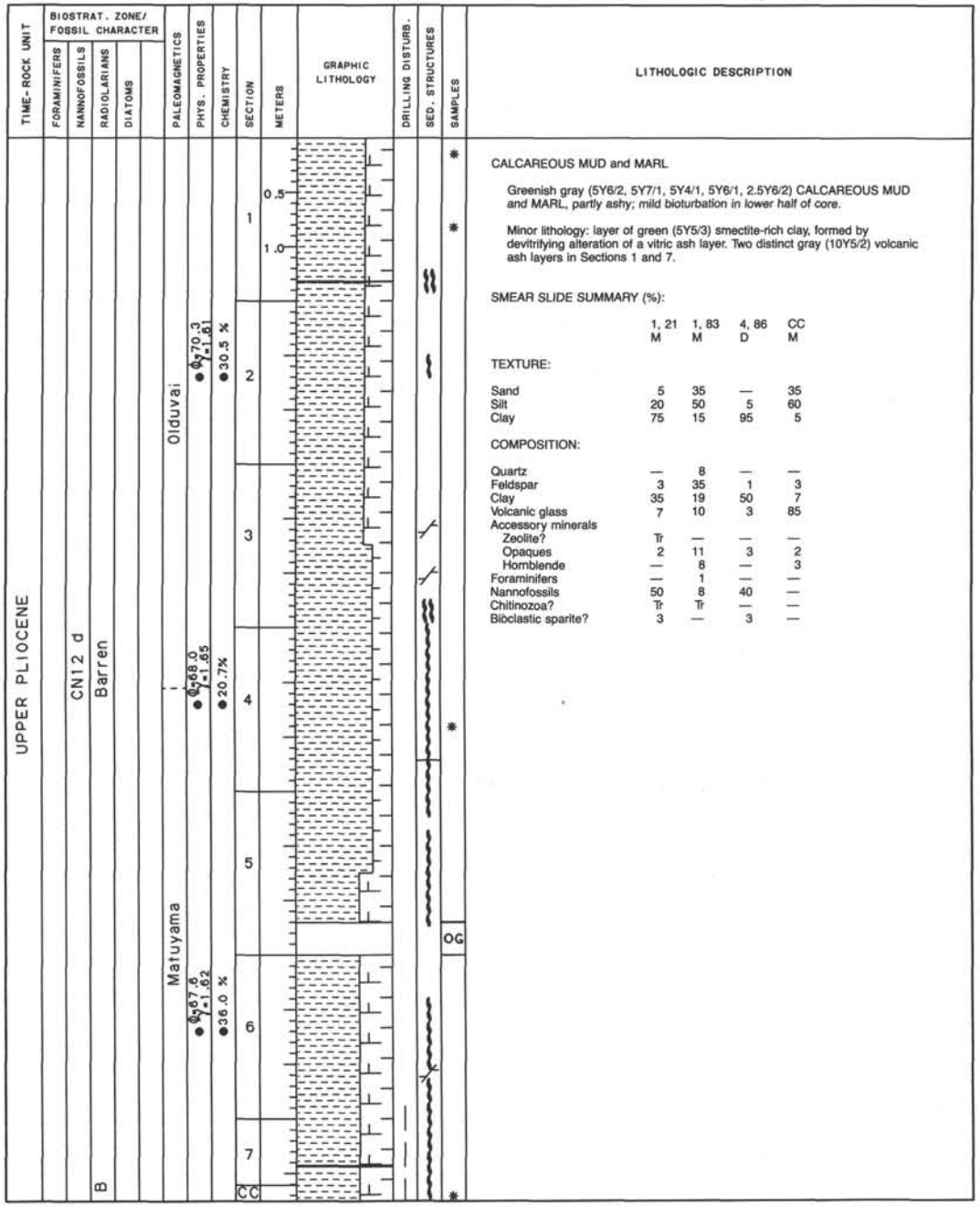

LITHOLOGIC DESCRIPTION

CALCAREOUS MUD and MARL

Greenish gray (5Y6/2, 5Y7/1, 5Y4/1, 5Y6/1, 2.5Y6/2) CALCAREOUS MUD and MARL, partly ashy; mild bioturbation in lower half of core.

Minor lithology: layer of green (5Y5/3) smectite-rich clay, formed by devitrifying alteration of a vitric ash layer. Two distinct gray (10Y5/2) volcanic ash layers in Sections 1 and 7.

SMEAR SLIDE SUMMARY (%):

	1, 21 M	1, 83 M	4, 86 D	CC M
TEXTURE:				
Sand	5	35	—	35
Silt	20	50	5	60
Clay	75	15	95	5
COMPOSITION:				
Quartz	—	8	—	—
Feldspar	3	35	1	3
Clay	35	19	50	7
Volcanic glass	7	10	3	85
Accessory minerals				
Zeolite?	Tr	—	—	—
Opaques	2	11	3	2
Hornblende	—	8	—	3
Foraminifers	—	1	—	—
Nannofossils	50	8	40	—
Chitinozoa?	Tr	Tr	—	—
Bioclastic sparite?	3	—	3	—

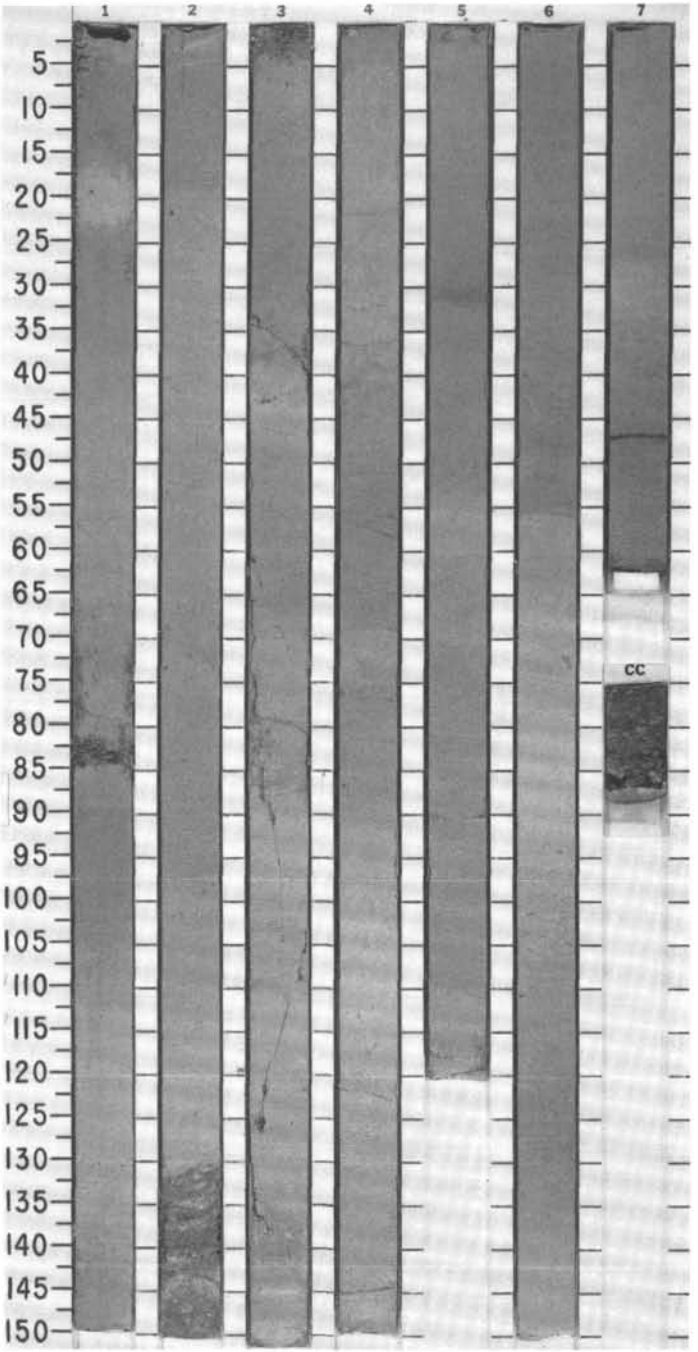

SITE 671 HOLE B CORE 6 H CORED INTERVAL 4977.1-4986.6 mbsl; 45.4-54.9 mbsf

TIME-ROCK UNIT: UPPER PLIOCENE
Globorotalia miocenica Zone (*G. exilis* subzone) (PL5)
BIOSTRAT. ZONE/FOSSIL CHARACTER: FORAMINIFERS: CN12 b; NANNOFOSSILS: Barren; RADIOLARIANS: B; DIATOMS
PALEOMAGNETICS
PHYS. PROPERTIES: ● 0-59.4 / 7-1.69; ● 0-63.0 / 7-1.68; ● 0-67.9 / 7-1.63
CHEMISTRY: ● 5.8 %; ● 40.7 %; ● 31.1 %
SECTION: 1, 2, 3, 4, 5, 6, 7, CC
METERS: 0.5, 1.0
GRAPHIC LITHOLOGY: VOID
DRILLING DISTURB.
SED. STRUCTURES
SAMPLES: IW

LITHOLOGIC DESCRIPTION

MUD, CLAY, and MARL

Greenish gray ((5Y6/2, 5Y6/1, 10Y5/1, 10Y6/2, 2.5Y6/2) MUD, CLAY, and MARL.

Minor lithology: three distinct gray volcanic ash beds in Sections 1, 2, and 4. One ashy mud horizon in Section 7.

SMEAR SLIDE SUMMARY (%):

	1, 79 D	1, 144 M	1, 148 M	2, 90 M	CC D
TEXTURE:					
Sand	15	65	30	—	—
Silt	5	15	50	50	6
Clay	80	20	20	50	94
COMPOSITION:					
Quartz	—	—	10	Tr	Tr
Feldspar	—	12	15	35	Tr
Clay	45	27	—	15	—
Volcanic glass	Tr	45	45	45	60
Accessory minerals					
Clinopyroxene	—	3	—	5	—
Opaques	—	10	5	—	—
Hornblende	—	3	—	—	Tr
Foraminifers	15	Tr	5	—	5
Nannofossils	40	Tr	10	Tr	35
Biolclasts	—	—	10	—	—

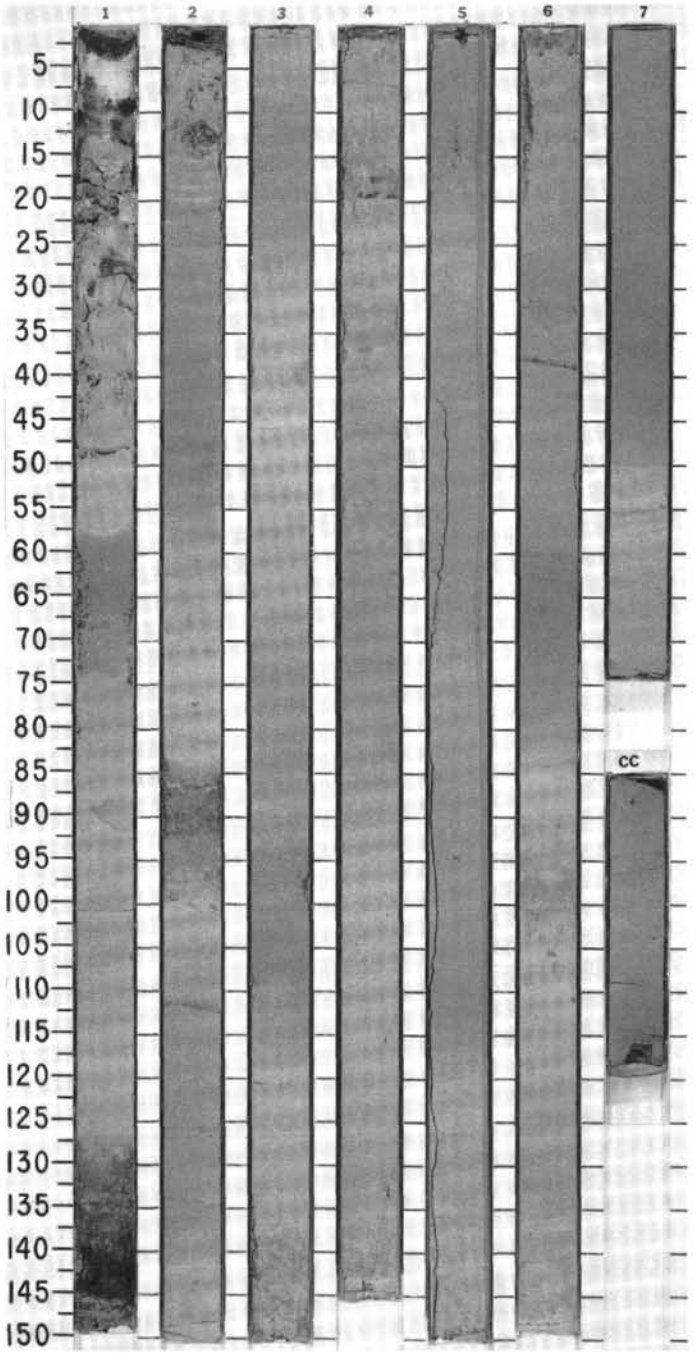

SITE 671 HOLE B CORE 7 H CORED INTERVAL 4986.6-4996.1 mbsl; 54.9-64.4 mbsf

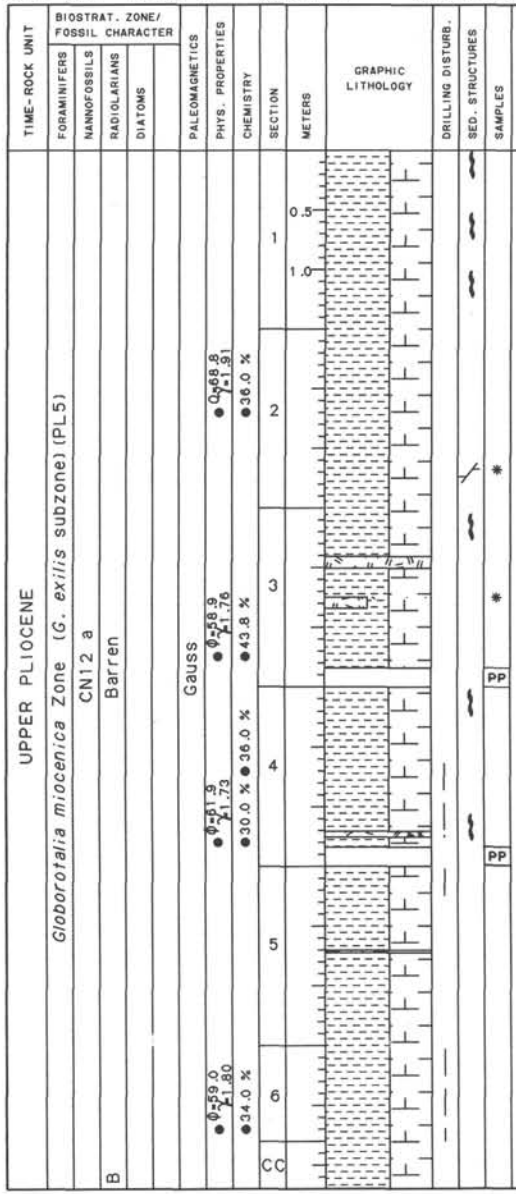

LITHOLOGIC DESCRIPTION

MARL

Light olive-gray to light brown (2.5Y6/2, 5Y6/2, 5Y7/2, 10Y7/1) MARL with patchy slight bioturbation.

Minor lithology: three distinct layers of gray volcanic ash.

SMEAR SLIDE SUMMARY (%):

	2, 122 M	3, 76 D
TEXTURE:		
Sand	2	2
Silt	70	8
Clay	28	90
COMPOSITION:		
Quartz	10	—
Feldspar	25	2
Clay	25	55
Volcanic glass	20	—
Accessory minerals		
Opaques	5	1
Hornblende	1	—
Foraminifers	2	—
Nannofossils	5	40
Bioclasts	7	2

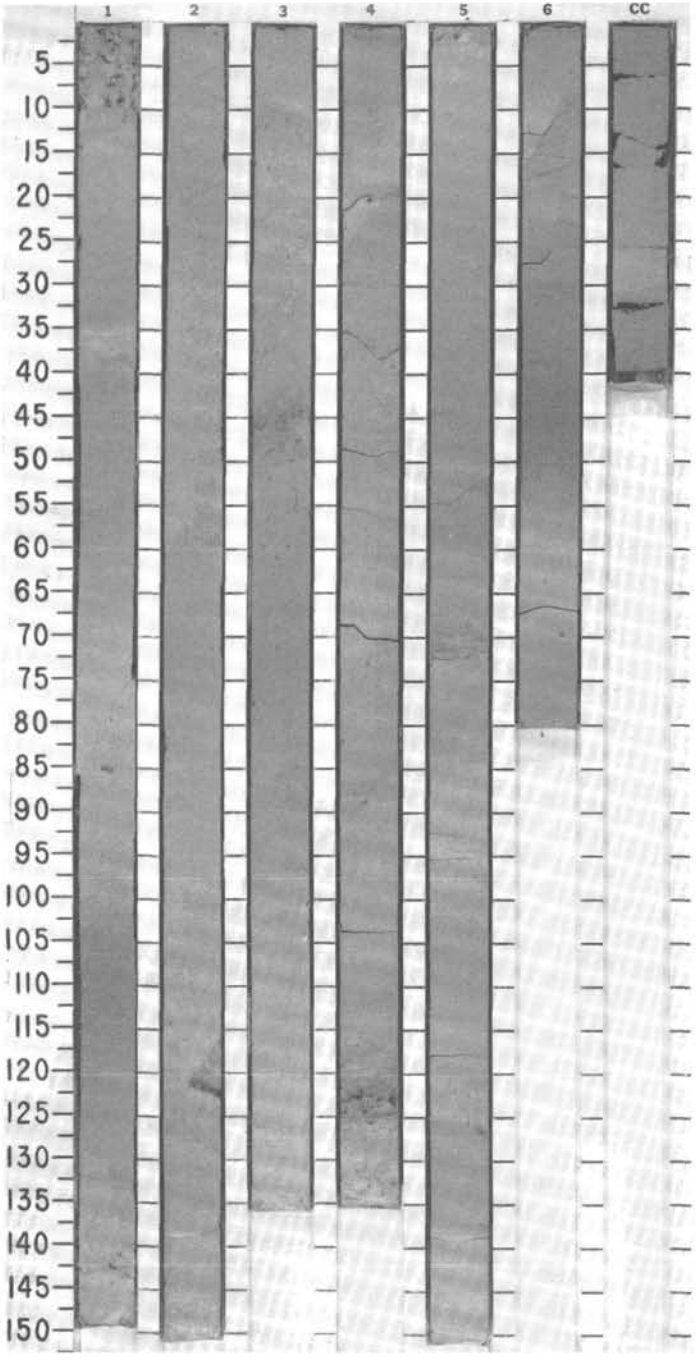

SITE 671 HOLE B CORE 8 H CORED INTERVAL 4996.1-5005.6 mbsl; 64.4-73.9 mbsf

TIME-ROCK UNIT	BIOSTRAT. ZONE/ FOSSIL CHARACTER: FORAMINIFERS	NANNOFOSSILS	RADIOLARIANS	DIATOMS	PALEOMAGNETICS	PHYS. PROPERTIES	CHEMISTRY	SECTION	METERS	GRAPHIC LITHOLOGY	DRILLING DISTURB.	SED. STRUCTURES	SAMPLES
LOWER PLIOCENE	*Globorotalia margaritae* Zone (PL2)	CN12 a	Barren	B	Gauss	Φ=61.2 ρ=1.76	43.4 %	1	0.5				*
									1.0				
								2					
						Φ=63.4 ρ=1.69	33.9 %	3					
								4					*
													TWC
								5					
													OG
						Φ=61.9 ρ=1.69	40.3 %	6					
								7					
								CC					

LITHOLOGIC DESCRIPTION

MARL

Light brown (2.5Y6/2, 5Y6/1, 5Y5/3) MARL, partly ashy, with mild to intense bioturbation.

Minor lithology: three distinct (5Y7/1) gray layers of bioturbated volcanic ash.

SMEAR SLIDE SUMMARY (%):

	1, 90 D	4, 16 D	4, 142 D
TEXTURE:			
Silt	5	5	31
Clay	95	95	69
COMPOSITION:			
Quartz	—	—	5
Feldspar	—	—	10
Clay	55	62	40
Volcanic glass	Tr	Tr	13
Accessory minerals	—	2	1
Glauconite	—	—	Tr
Clinopyroxene	—	—	Tr
Hornblende	—	—	Tr
Foraminifers	1	1	10
Nannofossils	40	35	20
Sponge spicules	Tr	—	—
Bioclasts	3	—	—

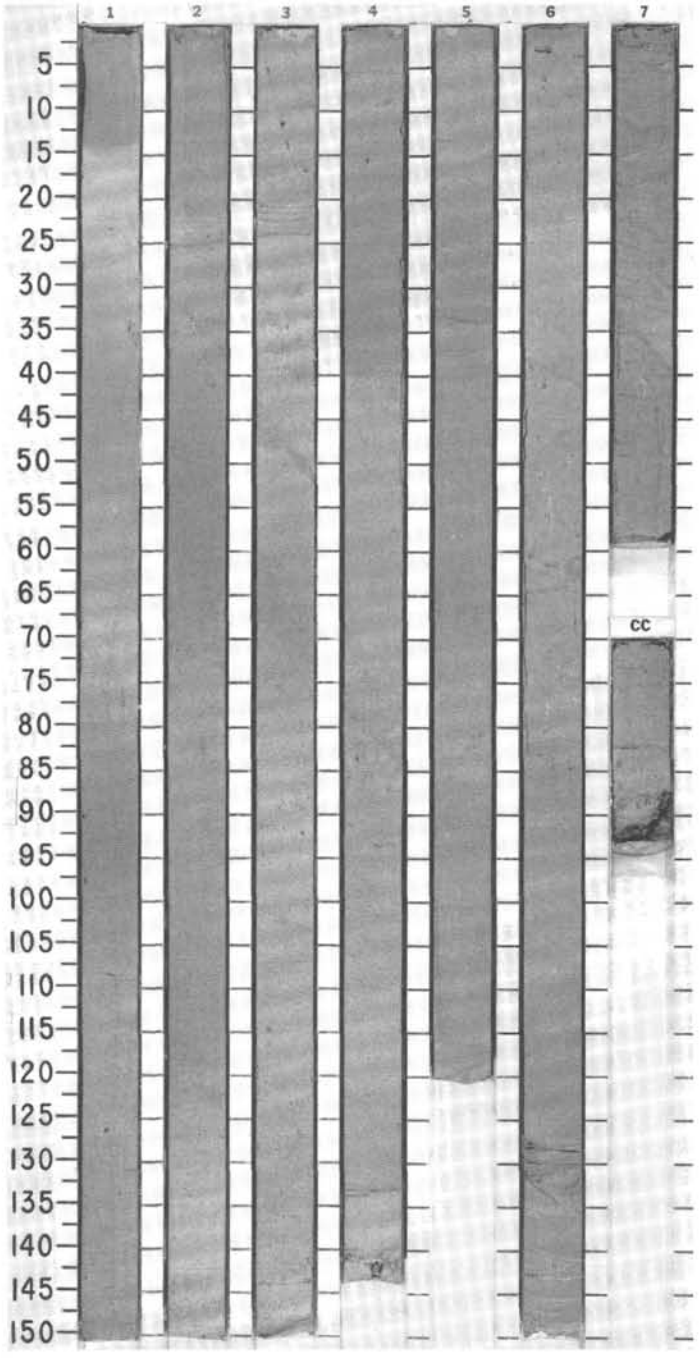

SITE 671 HOLE B CORE 9 H CORED INTERVAL 5005.6-5015.1 mbsl; 73.9-83.4 mbsf

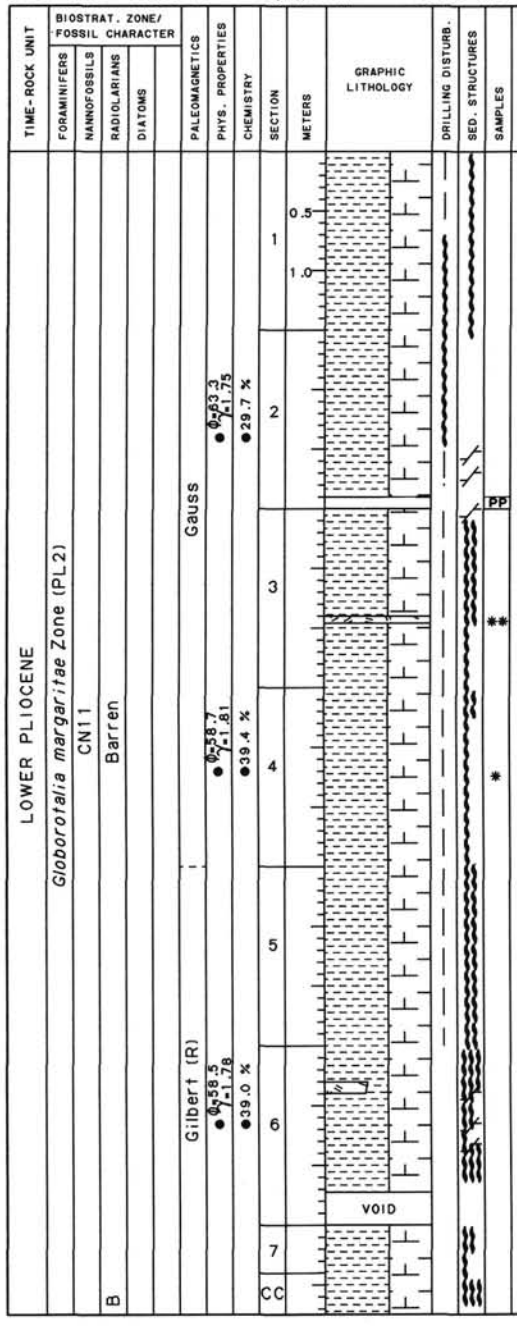

LITHOLOGIC DESCRIPTION

MARL

Olive-gray (5Y6/1 to 5Y7/1) to light green (5Y6/2 to 2.5Y6/2) MARL, moderately to strongly bioturbated.

Minor lithology: one distinct gray (2.5Y4/1) bed of vitric volcanic ash in Section 3.

SMEAR SLIDE SUMMARY (%):

	3, 95 M	3, 95 M	4, 80 D
TEXTURE:			
Sand	2	45	5
Silt	20	40	5
Clay	78	15	90
COMPOSITION:			
Feldspar	10	1	—
Clay	45	—	61
Volcanic glass	40	98	2
Accessory minerals			
Clinopyroxene	Tr	—	—
Foraminifers	—	—	2
Nannofossils	5	1	35

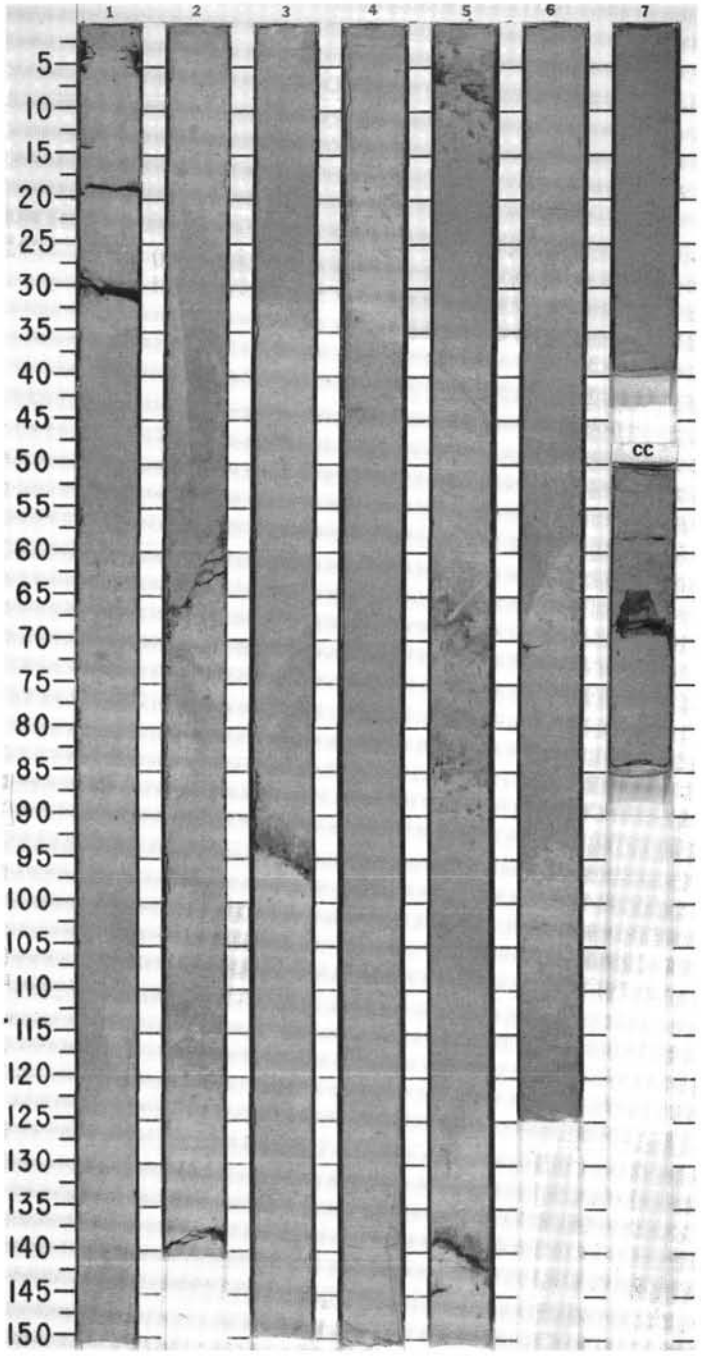

SITE 671 HOLE B CORE 10 H CORED INTERVAL 5015.1-5023.3 mbsl; 83.4-91.6 mbsf

TIME-ROCK UNIT	BIOSTRAT. ZONE/ FOSSIL CHARACTER: FORAMINIFERS	NANNOFOSSILS	RADIOLARIANS	DIATOMS	PALEOMAGNETICS	PHYS. PROPERTIES	CHEMISTRY	SECTION	METERS	GRAPHIC LITHOLOGY	DRILLING DISTURB.	SED. STRUCTURES	SAMPLES
LOWER PLIOCENE	*Globorotalia margaritae* Zone (PL2)	CN11	Barren		Gilbert (N) / Gilbert (R)	ϕ=58.8 ρ=1.76; ϕ=61.4 ρ=1.75; ϕ=61.7 ρ=1.70	40.8 %; 41.3 %; 29.4 %	1–6, CC	0.5; 1.0	VOID			PP, IW, PP

LITHOLOGIC DESCRIPTION

MARL

Whole core composed of greenish gray (5Y6/2 to 2.5Y6/2) to greenish (5Y7/2) ashy MARL, moderately to strongly bioturbated throughout core.

Minor lithology: three distinct dark gray (N3 to N6) ash beds in Sections 1 and 2.

SMEAR SLIDE SUMMARY (%):

	4, 61 D
TEXTURE:	
Sand	5
Silt	10
Clay	85
COMPOSITION:	
Clay	40
Volcanic glass	10
Foraminifers	5
Nannofossils	45

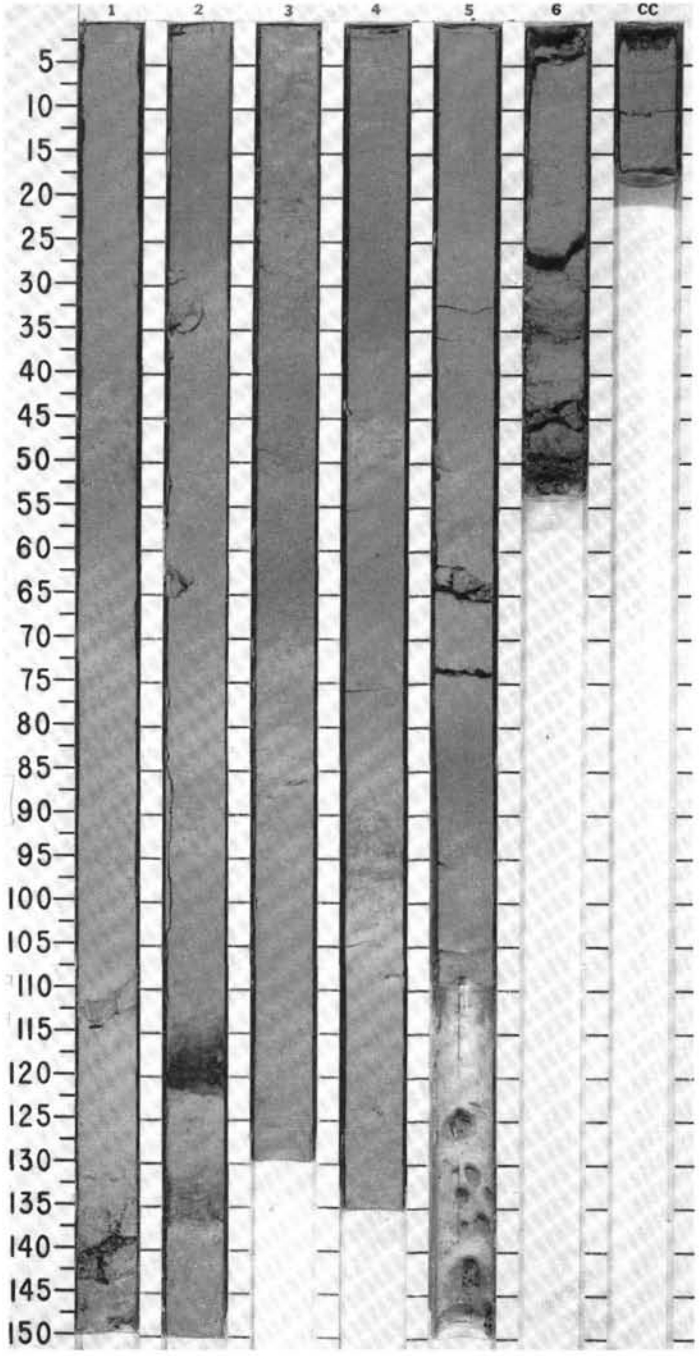

SITE 671 HOLE B CORE 11 X CORED INTERVAL 5023.3-5032.3 mbsl; 91.6-101.1 mbsf

TIME-ROCK UNIT	BIOSTRAT. ZONE/ FOSSIL CHARACTER: FORAMINIFERS	NANNOFOSSILS	RADIOLARIANS	DIATOMS	PALEOMAGNETICS	PHYS. PROPERTIES	CHEMISTRY	SECTION	METERS	GRAPHIC LITHOLOGY	DRILLING DISTURB.	SED. STRUCTURES	SAMPLES
LOWER PLIOCENE	*Globorotalia margaritae* Zone (PL1)	CN10 c	Barren			● Q=63.5 γ=1.71	● 43.7 %	1	0.5, 1.0				
								2					
								3					
						● Q=65.2 γ=1.68	● 33.5 %	4					* *
							34.6 %						OG
								5					
						● Q=57.3 γ=1.77	● 28.1 %	6					
								7					
			B					CC					*

LITHOLOGIC DESCRIPTION

MARL

Green-gray (5Y5/2, 5Y6/2, 5Y6/1, 5Y7/1) to olive-gray (2.5Y6/2) MARL, moderately to strongly bioturbated throughout core.

Minor lithology: three diffuse gray (5Y6/1 to N5) ashy mud layers in Section 3, one distinct, dark gray (N3) ash bed with sharp, but locally burrowed base in Section 5.

SMEAR SLIDE SUMMARY (%):

	4, 33 M	4, 75 D	CC, 17 D
TEXTURE:			
Sand	1	—	—
Silt	59	—	10
Clay	40	100	90
COMPOSITION:			
Feldspar	20	—	—
Clay	8	65	40
Volcanic glass	68	—	—
Accessory minerals	—	—	10
Clinopyroxene	2	—	—
Foraminifers	—	—	Tr
Nannofossils	2	35	50
Sponge spicules	Tr	—	Tr

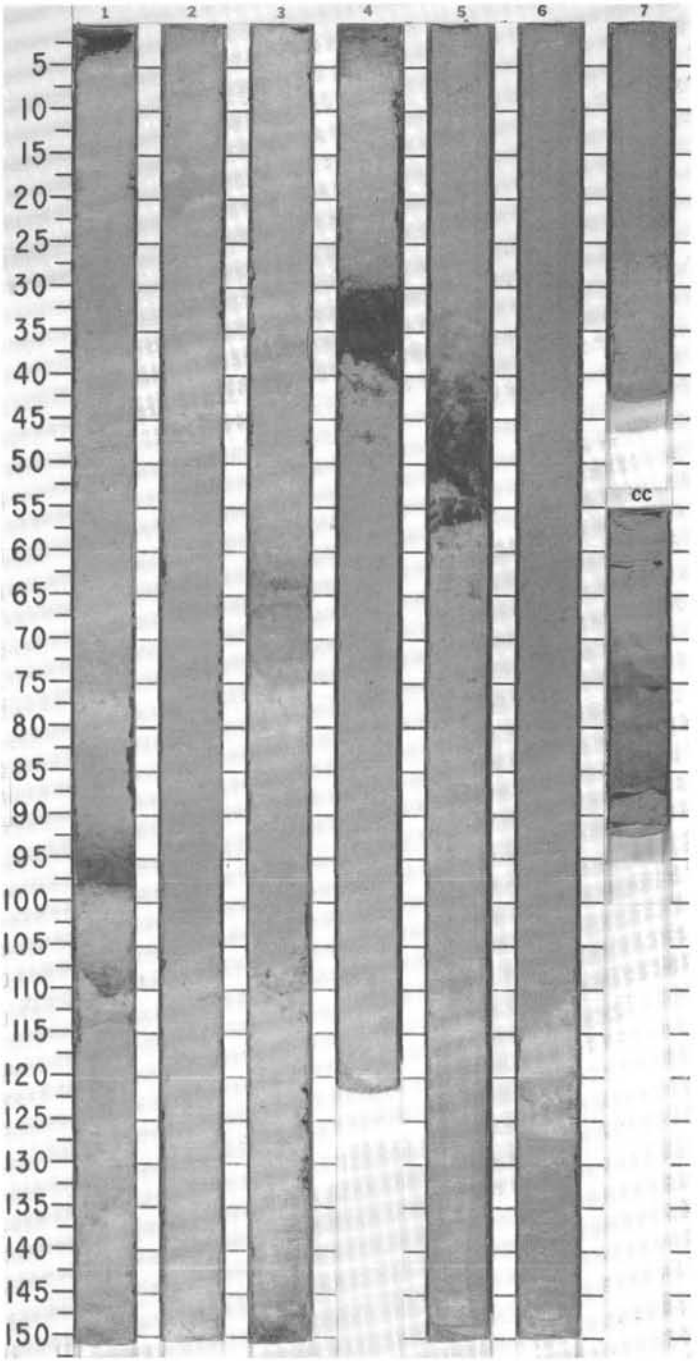

SITE 671 HOLE B CORE 12 X CORED INTERVAL 5032.8-5042.3 mbsl; 101.1-110.6 mbsf

TIME-ROCK UNIT	BIOSTRAT. ZONE/ FOSSIL CHARACTER: FORAMINIFERS	NANNOFOSSILS	RADIOLARIANS	DIATOMS	PALEOMAGNETICS	PHYS. PROPERTIES	CHEMISTRY	SECTION	METERS	GRAPHIC LITHOLOGY	DRILLING DISTURB.	SED. STRUCTURES	SAMPLES
LOWER PLIOCENE	*Globorotalia margaritae* Zone (PL1)	CN10 a	Barren	B		Φ=59.8 ρ=1.75 Φ=56.4 ρ=1.80 Φ=58.1 ρ=1.81	35.5 % 26.9 % 4.6 % 24.2 %	1 2 3 4 5 CC	0.5 1.0				*

LITHOLOGIC DESCRIPTION

CALCAREOUS MUD and MARL

Yellow-brown (10YR5/3, 10YR6/3, 10YR7/1, 2.5Y5/2, 2.5Y6/2) CALCAREOUS MUD in Sections 1 to 4. Section 5 contains light olive-gray (5Y6/2) MARL. Bioturbation is strong throughout the core.

Minor lithology: two distinct gray to blue-gray (5B4/1 to 5G7/1) layers of volcanic ash in Sections 2 and 5.

SMEAR SLIDE SUMMARY (%):

	2, 71 D	2, 121 D
TEXTURE:		
Silt	5	30
Clay	95	70
COMPOSITION:		
Clay	95	65
Volcanic glass	Tr	15
Nannofossils	5	20

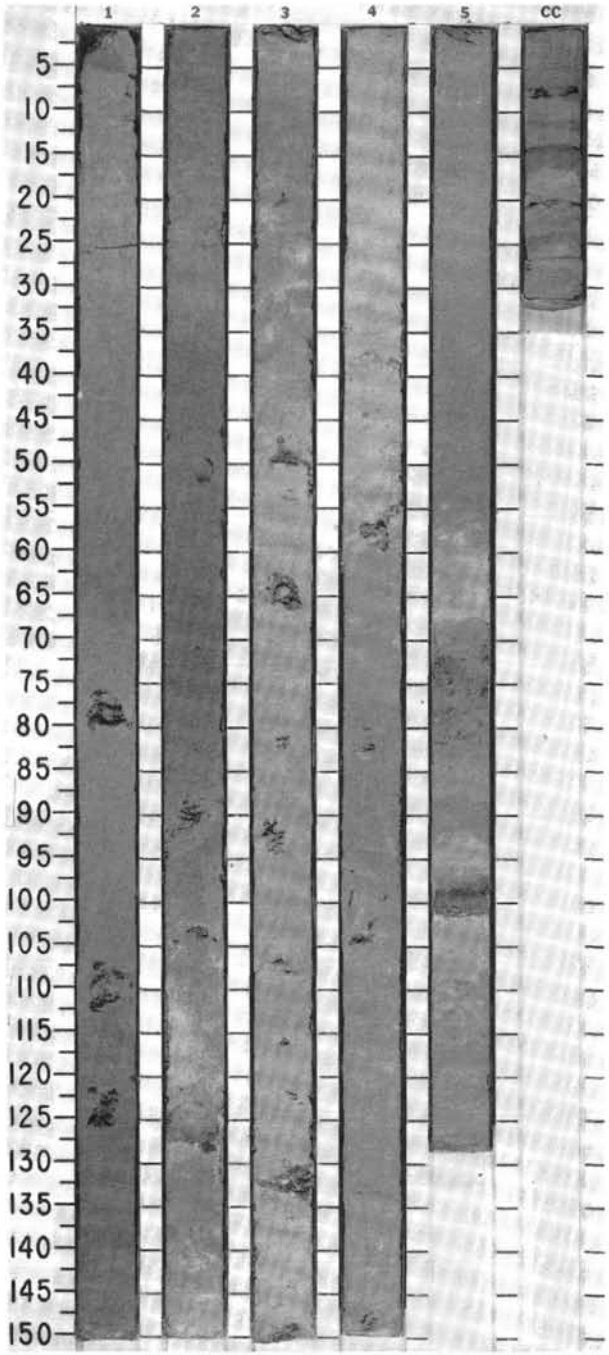

SITE 671 HOLE B CORE 13 X CORED INTERVAL 5042.3-5051.8 mbsl; 110.6-120.1 mbsf

TIME-ROCK UNIT: UPPER MIOCENE

BIOSTRAT. ZONE/FOSSIL CHARACTER:
- FORAMINIFERS: *Neogloboquadrina humerosa* Zone
- NANNOFOSSILS: CN9 b
- RADIOLARIANS: Barren
- DIATOMS: B

PALEOMAGNETICS: Chron 5

PHYS. PROPERTIES: Φ=55.9, Pb=1.84; Φ=62.9, γ=1.70; Φ=58.3 %, γ=1.79; Φ=71.2, γ=1.60

CHEMISTRY: 26.8 %; 10.5 %; 22.9 %; 23.4 %; 27.4 %

SECTION: 1, 2, 3, 4, 5, 6, CC

METERS: 0.5, 1.0

GRAPHIC LITHOLOGY

DRILLING DISTURB.

SED. STRUCTURES

SAMPLES: IW

LITHOLOGIC DESCRIPTION

CALCAREOUS MUD

Olive-gray (2.5Y6/3, 5Y5/2) CALCAREOUS MUD, strongly bioturbated, in parts with vitric ash components.

Minor lithology: three distinct gray (5G7/2) volcanic ash layers in Sections 1, 3, and 4, and two ashy mud layers in Section 5. Ashes are strongly bioturbated.

SMEAR SLIDE SUMMARY (%):

	2, 14 M	2, 85 D
TEXTURE:		
Sand	2	—
Silt	10	2
Clay	88	98
COMPOSITION:		
Feldspar	2	Tr
Clay	58	60
Volcanic glass	30	20
Nannofossils	10	20
Sponge spicules	—	Tr

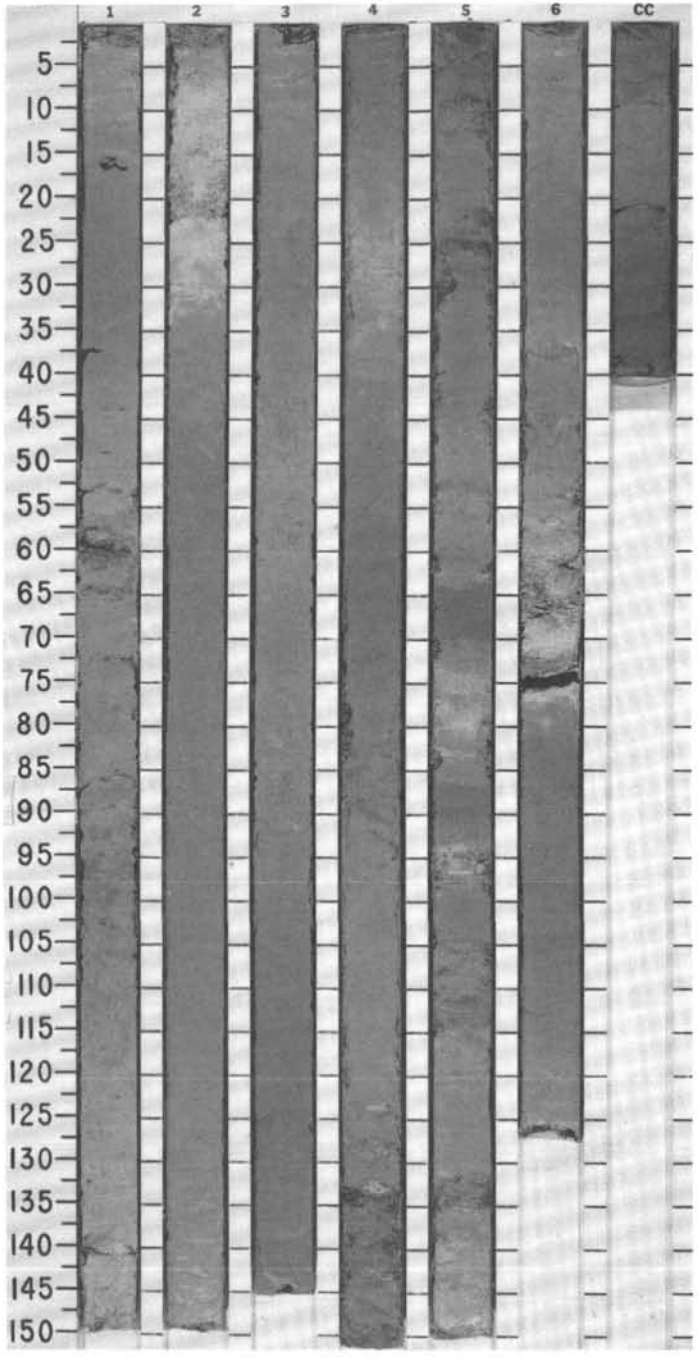

SITE 671 HOLE B CORE 14 X CORED INTERVAL 5051.8-5061.3 mbsl; 120.1-129.6 mbsf

TIME-ROCK UNIT: LOWER PLEISTOCENE

BIOSTRAT. ZONE/FOSSIL CHARACTER: *Globorotalia truncatulinoides* Zone (*G. hessi* subzone); *Pseudoemiliania lacunosa* Zone; B; Barren

FORAMINIFERS | NANNOFOSSILS | RADIOLARIANS | DIATOMS | PALEOMAGNETICS | PHYS. PROPERTIES | CHEMISTRY

SECTION | METERS | GRAPHIC LITHOLOGY | DRILLING DISTURB. | SED. STRUCTURES | SAMPLES

Φ=56.5 ρ=1.85 ● 8.9 %

Φ=55.8 ρ=1.83 ● 21.1 %

Φ=56.1 ρ=1.78 ● 21.8 %

Φ=61.1 ρ=1.77 ● 21.8 %

SAMPLES: OG

LITHOLOGIC DESCRIPTION

CALCAREOUS MUDSTONE and MARLSTONE

Olive-gray (2.5Y5/2 to 5Y5/2) to yellowish (10YR7/2 to 10YR6/2) ashy CLACAREOUS MUDSTONE, highly bioturbated, in Sections 1 to 6, 110 cm, tectonically underlain by olive-gray (5Y5/3) MARLSTONE.

Minor lithology: two distinct gray volcanic ash layers in tectonic footwall rocks in Sections 6 and 7.

SMEAR SLIDE SUMMARY (%):

	2, 36 D	6, 135 M	6, 139 M	7, 30 M	7, 47 M
TEXTURE:					
Sand	1	40	2	—	90
Silt	4	30	10	80	10
Clay	95	30	88	20	Tr
COMPOSITION:					
Quartz	—	—	—	20	5
Feldspar	2	5	—	50	45
Mica	—	—	—	Tr	—
Clay	55	30	58	20	—
Volcanic glass	Tr	60	40	—	10
Accessory minerals					
Clinopyroxene	—	Tr	—	2	15
Opaques	—	5	—	Tr	5
Hornblende	—	—	—	8	20
Nannofossils	40	Tr	2	—	—
Bioclasts	3	—	—	—	—

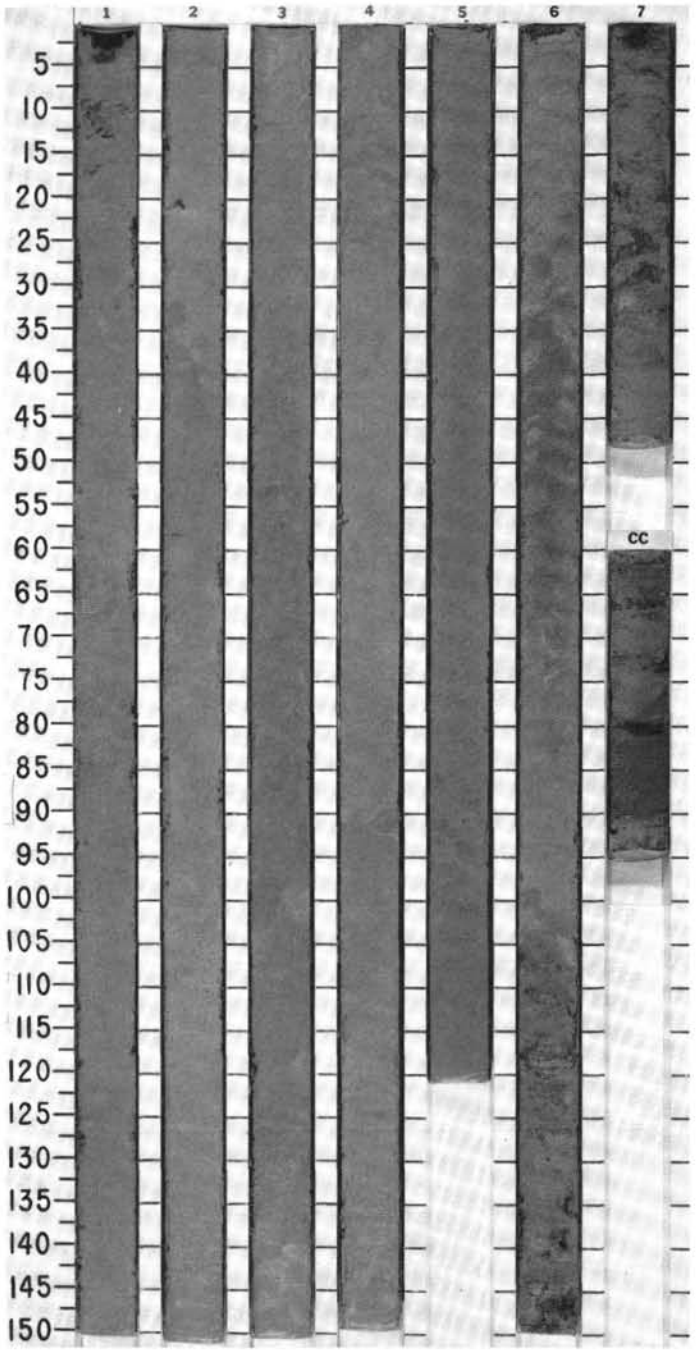

SITE 671 HOLE B CORE 15 X CORED INTERVAL 5061.3-5070.8 mbsl; 129.6-139.1 mbsf

TIME-ROCK UNIT: LOWER PLEISTOCENE

BIOSTRAT. ZONE/ FOSSIL CHARACTER: *Pseudoemiliania lacunosa* Zone

FORAMINIFERS

NANNOFOSSILS: B

RADIOLARIANS: Barren

DIATOMS

PALEOMAGNETICS

PHYS. PROPERTIES: Ø=65.8 ρ=1.70; Ø=61.8 ρ=1.77; Ø=69.5 ρ=1.66; Ø=68.0 ρ=1.71; Ø=58.4 ρ=1.79

CHEMISTRY: 15.6 ‰; ●6.7 %; ●14.3 %; ●18.1 %; ●6.3 %; ●0.4 %

SECTION: 1 2 3 4 5 6 7 CC

METERS: 0.5 1.0

GRAPHIC LITHOLOGY

DRILLING DISTURB.

SED. STRUCTURES

SAMPLES: * PP PP * * *

LITHOLOGIC DESCRIPTION

MUDSTONE and VOLCANIC ASH

Interbedded MUDSTONE and VOLCANIC ASH layers of gray to greenish gray (4Y4/3, 5Y5/3) color.

Minor lithology: ash-poor brown (2.5Y5/4) nannofossil-bearing mudstones with minor content of sand-sized foraminifers.

SMEAR SLIDE SUMMARY (%):

	1, 70 D	3, 27 D	4, 53 D	6, 112 D
TEXTURE:				
Sand	25	20	—	45
Silt	50	70	15	45
Clay	25	10	85	10
COMPOSITION:				
Feldspar	35	70	5	50
Rock fragments	—	1	—	—
Clay	24	—	58	11
Volcanic glass	20	—	—	10
Accessory minerals	—	14	—	3
Clinopyroxene	4	10	—	5
Hornblende	8	5	—	20
Chloritized min.	2	—	—	—
Foraminifers	Tr	—	Tr	1
Nannofossils	2	—	30	Tr
Diatoms	Tr	—	—	—
Sponge spicules	3	—	3	—
Bioclasts	2	—	4	—

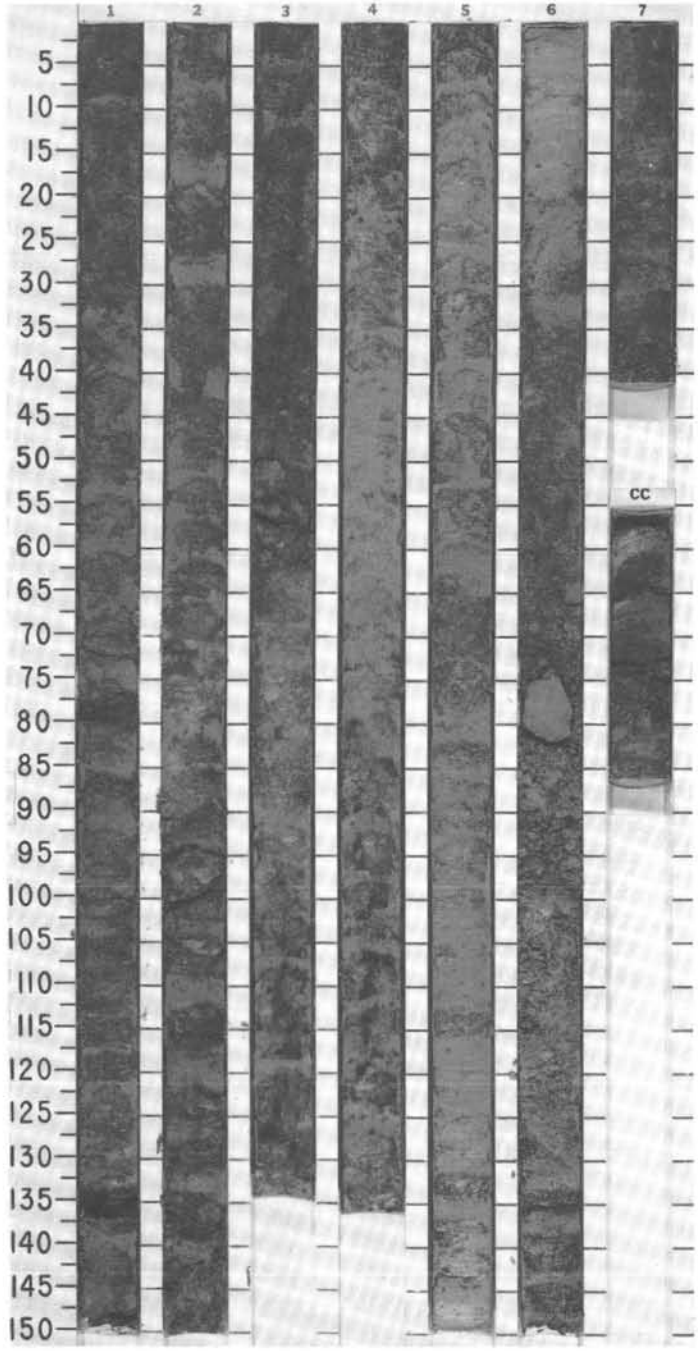

SITE 671 HOLE B CORE 16 X CORED INTERVAL 5070.8-5080.3 mbsl; 139.1-148.6 mbsf

TIME-ROCK UNIT	BIOSTRAT. ZONE/ FOSSIL CHARACTER: FORAMINIFERS	NANNOFOSSILS	RADIOLARIANS	DIATOMS	PALEOMAGNETICS	PHYS. PROPERTIES	CHEMISTRY	SECTION	METERS	GRAPHIC LITHOLOGY	DRILLING DISTURB.	SED. STRUCTURES	SAMPLES
LOWER PLEISTOCENE	*Globorotalia truncatulinoides* Zone (*G. hessi* subzone)	*Pseudoemiliania lacunosa* Zone	Barren			● Φ=58.1 γ=1.83	● 13.3 %	1, 2, 3, 4, 5, 6, 7, CC	0.5, 1.0	VOID			*

LITHOLOGIC DESCRIPTION

MUDSTONE and CALCAREOUS MUDSTONE

Dark greenish gray (5Y4/2) ash-bearing MUDSTONE with local dark gray patches of volcanic debris in Section 1. CALCAREOUS MUDSTONE, variably calcareous and a few dark gray specks of pyroclastic material in Sections 6 and 7.

SMEAR SLIDE SUMMARY (%):

	1, 19 D	6, 150 D
TEXTURE:		
Sand	—	5
Silt	15	10
Clay	85	85
COMPOSITION:		
Quartz	Tr	—
Feldspar	Tr	Tr
Clay	70	65
Volcanic glass	30	Tr
Accessory minerals		
Chlorite?	—	5
Foraminifers	Tr	10
Nannofossils	—	20
Sponge spicules	Tr	—
Bioclasts	Tr	—

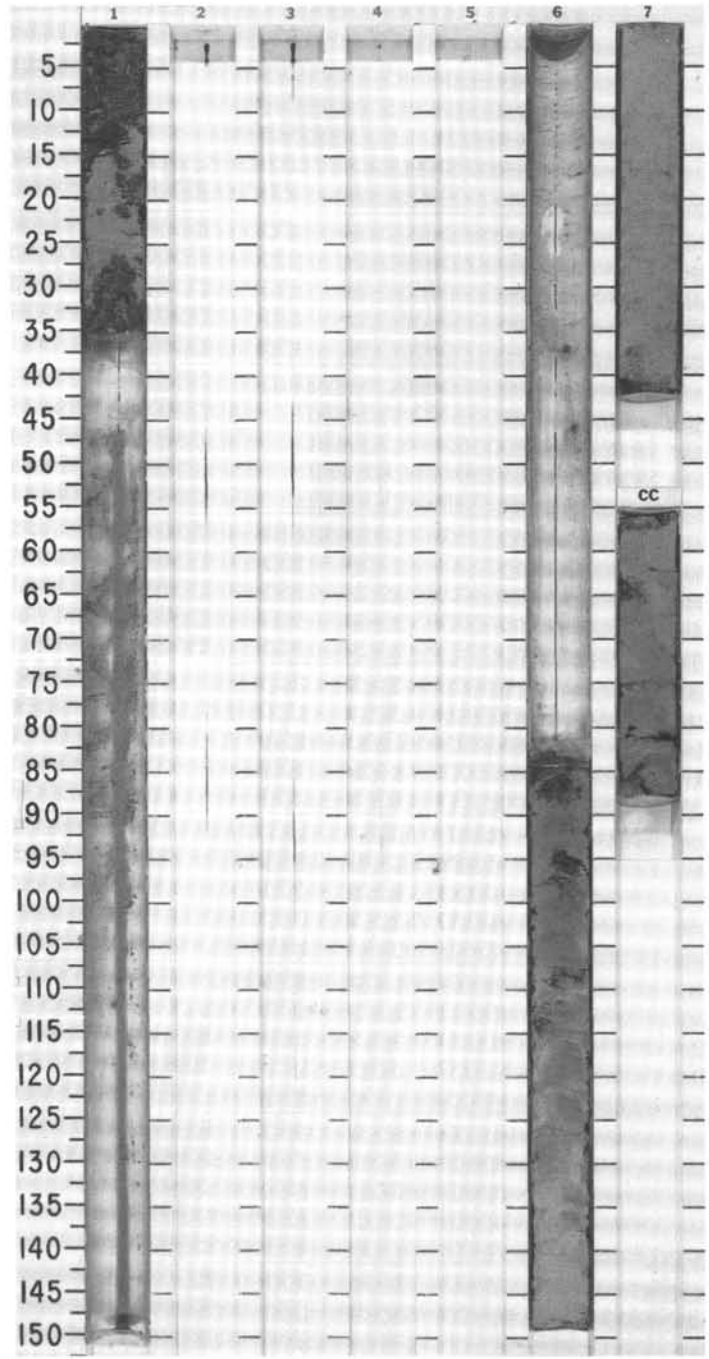

SITE 671 HOLE B CORE 17 X CORED INTERVAL 5080.3-5089.8 mbsl; 148.6-158.1 mbsf

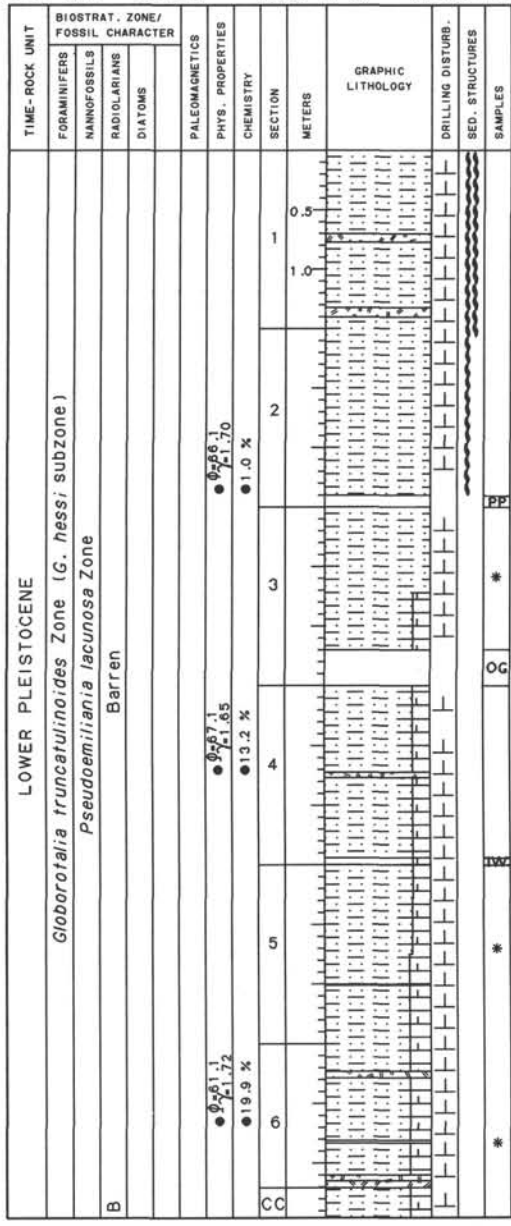

LITHOLOGIC DESCRIPTION

CALCAREOUS MUDSTONE

Variegated CALCAREOUS MUDSTONE, partly ashy. In Section 1 rapid color changes on a 10 cm-scale from greenish gray to brown through olive-gray (10Y6/2, 5GY5/2, 5Y5/2, 5Y5/1). Rest of core is dominantly olive-brown to olive-gray (2.5Y5/3). Bioturbation is strong to moderate in the first two sections.

Minor lithology: six thin distinct layers of gray (5Y3/1) volcanic ash beds in Sections 1, 4, and 6.

SMEAR SLIDE SUMMARY (%):

	3, 57 D	5, 67 D	6, 87 D
TEXTURE:			
Sand	—	—	Tr
Silt	25	15	45
Clay	75	85	55
COMPOSITION:			
Quartz	—	—	3
Feldspar	5	10	5
Clay	60	68	21
Volcanic glass	5	10	—
Accessory minerals			
Opaques	1	—	1
Foraminifers	1	—	5
Nannofossils	25	10	40
Bioclasts	3	2	25

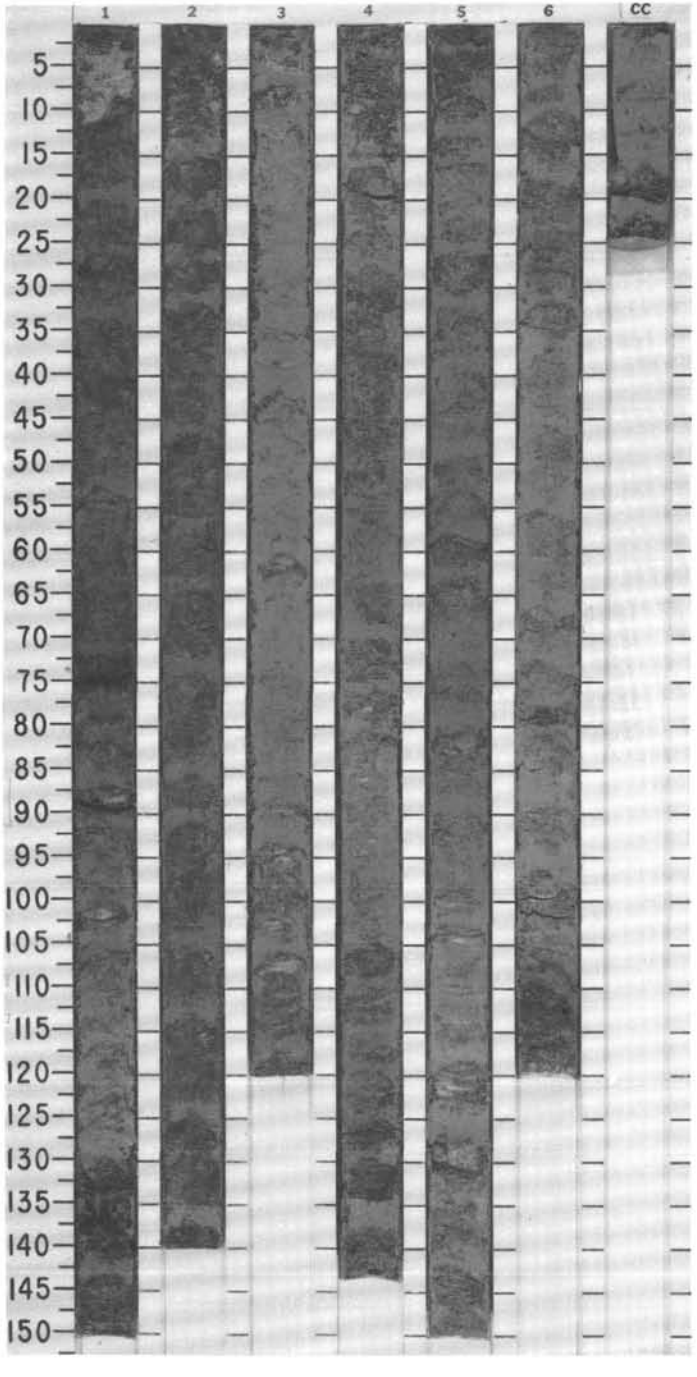

SITE 671 HOLE B CORE 18 X CORED INTERVAL 5089.8-5099.3 mbsl; 158.1-167.6 mbsf

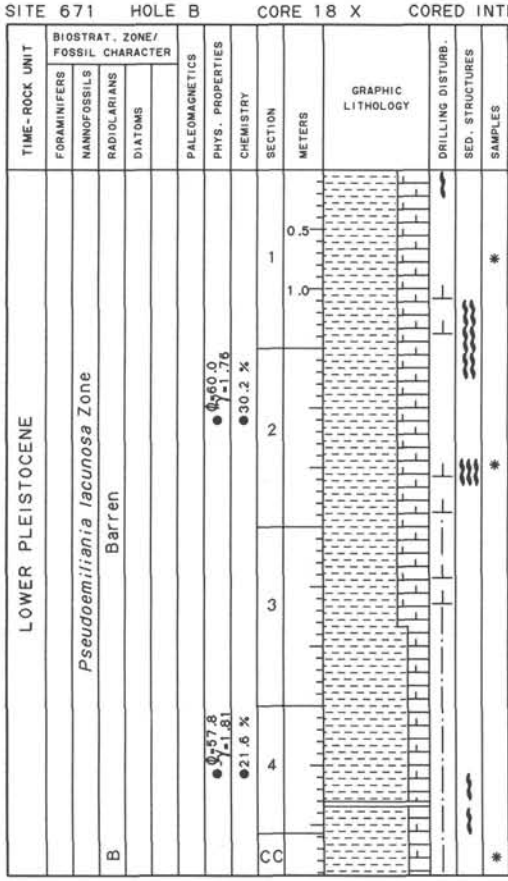

LITHOLOGIC DESCRIPTION

MARLSTONE

Olive-gray (2.5Y6/2, 5Y5/2, 5Y5/3) MARLSTONE, in parts ash-bearing (ashy blebs), foraminifer-bearing. Moderate to strong patchy bioturbation.

SMEAR SLIDE SUMMARY (%):

	1, 70 D	2, 93 D	CC D
TEXTURE:			
Sand	Tr	—	—
Silt	60	20	2
Clay	40	80	98
COMPOSITION:			
Quartz	—	Tr	—
Feldspar	4	Tr	—
Clay	55	73	97
Volcanic glass	2	2	Tr
Accessory minerals			
Fibrous zeolite	—	Tr	—
Opaques	—	—	1
Chloritized min.	1	—	—
Foraminifers	8	—	—
Nannofossils	30	25	2

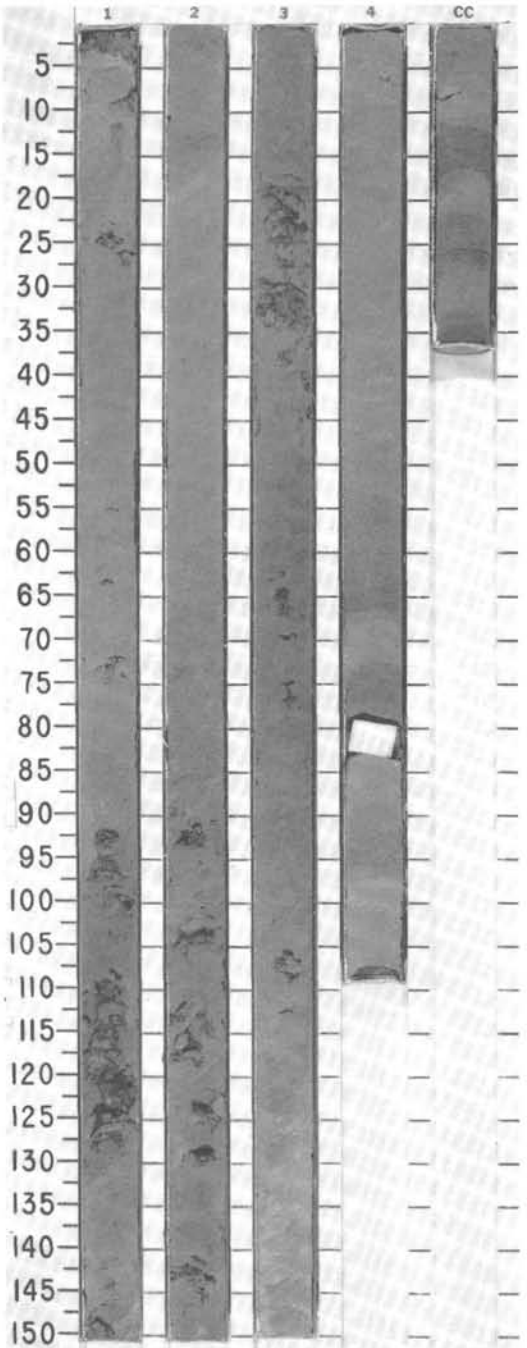

SITE 671 HOLE B CORE 19 X CORED INTERVAL 5099.3-5108.8 mbsl; 167.6-177.1 mbsf

TIME-ROCK UNIT	BIOSTRAT. ZONE/ FOSSIL CHARACTER: FORAMINIFERS	NANNOFOSSILS	RADIOLARIANS	DIATOMS	PALEOMAGNETICS	PHYS. PROPERTIES	CHEMISTRY	SECTION	METERS	GRAPHIC LITHOLOGY	DRILLING DISTURB.	SED. STRUCTURES	SAMPLES
LOWER PLEISTOCENE	*Globorotalia truncatulinoides* Zone (*G. hessi* subzone)	*Helicoportosphaera sellii* Zone	B Barren			● Φ=56.9 γ=1.83	● 35.3 %	1, 2, CC	0.5, 1.0				* IW *

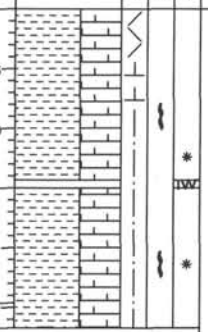

LITHOLOGIC DESCRIPTION

MARLSTONE

Gray (5Y6/1, 5Y5/2) MARLSTONE, partly ashy, partly bearing sand-sized foraminifers. Part of the burrow fills in bioturbated sections is provided by sulfide-rich clay.

SMEAR SLIDE SUMMARY (%):

	1, 125 D	2, 77 D
TEXTURE:		
Sand	5	2
Silt	35	23
Clay	60	75
COMPOSITION:		
Feldspar	3	—
Clay	40	70
Volcanic glass	2	10
Accessory minerals		
Opaques	—	15
Hornblende	—	5
Foraminifers	20	—
Nannofossils	30	—
Bioclasts, silt-size	5	—

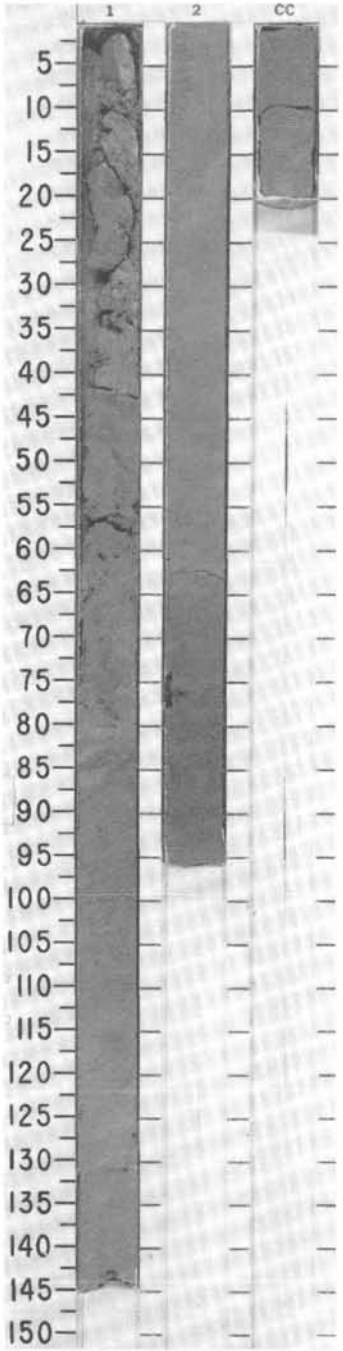

SITE 671 HOLE B CORE 20 X CORED INTERVAL 5108.8-5118.3 mbsl; 177.1-186.6 mbsf

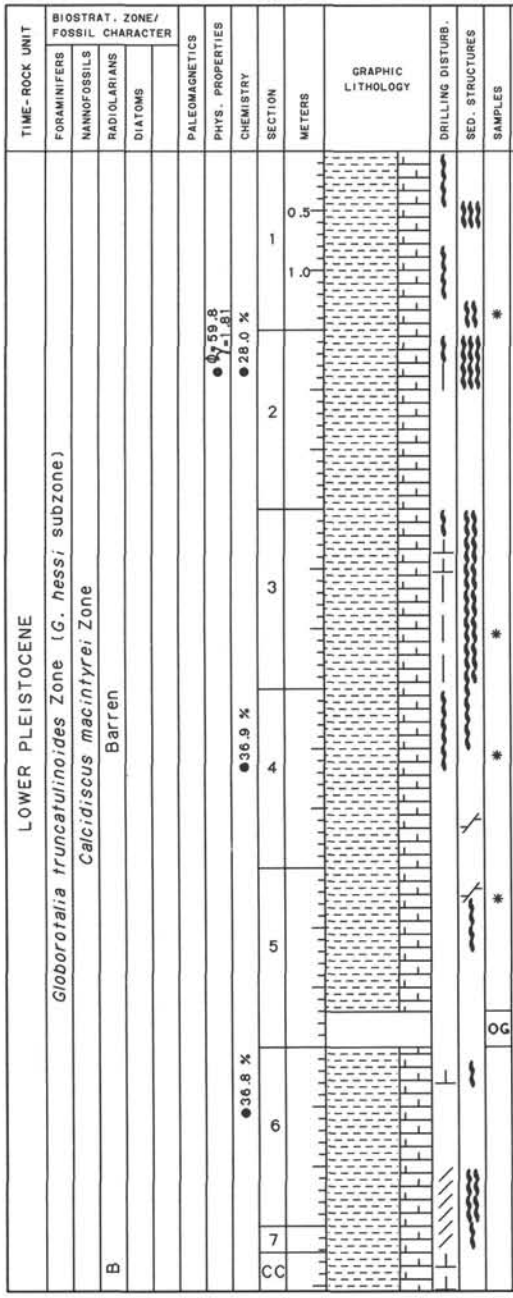

LITHOLOGIC DESCRIPTION

MARLSTONE and CALCAREOUS MUDSTONE

MARLSTONE and CALCAREOUS MUDSTONE, light gray, yellowish gray to olive-gray (5Y5/2 to 5Y6/3). In Sections 1 and 2 locally strong bioturbation by *Chondrites*. Moderate to slight bioturbation in rest of core. Two discrete low-angle faults in Sections 4 and 5. Slight to moderate drilling disturbance.

SMEAR SLIDE SUMMARY (%):

	1, 132 D	3, 100 D	4, 59 D	5, 27 M
TEXTURE:				
Sand	—	—	—	80
Silt	20	10	5	20
Clay	80	90	95	—
COMPOSITION:				
Feldspar	5	—	—	83
Mica	—	—	—	Tr
Clay	65	74	65	—
Volcanic glass	—	1	Tr	—
Accessory minerals				
Clinopyroxene	Tr	—	Tr	10
Opaques	—	—	—	2
Hornblende	—	—	Tr	5
Foraminifers	10	10	3	—
Nannofossils	20	15	30	—
Bioclasts	—	—	2	—

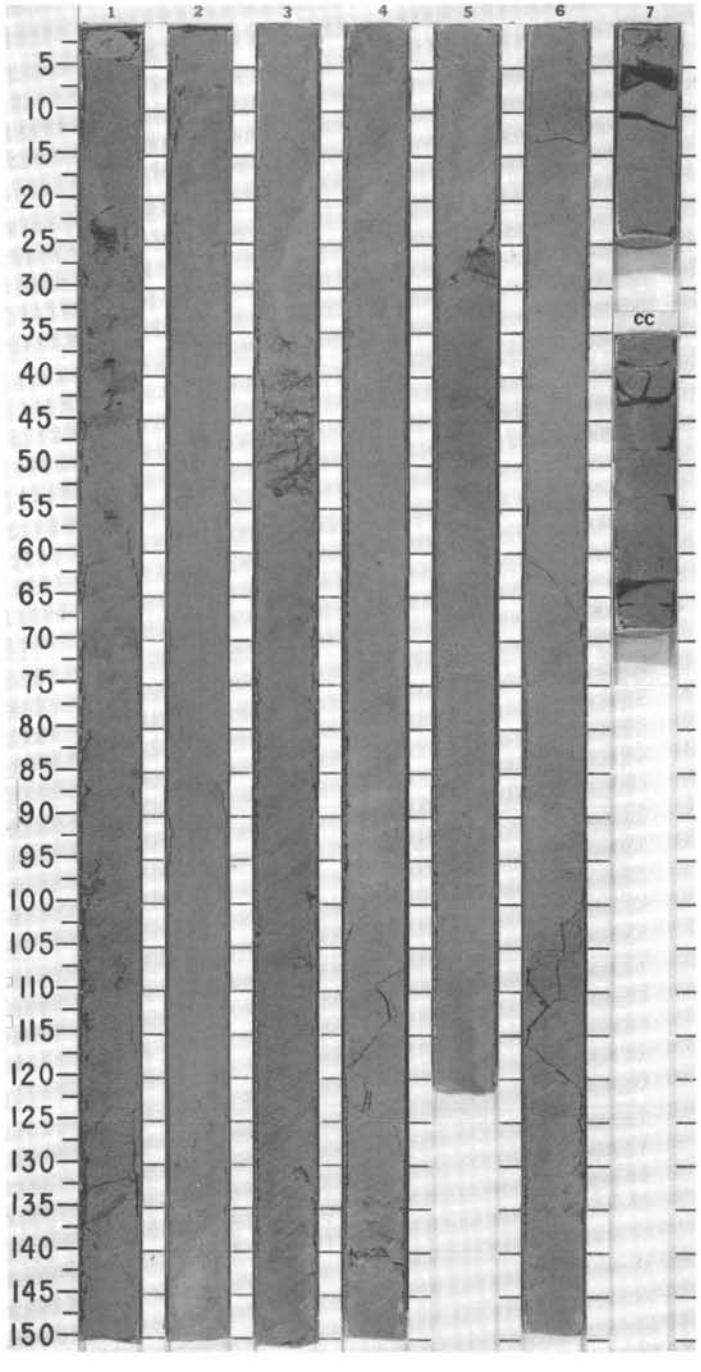

SITE 671 HOLE B CORE 21 X CORED INTERVAL 5118.3-5127.8 mbsl; 186.6-196.1 mbsf

TIME-ROCK UNIT	BIOSTRAT. ZONE/ FOSSIL CHARACTER: FORAMINIFERS	NANNOFOSSILS	RADIOLARIANS	DIATOMS	PALEOMAGNETICS	PHYS. PROPERTIES	CHEMISTRY	SECTION	METERS	GRAPHIC LITHOLOGY	DRILLING DISTURB.	SED. STRUCTURES	SAMPLES	LITHOLOGIC DESCRIPTION
LOWER PLEISTOCENE	*Globorotalia truncatulinoides* Zone	*Calcidiscus macintyrei* Zone	B	Barren		ϕ=55.7 ρ=1.81 ●33.2 %		1 2 CC	0.5 1.0				*	

CALCAREOUS MUDSTONE

Olive-gray to green-gray (5Y5/2 to 2.5Y5/2) CALCAREOUS MUDSTONE, in parts ashy, in parts sand-sized foraminifer-bearing. Bioturbation is weak in Section 1, but very intense in Section 2 and in the CC. At the bottom of Section 2 and in the CC there are discrete slickensided sub-horizontal fault surfaces.

SMEAR SLIDE SUMMARY (%):

	1, 145 D	2, 100 D
TEXTURE:		
Sand	6	2
Silt	—	5
Clay	94	93
COMPOSITION:		
Quartz	—	2
Feldspar	1	3
Clay	74	50
Volcanic glass	—	25
Calcite/dolomite	—	Tr
Foraminifers	5	—
Nannofossils	20	20

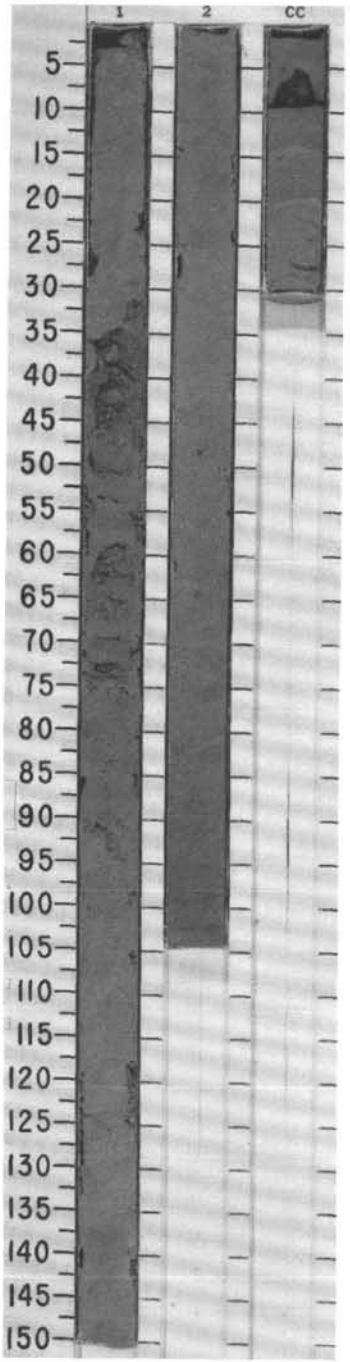

SITE 671 HOLE B CORE 22 X CORED INTERVAL 5127.8-5137.3 mbsl; 196.1-205.6 mbsf

TIME-ROCK UNIT: LOWER PLEISTOCENE
BIOSTRAT. ZONE/FOSSIL CHARACTER: FORAMINIFERS: *Globorotalia truncatulinoides* Zone (*G. viola* subzone); NANNOFOSSILS: *Calcidiscus macintyrei* Zone; RADIOLARIANS: Barren; DIATOMS: B
PALEOMAGNETICS
PHYS. PROPERTIES: ● Φ=54.2 γ=1.86; ● Φ=59.2 γ=1.82; ● Φ=57.9 γ=1.80
CHEMISTRY: ● 38.8 %; ● 25.7 %; 19.9 %; ● 33.2 %
SECTION: 1, 2, 3, 4, 5, 6, 7, CC
METERS: 0.5, 1.0
GRAPHIC LITHOLOGY
DRILLING DISTURB.
SED. STRUCTURES
SAMPLES: PP

LITHOLOGIC DESCRIPTION

CALCAREOUS MUDSTONE

Gray-brownish greenish (5Y5/1, 5Y6/1, 5Y5/2) CALCAREOUS MUDSTONE. Strong bioturbation. Bioturbation in Section 7 is caused by *Chondrites*. Sections 5 and 6 contain dispersed sand-sized foraminifers.

Minor lithology: the core contains one discrete layer of volcanic ash.

SMEAR SLIDE SUMMARY (%):

	2, 60 M	2, 88 D	4, 91 D
TEXTURE:			
Silt	30	10	20
Clay	70	90	80
COMPOSITION:			
Quartz	—	2	5
Feldspar	5	—	5
Clay	63	73	80
Volcanic glass	30	—	—
Accessory minerals			
Clinopyroxene	Tr	—	—
Foraminifers	1	—	Tr
Nannofossils	Tr	25	10

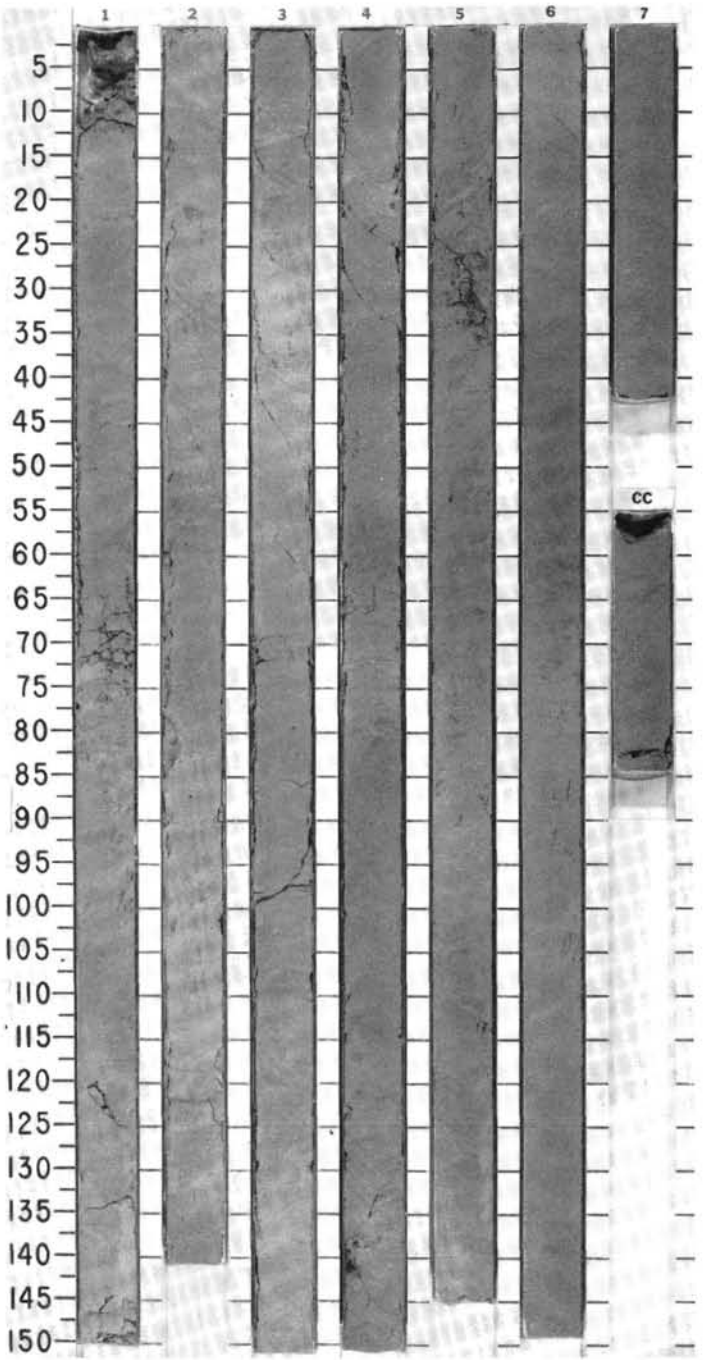

SITE 671 HOLE B CORE 23 X CORED INTERVAL 5137.3-5146.8 mbsl; 205.6-215.1 mbsf

TIME-ROCK UNIT	BIOSTRAT. ZONE/ FOSSIL CHARACTER: FORAMINIFERS	NANNOFOSSILS	RADIOLARIANS	DIATOMS	PALEOMAGNETICS	PHYS. PROPERTIES	CHEMISTRY	SECTION	METERS	GRAPHIC LITHOLOGY	DRILLING DISTURB.	SED. STRUCTURES	SAMPLES
LOWER PLIOCENE	*Globorotalia tosaensis* Zone (PL6)	CN12 d	B Barren			● ϕ=55.9 γ=1.82	● 33.6 %	1	0.5				
									1.0				
								2					*
													OG
								3		VOID			
						● ϕ=61.3 γ=1.74	● 30.3 %	4					
								CC					

LITHOLOGIC DESCRIPTION

CALCAREOUS MUDSTONE

Olive-gray (5Y5/2 to 5Y6/1) volcanic glass-bearing CALCAREOUS MUDSTONE, with scattered sand-sized foraminifers throughout Sections 3 and 4. Bioturbation is moderate to intense. *Zoophycos* is found in Section 2, *Chondrites* in Section 4.

SMEAR SLIDE SUMMARY (%):

	2, 73 D
TEXTURE:	
Sand	Tr
Silt	15
Clay	85
COMPOSITION:	
Clay	45
Volcanic glass	24
Foraminifers	1
Nannofossils	30

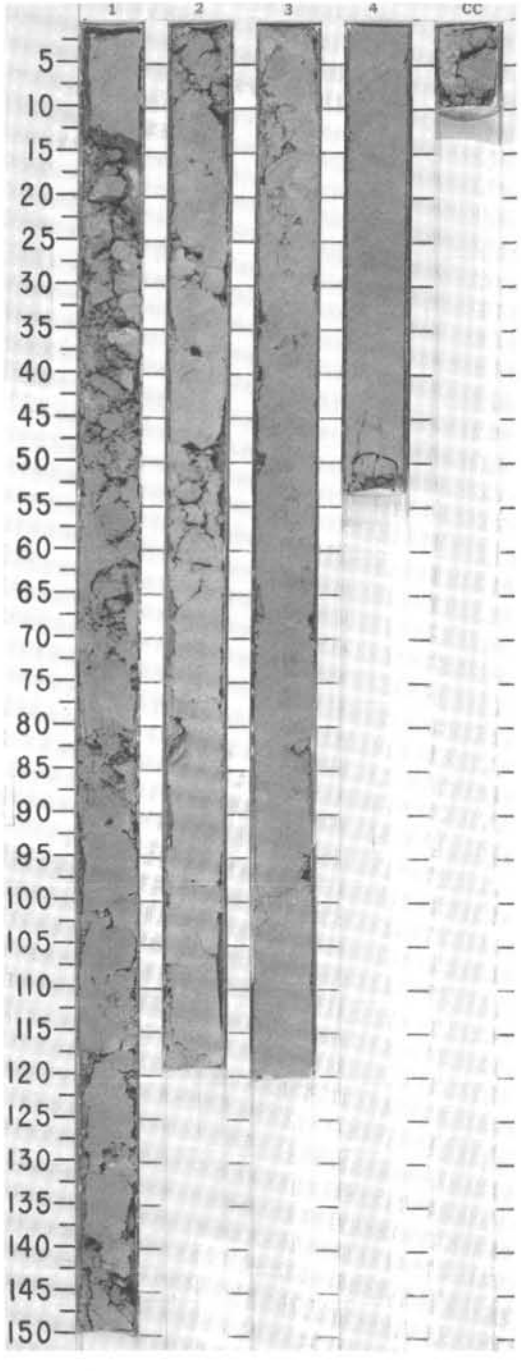

SITE 671 HOLE B CORE 24 X CORED INTERVAL 5146.8-5156.3 mbsl; 215.1-224.6 mbsf

TIME-ROCK UNIT	BIOSTRAT. ZONE/ FOSSIL CHARACTER: FORAMINIFERS	NANNOFOSSILS	RADIOLARIANS	DIATOMS	PALEOMAGNETICS	PHYS. PROPERTIES	CHEMISTRY	SECTION	METERS	GRAPHIC LITHOLOGY	DRILLING DISTURB.	SED. STRUCTURES	SAMPLES
UPPER PLIOCENE	*Globorotalia tosaensis* Zone (PL6)	CN12 d	Barren			● O=52.7 γ=1.88 ● O=50.0 γ=1.96 ● O=53.1 γ=1.89	● 44.7% ● 46.4 % ● 32.3 % ● 26.1 %	1 2 3 CC	0.5 1.0				* *

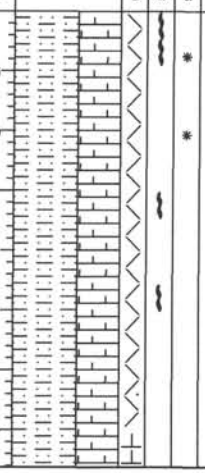

LITHOLOGIC DESCRIPTION

CALCAREOUS MUDSTONE

Light greenish gray to olive-gray (5Y5/2 to 5Y6/2) volcanic glass-bearing CALCAREOUS MUDSTONE, with foraminifers. Mild bioturbation in Section 1 by *Zoophycos* burrows. Section 1, 120 cm, downward is deformed into a scaly clay fabric.

SMEAR SLIDE SUMMARY (%):

	1, 37 D	1, 131 D
TEXTURE:		
Sand	5	Tr
Silt	15	3
Clay	80	97
COMPOSITION:		
Clay	40	55
Volcanic glass	10	10
Foraminifers	5	Tr
Nannofossils	45	35

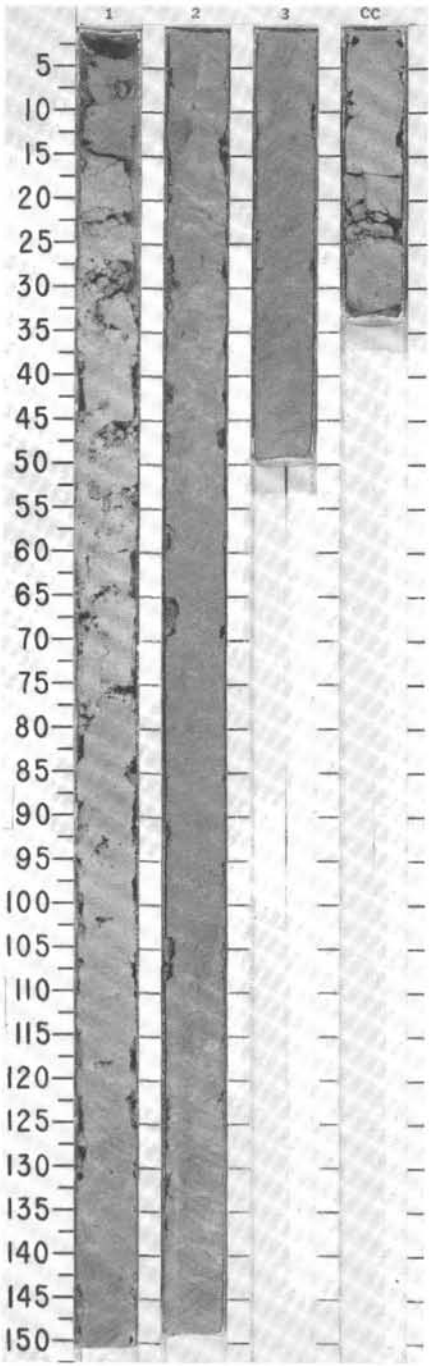

SITE 671 HOLE B CORE 25 X CORED INTERVAL 5156.3-5165.8 mbsl; 224.6-234.1 mbsf

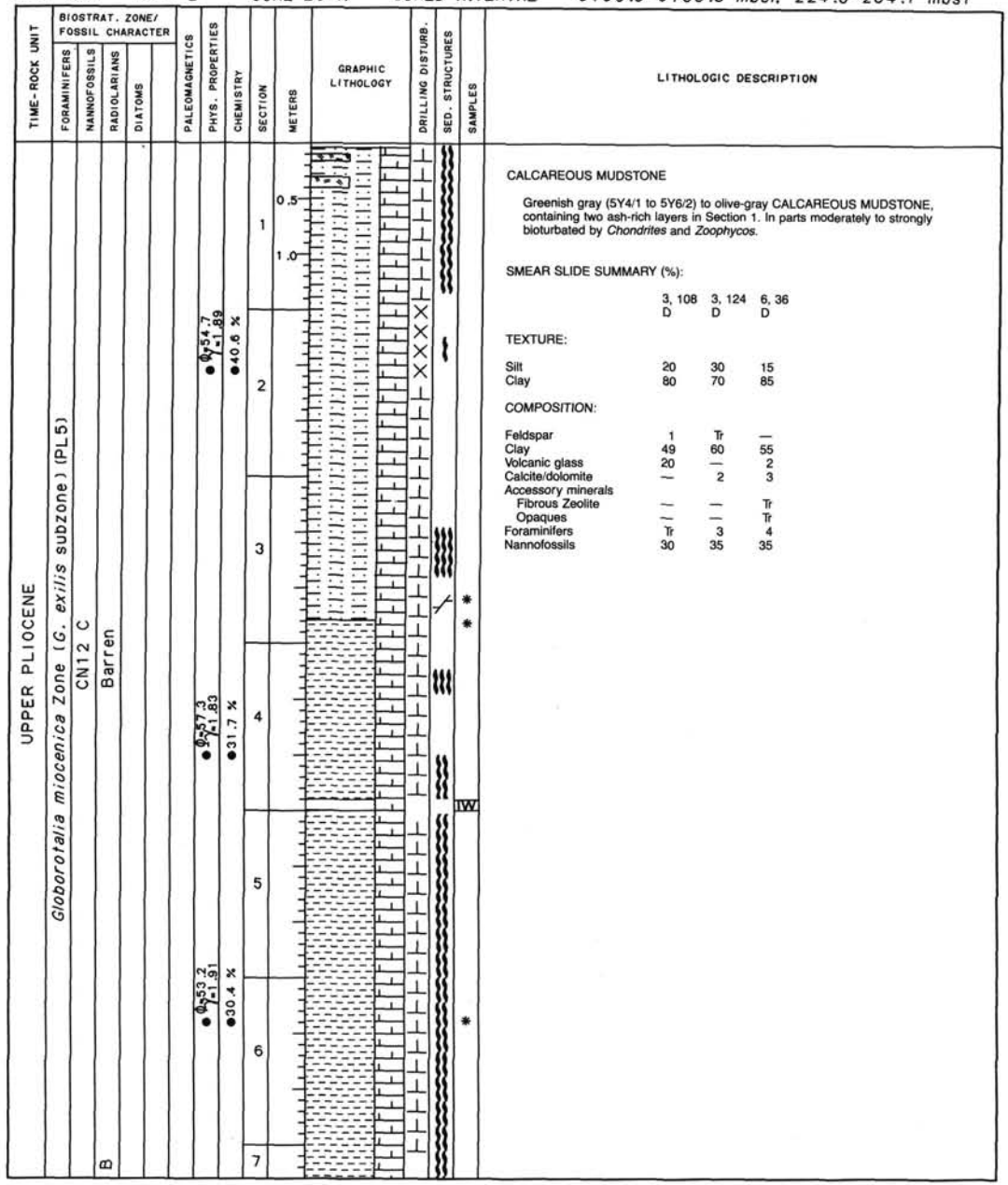

CALCAREOUS MUDSTONE

Greenish gray (5Y4/1 to 5Y6/2) to olive-gray CALCAREOUS MUDSTONE, containing two ash-rich layers in Section 1. In parts moderately to strongly bioturbated by *Chondrites* and *Zoophycos*.

SMEAR SLIDE SUMMARY (%):

	3, 108 D	3, 124 D	6, 36 D
TEXTURE:			
Silt	20	30	15
Clay	80	70	85
COMPOSITION:			
Feldspar	1	Tr	—
Clay	49	60	55
Volcanic glass	20	—	2
Calcite/dolomite	—	2	3
Accessory minerals			
Fibrous Zeolite	—	—	Tr
Opaques	—	—	Tr
Foraminifers	Tr	3	4
Nannofossils	30	35	35

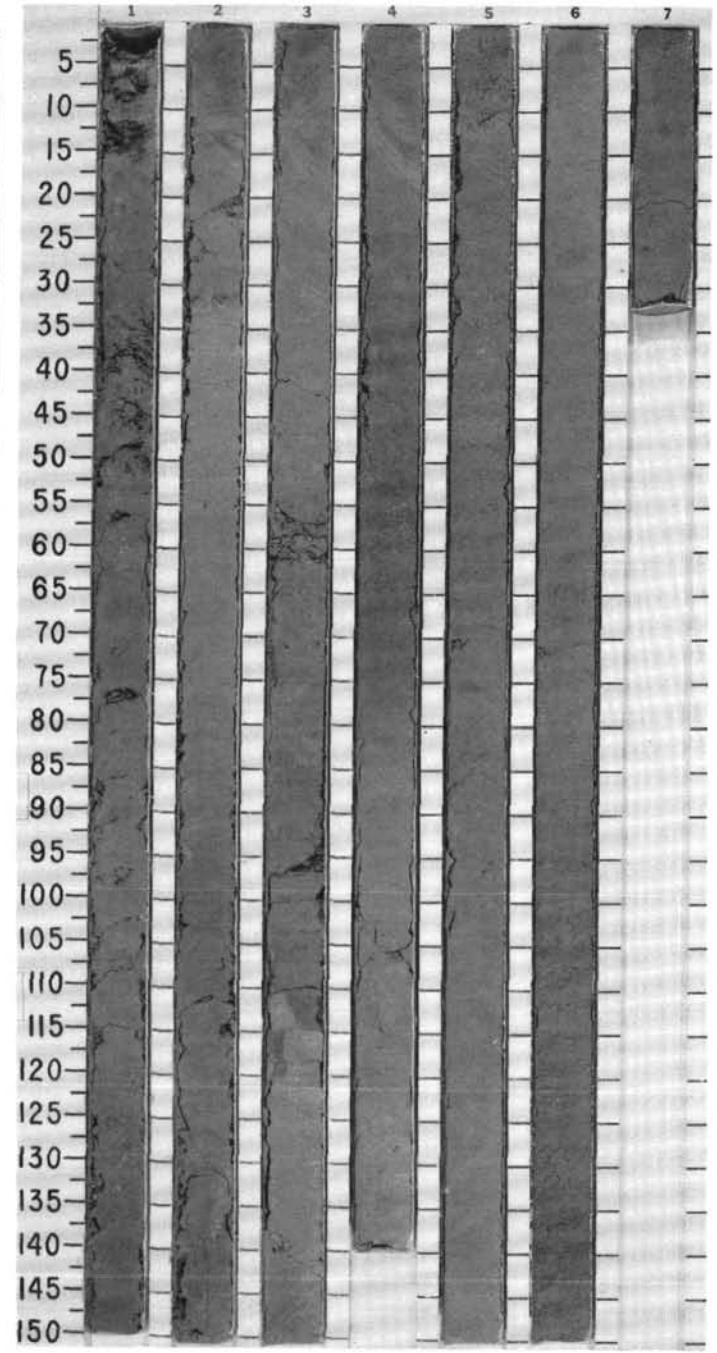

SITE 671 HOLE B CORE 26 X CORED INTERVAL 5165.8-5175.3 mbsl; 234.1-243.6 mbsf

TIME-ROCK UNIT	BIOSTRAT. ZONE/ FOSSIL CHARACTER: FORAMINIFERS	NANNOFOSSILS	RADIOLARIANS	DIATOMS	PALEOMAGNETICS	PHYS. PROPERTIES	CHEMISTRY	SECTION	METERS	GRAPHIC LITHOLOGY	DRILLING DISTURB.	SED. STRUCTURES	SAMPLES
UPPER PLIOCENE	*Globorotalia miocenica* Zone (*G. exilis* subzone) (PL5)	CN12b	Barren			● Φ=53.1 γ=1.89	● 25.9 %	1	0.5, 1.0				*
								2					*
													OG
								3					
			B					4					*
								CC					

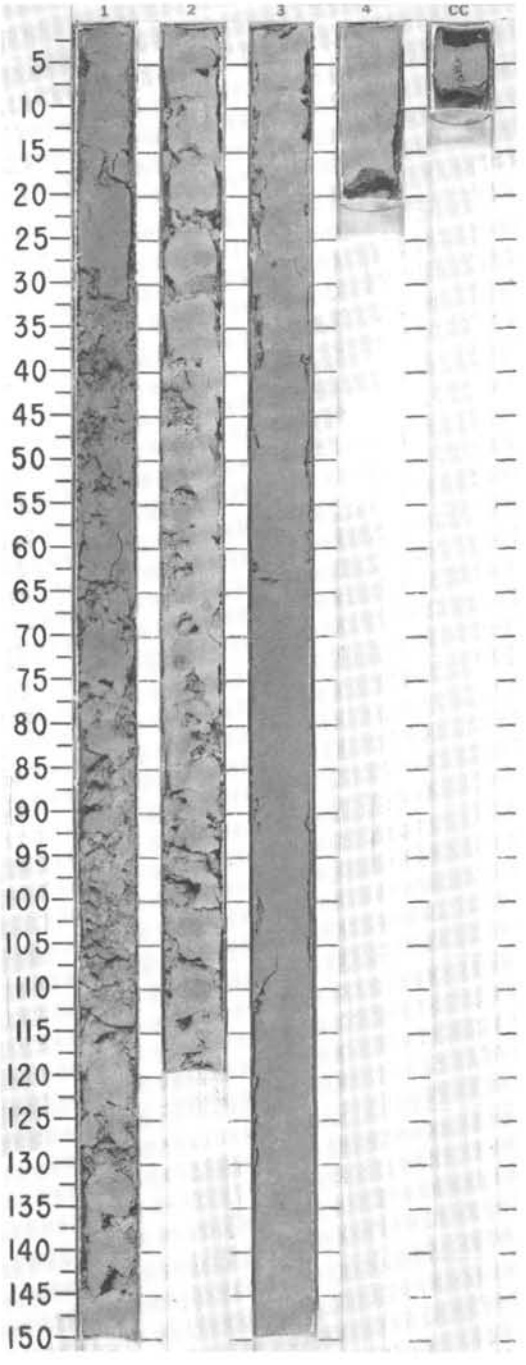

LITHOLOGIC DESCRIPTION

CALCAREOUS MUDSTONE

Gray (5Y5/1, 5Y6/1) CALCAREOUS MUDSTONE with local bioturbation. Section 1, 130–140 cm, shows mesoscopic calc-shelled foraminifers. High drilling disturbance.

SMEAR SLIDE SUMMARY (%):

	1, 71 D	2, 11 D	CC D
TEXTURE:			
Sand	—	—	5
Silt	5	10	15
Clay	95	90	80
COMPOSITION:			
Feldspar	Tr	1	2
Clay	65	60	53
Volcanic glass	Tr	2	—
Accessory minerals			
Opaques	Tr	—	—
Micronodules	Tr	—	—
Chloritized min.	—	Tr	—
Foraminifers	Tr	5	15
Nannofossils	34	32	30

TIME-ROCK UNIT: UPPER PLIOCENE

BIOSTRAT. ZONE/FOSSIL CHARACTER:
- FORAMINIFERS: *Globorotalia miocenica* Zone (PL 4)
- NANNOFOSSILS: CN12a
- RADIOLARIANS: Barren
- DIATOMS: B

PALEOMAGNETICS

PHYS. PROPERTIES: ● Φ=54.3 γ=1.89; ● Φ=52.5 γ=1.89

CHEMISTRY: ● 29.5 %; ● 34.4 %

SECTION: 1, 2, 3, 4, 5, CC

METERS: 0.5, 1.0

GRAPHIC LITHOLOGY

DRILLING DISTURB.

SED. STRUCTURES

SAMPLES: *, *

LITHOLOGIC DESCRIPTION

CALCAREOUS MUDSTONE and MUDSTONE

Sections 1 to 3: homogeneous light gray to olive-gray (5Y6/1 to 5Y5/2) CALCAREOUS MUDSTONE with moderate to strong bioturbation (mostly *Chondrites* burrows); foraminifers present. Sections 4, 5: olive-gray (5Y5/2) MUDSTONE, bioturbated mostly by *Planolites*, 20% by *Chondrites*; foraminifers present. Core moderately to totally fragmented by drilling.

SMEAR SLIDE SUMMARY (%):

	1, 143 D	2, 50 M
TEXTURE:		
Sand	—	Tr
Silt	5	10
Clay	95	90
COMPOSITION:		
Feldspar	Tr	2
Clay	70	55
Accessory minerals		
Chlorite	Tr	—
Opaques	—	12
Foraminifers	5	1
Nannofossils	25	30

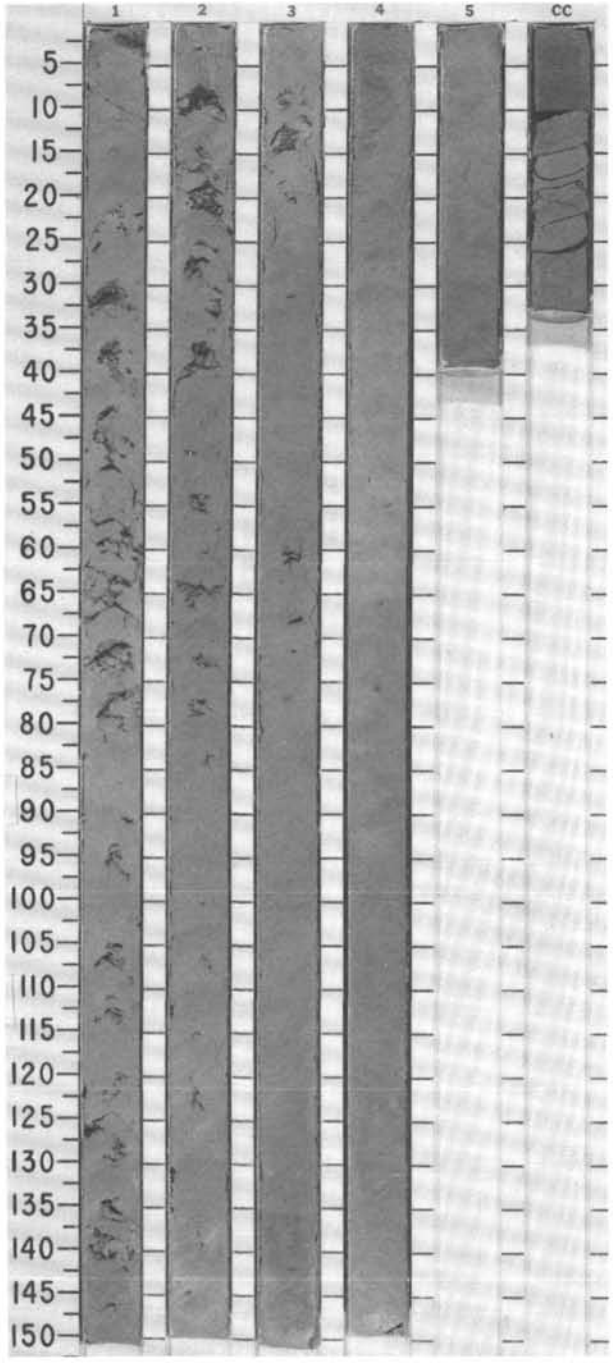

SITE 671 HOLE B CORE 28 X CORED INTERVAL 5184.8-5194.3 mbsl; 253.1-262.6 mbsf

TIME-ROCK UNIT: UPPER PLIOCENE

BIOSTRAT. ZONE/FOSSIL CHARACTER:
- FORAMINIFERS: *Globorotalia miocenica* Zone (PL3)
- NANNOFOSSILS: CN12a to CN11b
- RADIOLARIANS: Barren
- DIATOMS: B

PALEOMAGNETICS

PHYS. PROPERTIES: ● Φ=50.1 γ=1.96; ● Φ=49.8 γ=1.91; ● Φ=52.6 γ=1.89

CHEMISTRY: ● 38.9 %; ● 45.0 %; ● 35.1 %

SECTION: 1, 2, 3, 4, 5, 6, 7, CC

METERS: 0.5, 1.0

GRAPHIC LITHOLOGY: VOID

DRILLING DISTURB.

SED. STRUCTURES

SAMPLES: IW

LITHOLOGIC DESCRIPTION

CALCAREOUS MUDSTONE

Greenish gray (5Y5/1, 5Y5/2, 5Y6/1, 5Y6/2, 10Y6/1) to yellowish gray (6Y6/3) CALCAREOUS MUDSTONE, partly foraminifer-bearing, slightly bioturbated (*Planolites* and *Chondrites* burrows).

SMEAR SLIDE SUMMARY (%):

	1, 72 M	1, 146 D	6, 77 D
TEXTURE:			
Sand	2	2	—
Silt	70	2	3
Clay	28	96	97
COMPOSITION:			
Feldspar	65	1	1
Clay	14	56	72
Volcanic glass	—	1	—
Accessory minerals	3	—	—
Glauconite	1	Tr	Tr
Chlorite	1	Tr	Tr
Clinopyroxene	—	Tr	—
Foraminifers	2	2	2
Nannofossils	15	40	25

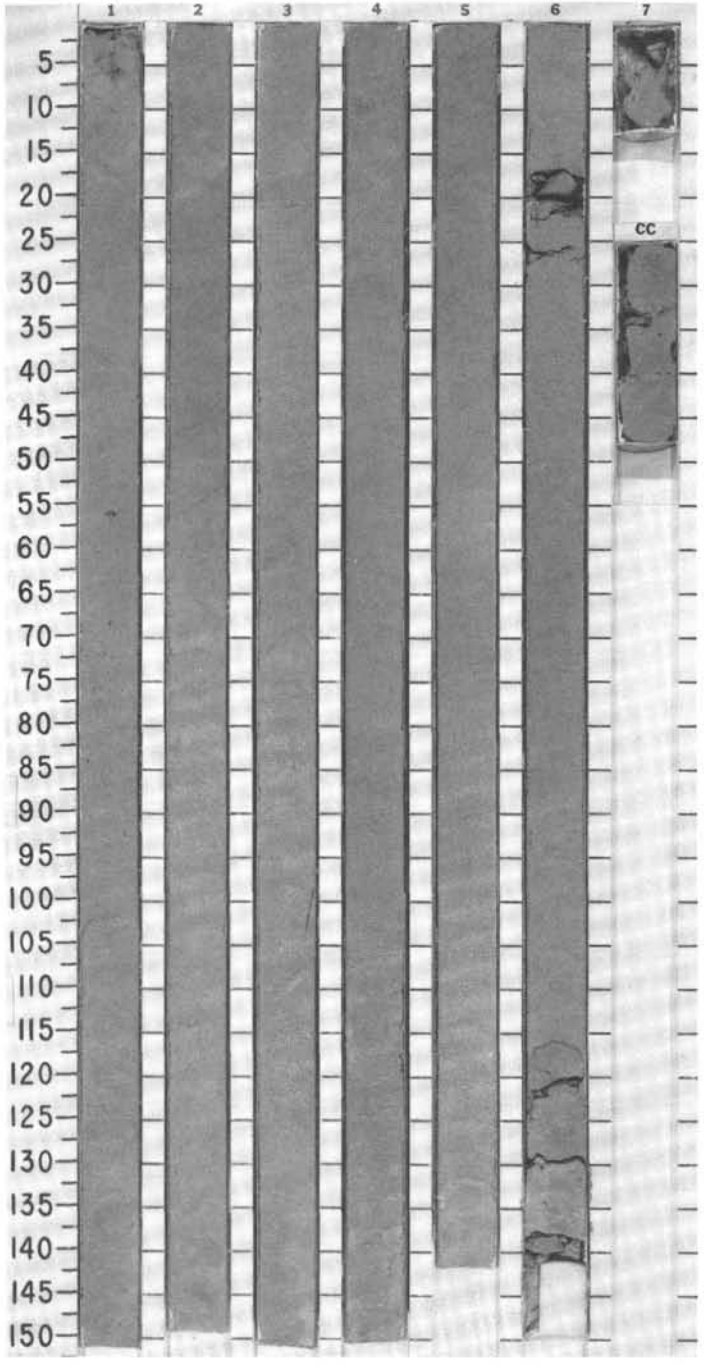

SITE 671 HOLE B CORE 29 X CORED INTERVAL 5194.3-5203.8 mbsl; 262.6-272.1 mbsf

TIME-ROCK UNIT	BIOSTRAT. ZONE/ FOSSIL CHARACTER: FORAMINIFERS	NANNOFOSSILS	RADIOLARIANS	DIATOMS	PALEOMAGNETICS	PHYS. PROPERTIES	CHEMISTRY	SECTION	METERS	GRAPHIC LITHOLOGY	DRILLING DISTURB.	SED. STRUCTURES	SAMPLES
LOWER PLIOCENE	*Globorotalia margaritae* Zone (PL2)	CN11	Barren			φ=49.3 γ=1.96	39.1%	1	0.5, 1.0			?	
								2				?	OG
								3					*
			B				32.2%	CC					

LITHOLOGIC DESCRIPTION

CALCAREOUS MUDSTONE

Dominantly gray (5Y6/1) CALCAREOUS MUDSTONE. Moderate (Section 1) to mild (Section 3) bioturbation of sediment. Burrows are darker gray than the rest of the sediment. Section 3 and CC contain disseminated sand-sized foraminifers with a maximum concentration at Section 3, 106 cm (5%).

SMEAR SLIDE SUMMARY (%):

	3, 82
	D
TEXTURE:	
Silt	20
Clay	80
COMPOSITION:	
Feldspar	Tr
Clay	55
Accessory minerals	
Clinopyroxene	Tr
Foraminifers	2
Nannofossils	40
Radiolarians	5

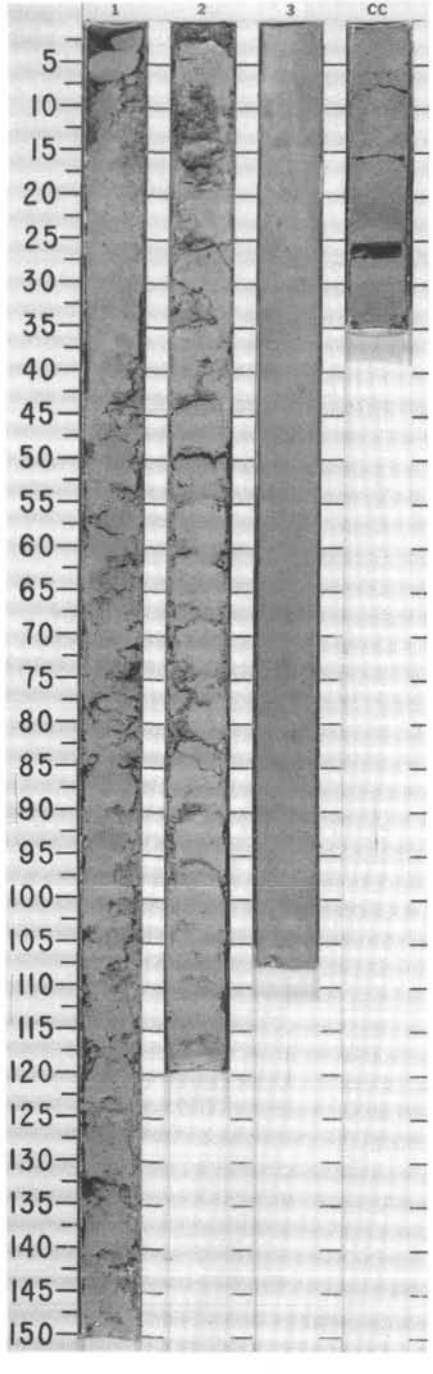

SITE 671 HOLE B CORE 30 X CORED INTERVAL 5203.8-5213.3 mbsl; 272.1-281.6 mbsf

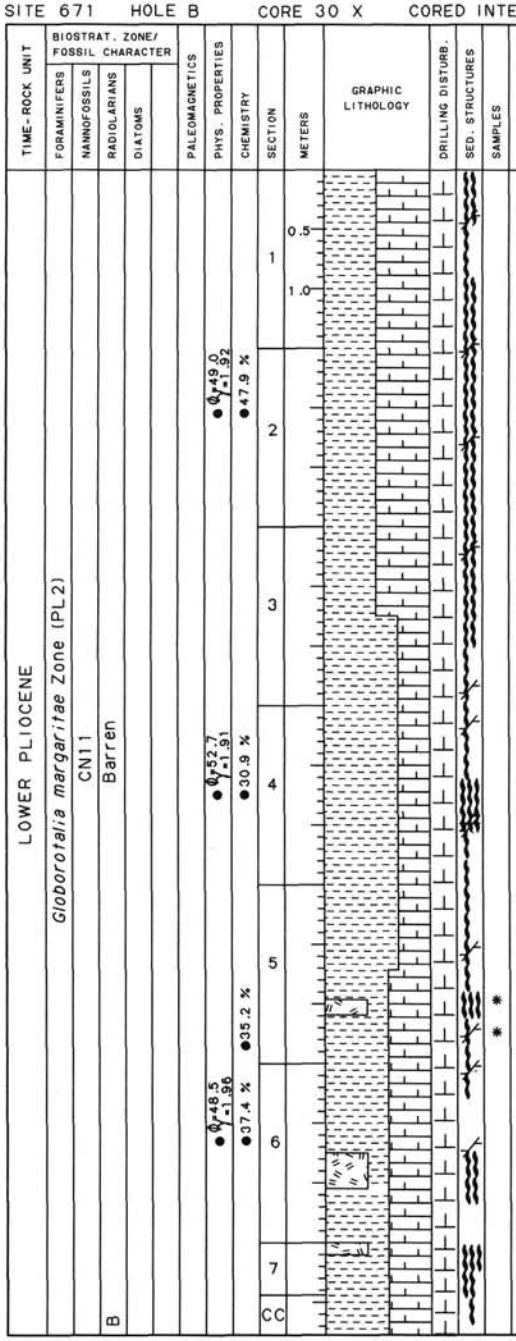

LITHOLOGIC DESCRIPTION

MARLSTONE and CALCAREOUS MUDSTONE

Gray (5Y6/1) to olive-gray (5Y5/1) MARLSTONE and CALCAREOUS MUDSTONE. Bioturbation is moderate to strong throughout the core. Sections 5 to 7 contain darker gray (2.5Y4/1) strongly bioturbated beds of ashy mudstone. Numerous small-scale high-angle faults throughout the core.

SMEAR SLIDE SUMMARY (%):

	5, 100 M	5, 132 D
TEXTURE:		
Sand	—	5
Silt	20	10
Clay	80	85
COMPOSITION:		
Feldspar	4	Tr
Clay	22	54
Volcanic glass	4	—
Accessory minerals	5	1
Clinopyroxene	Tr	Tr
Foraminifers	5	10
Nannofossils	60	35
Diatoms	Tr	Tr
Radiolarians	Tr	—

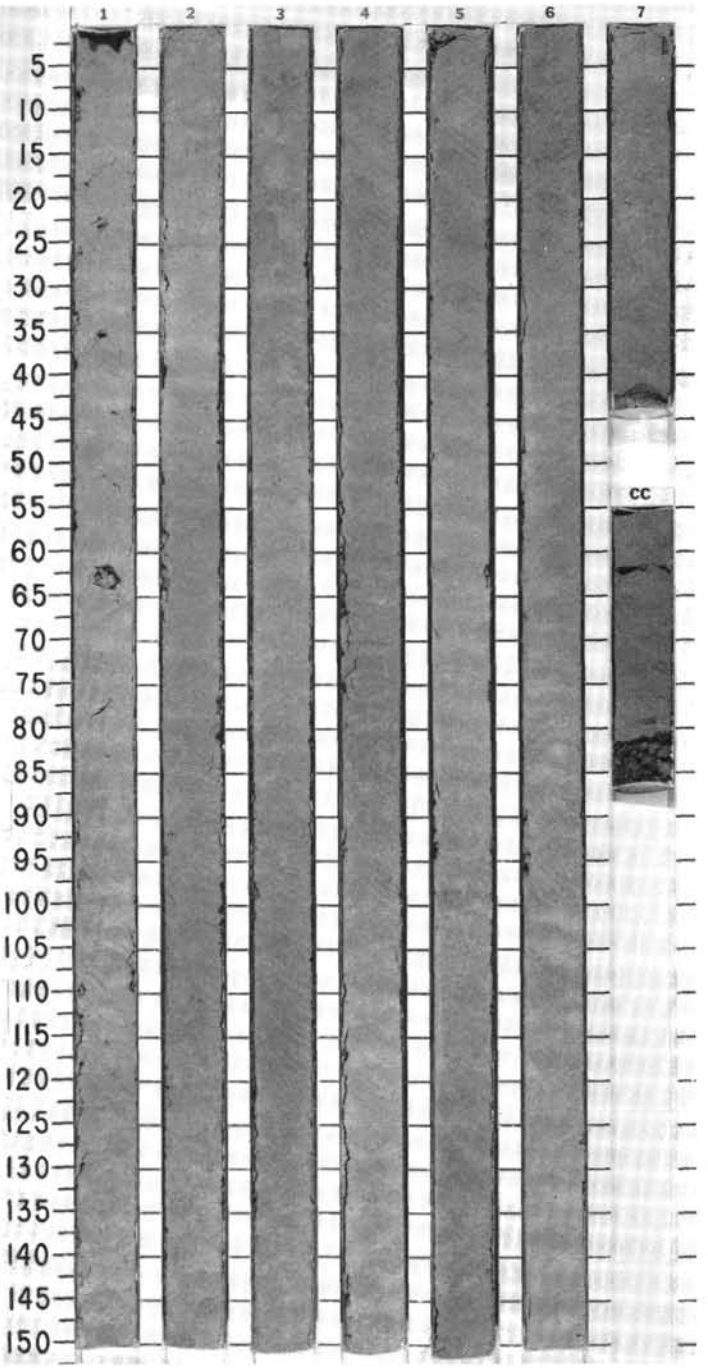

SITE 671 HOLE B CORE 31 X CORED INTERVAL 5213.3-5222.8 mbsl; 281.6-291.1 mbsf

TIME-ROCK UNIT	BIOSTRAT. ZONE/ FOSSIL CHARACTER: FORAMINIFERS	NANNOFOSSILS	RADIOLARIANS	DIATOMS	PALEOMAGNETICS	PHYS. PROPERTIES	CHEMISTRY	SECTION	METERS	GRAPHIC LITHOLOGY	DRILLING DISTURB.	SED. STRUCTURES	SAMPLES
LOWER PLIOCENE	*Globorotalia margaritae* Zone (PL2)	CN11	B Barren			● φ=50.4 γ=1.95	32.6 %	1, 2, CC	0.5, 1.0				* IW

LITHOLOGIC DESCRIPTION

CALCAREOUS MUDSTONE and MUDSTONE

Gray (5Y5/1 to 5Y6/1) CALCAREOUS MUDSTONE with one layer of ashy MUDSTONE in Section 1, 98–120 cm. The lower half of Section 1, Section 2, and the CC are moderately bioturbated.

SMEAR SLIDE SUMMARY (%):

	1, 5
	D
TEXTURE:	
Sand	5
Silt	10
Clay	85
COMPOSITION:	
Quartz	Tr
Feldspar	Tr
Clay	50
Volcanic glass	Tr
Accessory minerals	
Opaques	Tr
Foraminifers	5
Nannofossils	45
Diatoms	Tr
Radiolarians	Tr

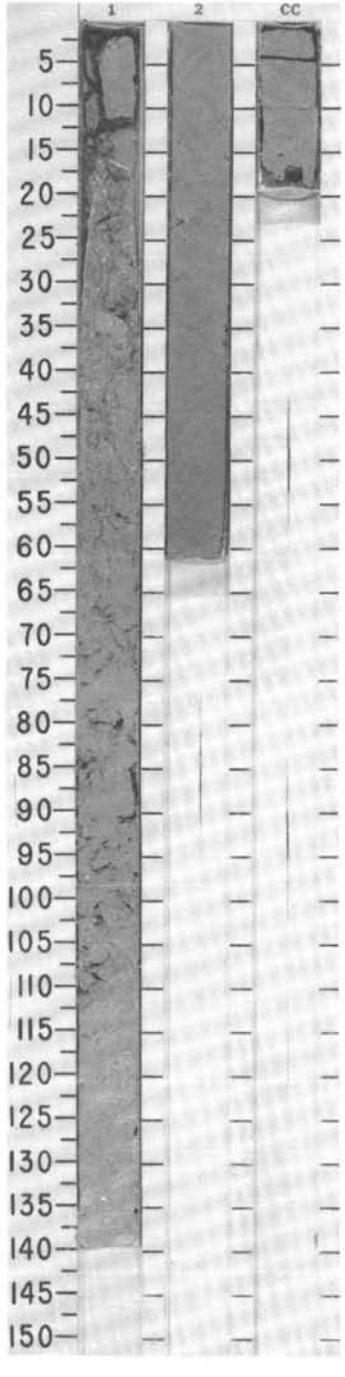

SITE 671 HOLE B CORE 32 X CORED INTERVAL 5222.8-5232.3 mbsl; 291.1-300.6 mbsf

TIME-ROCK UNIT	BIOSTRAT. ZONE/ FOSSIL CHARACTER: FORAMINIFERS	NANNOFOSSILS	RADIOLARIANS	DIATOMS	PALEOMAGNETICS	PHYS. PROPERTIES	CHEMISTRY	SECTION	METERS	GRAPHIC LITHOLOGY	DRILLING DISTURB.	SED. STRUCTURES	SAMPLES
LOWER PLIOCENE	*Globorotalia margaritae* Zone (PL2)	CN1Oc	Barren			● φ=55.2 γ=1.84	● 35.6 %	1	0.5, 1.0				
								2					
								3					*
						● φ=60.1 γ=1.77	● 21.7 %	4					OG
								5					*
						● φ=50.2 γ=1.92	● 45 %	6					
								7					
			B					CC					

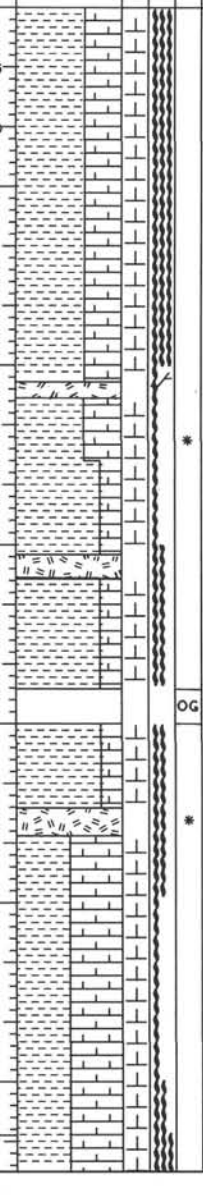

LITHOLOGIC DESCRIPTION

CALCAREOUS MUDSTONE and MARLSTONE

Gray (5Y5/1 to 5Y6/1) CALCAREOUS MUDSTONE in Sections 1 to 5, to MARLSTONE in lower part of Section 5 and in Section 6. Sections 1 and 2 are strongly bioturbated, and from Section 1, 100 cm, to the bottom of Section 2 there is a pronounced scaly fabric, which is truncated by a fault at the top of Section 3. Sections 3 to 7 are mildly to moderately bioturbated.

Minor lithology: three dark gray (N3) beds of volcanic vitric ash in Sections 3, 4, and 5.

SMEAR SLIDE SUMMARY (%):

	3, 66 D	5, 82 M
TEXTURE:		
Sand	2	2
Silt	5	15
Clay	93	83
COMPOSITION:		
Feldspar	Tr	Tr
Clay	93	50
Volcanic glass	5	47
Foraminifers	2	3

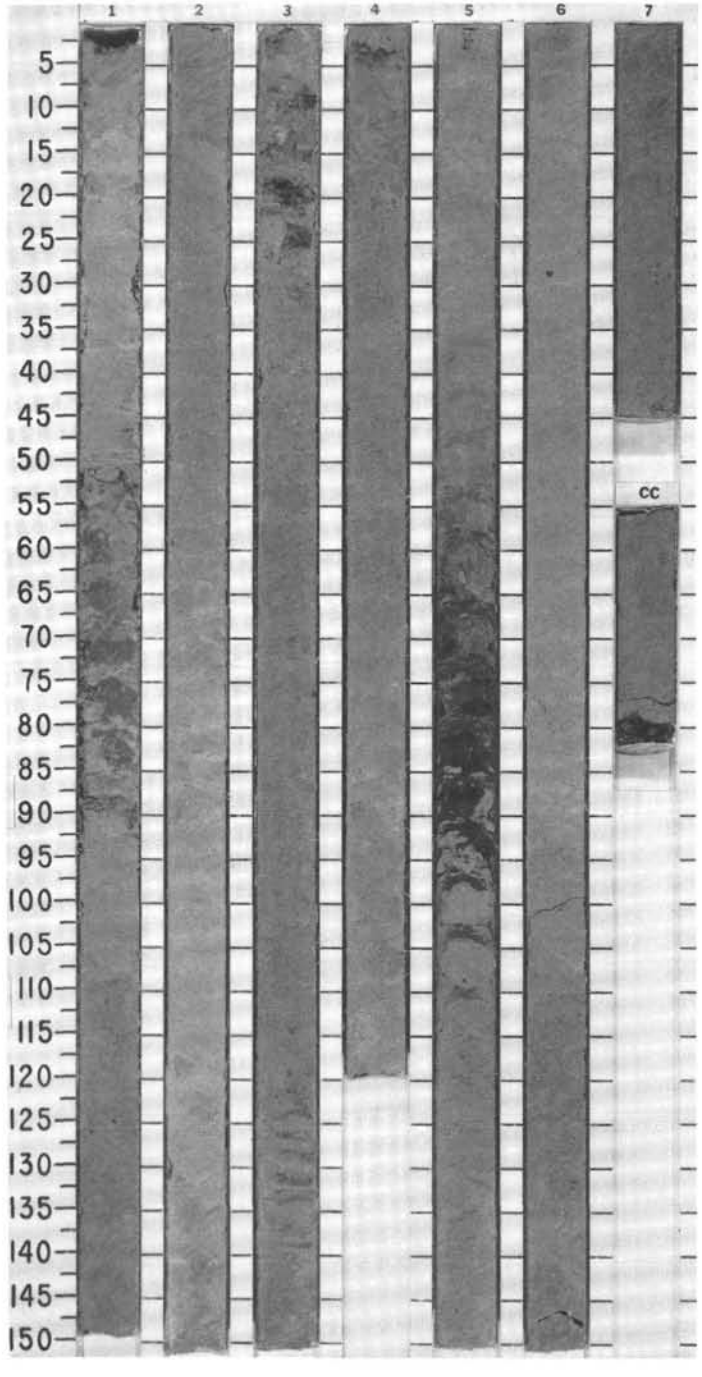

SITE 671 HOLE B CORE 33 X CORED INTERVAL 5232.3-5237.8 mbsl; 300.6-306.1 mbsf

TIME-ROCK UNIT	BIOSTRAT. ZONE/ FOSSIL CHARACTER: FORAMINIFERS	NANNOFOSSILS	RADIOLARIANS	DIATOMS	PALEOMAGNETICS	PHYS. PROPERTIES	CHEMISTRY	SECTION	METERS	GRAPHIC LITHOLOGY	DRILLING DISTURB.	SED. STRUCTURES	SAMPLES
LOWER PLIOCENE	*Globorotalia truncatulinodes* Zone (PL1)	CN10c	B Barren			● Φ=57.6 γ=1.86 ● Φ=48.7 γ=1.99	● 36.4% ● 36.7 %	1 2 CC	0.5 1.0				*

LITHOLOGIC DESCRIPTION

CALCAREOUS CLAYSTONE and CLAYSTONE

Gray (5Y4/1, 5Y6/1) to olive-gray (5Y6/2) or olive (5Y6/3) CALCAREOUS CLAYSTONE with two interbedded dark gray (2.5Y3/0) ashy CLAYSTONE layers. Moderate bioturbation in claystone, strong bioturbation in the ashy layers.

SMEAR SLIDE SUMMARY (%):

	1, 10 M	2, 1 D	2, 75 D
TEXTURE:			
Sand	2	1	—
Silt	80	—	5
Clay	18	99	95
COMPOSITION:			
Quartz	2	—	—
Feldspar	55	—	—
Clay	35	79	70
Volcanic glass	5	—	3
Accessory minerals			
Opaques	3	—	—
Foraminifers	—	1	—
Nannofossils	—	20	25
Bioclasts	—	—	2

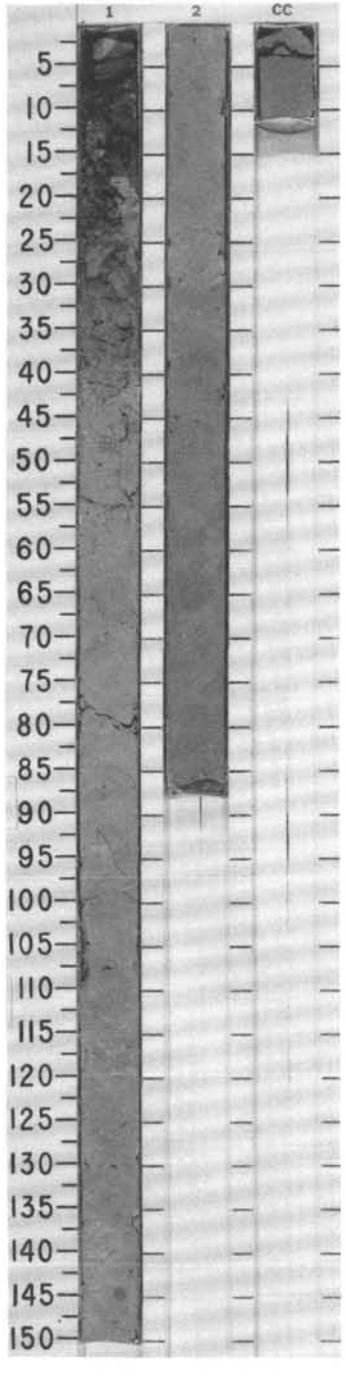

SITE 671 HOLE B CORE 34 X CORED INTERVAL 5237.8-5247.3 mbsl; 306.1-315.6 mbsf

TIME-ROCK UNIT: LOWER PLIOCENE

BIOSTRAT. ZONE/FOSSIL CHARACTER: FORAMINIFERS: *Globorotalia truncatulinoides* Zone (PL1); NANNOFOSSILS: CN10 c; RADIOLARIANS: Barren; DIATOMS: B

PALEOMAGNETICS

PHYS. PROPERTIES: ● Φ=55.2 γ=1.79; ● Φ=55.6 γ=1.85; ● Φ=46.6 γ=2.01

CHEMISTRY: ● 27.8%; ● 19.9 %; ● 21.7 %

SECTION: 1, 2, 3, 4, 5, 6, CC

METERS: 0.5, 1.0

GRAPHIC LITHOLOGY

DRILLING DISTURB.

SED. STRUCTURES

SAMPLES: IW

LITHOLOGIC DESCRIPTION

CALCAREOUS CLAYSTONE

Variegated (5Y6/1, 5Y5/2, 10YR6/1, 5Y6/2, 2.5Y5/2, 5G7/2) gray to olive-gray and greenish CALCAREOUS CLAYSTONE. In Section 3 there is a gray (2.5Y3/0) ashy layer with strong *Planolites* and *Teichinus* bioturbation. In addition, bioturbation is strong in the upper half of the core, and mild to moderate (by *Planolites* and *Chondrites*) in the lower half.

SMEAR SLIDE SUMMARY (%):

	1, 10 D	3, 31 M	4, 91 D	6, 8 D
TEXTURE:				
Silt	3	60	5	10
Clay	97	40	95	90
COMPOSITION:				
Feldspar	Tr	32	—	Tr
Clay	65	60	72	73
Volcanic glass	2	2	5	Tr
Accessory minerals				
Pyrite	—	4	Tr	—
Foraminifers	1	Tr	—	—
Nannofossils	30	2	20	25
Bioclasts	2	—	3	2

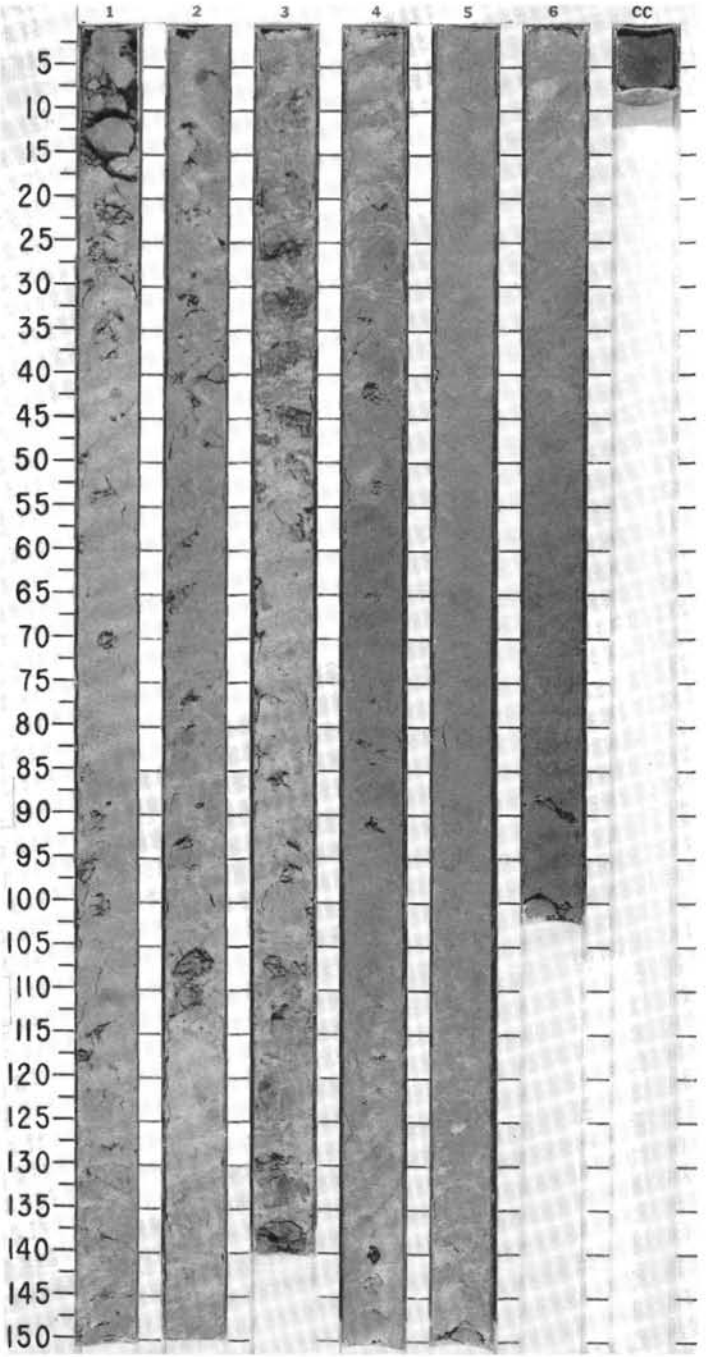

SITE 671 HOLE B CORE 35 X CORED INTERVAL 5247.3-5256.8 mbsl; 315.6-325.1 mbsf

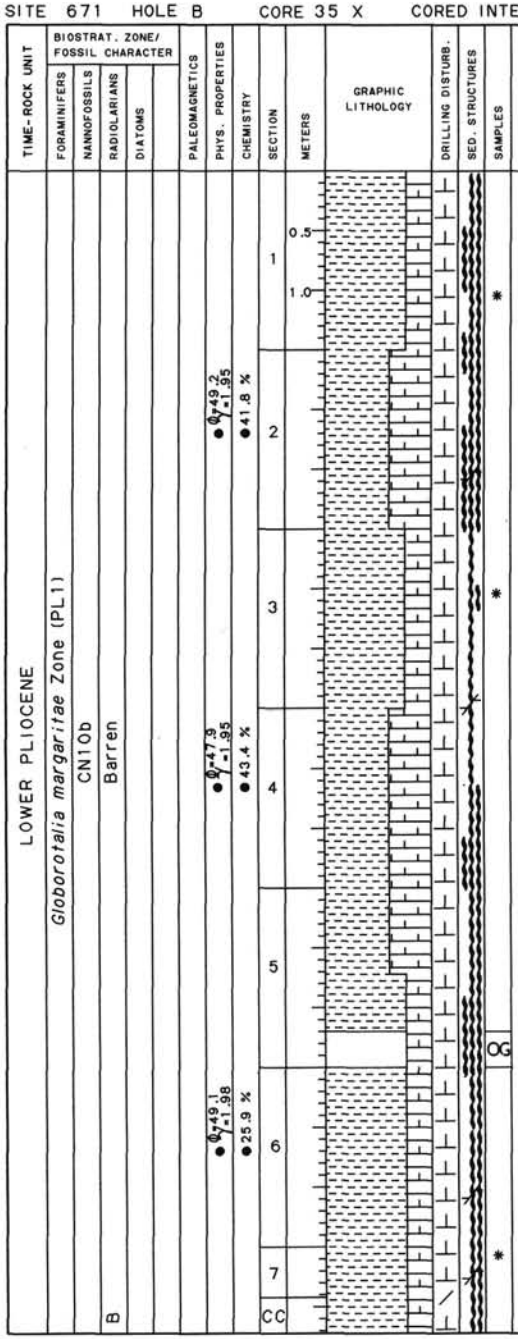

LITHOLOGIC DESCRIPTION

MARLSTONE, CALCAREOUS MUDSTONE, and CALCAREOUS CLAYSTONE

Grayish brown to light yellowish brown (2.5Y5/2 to 2.5Y6/3) MARLSTONE and CALCAREOUS MUDSTONE in Sections 1 and 2. Olive-gray to dark reddish brown CALCAREOUS CLAYSTONE in Section 3 with mild bioturbation. Section 3, 50–60 cm, shows burrowing by *Planolites*, and Section 3, 100–150 cm, is burrowed by *Zoophycos*. Light olive-gray to olive-brown (2.5Y6/2 to 2.5Y4/4) MARLSTONE in Section 4, moderately to highly bioturbated, partly by *Planolites*. Olive (5Y5/3) MARLSTONE to CALCAREOUS CLAYSTONE in Section 5, strong bioturbation by *Planolites* and *Chondrites*. In Sections 6, 7, and CC, olive-gray to pale olive (5Y6/2 to 5Y6/3) CALCAREOUS CLAYSTONE with scattered sand-sized foraminifers, strongly bioturbated.

SMEAR SLIDE SUMMARY (%):

	1, 94 D	3, 58 M	7, 4 D
TEXTURE:			
Silt	5	5	2
Clay	95	95	98
COMPOSITION:			
Feldspar	Tr	Tr	—
Mica	—	—	Tr
Clay	75	80	80
Volcanic glass	Tr	Tr	Tr
Accessory minerals			
Glauconite	—	—	Tr
Pyrite	—	1	—
Opaques	Tr	—	—
Foraminifers	—	Tr	Tr
Nannofossils	25	19	20
Bioclasts	Tr	—	—

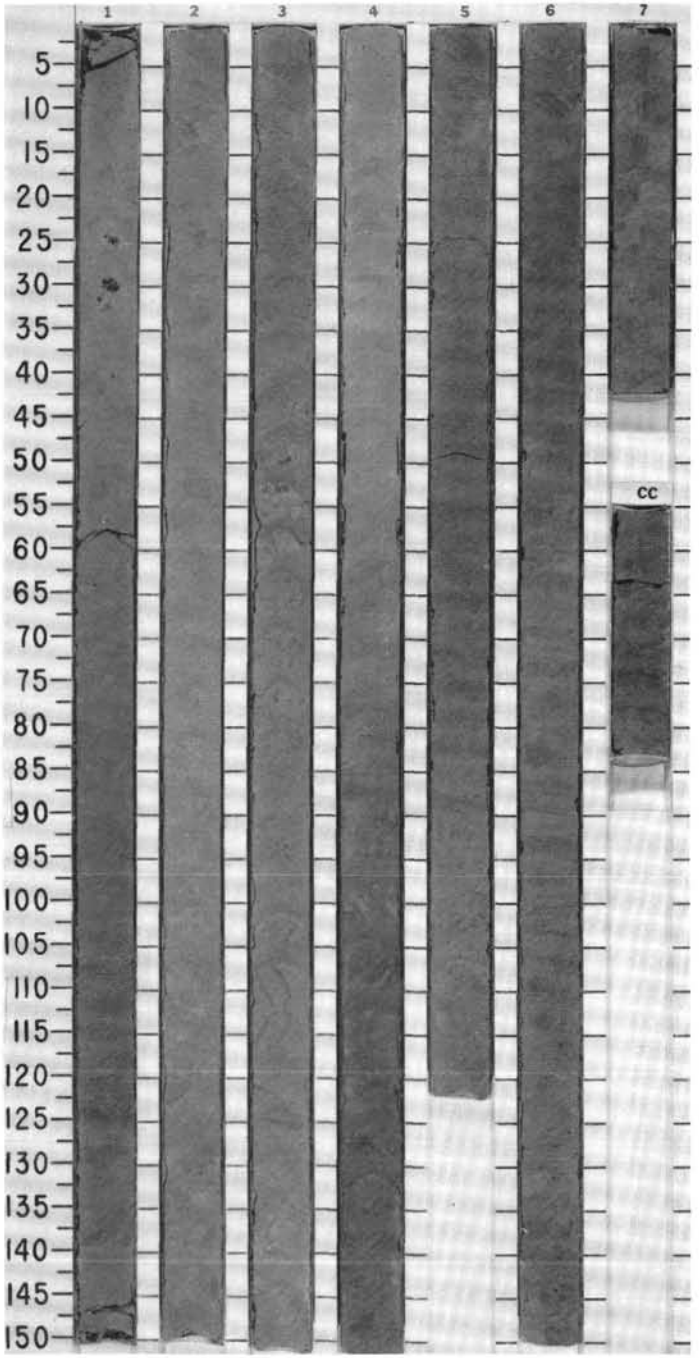

SITE 671 HOLE B CORE 36 X CORED INTERVAL 5256.8-5266.3 mbsl; 325.1-334.6 mbsf

TIME-ROCK UNIT	FORAMINIFERS	NANNOFOSSILS	RADIOLARIANS	DIATOMS	PALEOMAGNETICS	PHYS. PROPERTIES	CHEMISTRY	SECTION	METERS	GRAPHIC LITHOLOGY	DRILLING DISTURB.	SED. STRUCTURES	SAMPLES
LOWER PLIOCENE	*Globorotalia margaritae* Zone (PL1)	CN10b	Barren			● φ=49.5 γ=1.97	● 32.5 %	1	0.5 1.0				*
								2					
								3					
						● φ=58.0 γ=1.83	● 22.6 %	4					* *
								5					
						● φ=48.6 γ=1.97	● 38.9 %	6					
								7					
			B					CC					*

LITHOLOGIC DESCRIPTION

CALCAREOUS MUDSTONE and MARLSTONE

Light olive-gray to olive (5Y6/2 to 5Y5/3) or light brownish gray (2.5Y6/2) CALCAREOUS MUDSTONE in Sections 1 through 5, and MARLSTONE in Sections 6, 7, and CC. Mild to moderate bioturbation throughout the core.

Minor lithology: ashy marlstone, in part strongly bioturbated, throughout most of Section 7 and CC.

SMEAR SLIDE SUMMARY (%):

	1, 42 M	4, 71 D	4, 130 M	CC, 15 M
TEXTURE:				
Sand	—	—	10	2
Silt	Tr	15	50	63
Clay	100	85	40	35
COMPOSITION:				
Feldspar	Tr	Tr	45	20
Rock fragments	—	—	5	—
Clay	75	80	38	33
Volcanic glass	—	Tr	10	45
Accessory minerals				
Clinopyroxene	—	—	Tr	—
Opaques	—	—	2	2
Hornblende	—	—	Tr	Tr
Foraminifers	Tr	—	—	—
Nannofossils	25	20	—	—

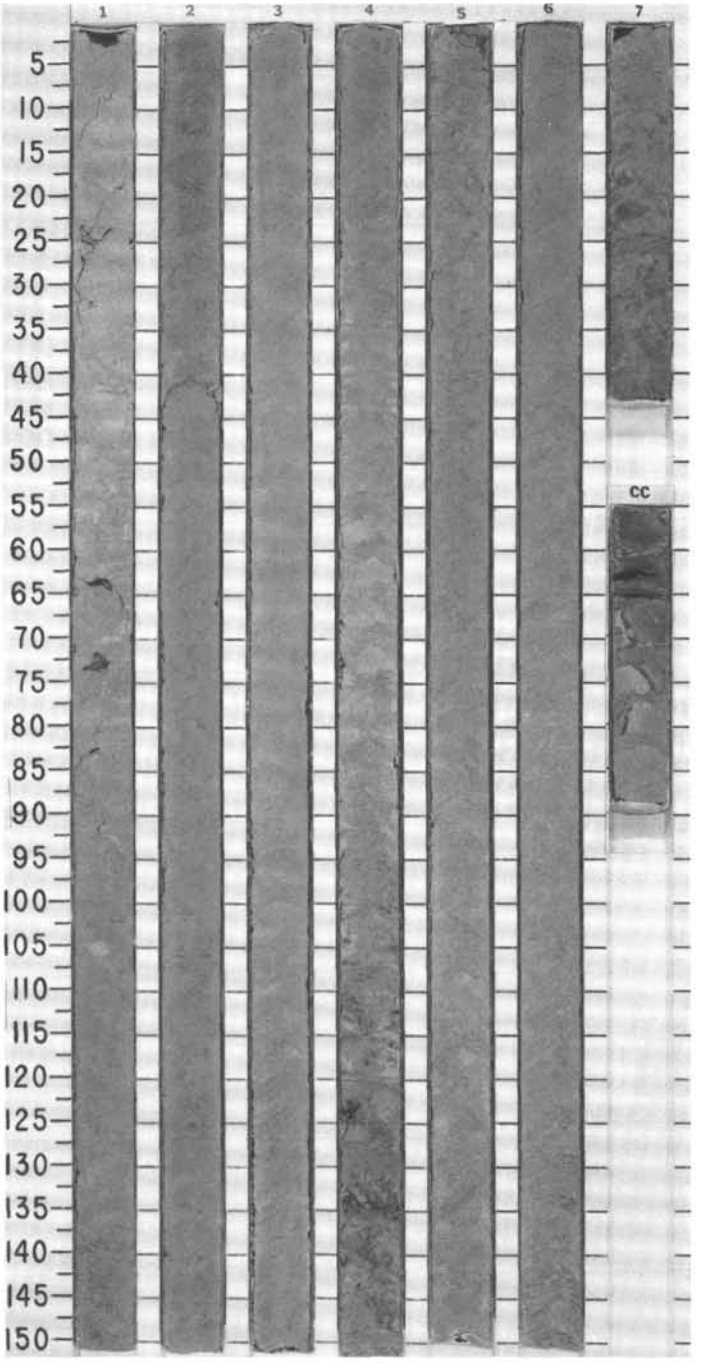

SITE 671 HOLE B CORE 37 X CORED INTERVAL 5266.3-5275.8 mbsl; 334.6-344.1 mbsf

TIME-ROCK UNIT	BIOSTRAT. ZONE/ FOSSIL CHARACTER: FORAMINIFERS	NANNOFOSSILS	RADIOLARIANS	DIATOMS	PALEOMAGNETICS	PHYS. PROPERTIES	CHEMISTRY	SECTION	METERS	GRAPHIC LITHOLOGY	DRILLING DISTURB.	SED. STRUCTURES	SAMPLES
UPPER MIOCENE	*Neogloboquadrina humerosa* Zone	CN10a	Barren			●φ=54.4 γ=1.87	●=9.2 %	1	0.5, 1.0				
								2					IW
						●φ=49.8 γ=1.92	●32.9 % 26.7 %	3					*
			B					CC					

LITHOLOGIC DESCRIPTION

CALCAREOUS MUDSTONE

Grayish brown to light brownish gray (2.5Y5/2 to 2.5Y6/2) ashy CALCAREOUS MUDSTONE with minor nannofossils and foraminifers. Mildly bioturbated, mainly by *Chondrites*.

SMEAR SLIDE SUMMARY (%):

	3, 72
	D
TEXTURE:	
Silt	12
Clay	88
COMPOSITION:	
Feldspar	Tr
Clay	76
Volcanic glass	12
Nannofossils	12

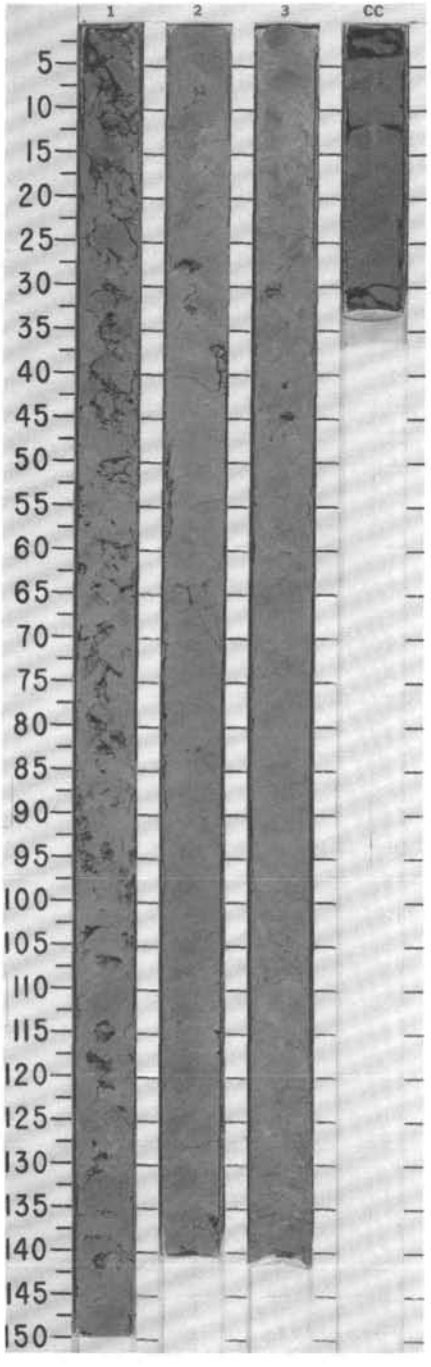

SITE 671 HOLE B CORE 38 X CORED INTERVAL 5275.8-5285.3 mbsl; 344.1-353.6 mbsf

TIME-ROCK UNIT	FORAMINIFERS	NANNOFOSSILS	RADIOLARIANS	DIATOMS	PALEOMAGNETICS	PHYS. PROPERTIES	CHEMISTRY	SECTION	METERS	GRAPHIC LITHOLOGY	DRILLING DISTURB.	SED. STRUCTURES	SAMPLES
LOWER MIOCENE	*Neogloboquadrina humerosa* Zone	CN9b	Barren			● φ=64.1 γ=1.76	● 7.9 %	1	0.5, 1.0				*
								2					OG
						● φ=51.1 γ=1.87	● 6.8 %	3					*
								CC					

LITHOLOGIC DESCRIPTION

MUDSTONE

Olive-brown to olive (2.5Y5/4 to 5Y5/3) or brown (10YR5/3) ashy MUDSTONE with minor nannofossils and foraminifers. Mild to intense bioturbation.

Minor lithology: one distinct 7 cm-thick bed of bluish gray (BG7/1) volcanic ash in Section 1, 8–20 cm.

SMEAR SLIDE SUMMARY (%):

	1, 7 M	3, 67 D
TEXTURE:		
Sand	5	10
Silt	25	20
Clay	70	70
COMPOSITION:		
Feldspar	Tr	2
Clay	45	53
Volcanic glass	50	25
Foraminifers	5	10
Nannofossils	—	10

SITE 671 HOLE B CORE 39 X CORED INTERVAL 5285.3-5294.8 mbsl; 353.6-363.1 mbsf

TIME-ROCK UNIT	FORAMINIFERS	NANNOFOSSILS	RADIOLARIANS	DIATOMS	PALEOMAGNETICS	PHYS. PROPERTIES	CHEMISTRY	SECTION	METERS	GRAPHIC LITHOLOGY	DRILLING DISTURB.	SED. STRUCTURES	SAMPLES
UPPER MIOCENE	*Neogloboquadrina humerosa* Zone	CN9b	Barren B					1					
								CC					

LITHOLOGIC DESCRIPTION

CLAYSTONE

Olive-gray (5Y5/2) CLAYSTONE, moderate bioturbation in CC.

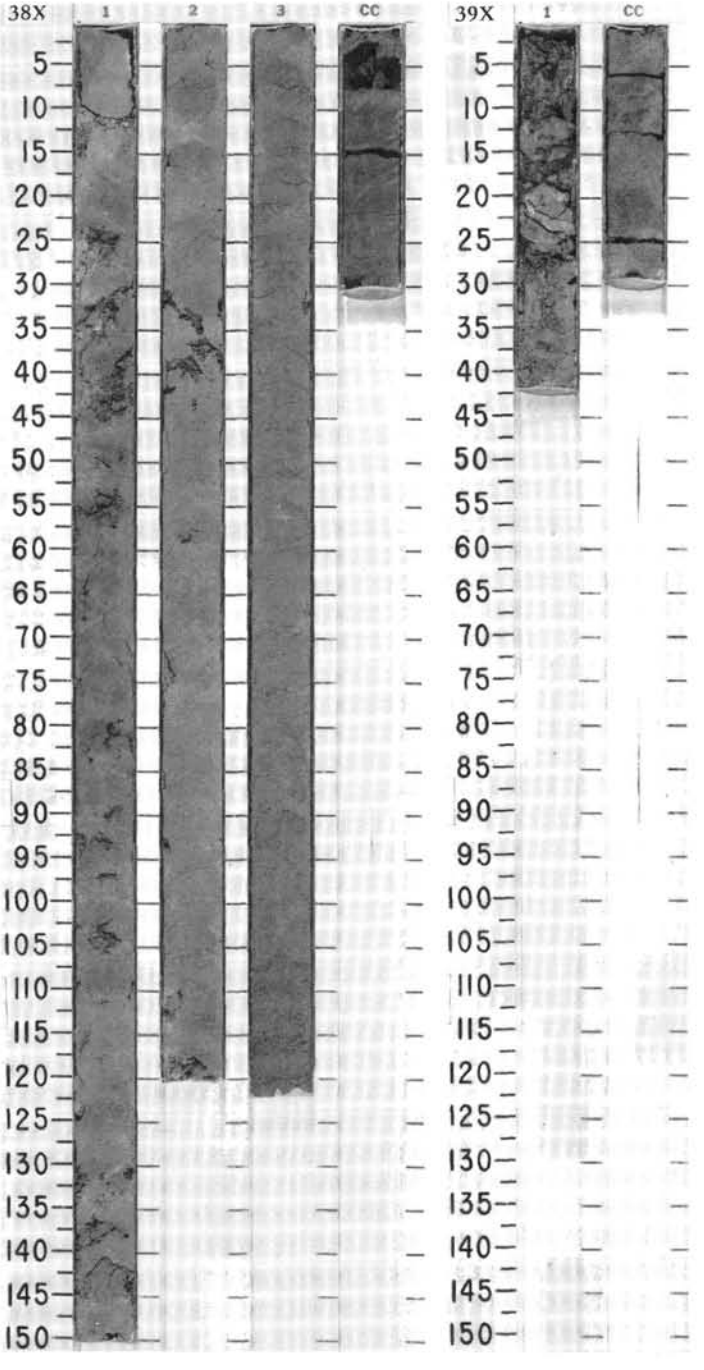

SITE 671 HOLE B CORE 40 X CORED INTERVAL 5294.8-5304.3 mbsl; 363.1-372.6 mbsf

TIME-ROCK UNIT	BIOSTRAT. ZONE/ FOSSIL CHARACTER: FORAMINIFERS	NANNOFOSSILS	RADIOLARIANS	DIATOMS	PALEOMAGNETICS	PHYS. PROPERTIES	CHEMISTRY	SECTION	METERS	GRAPHIC LITHOLOGY	DRILLING DISTURB.	SED. STRUCTURES	SAMPLES
UPPER MIOCENE	*Neoglobquadrina humerosa* Zone	CN9b	B	Barren		● Φ=49.9 ρ=1.93	● 8.0 %	4					
						● Φ=55.1 ρ=1.87	● 7.2 %	2					
								1	0.5				
									1.0				
								3					
								CC					

LITHOLOGIC DESCRIPTION

MUDSTONE

Olive-gray (5Y5/2, 5Y4/2) ashy MUDSTONE, with scattered sand-sized foraminifers. Sections 2, 3, and CC are mildly to moderately bioturbated.

SMEAR SLIDE SUMMARY (%):

	CC, 17 D
TEXTURE:	
Silt	10
Clay	90
COMPOSITION:	
Clay	88
Volcanic glass	10
Nannofossils	2

SITE 671 HOLE B CORE 41 X CORED INTERVAL 5304.3-5309.4 mbsl; 372.6-377.7 mbsf

TIME-ROCK UNIT	BIOSTRAT. ZONE/ FOSSIL CHARACTER: FORAMINIFERS	NANNOFOSSILS	RADIOLARIANS	DIATOMS	PALEOMAGNETICS	PHYS. PROPERTIES	CHEMISTRY	SECTION	METERS	GRAPHIC LITHOLOGY	DRILLING DISTURB.	SED. STRUCTURES	SAMPLES
UPPER MIOCENE		CN9b	Barren			● Φ=54.7 γ=1.93	● 4.0 %	1	0.5, 1.0				
								2					*
						● Φ=53.7 γ=1.89	● 7.1 %	3					
								4					*
								5					
						● Φ=45.8 γ=2.01	● 28.4 %	6					
								7					
			B					CC					

LITHOLOGIC DESCRIPTION

CLAYSTONE

CLAYSTONE, olive-gray (5Y4/2) in Sections 1 through 4, grayish brown (2.5Y5/2) in Section 5, and pale brown to brown (10YR6/3 to 10YR4/3) in Sections 6 and 7; in lower part of core nannofossil-bearing and calcareous. Bioturbation, by *Planolites* and *Chondrites*, is moderate throughout the core.

SMEAR SLIDE SUMMARY (%):

	2, 72 D	4, 131 D
TEXTURE:		
Silt	5	2
Clay	95	98
COMPOSITION:		
Feldspar	Tr	Tr
Clay	93	80
Volcanic glass	—	Tr
Accessory minerals		
Opaques	2	Tr
Nannofossils	5	20

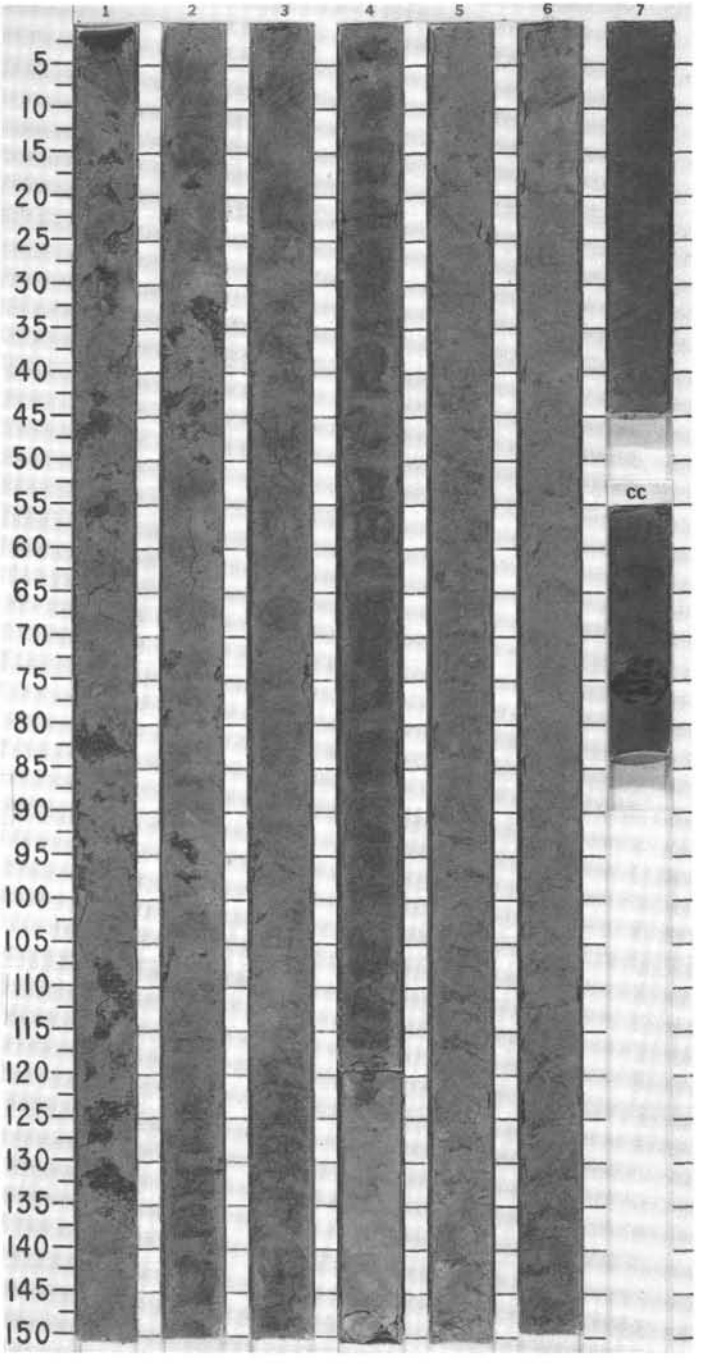

SITE 671 HOLE B CORE 42 X CORED INTERVAL 5309.4-5318.9 mbsl; 377.7-387.2 mbsf

TIME-ROCK UNIT	BIOSTRAT. ZONE/ FOSSIL CHARACTER: FORAMINIFERS	NANNOFOSSILS	RADIOLARIANS	DIATOMS	PALEOMAGNETICS	PHYS. PROPERTIES	CHEMISTRY	SECTION	METERS	GRAPHIC LITHOLOGY	DRILLING DISTURB.	SED. STRUCTURES	SAMPLES
UPPER MIOCENE	*Neogloboquadrina humerosa* Zone	CN9b	Barren			● φ=48.6 γ=1.98	● 8.0 %	1	0.5, 1.0				
								2					*
								3					*
						● φ=53.8 γ=1.88	● 12.5 %	4					
								5					
						● φ=53.5 γ=1.93	● 6.7 %	6					*
								7					
			B					CC					

LITHOLOGIC DESCRIPTION

CLAYSTONE and MUDSTONE

CLAYSTONE and MUDSTONE, pale olive to olive (5Y6/3, 5Y4/3, 5Y5/4) in Sections 1 through 3, and grayish brown (2.5Y5/2) and dark grayish brown (2.5Y4/2) in Sections 4 through 7, with an interval of vitric ashy clay in Section 3, 15–58 cm. Patchy moderate bioturbation. *Planolites* and *Chondrites* burrows were identified in Sections 5 and 7, and CC.

SMEAR SLIDE SUMMARY (%):

	2, 74 D	3, 30 M	6, 82 D
TEXTURE:			
Sand	—	—	20
Silt	2	70	5
Clay	98	30	75
COMPOSITION:			
Quartz	—	Tr	—
Feldspar	—	30	1
Clay	90	30	89
Volcanic glass	2	40	—
Calcite/dolomite	—	—	—
Accessory minerals			
Pyrite	—	—	5
Pyroxene	Tr	Tr	Tr
Hornblende	Tr	Tr	—
Nannofossils	8	Tr	5

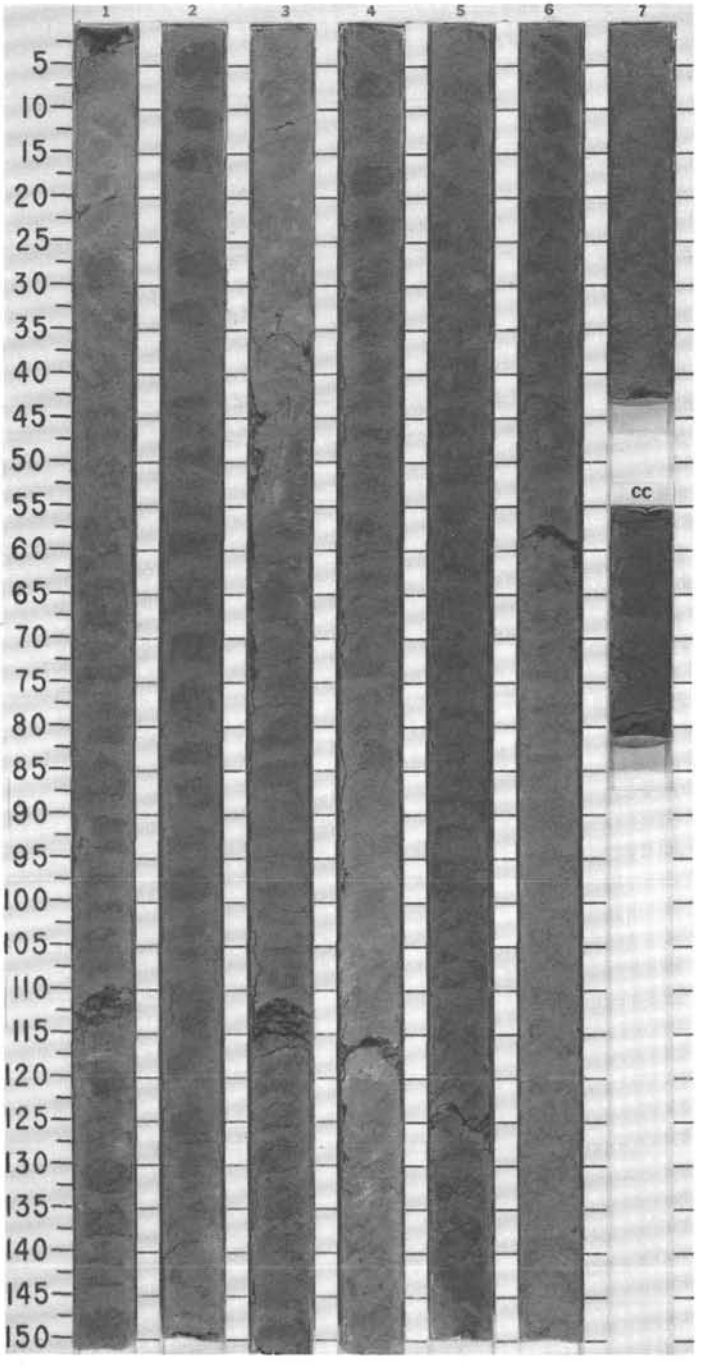

SITE 671 HOLE B CORE 43 X CORED INTERVAL 5318.9-5328.4 mbsl; 387.2-396.7 mbsf

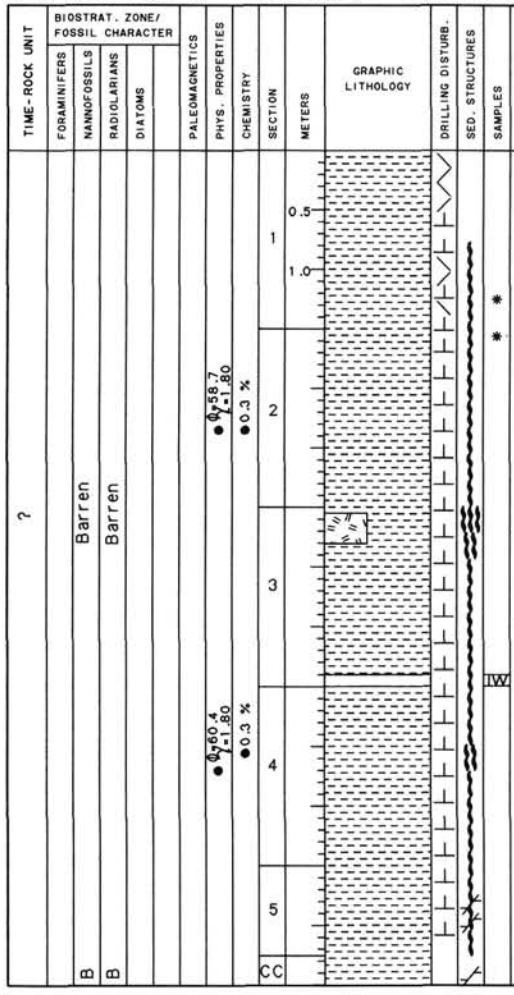

LITHOLOGIC DESCRIPTION

CLAYSTONE

Dark grayish brown (2.5Y4/2) to dark olive-gray (5Y3/2) CLAYSTONE, slightly to moderately bioturbated. One ashy interval in Section 3.

SMEAR SLIDE SUMMARY (%):

	1, 118 D	2, 7 M
TEXTURE:		
Silt	5	7
Clay	95	93
COMPOSITION:		
Feldspar	Tr	2
Clay	95	93
Volcanic glass	5	—
Accessory minerals		
Opaques	—	5
Nannofossils	—	Tr

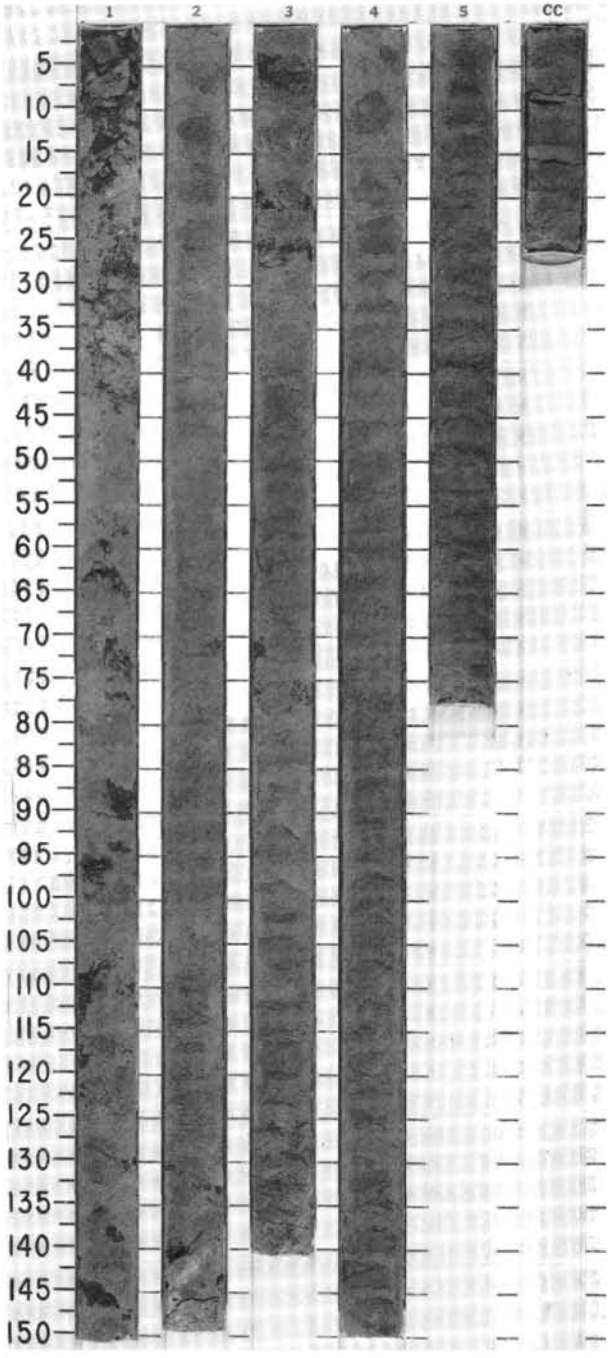

SITE 671 HOLE B CORE 44 X CORED INTERVAL 5328.4-5337.9 mbsl; 396.7-406.2 mbsf

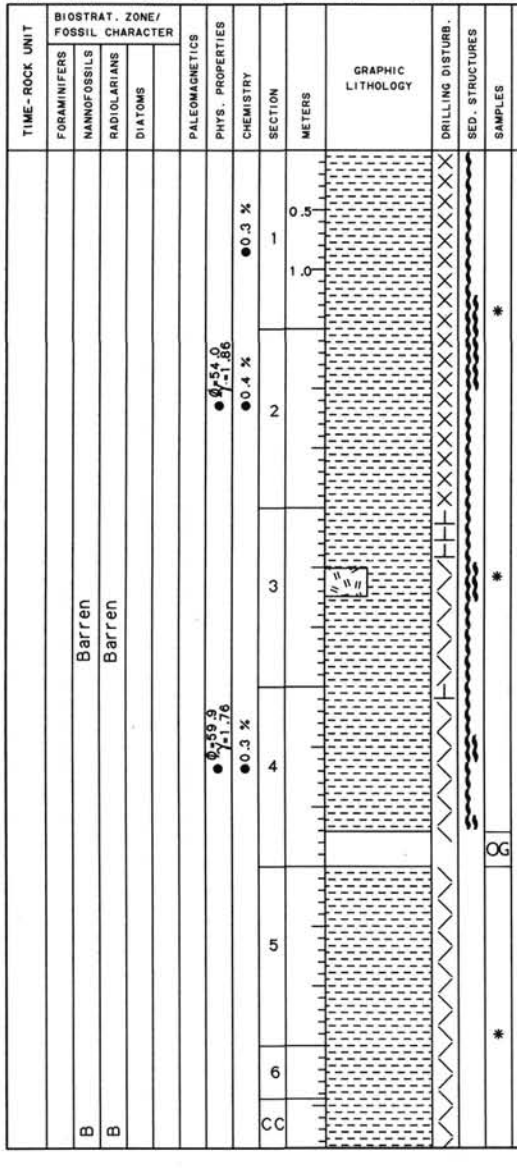

LITHOLOGIC DESCRIPTION

CLAYSTONE

Gray to olive-gray (5Y5/1 to 5Y5/2) CLAYSTONE, slightly to moderately bioturbated throughout section.

SMEAR SLIDE SUMMARY (%):

	1, 83 D	3, 55 M	5, 145 D
TEXTURE:			
Silt	Tr	5	3
Clay	100	95	97
COMPOSITION:			
Quartz	—	Tr	—
Feldspar	—	Tr	1
Clay	99	95	97
Volcanic glass	Tr	Tr	—
Accessory minerals			
Chlorite?	—	—	Tr
Opaques	1	4	2

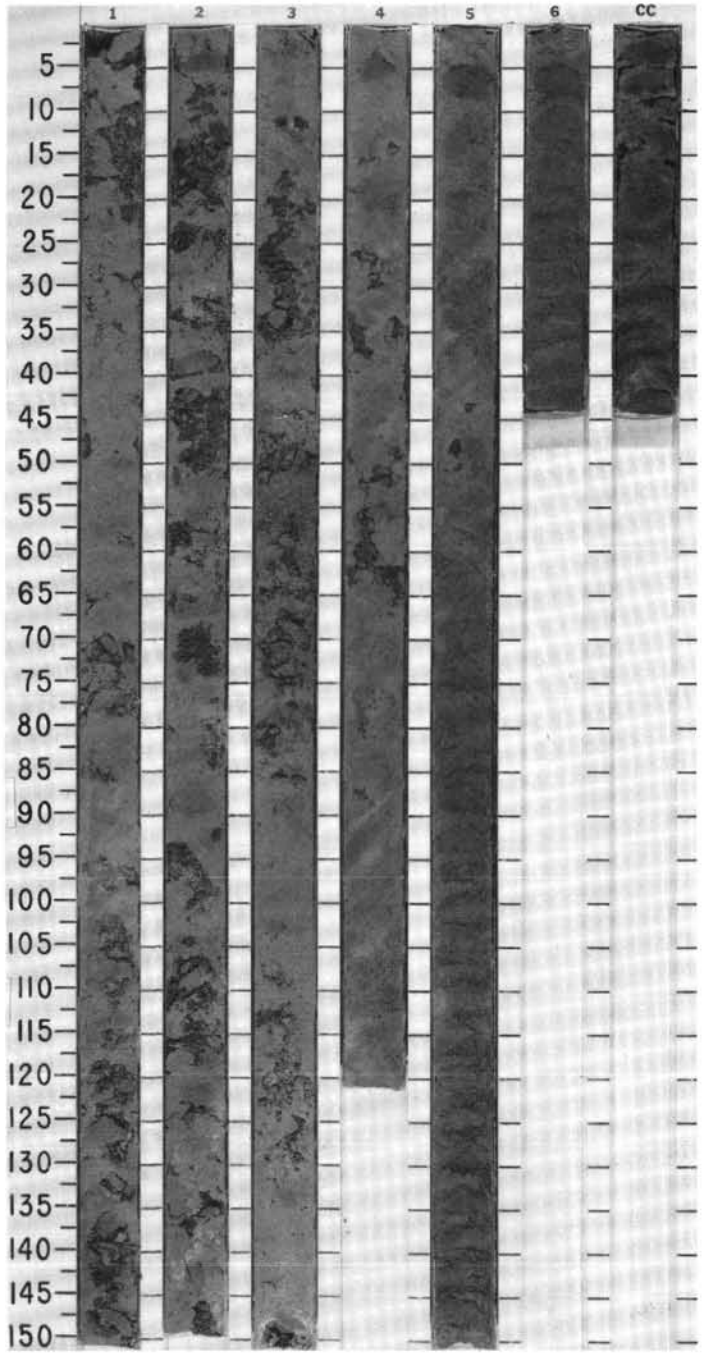

SITE 671 HOLE B CORE 45 X CORED INTERVAL 5337.9-5347.4 mbsl; 406.2-415.7 mbsf

TIME-ROCK UNIT	BIOSTRAT. ZONE/ FOSSIL CHARACTER: FORAMINIFERS	NANNOFOSSILS	RADIOLARIANS	DIATOMS	PALEOMAGNETICS	PHYS. PROPERTIES	CHEMISTRY	SECTION	METERS	GRAPHIC LITHOLOGY	DRILLING DISTURB.	SED. STRUCTURES	SAMPLES
?	B Barren	B Barren	B Barren			● Ø=64.5 %=1.78	● 0.3 %	1	0.5				*
									1.0				*
								2					
								3					
								4					
								CC					*

LITHOLOGIC DESCRIPTION

MUDSTONE

Dark greenish gray (5Y5/1 to 5G5/1) MUDSTONE, moderately bioturbated; ashy mud intercalation in Sections 1 and 4 (5G4/1); gradational contact between clay and more silty layers.

SMEAR SLIDE SUMMARY (%):

	1, 74 D	1, 121 M	CC, 22 M
TEXTURE:			
Sand	—	5	—
Silt	—	10	15
Clay	100	85	85
COMPOSITION:			
Feldspar	—	1	5
Clay	100	60	85
Volcanic glass	—	25	—
Accessory minerals			
Opaques	—	14	10

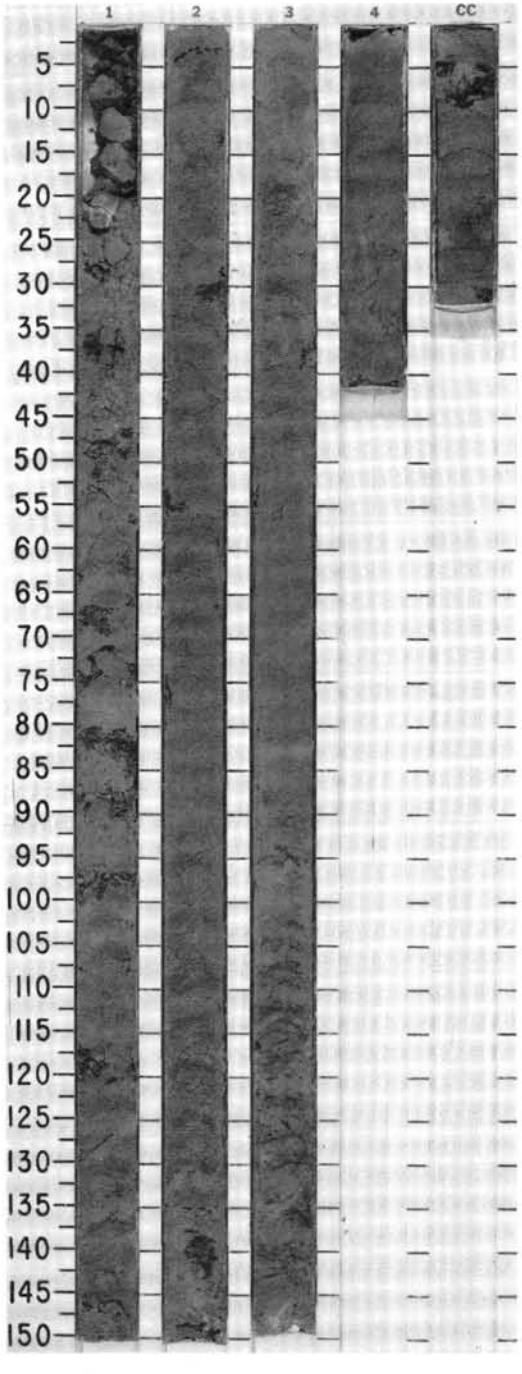

SITE 671 HOLE B CORE 46 X CORED INTERVAL 5347.4-5356.9 mbsl; 415.7-425.2 mbsf

TIME-ROCK UNIT	BIOSTRAT. ZONE/ FOSSIL CHARACTER: FORAMINIFERS	NANNOFOSSILS	RADIOLARIANS	DIATOMS	PALEOMAGNETICS	PHYS. PROPERTIES	CHEMISTRY	SECTION	METERS	GRAPHIC LITHOLOGY	DRILLING DISTURB.	SED. STRUCTURES	SAMPLES
UPPER MIOCENE	*Neogloboquadrina humerosa* Zone	CN9a	Barren			● φ=60.2 γ=1.83	● 0.7 %	1	0.5, 1.0				
								2					
						● φ=63.8 γ=1.74	● 0.2 %	3					IW
						● φ=55.3 γ=1.88	● 0.2 %	4					
			B			● φ=49.6 γ=2.04	● 13.2 %	5					*
								CC					

LITHOLOGIC DESCRIPTION

MUDSTONE

Moderately bioturbated MUDSTONE (locally slightly calcareous), greenish gray (10Y5/2 to 5G4/1) to dark greenish gray (5G5/1).

Minor lithology: dark gray (10Y4/2) mudstone with minor amount of ash (in Sections 2, 3, and 4).

SMEAR SLIDE SUMMARY (%):

	4, 145
	D
TEXTURE:	
Silt	25
Clay	75
COMPOSITION:	
Clay	75
Volcanic glass	23
Nannofossils	2

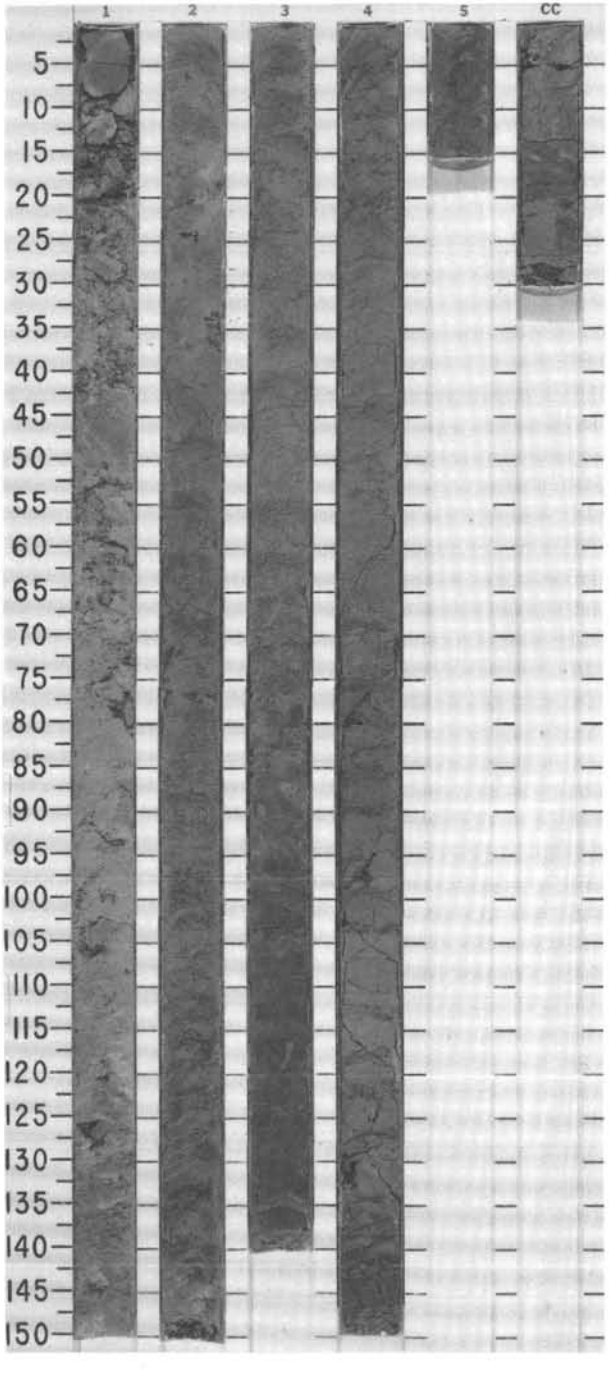

SITE 671 HOLE B CORE 47 X CORED INTERVAL 5356.9-5366.4 mbsl; 425.2-434.7 mbsf

TIME-ROCK UNIT	BIOSTRAT. ZONE/ FOSSIL CHARACTER: FORAMINIFERS	NANNOFOSSILS	RADIOLARIANS	DIATOMS	PALEOMAGNETICS	PHYS. PROPERTIES	CHEMISTRY	SECTION	METERS	GRAPHIC LITHOLOGY	DRILLING DISTURB.	SED. STRUCTURES	SAMPLES
UPPER MIOCENE		CN8a	Barren			● Φ=60.8 γ=1.78	● 0.4 %	1	0.5, 1.0				
								2					
								3					
						● Φ=56.8 γ=1.89	● 0.5 %	4					*
								5					OG
						● Φ=55.3 γ=1.83	● 8.3 %	6					
								7					
			B					CC					

LITHOLOGIC DESCRIPTION

CLAYSTONE

Dark to medium greenish gray CLAYSTONE (10Y4/2 to 10Y5/2), moderately bioturbated; two darker intercalations (Sections 1 and 2) corresponding to small amount of ash (5G5/1); these layers have diffuse contacts (top and bottom) and seem to be more bioturbated.

SMEAR SLIDE SUMMARY (%):

	4, 76
	D
TEXTURE:	
Silt	3
Clay	97
COMPOSITION:	
Quartz	Tr
Feldspar	3
Clay	97
Accessory minerals	
Opaques	Tr
Nannofossils	Tr

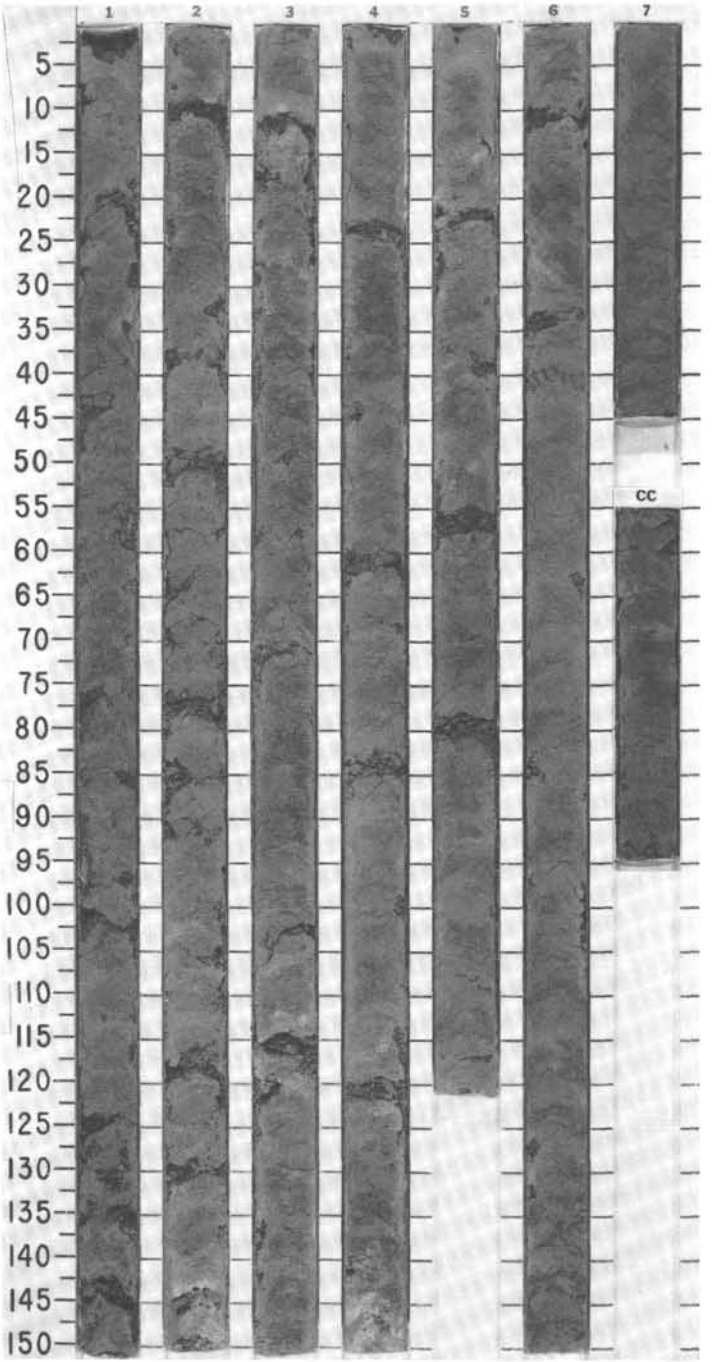

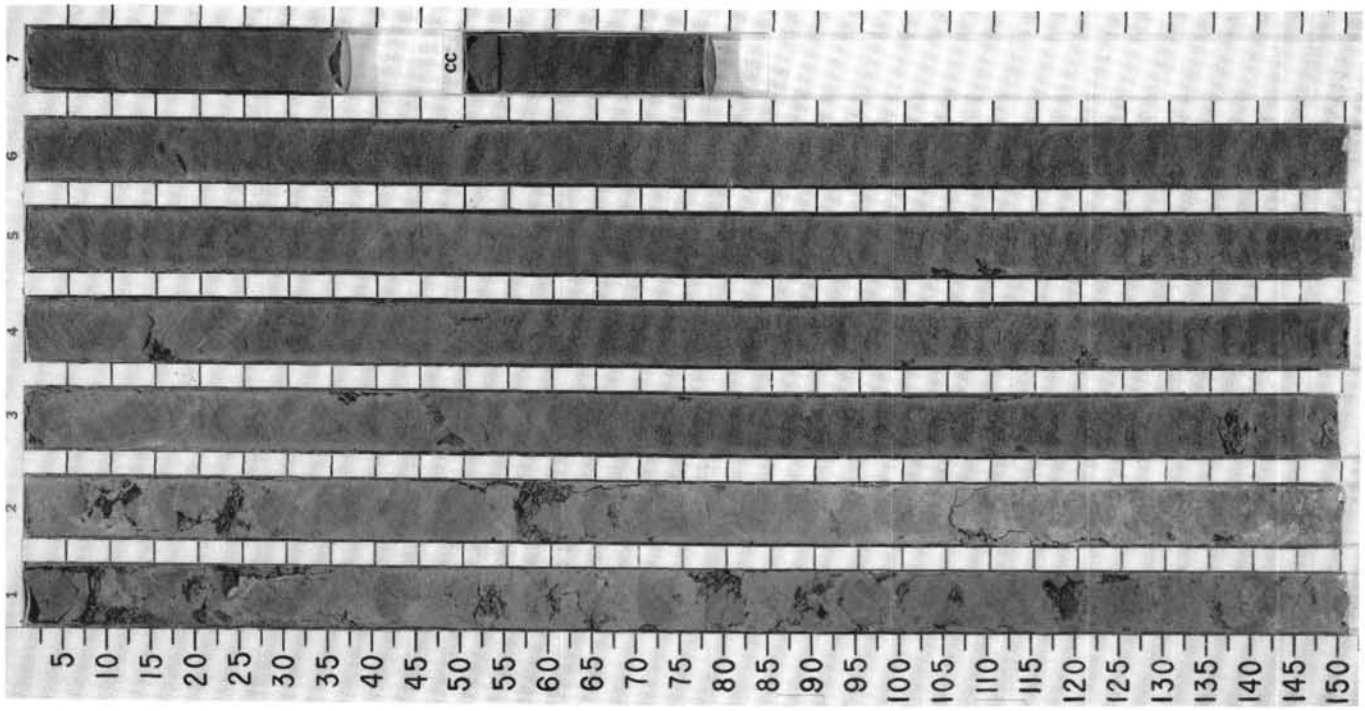

SITE 671 HOLE B CORE 48 X CORED INTERVAL 5366.4-5375.9 mbsl; 434.7-444.2 mbsf

TIME-ROCK UNIT	BIOSTRAT. ZONE/ FOSSIL CHARACTER: FORAMINIFERS	NANNOFOSSILS	RADIOLARIANS	DIATOMS		PALEOMAGNETICS	PHYS. PROPERTIES	CHEMISTRY	SECTION	METERS	GRAPHIC LITHOLOGY	DRILLING DISTURB.	SED. STRUCTURES	SAMPLES	LITHOLOGIC DESCRIPTION
?	B	B	B				● Φ=57.3 γ=1.81	● 10.4 %	1	0.5 1.0					CLAYSTONE Greenish gray (5G5/1 to 10Y4/2) moderately bioturbated CLAYSTONE; homogeneous.
	Barren	Barren	Barren				● Φ=55.4 γ=1.87	● 28.4 %	2						
							● Φ=60.1 γ=1.76	● 1.0 %	3 4 5						
							● Φ=54.8 γ=1.86	● 7.1 %	6 7 CC						

SITE 671 HOLE B CORE 49 X CORED INTERVAL 5375.9-5385.4 mbsl; 444.2-453.7 mbsf

TIME-ROCK UNIT	BIOSTRAT. ZONE/ FOSSIL CHARACTER: FORAMINIFERS	NANNOFOSSILS	RADIOLARIANS	DIATOMS	PALEOMAGNETICS	PHYS. PROPERTIES	CHEMISTRY	SECTION	METERS	GRAPHIC LITHOLOGY	DRILLING DISTURB.	SED. STRUCTURES	SAMPLES
?	Barren	Barren	Barren			●φ=58.1 γ=1.87 ●φ=55.5 γ=1.85 ●φ=53.4 γ=1.87	●0.2 % ●0.2 % ●0.2 %	1 2 3 4 CC	0.5 1.0				IW *
	B	B	B										

LITHOLOGIC DESCRIPTION

CLAYSTONE

Greenish gray (10Y5/2), moderately bioturbated CLAYSTONE; with local brownish (10YR5/6 to 10YR4/4) diffuse intercalations in Sections 2 and 3.

SMEAR SLIDE SUMMARY (%):

	3, 88
	D
TEXTURE:	
Silt	2
Clay	98
COMPOSITION:	
Feldspar	1
Clay	98
Accessory minerals	
Opaques	Tr
Nannofossils	Tr

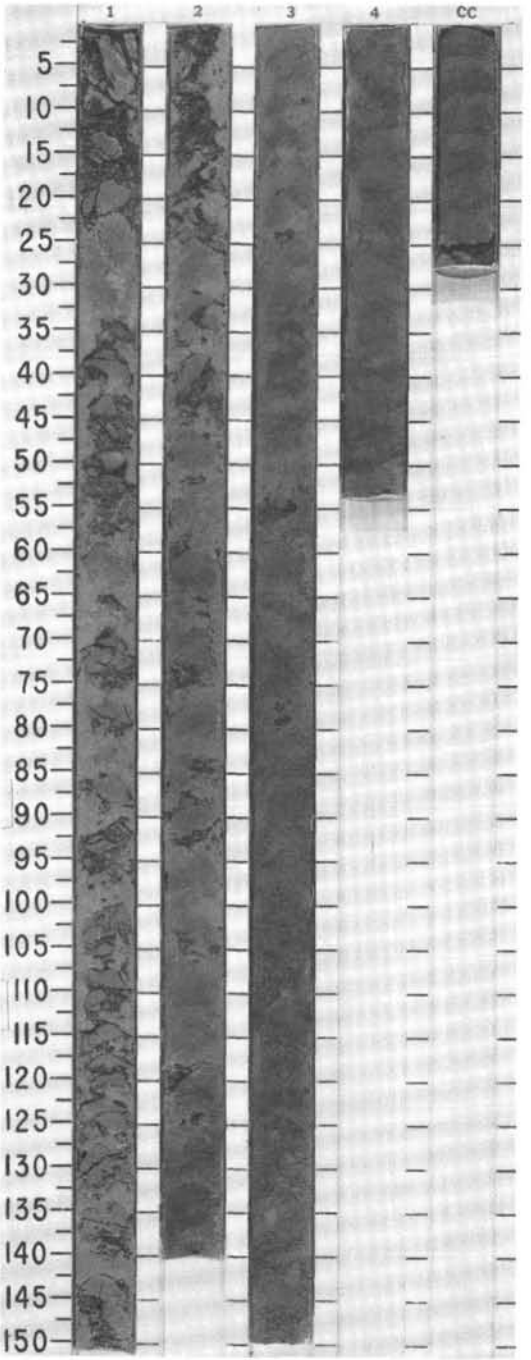

SITE 671 HOLE B CORE 50 X CORED INTERVAL 5385.4-5394.9 mbsl; 453.7-463.2 mbsf

TIME-ROCK UNIT	BIOSTRAT. ZONE/ FOSSIL CHARACTER: FORAMINIFERS	NANNOFOSSILS	RADIOLARIANS	DIATOMS	PALEOMAGNETICS	PHYS. PROPERTIES	CHEMISTRY	SECTION	METERS	GRAPHIC LITHOLOGY	DRILLING DISTURB.	SED. STRUCTURES	SAMPLES
?	Barren	Barren	Barren			●φ=52.1 γ=1.91	●0.3 %	1	0.5, 1.0				
								2					
								3					
						●φ=53.3 γ=1.90	●0.3 %	4					*
								5					OG
						●φ=57.0 γ=1.82	●0.3 %	6		VOID			
	B	B	B					7					*

LITHOLOGIC DESCRIPTION

CLAYSTONE

Greenish to brownish gray CLAYSTONE (5Y4/3 to 2.5Y4/3), moderately bioturbated; with minor scattered silt-sized ash debris (visible in smear slide), and an ashy layer at bottom of Section 7.

SMEAR SLIDE SUMMARY (%):

	4, 72 D	7, 35 M
TEXTURE:		
Sand	—	Tr
Silt	5	5
Clay	95	95
COMPOSITION:		
Feldspar	—	Tr
Clay	85	90
Volcanic glass	15	2
Accessory minerals		
Opaques	—	8

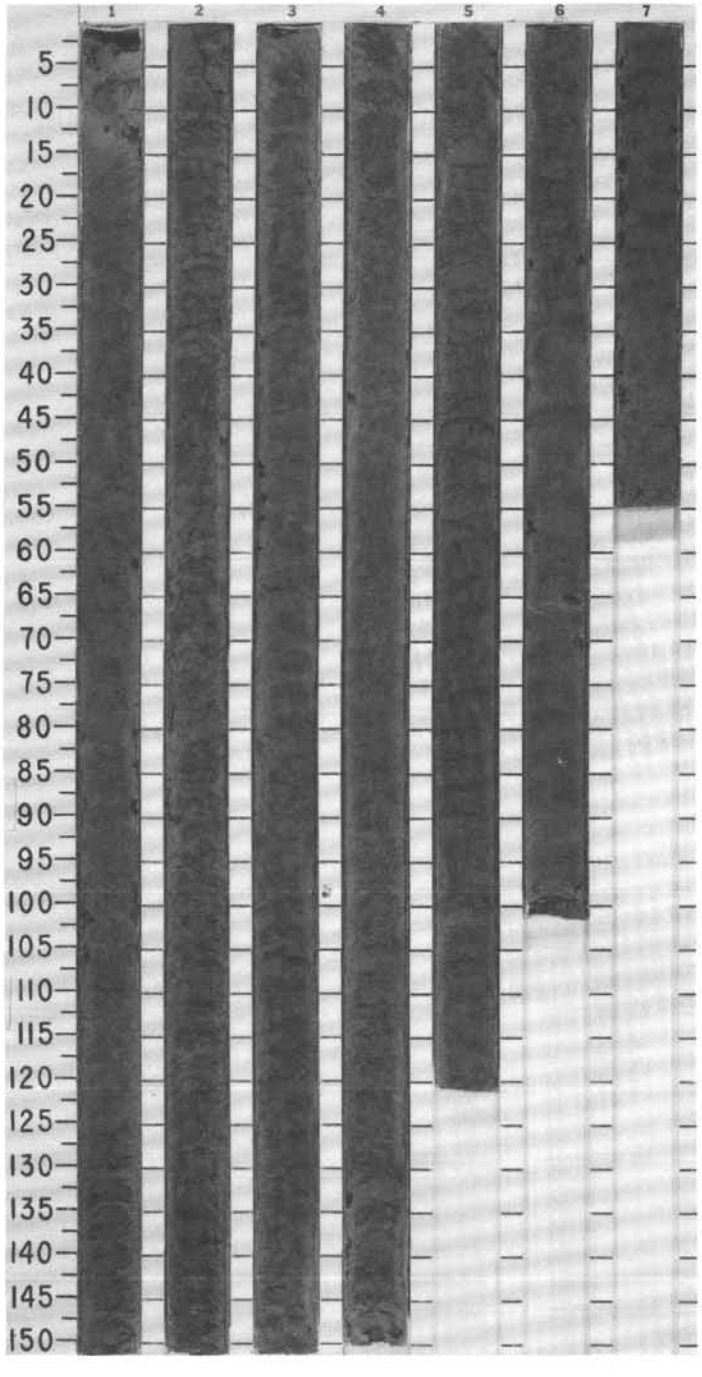

SITE 671 HOLE B CORE 51 X CORED INTERVAL 5394.9-5404.4 mbsl; 463.2-472.7 mbsf

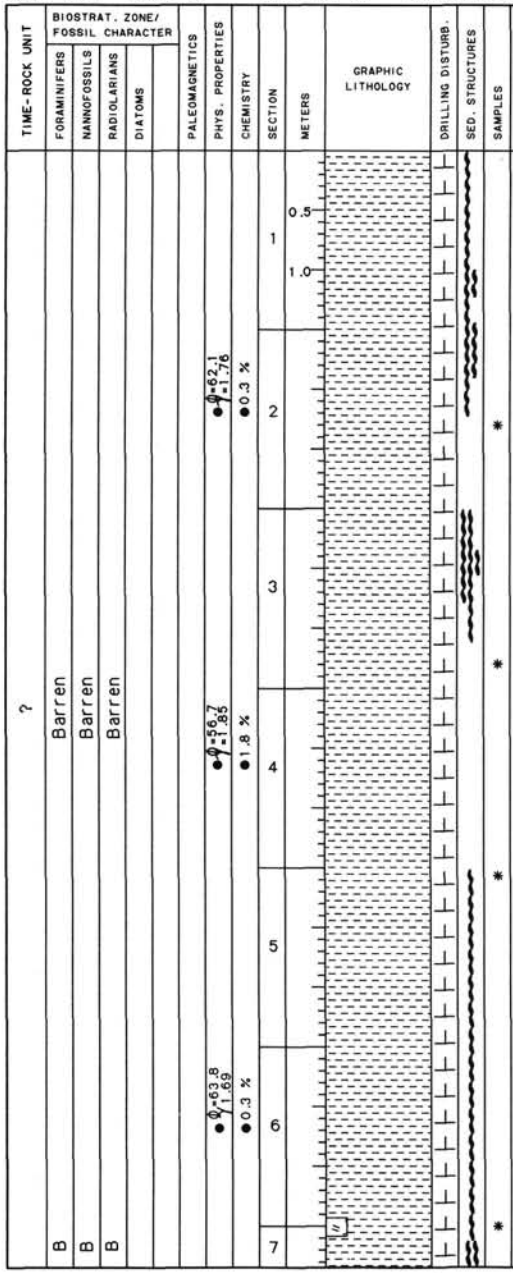

LITHOLOGIC DESCRIPTION

CLAYSTONE

Greenish gray CLAYSTONE (10Y4/2), moderately bioturbated; Section 3 shows a darker interval (10Y4/1) with gradational contacts (top and bottom) and intensively bioturbated; this interval contains a small amount of opaque minerals and ash.

SMEAR SLIDE SUMMARY (%):

	2, 82 D	3, 139 D	5, 5 M	7, 2 M
TEXTURE:				
Silt	2	1	5	5
Clay	98	99	95	95
COMPOSITION:				
Quartz	Tr	—	Tr	3
Feldspar	1	1	Tr	2
Clay	98	99	96	90
Volcanic glass	—	Tr	Tr	—
Accessory minerals				
Opaques	Tr	Tr	3	3
Hornblende	—	—	Tr	Tr
Chloritized Fe–Mn min.	Tr	—	—	2
Nannofossils	—	Tr	—	—
Bioclasts	—	—	Tr	—

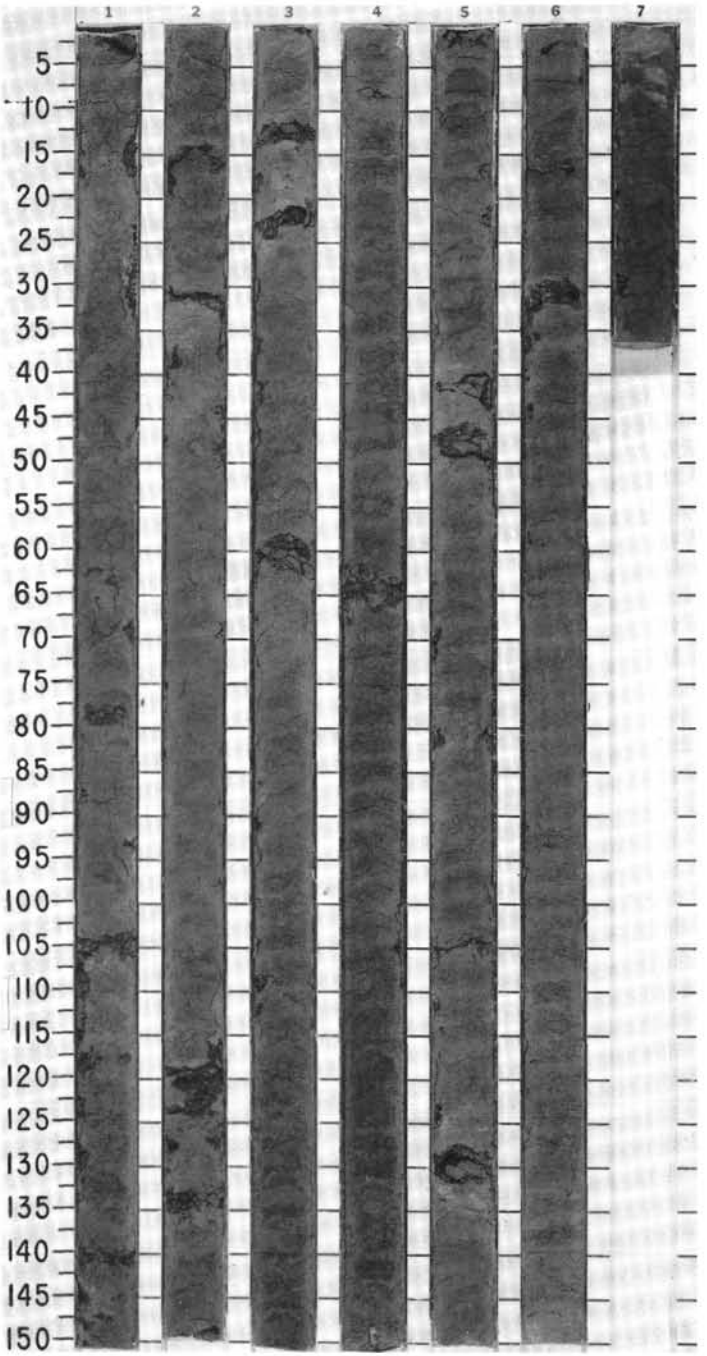

SITE 671 HOLE B CORE 52 X CORED INTERVAL 5404.4-5413.9 mbsl; 472.7-482.2 mbsf

TIME-ROCK UNIT	BIOSTRAT. ZONE/ FOSSIL CHARACTER: FORAMINIFERS	NANNOFOSSILS	RADIOLARIANS	DIATOMS	PALEOMAGNETICS	PHYS. PROPERTIES	CHEMISTRY	SECTION	METERS	GRAPHIC LITHOLOGY	DRILLING DISTURB.	SED. STRUCTURES	SAMPLES
UPPER MIOCENE	Barren	CN9a	Barren			●φ=65.8 ●φ=58.3 γ=1.64 γ=1.82	●0.7 % ●0.3 %	1	0.5 1.0				
								2					
								3					IW
						●φ=62.1 γ=1.72	●1.5 %	4					
	B		B					CC					*

LITHOLOGIC DESCRIPTION

CLAYSTONE and MUDSTONE

Brownish to greenish dark gray CLAYSTONE (2.5Y4/4 to 5Y4/3, or 10Y4/2) with discrete bioturbation; locally reaching the MUDSTONE class with 10–12% silt-sized debris (mostly opaque and altered ferromagnesian minerals).

SMEAR SLIDE SUMMARY (%):

	CC
	D
TEXTURE:	
Silt	10
Clay	90
COMPOSITION:	
Feldspar	2
Clay	95
Volcanic glass	1
Accessory minerals	
Opaques	1
Rutile?	Tr
Nannofossils	—
Bioclasts	Tr

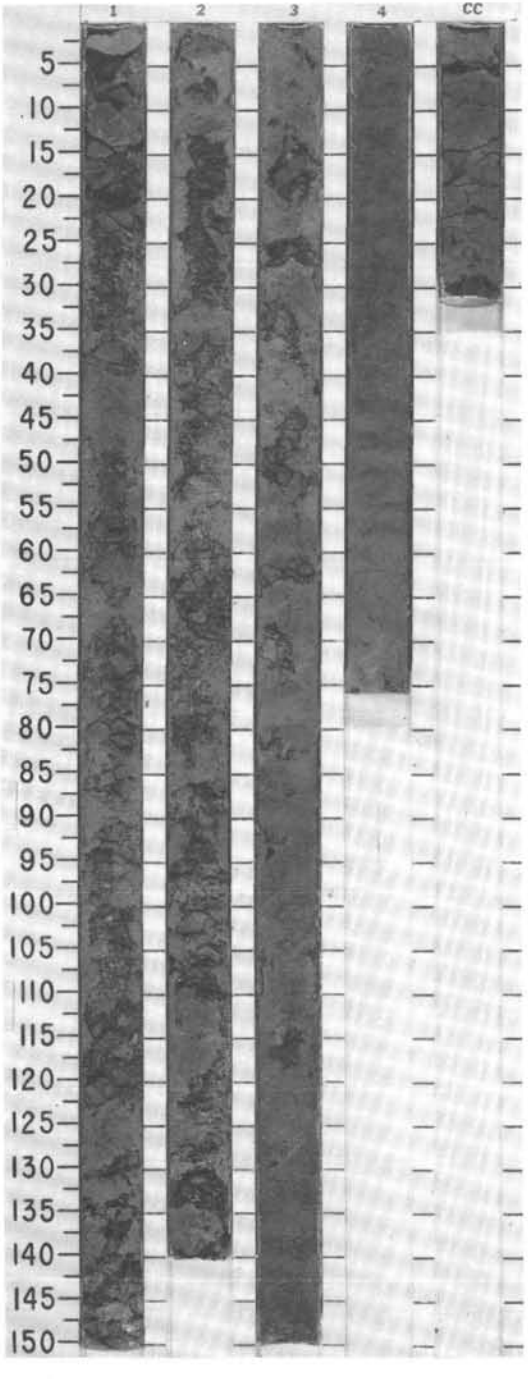

SITE 671 HOLE B CORE 53 X CORED INTERVAL 5413.9-5423.4 mbsl; 482.2-491.7 mbsf

TIME-ROCK UNIT	BIOSTRAT. ZONE/ FOSSIL CHARACTER: FORAMINIFERS	NANNOFOSSILS	RADIOLARIANS	DIATOMS	PALEOMAGNETICS	PHYS. PROPERTIES	CHEMISTRY	SECTION	METERS	GRAPHIC LITHOLOGY	DRILLING DISTURB.	SED. STRUCTURES	SAMPLES
?	Barren	Barren	Barren					1	0.5		X X X		* *

LITHOLOGIC DESCRIPTION

CLAYSTONE

Brownish to greenish CLAYSTONE (2.5Y4/4 to 5Y4/3, and 2.5Y5/3), with minor bioturbation and locally increased opaque content.

SMEAR SLIDE SUMMARY (%):

	1, 9 D	1, 57 D
TEXTURE:		
Silt	2	5
Clay	98	95
COMPOSITION:		
Feldspar	1	1
Clay	98	92
Volcanic glass	—	5
Accessory minerals		
Opaques (pyrite)	1	2

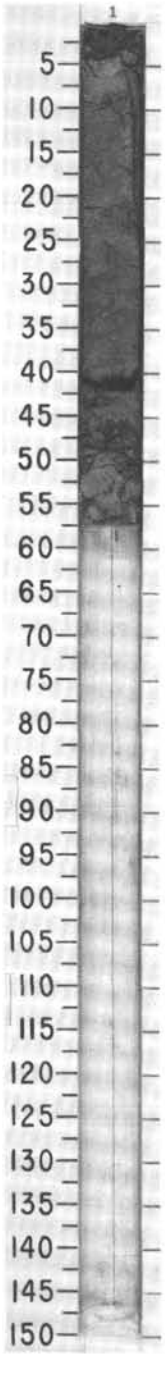

SITE 671 HOLE B CORE 54 X CORED INTERVAL 5423.4-5432.9 mbsl; 491.7-501.2 mbsf

TIME-ROCK UNIT	BIOSTRAT. ZONE/ FOSSIL CHARACTER: FORAMINIFERS	NANNOFOSSILS	RADIOLARIANS	DIATOMS	PALEOMAGNETICS	PHYS. PROPERTIES	CHEMISTRY	SECTION	METERS	GRAPHIC LITHOLOGY	DRILLING DISTURB.	SED. STRUCTURES	SAMPLES
?	B Barren	B Barren	vR/vP indet.			ϕ=61.4 ρ=1.73	0.3 %	6					
						ϕ=57.8 ρ=1.83	0.4 %	5					OG
						ϕ=59.9 ρ=1.81	0.5 %	4					*
								3					*
								2					*
								1	0.5				*
									1.0				

LITHOLOGIC DESCRIPTION

CLAYSTONE

Greenish to dark greenish CLAYSTONE (2.5Y5/3 to 10Y5/3); strongly bioturbated in Section 4 (top) and Section 6 (bottom).

SMEAR SLIDE SUMMARY (%):

	1, 115 D	1, 132 D	3, 66 M
TEXTURE:			
Silt	10	3	3
Clay	90	97	97
COMPOSITION:			
Feldspar	Tr	2	Tr
Clay	93	98	97
Volcanic glass	2	—	3
Calcite/dolomite	—	Tr	—
Accessory minerals			
Pyrite	1	—	—
Fe–Mn minerals	2	—	—
Fe oxides	—	Tr	Tr
Bioclasts	2	—	—

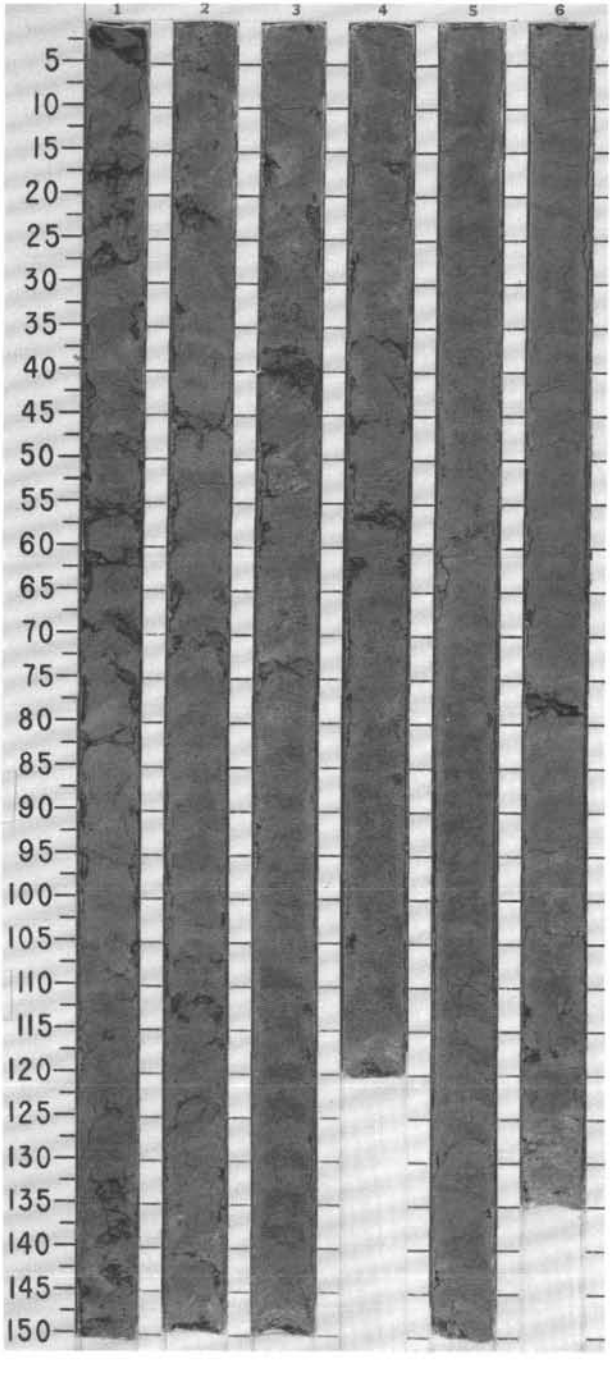

SITE 671 HOLE B CORE 55 X CORED INTERVAL 5432.9-5442.2 mbsl; 501.2-510.7 mbsf

TIME-ROCK UNIT	BIOSTRAT. ZONE/FOSSIL CHARACTER: FORAMINIFERS	NANNOFOSSILS	RADIOLARIANS	DIATOMS	PALEOMAGNETICS	PHYS. PROPERTIES	CHEMISTRY	SECTION	METERS	GRAPHIC LITHOLOGY	DRILLING DISTURB.	SED. STRUCTURES	SAMPLES
?	B Barren	B Barren	vR/vP indet.			ϕ=56.2 ρ=1.81	0.3 %	1	0.5				
									1.0				
						ϕ=52.0 ρ=1.91	0.2 %	2				*	
								3				*	
								4					
								5					IW
						ϕ=50.9 ρ=1.92	0.2 %	6					
								7					

LITHOLOGIC DESCRIPTION

CLAYSTONE

Yellowish to brownish gray (10YR5/6 to 10YR5/5) CLAYSTONE, moderately bioturbated.

Minor lithology: dark gray ashy layers (10YR3/1) in Sections 1 and 2, with minor amount of sand-sized volcanic debris.

SMEAR SLIDE SUMMARY (%):

	2, 80 D	2, 101 M	2, 101 M	5, 137 D
TEXTURE:				
Sand	—	15	15	—
Silt	—	25	30	10
Clay	100	60	55	90
COMPOSITION:				
Feldspar	—	2	—	Tr
Clay	15	60	50	90
Volcanic glass	—	38	50	10
Accessory minerals				
Zeolite	85	—	—	—

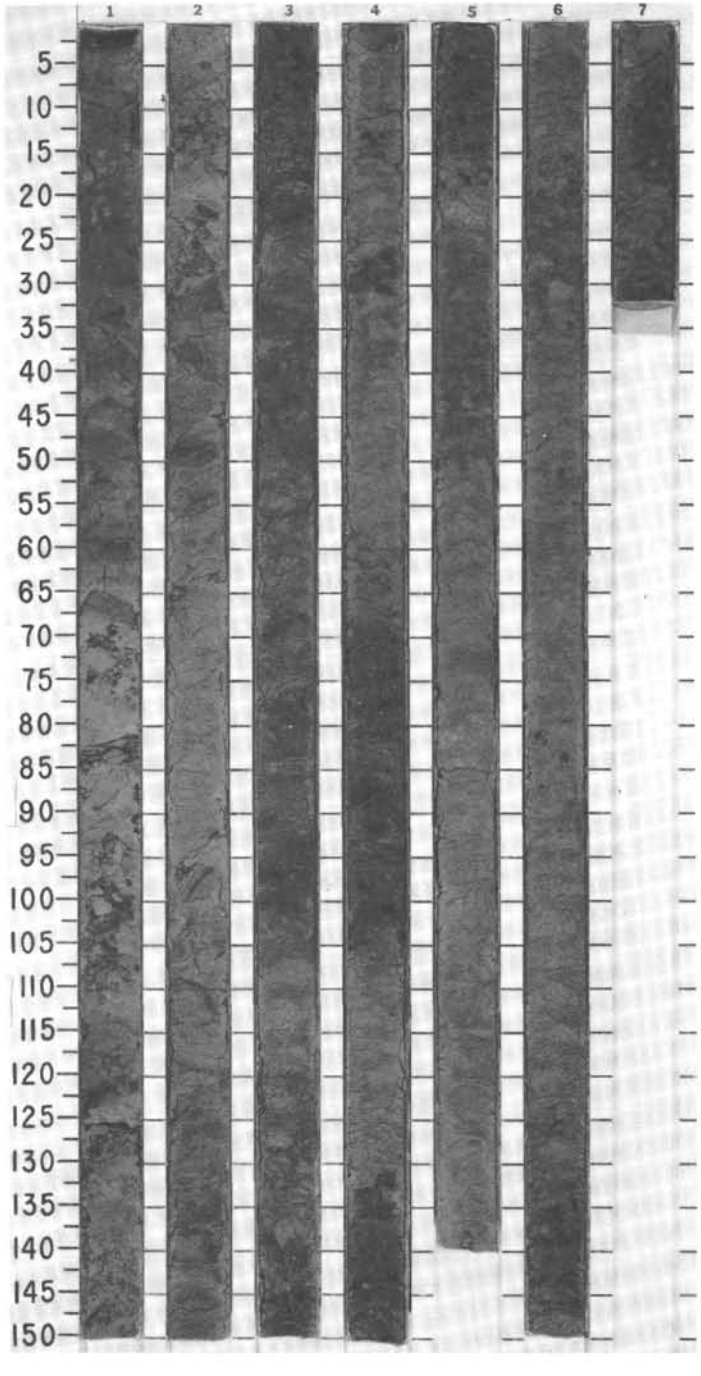

SITE 671 HOLE B CORE 56 X CORED INTERVAL 5442.2-5451.9 mbsl; 510.7-520.2 mbsf

TIME-ROCK UNIT	BIOSTRAT. ZONE/ FOSSIL CHARACTER: FORAMINIFERS	NANNOFOSSILS	RADIOLARIANS	DIATOMS	PALEOMAGNETICS	PHYS. PROPERTIES	CHEMISTRY	SECTION	METERS	GRAPHIC LITHOLOGY	DRILLING DISTURB.	SED. STRUCTURES	SAMPLES
?	B	B	C/vP			ϕ=55.9 ρ=1.87	0.3 %	1	0.5				
	Barren	Barren	indet.						1.0				
						ϕ=47.7 ρ=2.02	0.2 %	2					
								3					*
								4					
						ϕ=50.3 ρ=2.00	0.2 %	5					OG
								6					
								7					
								CC					

LITHOLOGIC DESCRIPTION

CLAYSTONE

Homogeneous (strongly scaly) dark greenish gray CLAYSTONE (5Y6/3 to 2.5Y5/3), with minor amount of silt-sized quartz grains; several whitish, mm-sized concretions and veinlets of clinoptilolite occur along scaly surfaces.

SMEAR SLIDE SUMMARY (%):

	3, 55 D
TEXTURE:	
Silt	5
Clay	95
COMPOSITION:	
Quartz	5
Clay	95

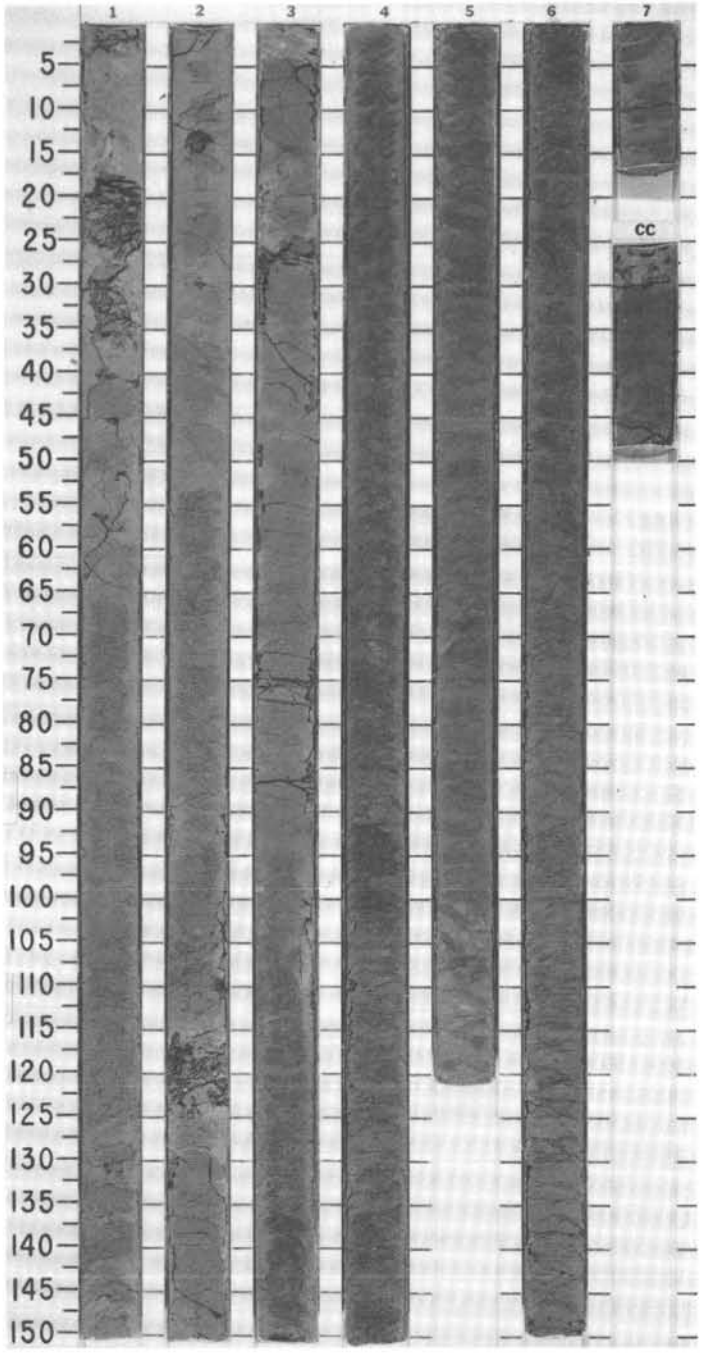

SITE 671 HOLE B CORE 57 X CORED INTERVAL 5451.9-5461.4 mbsl; 520.2-529.7 mbsf

TIME-ROCK UNIT	BIOSTRAT. ZONE/ FOSSIL CHARACTER: FORAMINIFERS	NANNOFOSSILS	RADIOLARIANS	DIATOMS	PALEOMAGNETICS	PHYS. PROPERTIES	CHEMISTRY	SECTION	METERS	GRAPHIC LITHOLOGY	DRILLING DISTURB.	SED. STRUCTURES	SAMPLES	LITHOLOGIC DESCRIPTION
?	Barren	Barren	indent.					CC			X			CLAYSTONE Major lithology: Claystone, olive (5Y 5/2), featureless except for 1–2 mm spherical white concretions.
	B	B	C/vP											

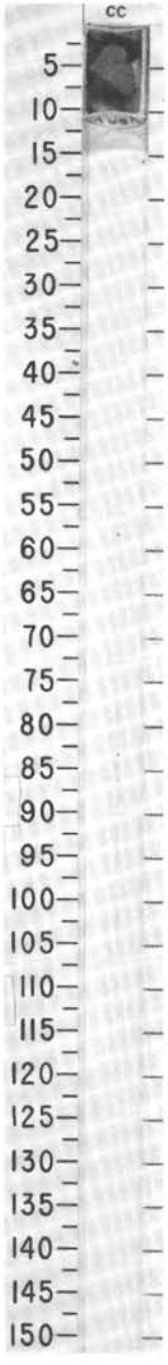

SITE 671 HOLE B CORE 58 X CORED INTERVAL 5461.4-5470.9 mbsl; 529.7-539.2 mbsf

TIME-ROCK UNIT: UPPER OLIGOCENE

BIOSTRAT. ZONE/FOSSIL CHARACTER: FORAMINIFERS: B; Barren; CP19. NANNOFOSSILS: B; Barren. RADIOLARIANS. DIATOMS.

PALEOMAGNETICS

PHYS. PROPERTIES: ρ=51.5, γ=1.89; ρ=53.0, γ=1.89; ρ=57.3, γ=1.82

CHEMISTRY: 0.2 %; 0.3 %; 0.3 %

SECTION: 1, 2, 3, 4, 5, 6, CC

METERS: 0.5; 1.0

GRAPHIC LITHOLOGY

DRILLING DISTURB.

SED. STRUCTURES

SAMPLES: IW

LITHOLOGIC DESCRIPTION

CLAYSTONE and MUDSTONE

Varicolored green (5G6/2) and dark olive-green-gray (10Y3/1) CLAYSTONE, with intervals of dark olive-green-gray (10Y3/1) MUDSTONE in Section 3, 140–150 cm, and Section 4, 0–23, 103–112, and 140–150 cm. Entire core slightly to moderately bioturbated. mm-thick planar laminations occur locally throughout core.

Minor lithology: feldspar-bearing sand, gray (N7). Cross-laminated base. Possible normal grading in upper portion.

SMEAR SLIDE SUMMARY (%):

	1, 70 D	2, 72 M	4, 12 D	4, 54 D	6, 14 M	CC, 30 M	CC, 38 M
TEXTURE:							
Sand	—	—	—	Tr	—	95	—
Silt	Tr	98	15	5	100	2	40
Clay	100	2	85	95	—	3	60
COMPOSITION:							
Quartz	—	60	Tr	25	—	1	—
Feldspar	Tr	37	10	—	96	90	—
Clay	100	—	85	72	1	2	50
Volcanic glass	—	—	—	—	1	—	—
Calcite/dolomite	—	—	—	—	—	—	40
Accessory minerals							
Glauconite	—	—	—	—	—	1	—
Opaques	Tr	3	3	—	1	4	—
Fe-Mn minerals	Tr	Tr	2	—	1	Tr	—
Microcline	—	Tr	—	—	—	—	—
Foraminifers	—	—	—	3	—	Tr	—
Nannofossils	—	—	—	—	Tr	1	10
Bioclasts	—	—	—	—	—	1	—

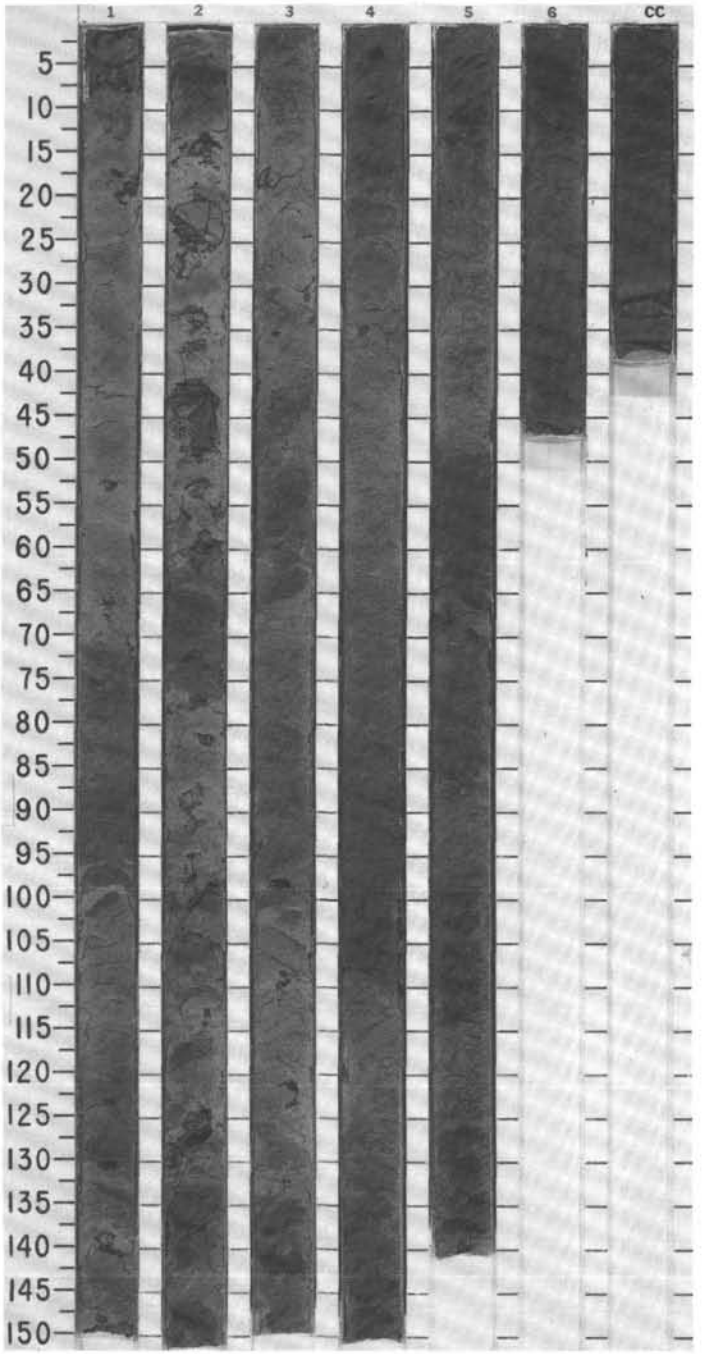

SITE 671 HOLE B CORE 59 X CORED INTERVAL 5470.9-5480.4 mbsl; 539.2-548.7 mbsf

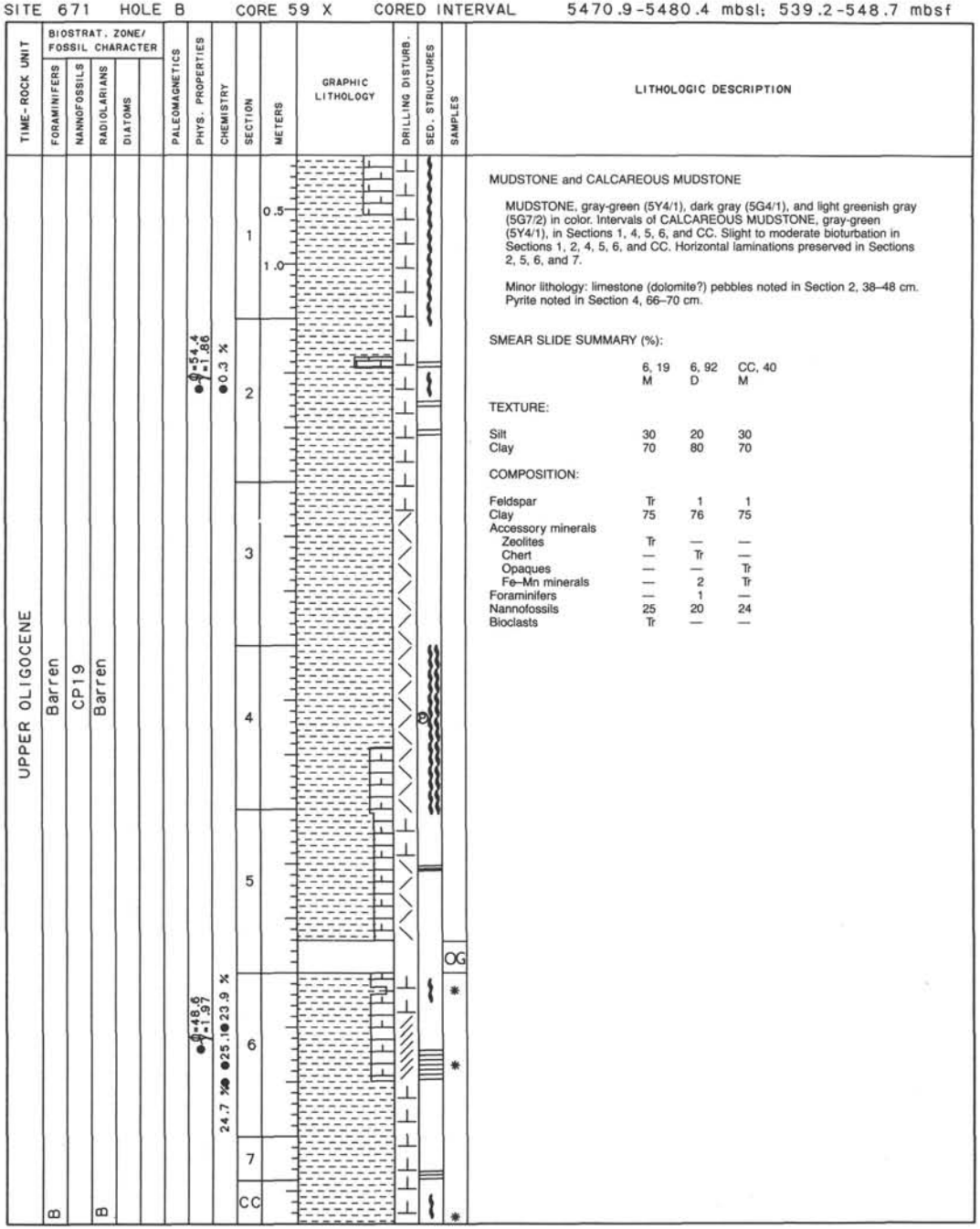

MUDSTONE and CALCAREOUS MUDSTONE

MUDSTONE, gray-green (5Y4/1), dark gray (5G4/1), and light greenish gray (5G7/2) in color. Intervals of CALCAREOUS MUDSTONE, gray-green (5Y4/1), in Sections 1, 4, 5, 6, and CC. Slight to moderate bioturbation in Sections 1, 2, 4, 5, 6, and CC. Horizontal laminations preserved in Sections 2, 5, 6, and 7.

Minor lithology: limestone (dolomite?) pebbles noted in Section 2, 38–48 cm. Pyrite noted in Section 4, 66–70 cm.

SMEAR SLIDE SUMMARY (%):

	6, 19 M	6, 92 D	CC, 40 M
TEXTURE:			
Silt	30	20	30
Clay	70	80	70
COMPOSITION:			
Feldspar	Tr	1	1
Clay	75	76	75
Accessory minerals			
Zeolites	Tr	—	—
Chert	—	Tr	—
Opaques	—	—	Tr
Fe–Mn minerals	—	2	Tr
Foraminifers	—	1	—
Nannofossils	25	20	24
Bioclasts	Tr	—	—

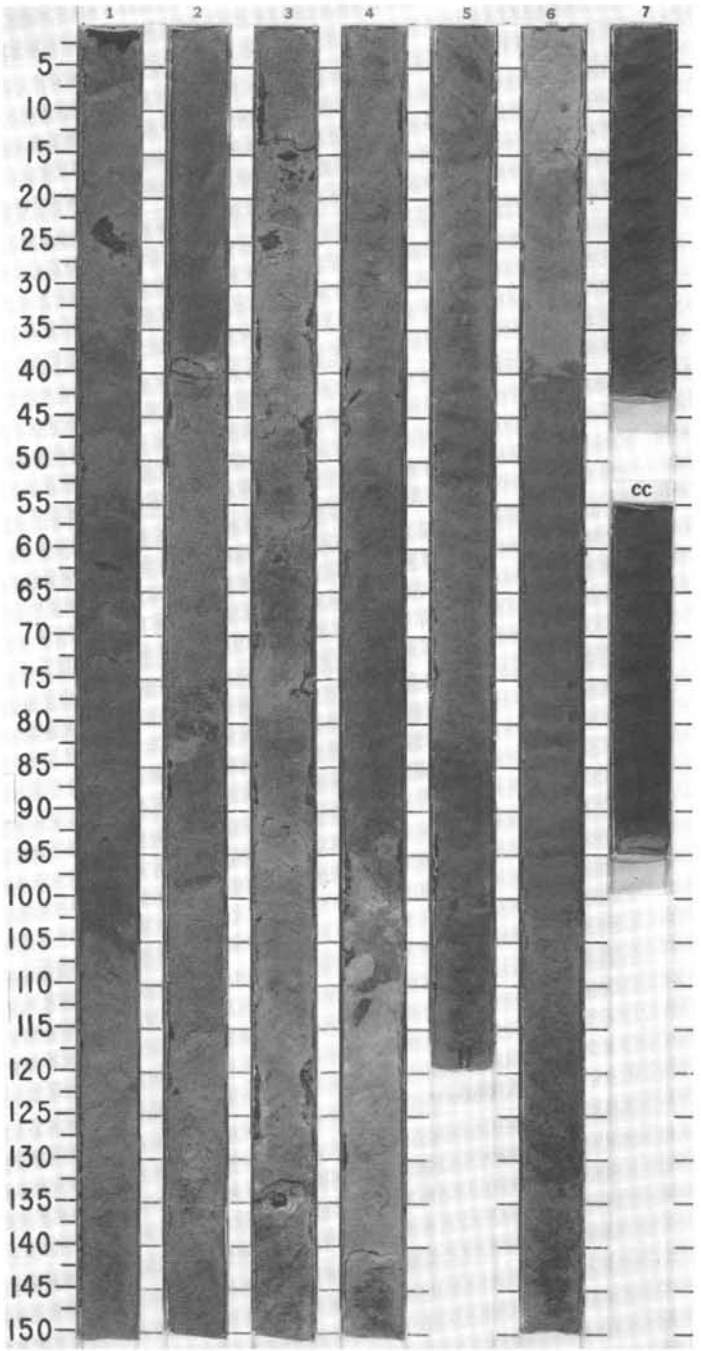

SITE 671 HOLE B CORE 60 X CORED INTERVAL 5480.4-5489.9 mbsl; 548.7-558.2 mbsf

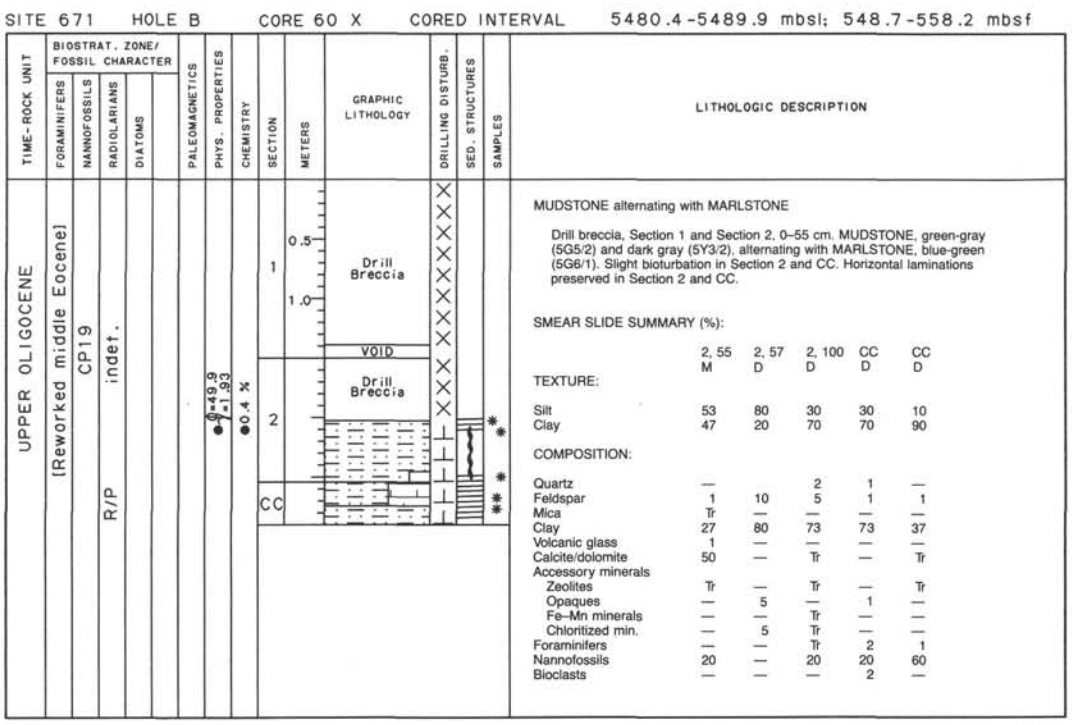

LITHOLOGIC DESCRIPTION

MUDSTONE alternating with MARLSTONE

Drill breccia, Section 1 and Section 2, 0–55 cm. MUDSTONE, green-gray (5G5/2) and dark gray (5Y3/2), alternating with MARLSTONE, blue-green (5G6/1). Slight bioturbation in Section 2 and CC. Horizontal laminations preserved in Section 2 and CC.

SMEAR SLIDE SUMMARY (%):

	2, 55 M	2, 57 D	2, 100 D	CC D	CC D
TEXTURE:					
Silt	53	80	30	30	10
Clay	47	20	70	70	90
COMPOSITION:					
Quartz	—		2	1	—
Feldspar	1	10	5	1	1
Mica	Tr	—	—	—	—
Clay	27	80	73	73	37
Volcanic glass	1	—	—	—	—
Calcite/dolomite	50	—	Tr	—	Tr
Accessory minerals					
Zeolites	Tr	—	Tr	—	Tr
Opaques	—	5	—	1	—
Fe–Mn minerals	—	—	Tr	—	—
Chloritized min.	—	5	Tr	—	—
Foraminifers	—	—	Tr	2	1
Nannofossils	20	—	20	20	60
Bioclasts	—	—	—	2	—

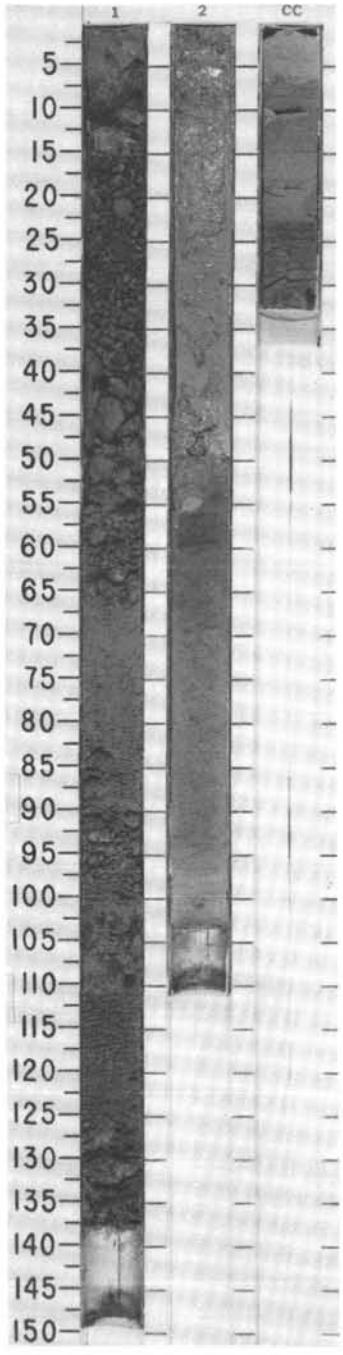

SITE 671 HOLE B CORE 61 X CORED INTERVAL 5489.9-5499.4 mbsl; 558.2-567.7 mbsf

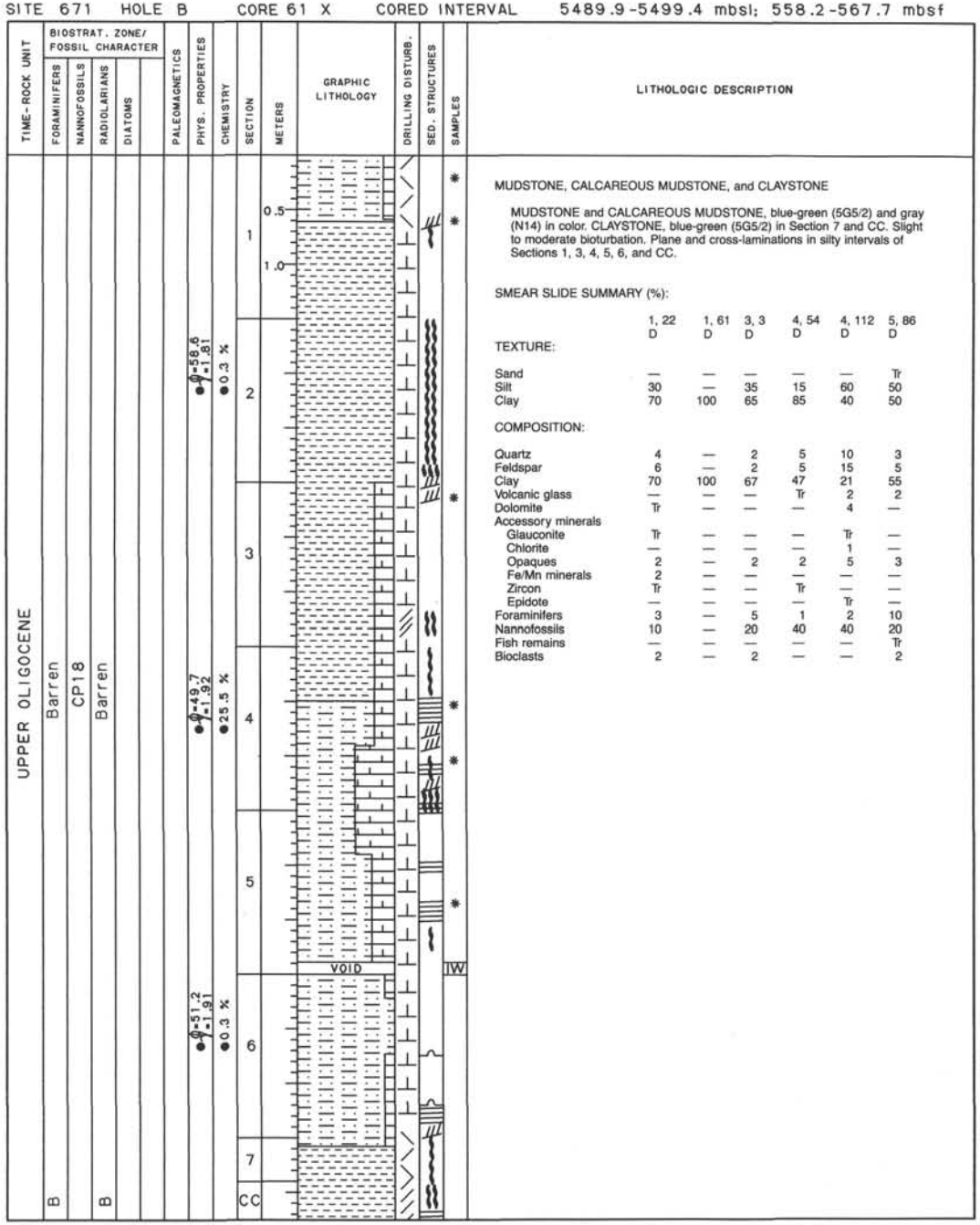

LITHOLOGIC DESCRIPTION

MUDSTONE, CALCAREOUS MUDSTONE, and CLAYSTONE

MUDSTONE and CALCAREOUS MUDSTONE, blue-green (5G5/2) and gray (N14) in color. CLAYSTONE, blue-green (5G5/2) in Section 7 and CC. Slight to moderate bioturbation. Plane and cross-laminations in silty intervals of Sections 1, 3, 4, 5, 6, and CC.

SMEAR SLIDE SUMMARY (%):

	1, 22 D	1, 61 D	3, 3 D	4, 54 D	4, 112 D	5, 86 D
TEXTURE:						
Sand	—	—	—	—	—	Tr
Silt	30	—	35	15	60	50
Clay	70	100	65	85	40	50
COMPOSITION:						
Quartz	4	—	2	5	10	3
Feldspar	6	—	2	5	15	5
Clay	70	100	67	47	21	55
Volcanic glass	—	—	—	Tr	2	2
Dolomite	Tr	—	—	—	4	—
Accessory minerals						
Glauconite	Tr	—	—	—	Tr	—
Chlorite	—	—	—	—	1	—
Opaques	2	—	2	2	5	3
Fe/Mn minerals	2	—	—	—	—	—
Zircon	Tr	—	—	Tr	—	—
Epidote	—	—	—	—	Tr	—
Foraminifers	3	—	5	1	2	10
Nannofossils	10	—	20	40	40	20
Fish remains	—	—	—	—	—	Tr
Bioclasts	2	—	2	—	—	2

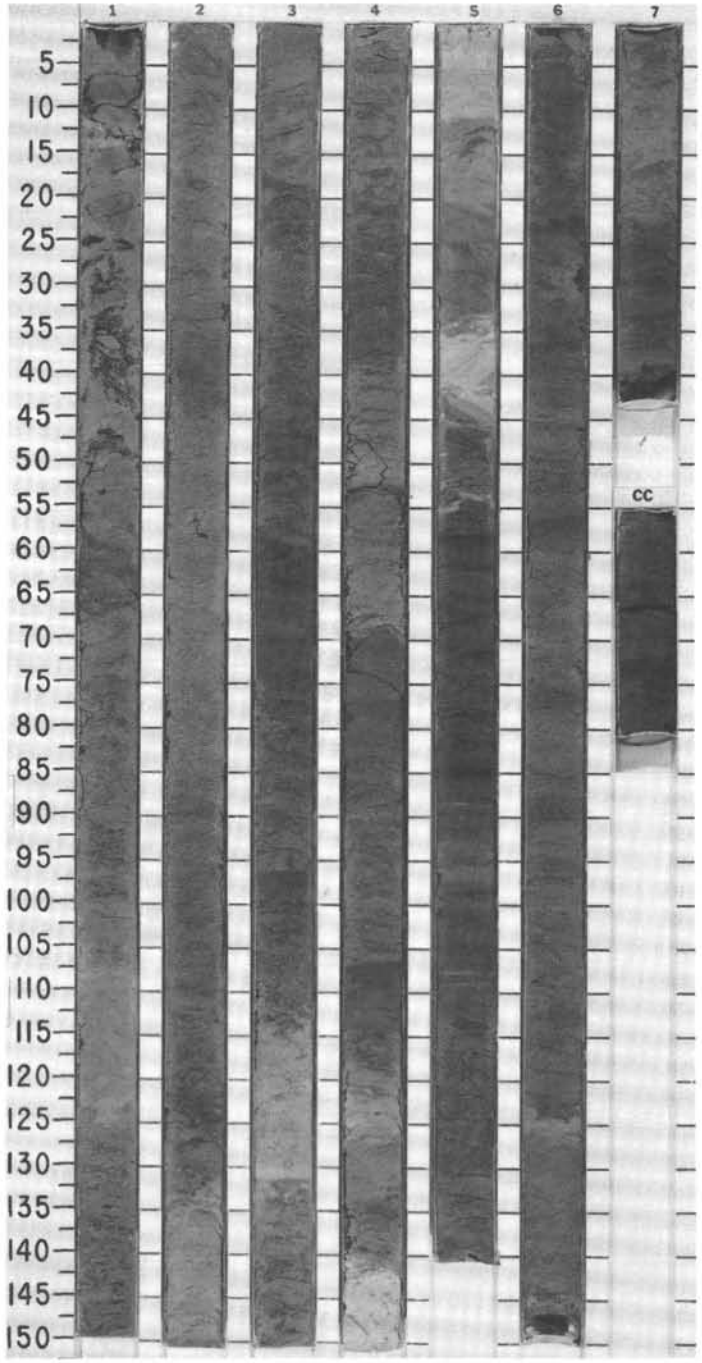

SITE 671 HOLE B CORE 62 X CORED INTERVAL 5499.4-5508.9 mbsl; 567.7-577.2 mbsf

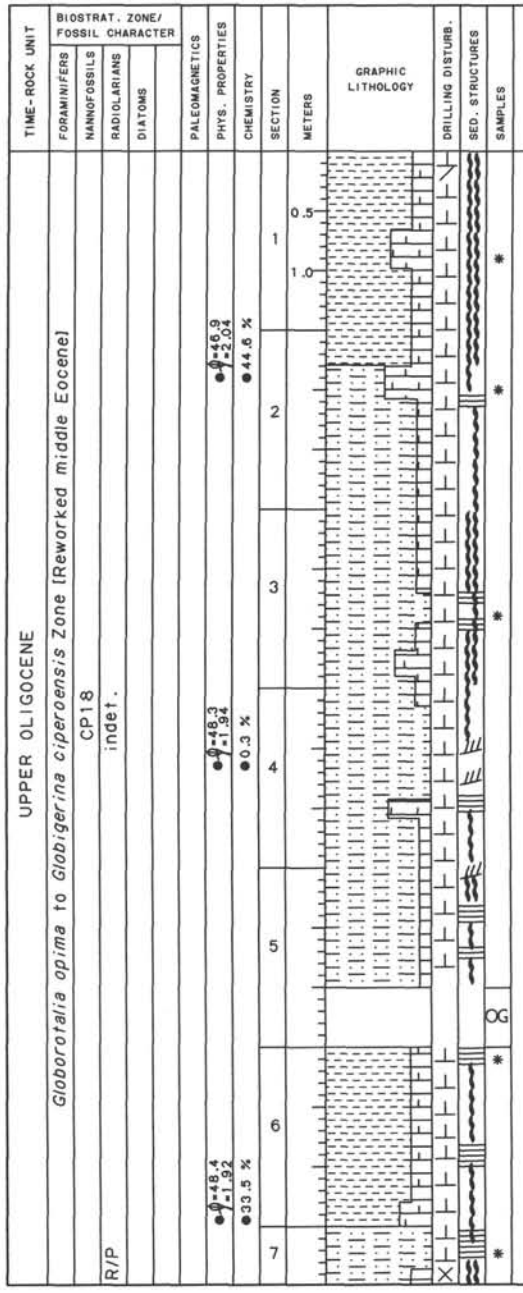

LITHOLOGIC DESCRIPTION

MUDSTONE, CALCAREOUS MUDSTONE, and MARLSTONE

MUDSTONE and CALCAREOUS MUDSTONE, gray-green (5G4/1). Intervals of MARLSTONE, pale gray-green (5GY6/1), in Sections 1, 2, 3, 4, and 6. Moderate bioturbation in Sections 1, 2, 3, and 7. Slight bioturbation in Sections 4, 5, and 6. Plane and cross-laminations and microripples in Sections 2, 3, 4, 5, 6, and 7.

SMEAR SLIDE SUMMARY (%):

	1, 89 D	2, 50 D	3, 87 M	6, 18 D	7, 22 M
TEXTURE:					
Sand	—	—	—	—	10
Silt	—	15	50	10	10
Clay	100	85	50	90	80
COMPOSITION:					
Quartz	Tr	10	50	5	20
Feldspar	Tr	Tr	—	Tr	—
Clay	60	50	50	75	50
Accessory minerals					
Opaques	Tr	Tr	Tr	Tr	20
Spinel?	—	—	—	—	10
Foraminifers	—	10	—	5	—
Nannofossils	40	30	Tr	15	—
Diatoms	—	—	—	Tr	—

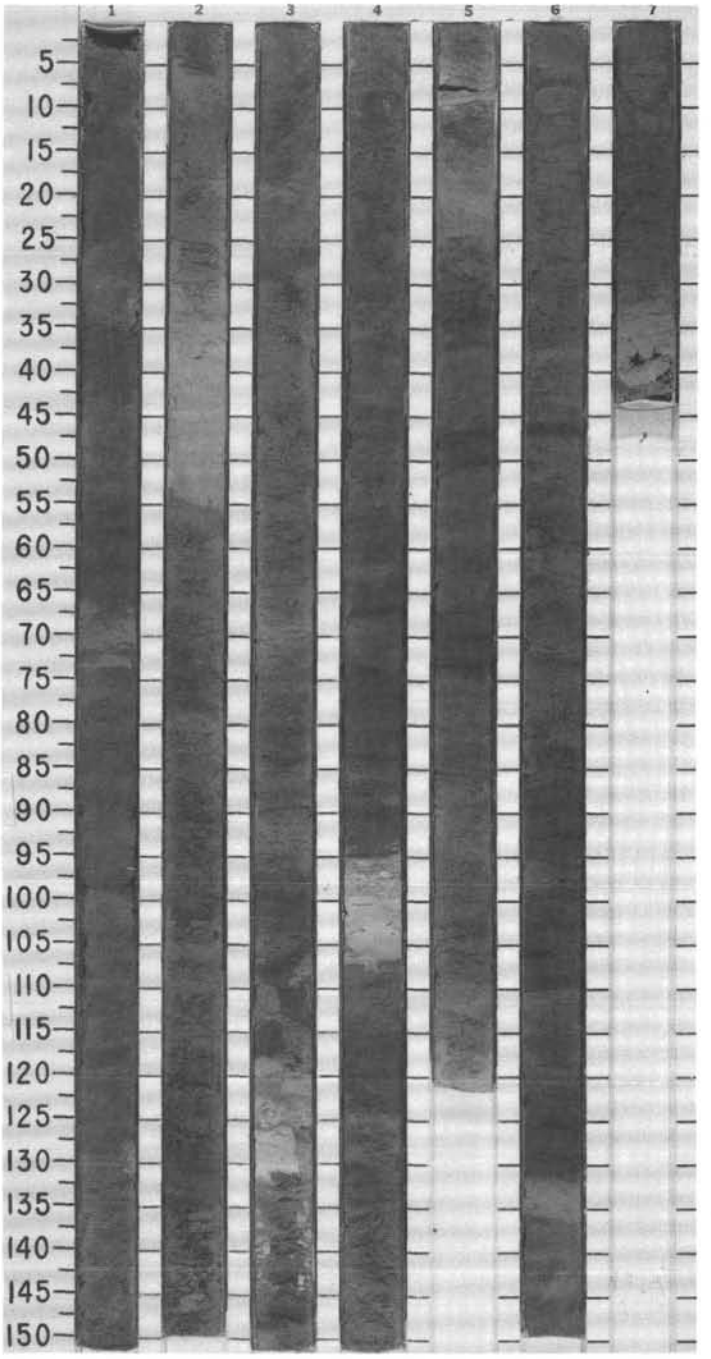

SITE 671 HOLE B CORE 63 X CORED INTERVAL 5508.9-5518.4 mbsl; 577.2-586.7 mbsf

TIME-ROCK UNIT	BIOSTRAT. ZONE/FOSSIL CHARACTER: FORAMINIFERS	NANNOFOSSILS	RADIOLARIANS	DIATOMS	PALEOMAGNETICS	PHYS. PROPERTIES	CHEMISTRY	SECTION	METERS	GRAPHIC LITHOLOGY	DRILLING DISTURB.	SED. STRUCTURES	SAMPLES
UPPER OLIGOCENE	B Barren	CP18	B Barren			ϕ=51.1 ρ=1.89 ϕ=56.2 ρ=1.85 ϕ=51.5 ρ=1.93	0.3 % 0.2 % 0.2 %	1 2 3 4 5 6 7	0.5 1.0	VOID			* * * IW

LITHOLOGIC DESCRIPTION

MUDSTONE

MUDSTONE, gray-green (5G5/1 and 5GY4/1), slightly bioturbated throughout. Plane and cross-laminations preserved in Sections 1, 3, 4, and 7. Apparent slump structures in Sections 1 and 3.

SMEAR SLIDE SUMMARY (%):

	1, 50 D	4, 87 D	5, 78 D
TEXTURE:			
Silt	10	20	15
Clay	90	80	85
COMPOSITION:			
Quartz	5	20	10
Feldspar	5	10	10
Clay	75	68	72
Volcanic glass	—	2	—
Foraminifers	—	—	Tr
Nannofossils	15	—	8

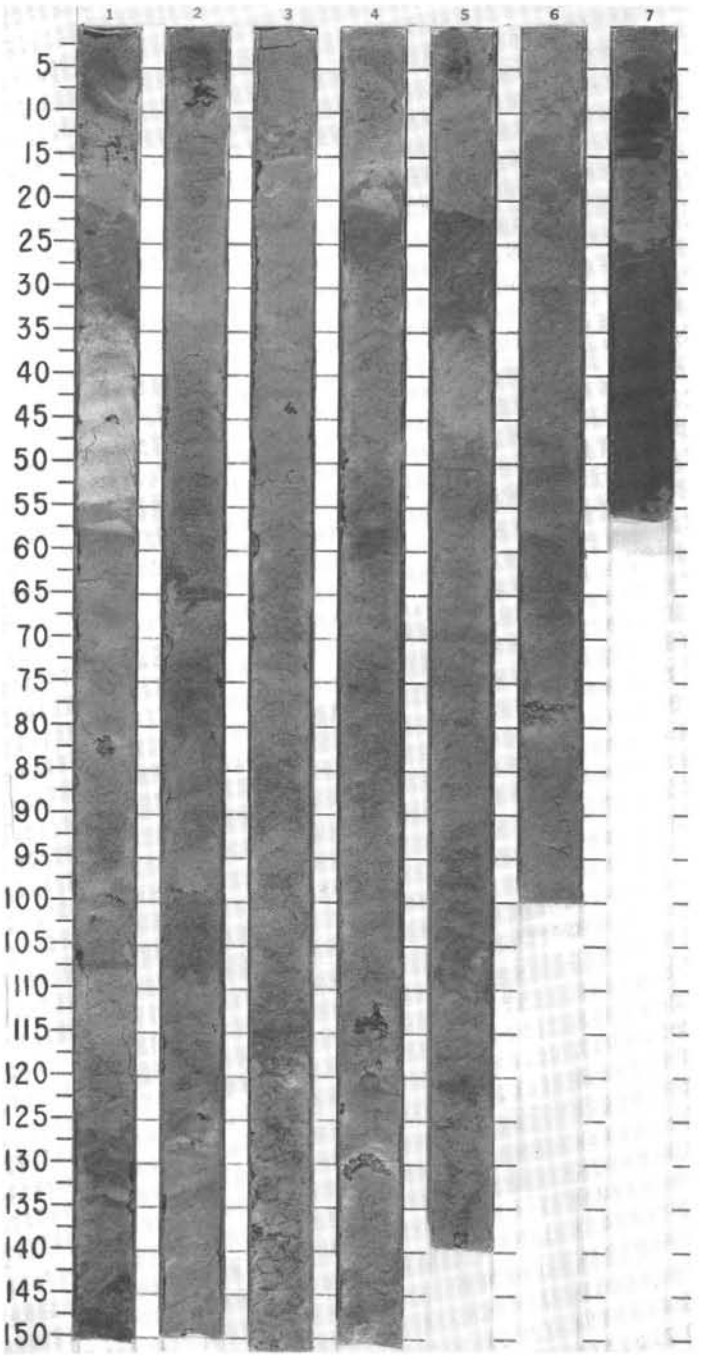

SITE 671 HOLE B CORE 64 X CORED INTERVAL 5518.4-5527.9 mbsl; 586.7-596.2 mbsf

TIME-ROCK UNIT	BIOSTRAT. ZONE/ FOSSIL CHARACTER: FORAMINIFERS	NANNOFOSSILS	RADIOLARIANS	DIATOMS	PALEOMAGNETICS	PHYS. PROPERTIES	CHEMISTRY	SECTION	METERS	GRAPHIC LITHOLOGY	DRILLING DISTURB.	SED. STRUCTURES	SAMPLES
UPPER OLIGOCENE	Barren	CP18	*Theocyrtis tuberosa* Z. to *Dorcadospyris ateuchus* Z.			●φ=53.6 γ=1.86	●0.3 %	1	0.5, 1.0	VOID			*
								2					
								3					*
						●φ=49.7 γ=1.93	●0.8%	4					
								5					
	B		R/vP			●φ=50.0 γ=1.91	●33.0 %	6					

LITHOLOGIC DESCRIPTION

MUDSTONE and SILTY MUDSTONE

MUDSTONE and SILTY MUDSTONE, green (5G5/2), gray-green (5BG4/1), and olive-green (5GY4/1). Intervals of mm-thick planar lamination occur throughout core. Local slight to intense bioturbation.

Minor lithology: marlstone, pale green-gray (5GY7/1 to 5Y6/1). Bases of these intervals commonly planar laminated while tops are typically bioturbated.

SMEAR SLIDE SUMMARY (%):

	1, 94 M	3, 22 M
TEXTURE:		
Silt	35	20
Clay	65	80
COMPOSITION:		
Quartz	25	20
Feldspar	25	—
Clay	49	78
Volcanic glass	—	2
Foraminifers	Tr	—
Nannofossils	1	Tr

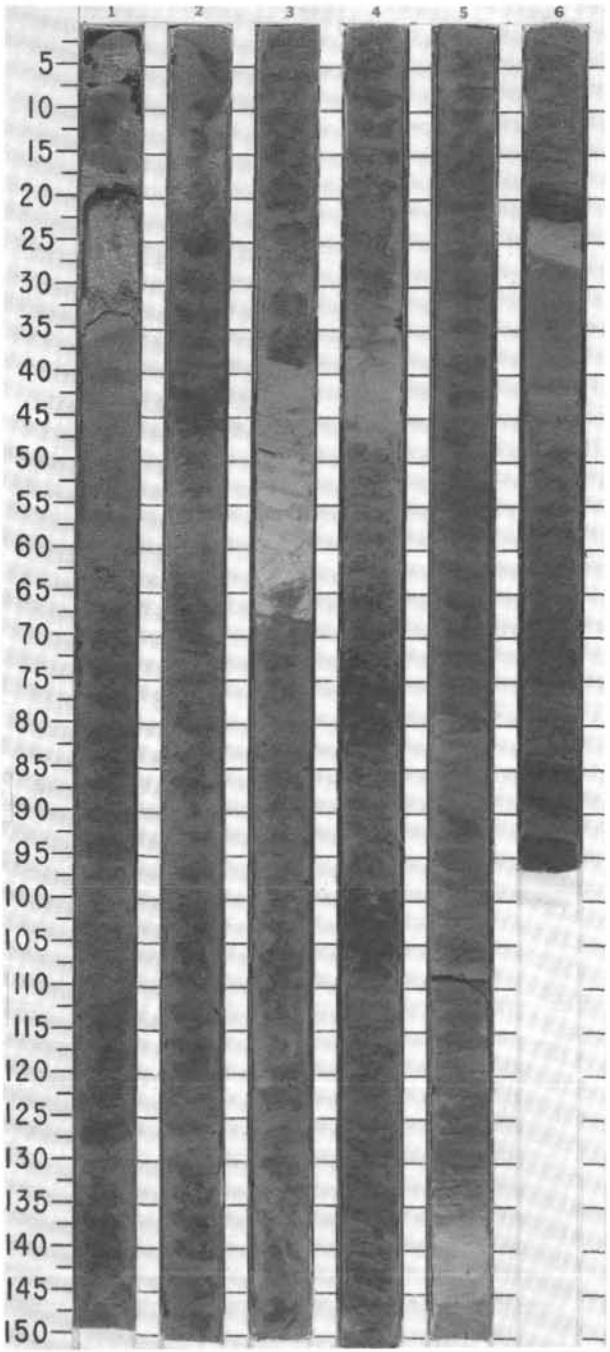

SITE 671 HOLE B CORE 65 X CORED INTERVAL 5527.9-5537.4 mbsl; 596.2-605.7 mbsf

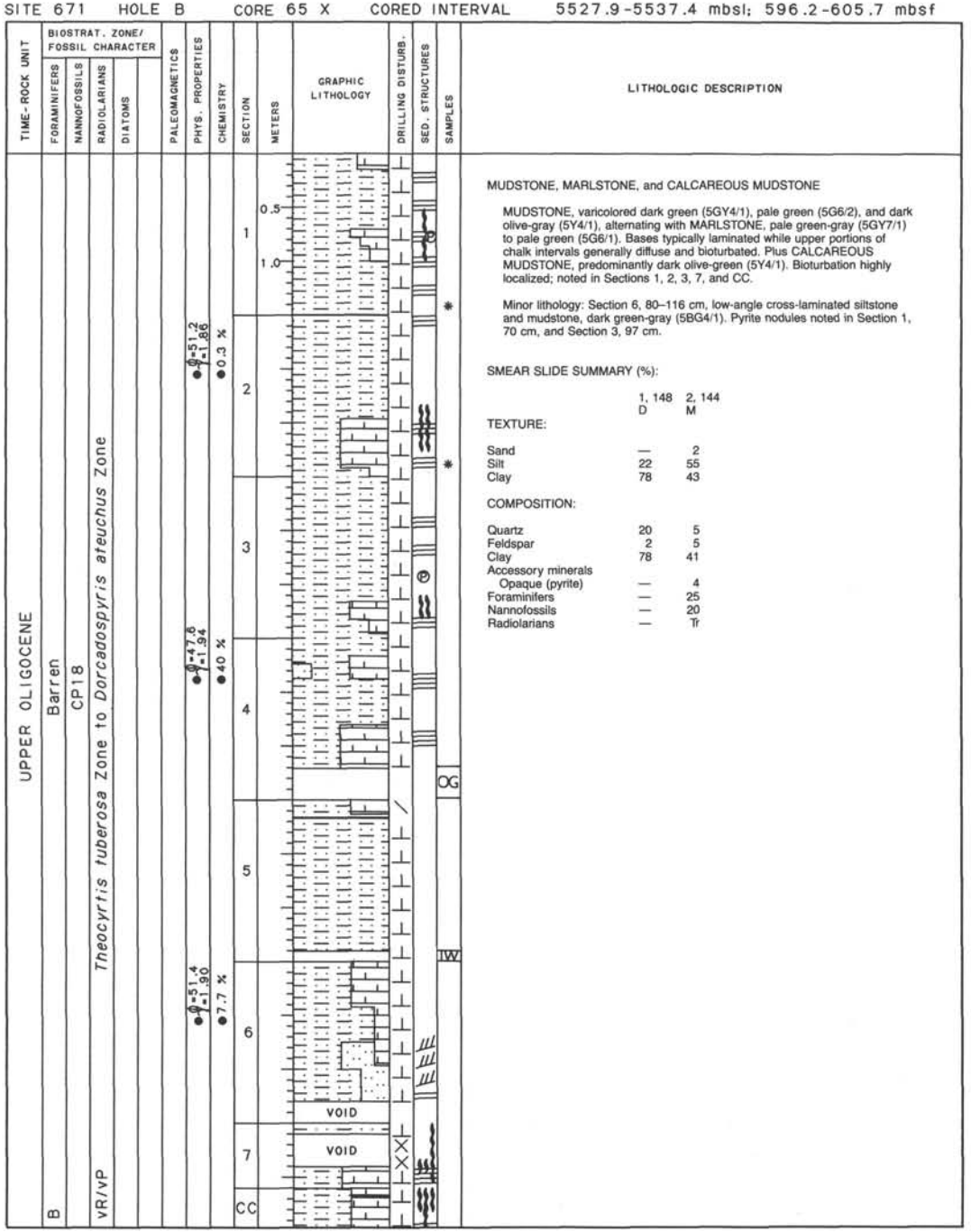

MUDSTONE, MARLSTONE, and CALCAREOUS MUDSTONE

MUDSTONE, varicolored dark green (5GY4/1), pale green (5G6/2), and dark olive-gray (5Y4/1), alternating with MARLSTONE, pale green-gray (5GY7/1) to pale green (5G6/1). Bases typically laminated while upper portions of chalk intervals generally diffuse and bioturbated. Plus CALCAREOUS MUDSTONE, predominantly dark olive-green (5Y4/1). Bioturbation highly localized; noted in Sections 1, 2, 3, 7, and CC.

Minor lithology: Section 6, 80–116 cm, low-angle cross-laminated siltstone and mudstone, dark green-gray (5BG4/1). Pyrite nodules noted in Section 1, 70 cm, and Section 3, 97 cm.

SMEAR SLIDE SUMMARY (%):

	1, 148 D	2, 144 M
TEXTURE:		
Sand	—	2
Silt	22	55
Clay	78	43
COMPOSITION:		
Quartz	20	5
Feldspar	2	5
Clay	78	41
Accessory minerals		
Opaque (pyrite)	—	4
Foraminifers	—	25
Nannofossils	—	20
Radiolarians	—	Tr

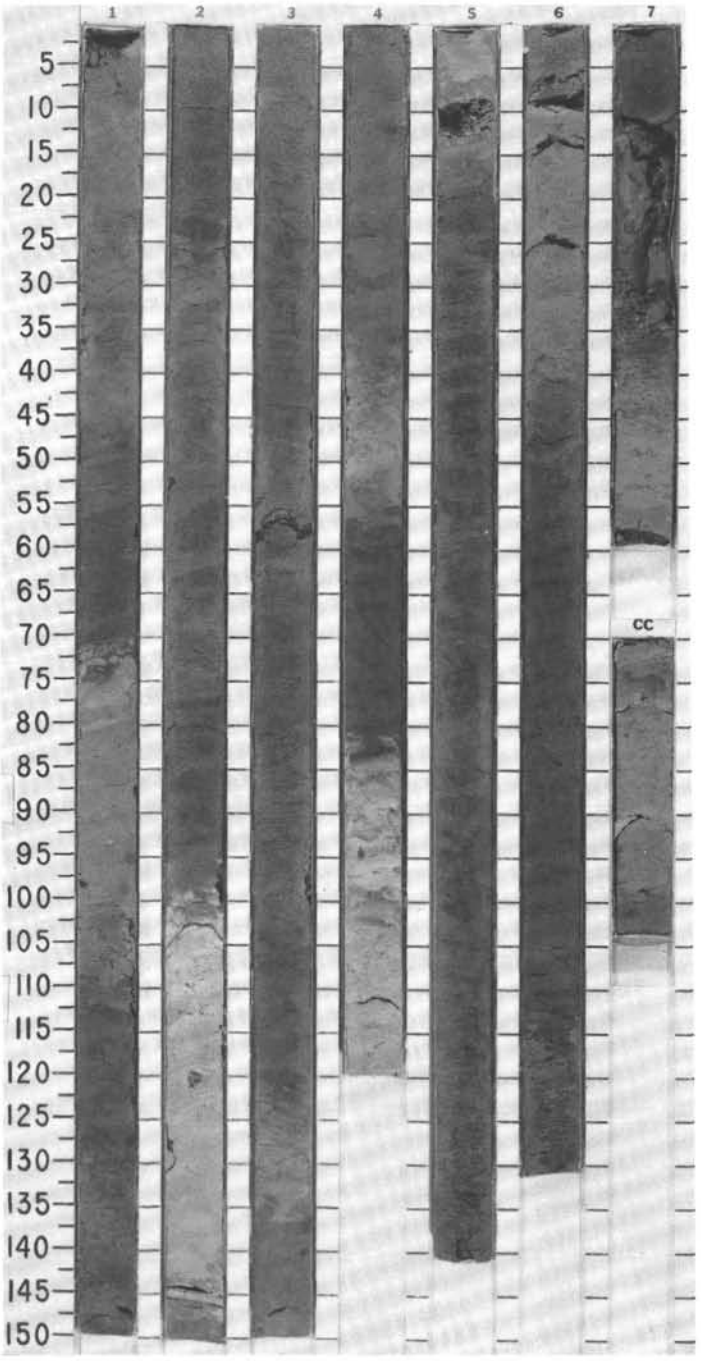

SITE 671 HOLE B CORE 66 X CORED INTERVAL 5537.4-5546.9 mbsl; 605.7-615.2 mbsf

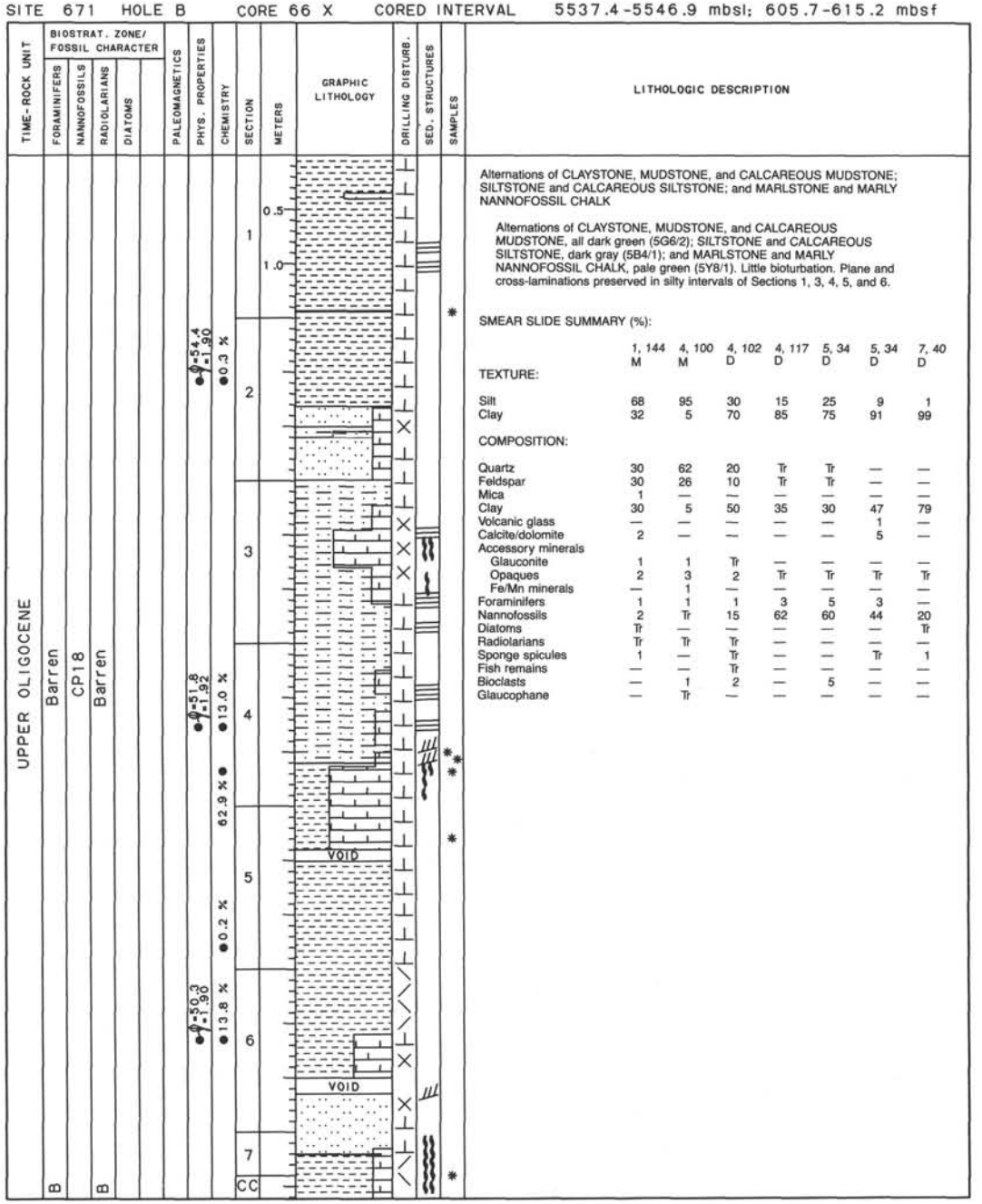

LITHOLOGIC DESCRIPTION

Alternations of CLAYSTONE, MUDSTONE, and CALCAREOUS MUDSTONE; SILTSTONE and CALCAREOUS SILTSTONE; and MARLSTONE and MARLY NANNOFOSSIL CHALK

Alternations of CLAYSTONE, MUDSTONE, and CALCAREOUS MUDSTONE, all dark green (5G6/2); SILTSTONE and CALCAREOUS SILTSTONE, dark gray (5B4/1); and MARLSTONE and MARLY NANNOFOSSIL CHALK, pale green (5Y8/1). Little bioturbation. Plane and cross-laminations preserved in silty intervals of Sections 1, 3, 4, 5, and 6.

SMEAR SLIDE SUMMARY (%):

	1, 144 M	4, 100 M	4, 102 D	4, 117 D	5, 34 D	5, 34 D	7, 40 D
TEXTURE:							
Silt	68	95	30	15	25	9	1
Clay	32	5	70	85	75	91	99
COMPOSITION:							
Quartz	30	62	20	Tr	Tr	—	—
Feldspar	30	26	10	Tr	Tr	—	—
Mica	1	—	—	—	—	—	—
Clay	30	5	50	35	30	47	79
Volcanic glass	—	—	—	—	—	1	—
Calcite/dolomite	2	—	—	—	—	5	—
Accessory minerals							
Glauconite	1	1	Tr	—	—	—	—
Opaques	2	3	2	Tr	Tr	Tr	Tr
Fe/Mn minerals	—	1	—	—	—	—	—
Foraminifers	1	1	1	3	5	3	—
Nannofossils	2	Tr	15	62	60	44	20
Diatoms	Tr	—	—	—	—	—	Tr
Radiolarians	Tr	Tr	Tr	—	—	—	—
Sponge spicules	1	—	Tr	—	—	Tr	1
Fish remains	—	—	Tr	—	—	—	—
Bioclasts	—	1	2	—	5	—	—
Glaucophane	—	Tr	—	—	—	—	—

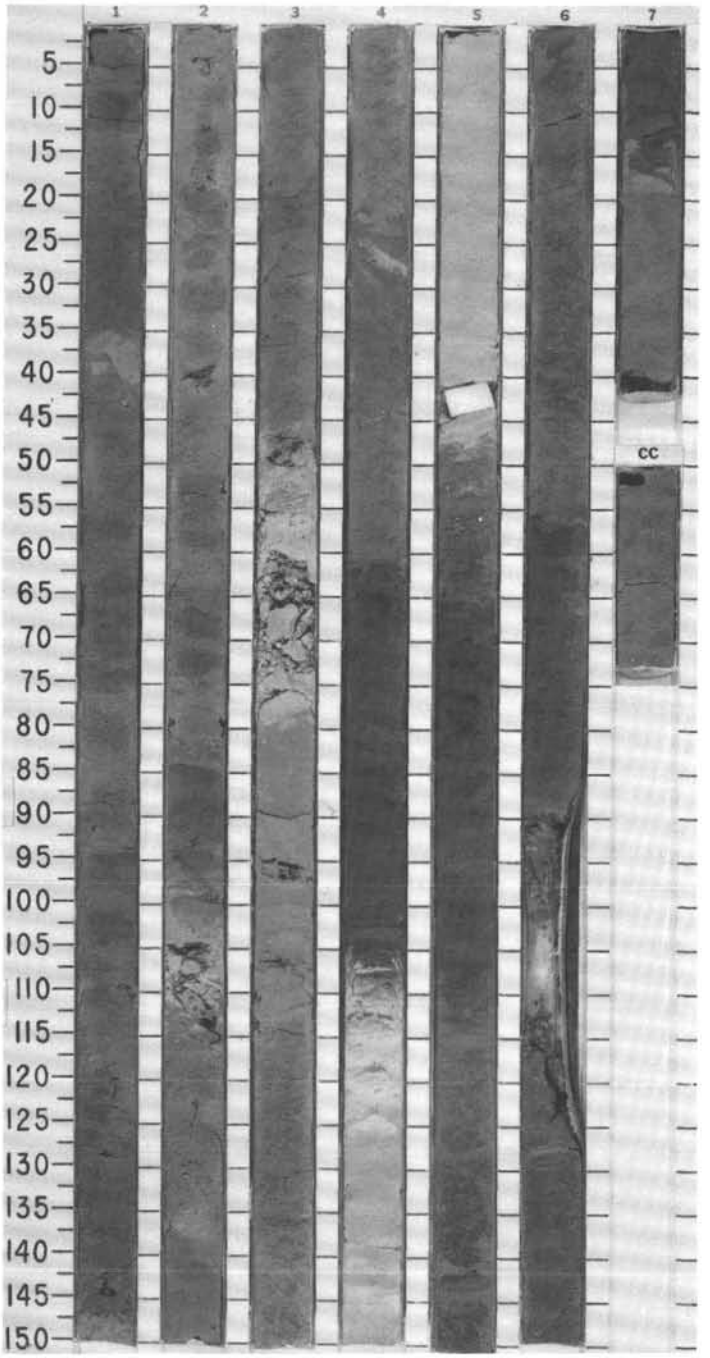

SITE 671 HOLE B CORE 67 X CORED INTERVAL 5546.9-5556.4 mbsl; 615.2-624.7 mbsf

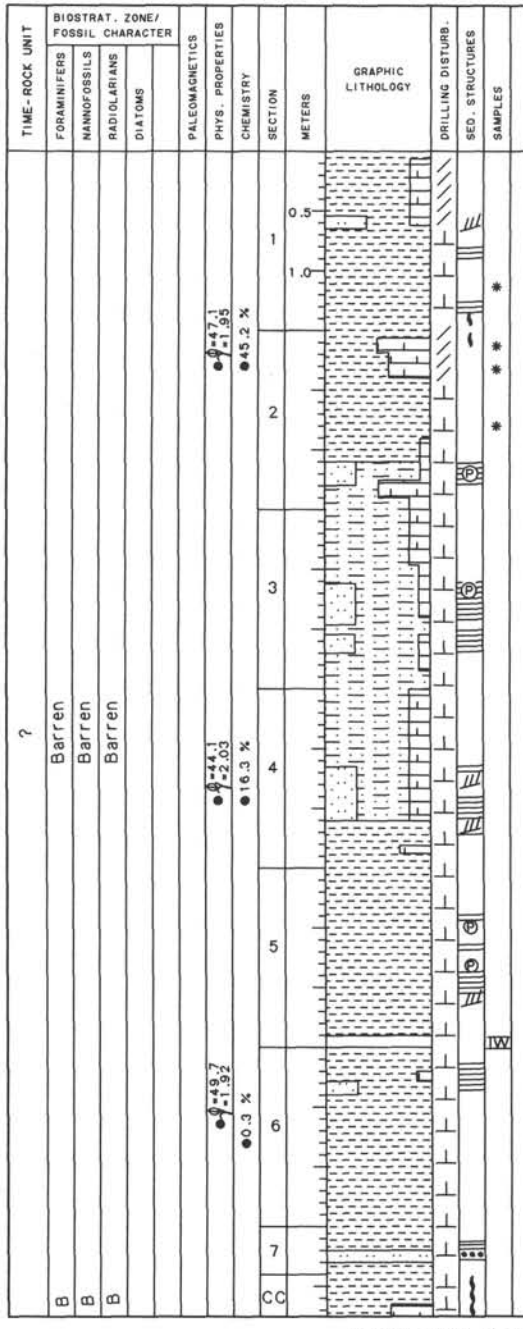

LITHOLOGIC DESCRIPTION

CALCAREOUS MUDSTONE, alternating with MUDSTONE and CLAYSTONE; and MARLSTONE

Nannofossil-bearing CALCAREOUS MUDSTONE, dark olive-green (5Y3/1, 5Y4/1), alternating with MUDSTONE and CLAYSTONE, green (5G4/2, 5G5/2). Plus MARLSTONE, pale green-gray (5G7/1). Minor bioturbation in Section 1 and CC. mm-thick planar lamination and low-angle cross-laminations occur in Sections 1, 2, 3, 4, 5, 6, and 7. These intervals commonly include silt laminae.

Minor lithology: siltstone, dark green (5BG5/1). Normally graded, possible turbidite. Pyrite nodules noted in Sections 2, 3, and 5.

SMEAR SLIDE SUMMARY (%):

	1, 115 D	2, 11 D	2, 32 D	2, 80 D
TEXTURE:				
Silt	5	5	10	Tr
Clay	95	95	90	100
COMPOSITION:				
Quartz	2	—	—	Tr
Feldspar	1	—	—	Tr
Clay	97	15	40	100
Accessory minerals				
Opaques	—	5	—	Tr
Microcline	Tr	—	—	—
Foraminifers	—	—	Tr	—
Nannofossils	—	80	60	—
Bioclasts	—	—	Tr	—

CORE 68X NO RECOVERY

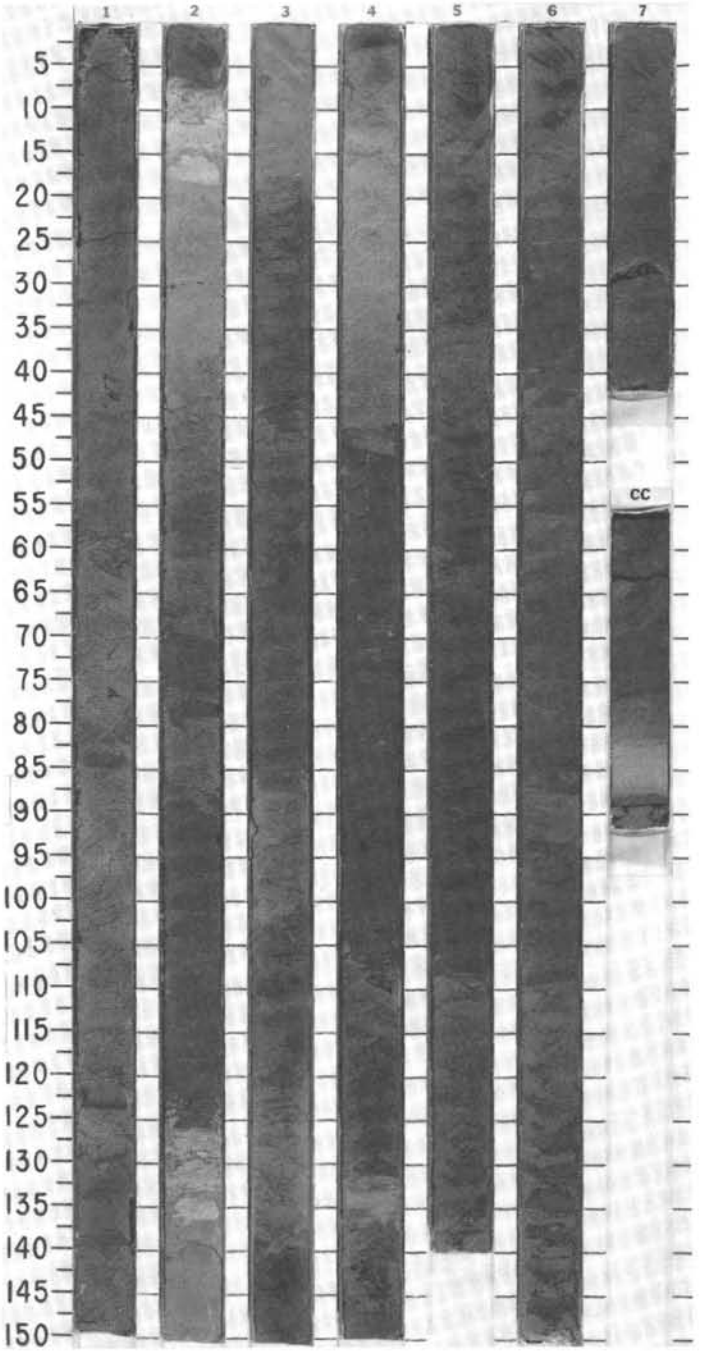

SITE 671 HOLE B CORE 69 X CORED INTERVAL 5565.9-5575.4 mbsl; 634.2-643.7 mbsf

TIME-ROCK UNIT	BIOSTRAT. ZONE/ FOSSIL CHARACTER: FORAMINIFERS	NANNOFOSSILS	RADIOLARIANS	DIATOMS	PALEOMAGNETICS	PHYS. PROPERTIES	CHEMISTRY	SECTION	METERS	GRAPHIC LITHOLOGY	DRILLING DISTURB.	SED. STRUCTURES	SAMPLES	LITHOLOGIC DESCRIPTION
UPPER OLIGOCENE	B Barren	CP17	B Barren				● 2.5 %	1 2 3 CC	0.5 1.0	All Drilling Breccia; All Drilling Breccia		Ⓟ	*	

CALCAREOUS CLAYSTONE and CLAYSTONE

Drill breccias, Sections 1, 2, and 3, 0–78 and 85–105 cm. Section 3, 78–85 cm, composed of CALCAREOUS CLAYSTONE probably *in situ*, varicolored green (5G6/1, 10Y6/2, and 5G5/2), planar laminated, and slightly bioturbated. CC consists of dark bluish green (5BG4/1) CLAYSTONE. *Planolites* observed in CC, 22–27 cm.

SMEAR SLIDE SUMMARY (%):

	CC M
TEXTURE:	
Clay	100
COMPOSITION:	
Accessory minerals	
Opaques (amorphous opaque material, org. matter?)	100

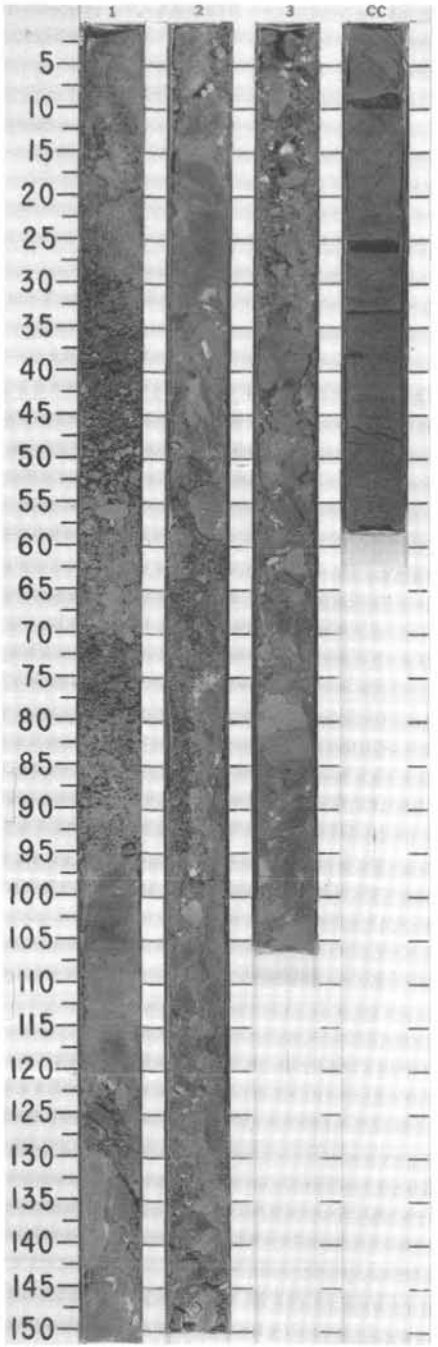

SITE 671 HOLE B CORE 70 X CORED INTERVAL 5575.4-5584.9 mbsl; 643.7-653.2 mbsf

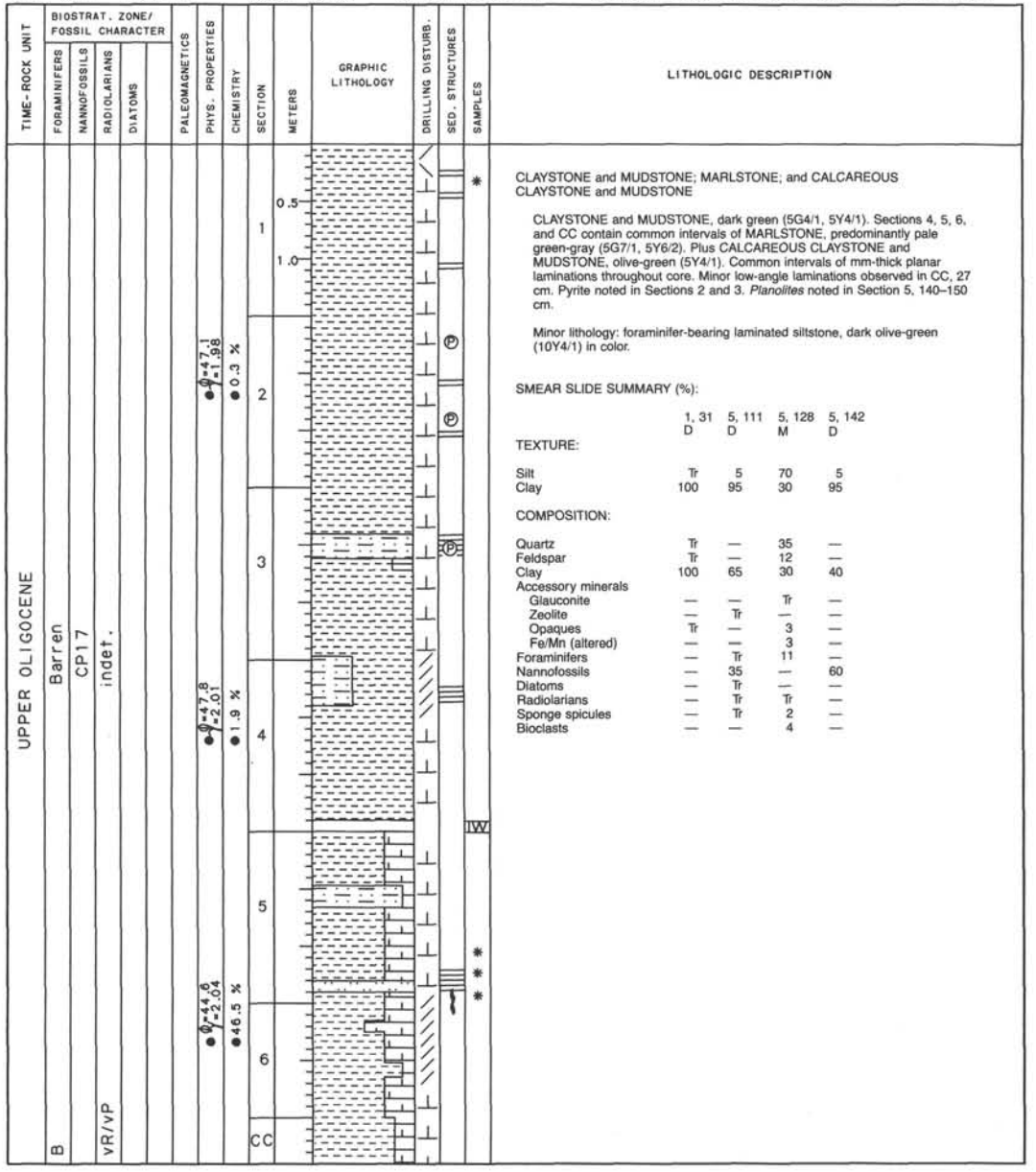

LITHOLOGIC DESCRIPTION

CLAYSTONE and MUDSTONE; MARLSTONE; and CALCAREOUS CLAYSTONE and MUDSTONE

CLAYSTONE and MUDSTONE, dark green (5G4/1, 5Y4/1). Sections 4, 5, 6, and CC contain common intervals of MARLSTONE, predominantly pale green-gray (5G7/1, 5Y6/2). Plus CALCAREOUS CLAYSTONE and MUDSTONE, olive-green (5Y4/1). Common intervals of mm-thick planar laminations throughout core. Minor low-angle laminations observed in CC, 27 cm. Pyrite noted in Sections 2 and 3. *Planolites* noted in Section 5, 140–150 cm.

Minor lithology: foraminifer-bearing laminated siltstone, dark olive-green (10Y4/1) in color.

SMEAR SLIDE SUMMARY (%):

	1, 31 D	5, 111 D	5, 128 M	5, 142 D
TEXTURE:				
Silt	Tr	5	70	5
Clay	100	95	30	95
COMPOSITION:				
Quartz	Tr	—	35	—
Feldspar	Tr	—	12	—
Clay	100	65	30	40
Accessory minerals				
Glauconite	—	—	Tr	—
Zeolite	—	Tr	—	—
Opaques	Tr	—	3	—
Fe/Mn (altered)	—	—	3	—
Foraminifers	—	Tr	11	—
Nannofossils	—	35	—	60
Diatoms	—	Tr	—	—
Radiolarians	—	Tr	Tr	—
Sponge spicules	—	Tr	2	—
Bioclasts	—	—	4	—

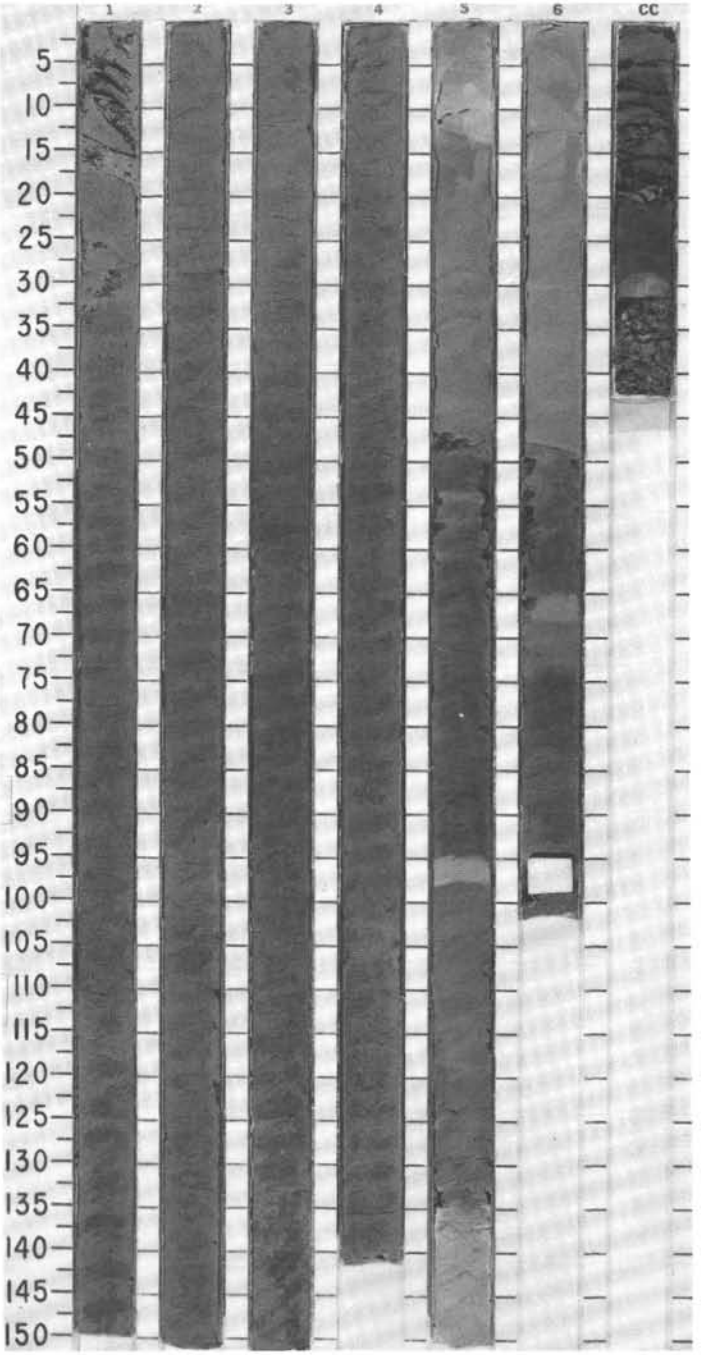

SITE 671 HOLE B CORE 71 X CORED INTERVAL 5584.9-5594.4 mbsl; 653.2-662.7 mbsf

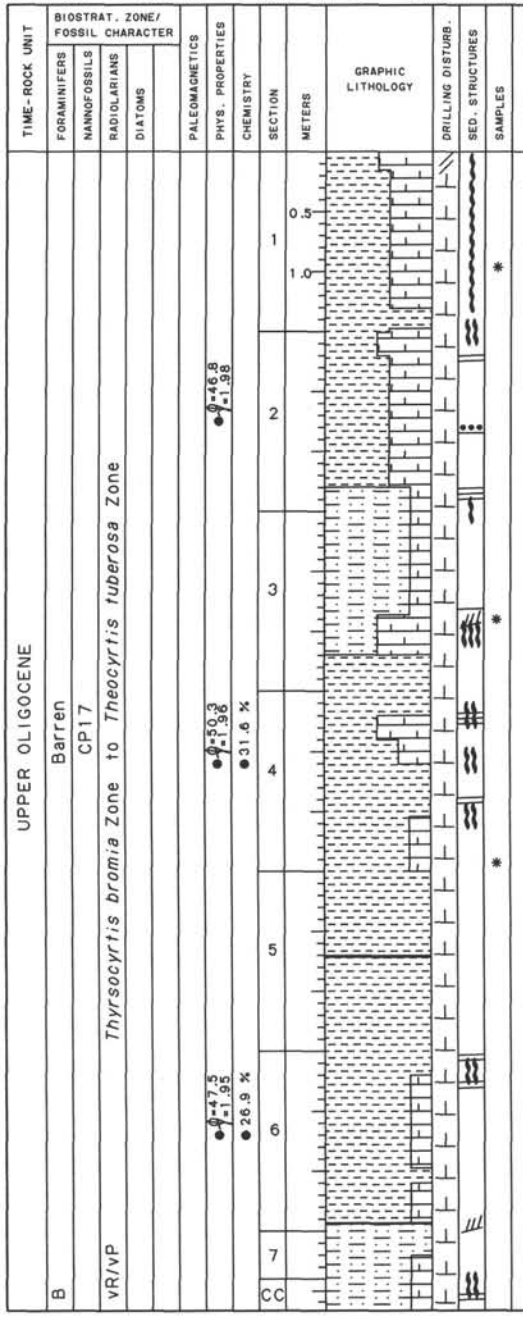

LITHOLOGIC DESCRIPTION

MARLSTONE, alternating with CALCAREOUS CLAYSTONE and MUDSTONE; and CLAYSTONE and MUDSTONE

MARLSTONE, green (5GY5/1) to pale green-gray (5GY7/1) (pale green horizons appear to contain higher percentages of nannofossils); alternating with CALCAREOUS CLAYSTONE and MUDSTONE, olive-green (5Y4/1) to green (5G5/2); and CLAYSTONE and MUDSTONE, predominantly dark green (5G4/2) with common intervals of dark olive-gray (5Y3/1). Intervals of mm-thick planar laminae occur throughout core. Low-angle cross-laminations occur in Sections 3 and 6. Local bioturbation noted in Sections 1, 2, 3, 4, 6, and CC.

Minor lithology: mm-thick silty foraminifer-rich bed in Section 5, 70 cm, and siltstone bed with low-angle cross-laminations in Section 6, 142–146 cm. One thin graded bed of pyrite-rich mudstone noted in Section 2, 95 cm.

SMEAR SLIDE SUMMARY (%):

	1, 90 D	3, 90 D	4, 141 D
TEXTURE:			
Sand	—	3	—
Silt	—	30	2
Clay	100	67	98
COMPOSITION:			
Quartz	—	30	2
Feldspar	—	5	—
Clay	30	55	98
Volcanic glass	Tr	Tr	—
Calcite/dolomite	Tr	—	—
Accessory minerals			
Pyrite	—	5	—
Foraminifers	—	2	—
Nannofossils	70	3	—

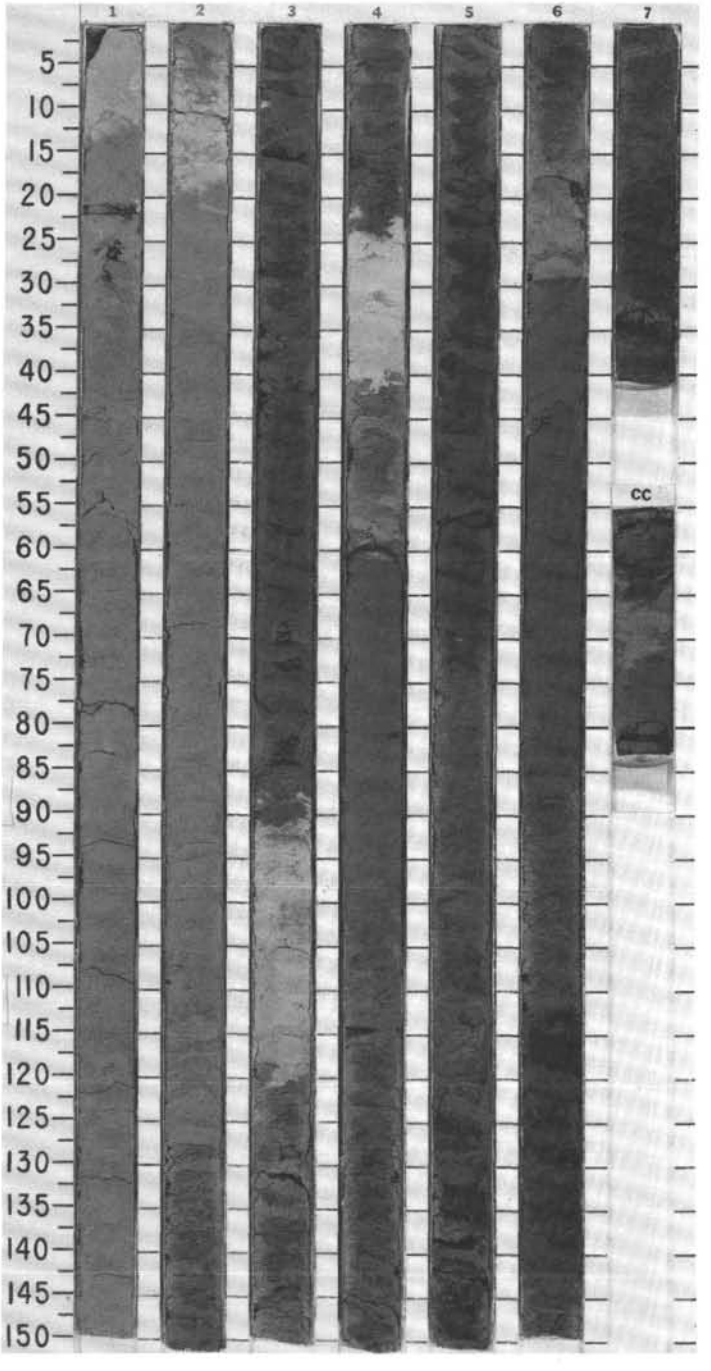

SITE 671 HOLE B CORE 72 X CORED INTERVAL 5594.4-5603.9 mbsl; 662.7-672.2 mbsf

TIME-ROCK UNIT: LOWER OLIGOCENE

BIOSTRAT. ZONE/FOSSIL CHARACTER: FORAMINIFERS: B; Barren; NANNOFOSSILS: CP16; RADIOLARIANS: indet.; DIATOMS: vR/vP

PALEOMAGNETICS

PHYS. PROPERTIES: ●ϕ=50.3 / ρ=1.97; ●ϕ=45.9 / ρ=1.98; ●ϕ=46.0 / ρ=2.01

CHEMISTRY: ●0.3 %; ●34.5 %; ●46.4 %

SECTION: 1, 2, 3, 4, 5, 6, 7, CC

METERS: 0.5, 1.0

GRAPHIC LITHOLOGY

DRILLING DISTURB.

SED. STRUCTURES

SAMPLES: OG

LITHOLOGIC DESCRIPTION

CLAYSTONE and MUDSTONE, alternating with CALCAREOUS CLAYSTONE and MUDSTONE, and MARLSTONE

CLAYSTONE and MUDSTONE, green (5G4/2), alternating with CALCAREOUS CLAYSTONE and MUDSTONE, olive-green (5Y4/1) to green (5G4/1). Plus MARLSTONE, pale green-gray (5G7/1) to pale green (5GY6/1). mm-thick planar lamination and low-angle cross-laminations noted in Sections 2, 3, 4, 5, 6, 7, and CC. Local bioturbation occurs in Sections 3, 4, 5, and 7. Thin *Zoophycos* burrows noted in Section 5, 4–10 cm.

SMEAR SLIDE SUMMARY (%):

	5, 75 D	6, 80 D	6, 135 D
TEXTURE:			
Sand	1	—	4
Silt	10	10	46
Clay	89	90	50
COMPOSITION:			
Quartz	5	10	10
Feldspar	5	—	10
Clay	80	49	48
Volcanic glass	Tr	—	—
Accessory minerals			
Pyrite	—	1	5
Foraminifers	—	5	12
Nannofossils	10	35	15

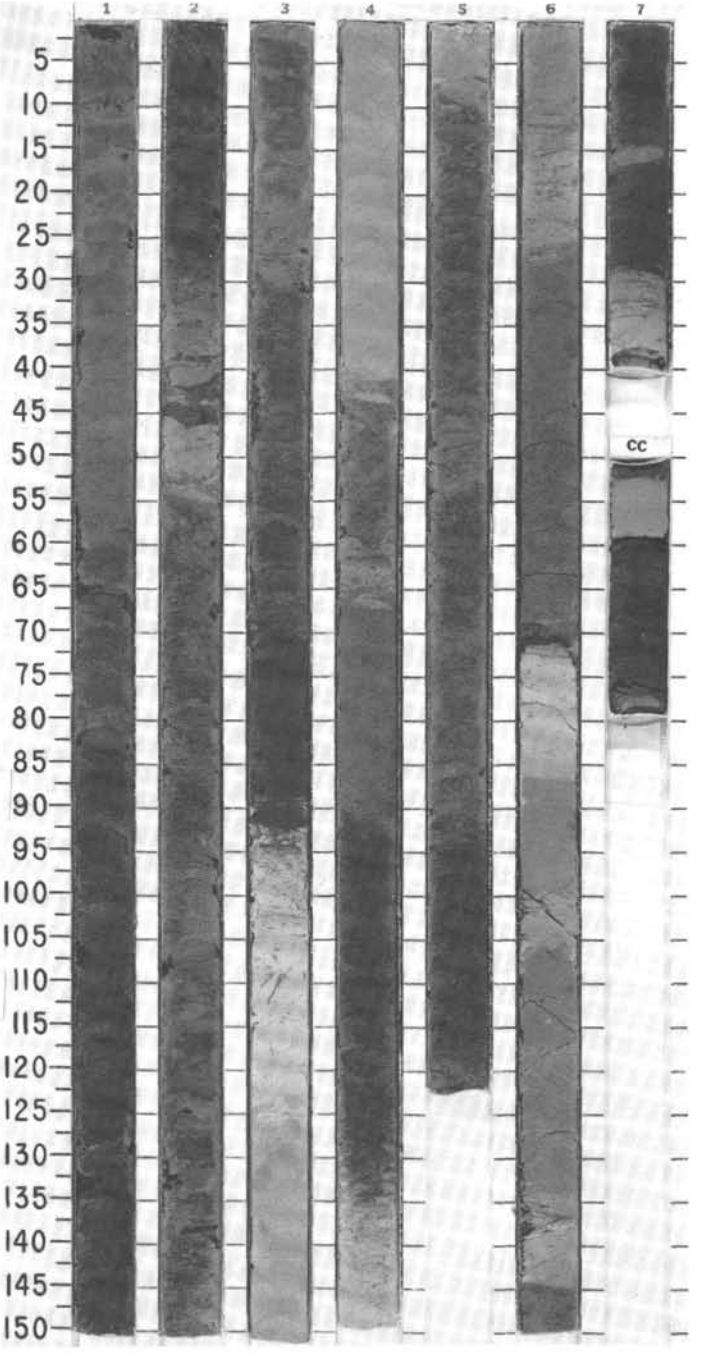

SITE 671 HOLE B CORE 73 X CORED INTERVAL 5603.9-5613.4 mbsl; 672.2-681.7 mbsf

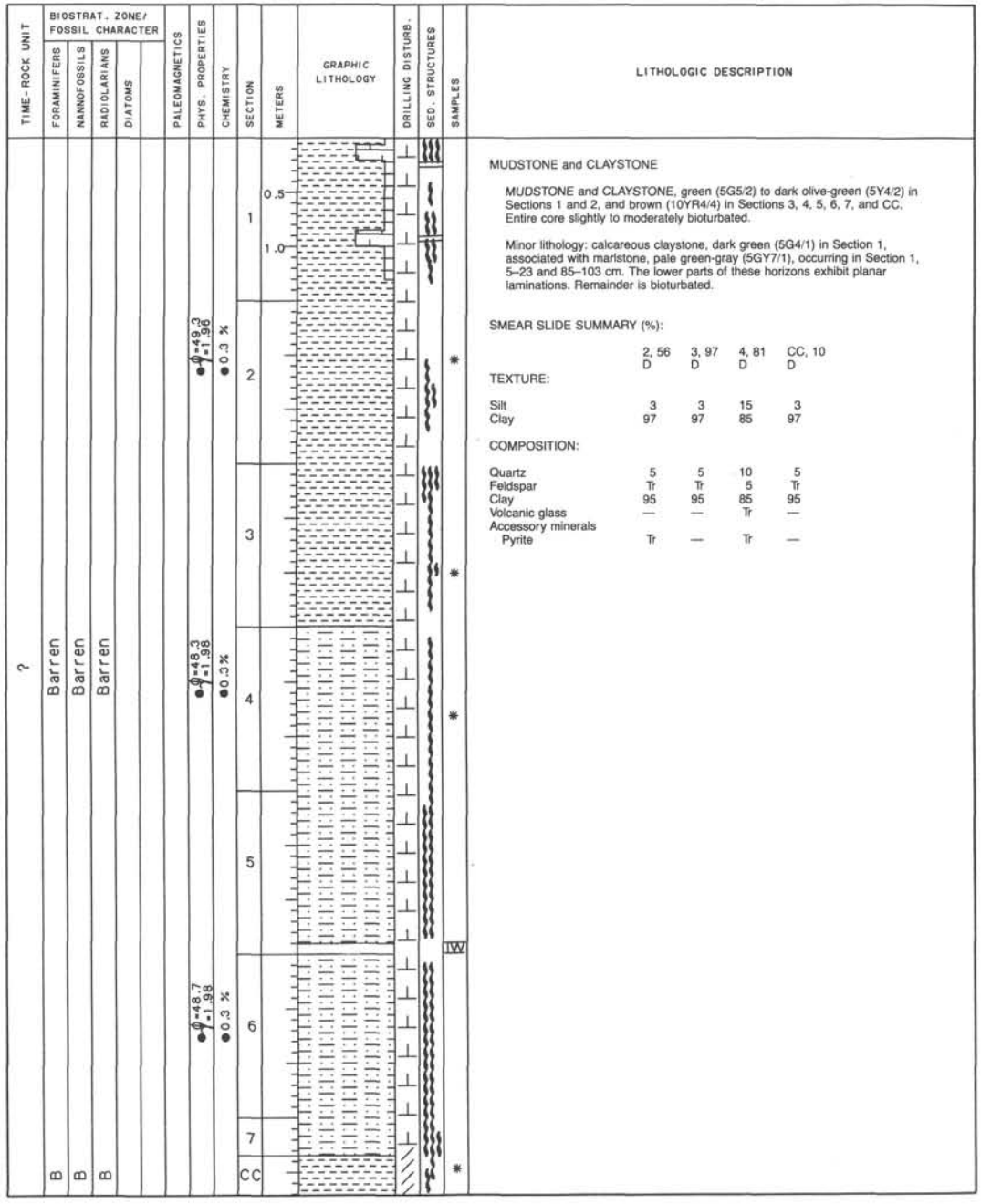

LITHOLOGIC DESCRIPTION

MUDSTONE and CLAYSTONE

MUDSTONE and *CLAYSTONE*, green (5G5/2) to dark olive-green (5Y4/2) in Sections 1 and 2, and brown (10YR4/4) in Sections 3, 4, 5, 6, 7, and CC. Entire core slightly to moderately bioturbated.

Minor lithology: calcareous claystone, dark green (5G4/1) in Section 1, associated with marlstone, pale green-gray (5GY7/1), occurring in Section 1, 5–23 and 85–103 cm. The lower parts of these horizons exhibit planar laminations. Remainder is bioturbated.

SMEAR SLIDE SUMMARY (%):

	2, 56 D	3, 97 D	4, 81 D	CC, 10 D
TEXTURE:				
Silt	3	3	15	3
Clay	97	97	85	97
COMPOSITION:				
Quartz	5	5	10	5
Feldspar	Tr	Tr	5	Tr
Clay	95	95	85	95
Volcanic glass	—	—	Tr	—
Accessory minerals				
Pyrite	Tr	—	Tr	—

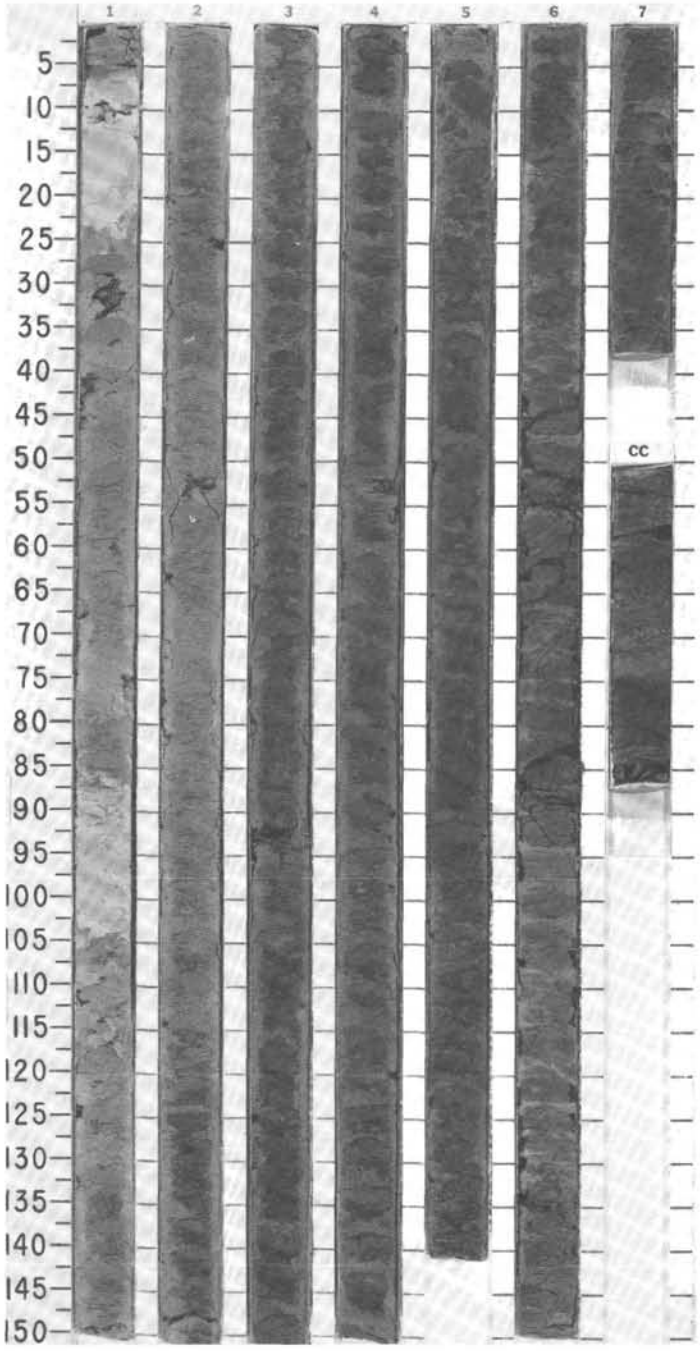

SITE 671 HOLE B CORE 74 X CORED INTERVAL 5613.4-5622.9 mbsl; 681.7-691.2 mbsf

TIME-ROCK UNIT	BIOSTRAT. ZONE/ FOSSIL CHARACTER: FORAMINIFERS	NANNOFOSSILS	RADIOLARIANS	DIATOMS	PALEOMAGNETICS	PHYS. PROPERTIES	CHEMISTRY	SECTION	METERS	GRAPHIC LITHOLOGY	DRILLING DISTURB.	SED. STRUCTURES	SAMPLES
?	B	reworked	C/vP indet.					1	0.5 1.0				** * *

LITHOLOGIC DESCRIPTION

MUDSTONE and GLAUCONITIC QUARTZ SAND

MUDSTONE, green (predominantly 5G5/1), from Section 1, 0–100 cm, grading down to GLAUCONITIC QUARTZ SAND, 1 cm bed in Section 1, 38–39 cm, and drill slurry of unlithified sand, Section 1, 100–128 cm. Interval contains abundant mudstone (a/a) and several 1 cm-diameter chips of lithified sandstone.

Minor lithology: pyrite-bearing siltstone, 0.5–1 cm beds at Section 1, 14, 17, and 48 cm.

SMEAR SLIDE SUMMARY (%):

	1, 15 D	1, 15 M	1, 35 D	1, 75 M
TEXTURE:				
Sand	7	10	—	18
Silt	23	60	20	32
Clay	70	30	80	50
COMPOSITION:				
Quartz	8	10	15	30
Feldspar	22	25	5	30
Clay	48	30	77	—
Volcanic glass	10	16	3	35
Accessory minerals				
Glauconite	2	4	—	3
Pyrite	10	15	—	2
Clinopyroxene	Tr	—	—	—
Chert	—	Tr	—	—
Microcline	—	—	—	Tr

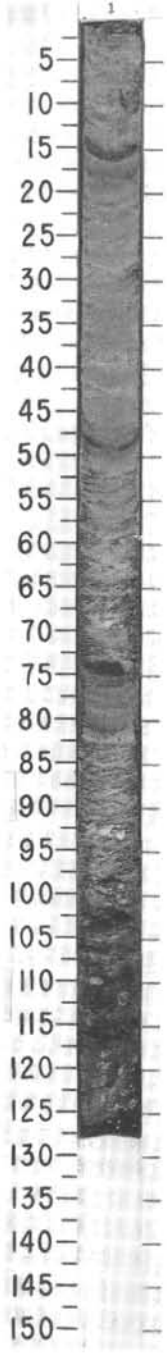

SITE 671 HOLE C CORE 1 X CORED INTERVAL 5432.2-5441.7 mbsl; 495.7-505.2 mbsf

TIME-ROCK UNIT: LOWER MIOCENE

BIOSTRAT. ZONE/FOSSIL CHARACTER: FORAMINIFERS: Barren; NANNOFOSSILS: Barren; RADIOLARIANS: *Stichocorys wolffii* Zone; DIATOMS: *C. tetrapera* Z.

PALEOMAGNETICS: A/M; PHYS. PROPERTIES: C/M; CHEMISTRY

SECTION: 1, 2, 3, 4, 5, 6, 7, CC

METERS: 0.5, 1.0

GRAPHIC LITHOLOGY

DRILLING DISTURB.

SED. STRUCTURES

SAMPLES: IW

LITHOLOGIC DESCRIPTION

CLAYSTONE

CLAYSTONE, alternating brown (10YR6/4) and dark gray-brown (10YR3/1). Local radiolarian fragments occur in Section 1. All contacts gradational.

SMEAR SLIDE SUMMARY (%):

	1, 53 D	1, 60 D	1, 94 M	1, 120 D
TEXTURE:				
Silt	15	8	75	25
Clay	85	92	25	75
COMPOSITION:				
Quartz	Tr	—	15	Tr
Feldspar	Tr	Tr	10	Tr
Clay	89	92	30	77
Volcanic glass	—	—	43	1
Accessory minerals				
Pyroxene	—	—	Tr	—
Opaques	Tr	Tr	2	—
Mn oxide	—	—	—	8
Radiolarians	10	6	Tr	12
Sponge spicules	1	1	Tr	2

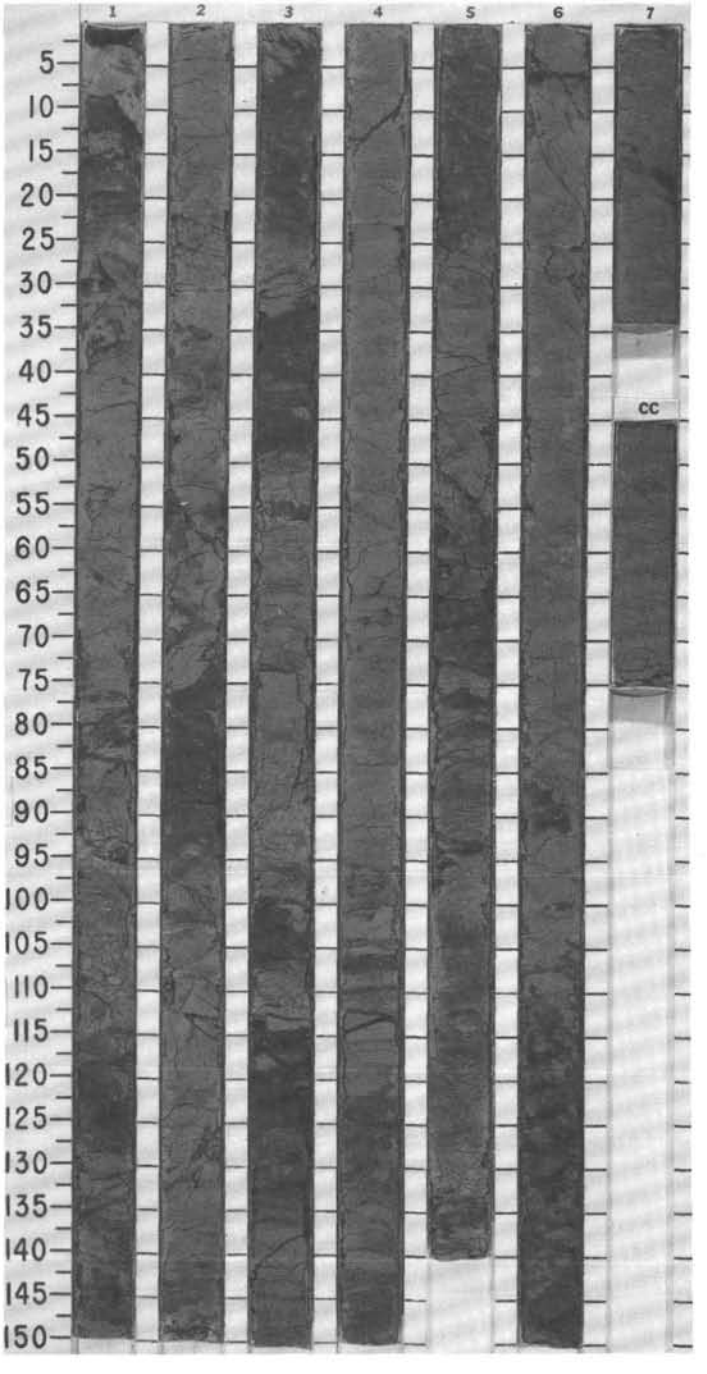

SITE 671 HOLE C CORE 2 X CORED INTERVAL 5441.7-5451.2 mbsl; 505.2-514.7 mbsf

TIME-ROCK UNIT	FORAMINIFERS	NANNOFOSSILS	RADIOLARIANS	DIATOMS	PALEOMAGNETICS	PHYS. PROPERTIES	CHEMISTRY	SECTION	METERS	GRAPHIC LITHOLOGY	DRILLING DISTURB.	SED. STRUCTURES	SAMPLES
?	Barren	Barren	F/vP	indet.				1	0.5				TW
									1.0				
								2					*
								3					*
								4					TW
								5					TW
								CC					*

LITHOLOGIC DESCRIPTION

CLAYSTONE

CLAYSTONE, brown (10YR 6/4) and dark gray-brown (10YR 3/1). Dark colors probably due to manganese oxides. Core highly disturbed by drilling. 0–5% radiolarian fragments occur scattered through core. Bottom of Section 5 and CC consists of green-gray (5Y6/3) CLAYSTONE with scattered 1 mm white clinoptilolite spherules.

SMEAR SLIDE SUMMARY (%):
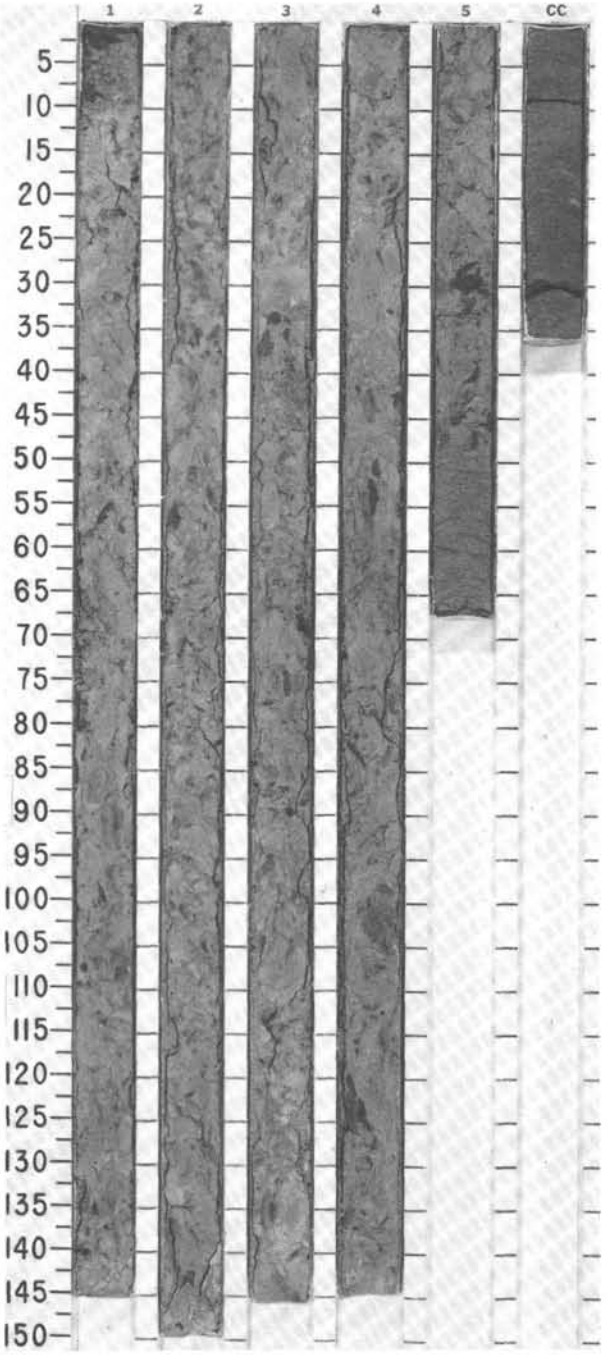
	2, 37 D	3, 36 D	CC, 5 D
TEXTURE:			
Silt	2	10	2
Clay	98	90	98
COMPOSITION:			
Feldspar	Tr	1	—
Clay	98	92	98
Volcanic glass	Tr	Tr	1
Accessory minerals			
Opaques	Tr	Tr	1
Radiolarians	1	5	—
Sponge spicules	Tr	2	—